UNIVERSITY OF CALIFORNIA SAN DIEGO

A Role for the Medial Entorhinal Cortex in Multimodal Information Processing and Episodic Memory

A dissertation submitted in partial satisfaction of the
requirements for the degree Doctor of Philosophy

in

Neurosciences

by

Geoffrey W. Diehl

Committee in charge:

Professor Jill Leutgeb, Chair
Professor Timothy Gentner
Professor Stefan Leutgeb
Professor Byungkook Lim
Professor Terrence Sejnowski
Professor Larry Squire

2018

The Dissertation of Geoffrey W. Diehl is approved, and it is acceptable in quality and form for publication on microfilm and electronically:

_____

_____

_____

_____

_____

_____

Chair

University of California San Diego

2018

DEDICATION

I would like to dedicate this dissertation, and all of the work behind it, to the people that have provided the support and guidance to make it all possible. Most importantly to my family, who have always been there and always will be. To my friends who have gone along for the ride. And to all of the mentors, teachers, coaches, and advisors that have put in the time and effort to help me get to where I am.

EPIGRAPH

It's good to be curious about many things.

— Mr. Rogers

TABLE OF CONTENTS

LIST OF ABBREVIATIONS

AP	Anterior-Posterior
ATN	Anterior thalamic nucleus
CDF	Cumulative density function
COM	Center of mass
DG	Dentate Gyrus
DV	Dorso-Ventral
EC	Entorhinal cortex
HCN1	Hyperpolarization-activated cyclic nucleotide gated
HD	Head direction
HRP	Horseradish peroxidase
HSD	Honestly significant difference
IQR	Inter quartile range
lEC	Lateral entorhinal cortex
LFP	Local field potential
LTP	Long-term potentiation
mEC	Medial entorhinal cortex
ML	Medial-Lateral
MRL	Mean resultant length
MSA	Medial septal area
MTL	Medial temporal lobe
NGS	Non-grid spatial
ns	Non-significant

PI	Path integration
PV	Population vector
Pvalb	Parvalbumin
ROC	Receiver operating characteristic
RSC	Rate-speed correlation
RV	Firing rate vector
SEM	Standard error of the mean
SI	Spatial information
SOM	Somatostatin
SS	Speed score
SWR	Sharp-wave ripple
TT	Tetrode
WSC	Within session correlation

LIST OF FIGURES

LIST OF TABLES

ACKNOWLEDGEMENTS

I would like to acknowledge Jill Leutgeb for her support and mentorship over the last several years. From the start she has been excited and engaged and without her none of this would have been possible. I would also like to acknowledge Stefan Leutgeb for his dedication to this work, as well as the rest of my committee who have been instrumental in my development and success as a scientist.

I want to thank the rest of my lab-mates who have provided guidance, advice, and support whenever I needed it. Emily Mankin, Laura Ewell, Olivia Hon, Magda Schlesiger, Ipshita Zutshi, Marta Sabariego Collet, Mandy Wong, and Anna-Lena Schlenner have all helped me so many times in so many ways, and for all that they have done I am grateful.

Last, I want to thank the UCSD Neurosciences Graduate Program. Erin Gilbert and Linh Vandermar for making everything work, always. Tim Gentner for being the program director we all love. And my classmates, for the comradery that makes it all manageable.

Chapter 1, in full, is material as it appears in *Neuron*, 2017, Diehl, Geoffrey W., Hon, Olivia J., Leutgeb, Stefan, and Leutgeb, Jill K. The dissertation author was the primary researcher and author of this paper.

Chapter 2, in full, is material as it appears in *Neuron*, 2015, Mankin, Emily A., Diehl, Geoffrey W., Sparks, Fraser T., Leutgeb, Stefan, and Leutgeb, Jill K. The dissertation author was a primary researcher and author of this paper.

Chapter 3, in full, is material as it has been submitted to *Hippocampus.* Diehl, Geoffrey W., Hon, Olivia J., Leutgeb, Stefan, and Leutgeb, Jill K. The dissertation author was the primary researcher and author of this paper.

VITA

Bachelor of Arts, Oberlin College, Oberlin, OH

Doctor of Philosophy, University of California San Diego, CA

PUBLICATIONS

Paine TA, Asinof SK*, Diehl GW*, Frackman A*, Leffler J* "Medial prefrontal cortex lesions impair decision-making on a rodent gambling task: Reversal by D1 receptor antagonist administration." *Behavioural Brain Research.* 243:247-54. 2013

Diehl GW*, Wachtel JM*, Paine TA "Cue-induced conditioned activity does not incubate but is mediated by the basolateral amygdala." *Pharmacology, Biochemistry and Behavior*. 104:69-79. 2013

Mankin EA, Diehl GW, Sparks FT, Leutgeb S, Leutgeb JK "Hippocampal CA2 activity patterns change over time to a larger extent than between spatial contexts." *Neuron*. 85:190-201. 2015

Diehl GW, Hon OJ, Leutgeb S, Leutgeb JK (2017) Grid and nongrid cells in medial entorhinal cortex represent spatial location and environmental features with complementary coding schemes. *Neuron*. 94:83-92. 2017

Diehl GW, Hon OJ, Leutgeb S, Leutgeb JK "Stability of medial entorhinal cortex representations over time." In Revision

FIELDS OF STUDY

Major Field: Neurosciences

Studies in Neurosciences
Professor Jill Leutgeb

Studies in Neuroscience
Professor Tracie Paine

ABSTRACT OF THE DISSERTATION

A Role for the Medial Entorhinal Cortex in Multimodal Information Processing and Episodic Memory

by

Geoffrey W. Diehl

Doctor of Philosophy in Neurosciences

University of California, San Diego, 2018

Professor Jill Leutgeb, Chair

The hippocampus and medial entorhinal cortex (mEC) have been together implicated in the cognitive processes of episodic memory and spatial navigation. Through collective network activity, hippocampal place cells provide a map of the world that could support navigation. In conjunction, remapping in the place cell network provides a mechanism to support episodic memory, allowing for individual episodes to be readily distinguished and reliably recalled. Upstream in mEC, spatial firing patterns are robust, but the ability of mEC cells to remap and

provide a signal to support episodic memory has remained largely untested. We recorded mEC cells while altering the features of an explored environment to determine if mEC may play a role in episodic memory processing. Indeed, we observed changes in the firing rates of mEC grid cells and the spatial firing patterns of non-grid spatial cells in response to environment manipulations, indicating that information necessary to distinguish between experiences was contained in mEC network activity. Yet, while distinguishing between events represents a central tenant of episodic memory, an additional requirement is the evaluation of a temporal component. How long ago experiences occur, and in what order, can be just as relevant as what actually happened. Systematic drift in network representations over time represents a candidate mechanism for encoding such temporal information. Drift has been repeatedly observed in the CA1 network, but the origin of such a signal remains unclear. To pursue this question, we recorded CA2 and mEC cells over many hours, evaluating how representations changed, or remained stable, over time. In CA2 we found considerable variation over time, well in excess of that in CA1. Upstream in mEC, a small minority of cells exhibited temporal drift, but overall the representation was reliable, suggesting the primary role of mEC may be to anchor downstream hippocampal representations. Collectively, our work indicates that the conjunctive coding schemes observed in place cells are not unique to the hippocampus, but that upstream the mEC appears to serve a similar role in providing a multimodal representation of an animal's interactions with the outside world to support both spatial navigation and episodic memory.

INTRODUCTION

Dual roles of the medial temporal lobe

Perhaps one of the most impressive facets of the brain is its ability to utilize past experiences to inform and modulate future decisions. In virtually all instances, the role of the brain is not simply to act as a reflexive cause and effect system, responding to a set of incoming sensory stimuli with a set of predefined motor outputs. Instead, the motor responses reflect an organism's state in a broader contextual framework, accounting for past actions and events in order to adapt a stimulus response accordingly. At the most basic level, memory can lead to simple changes, such as adaptation to a stimulus. But it can also lead to much more profound and long lasting modifications to an animal's behavior. Such an ability to form memories of past events assists animals in everything from consistently returning to the same food locations, to avoiding dangerous areas, to rapidly adapting to new situations. For humans, memory expands to serve a role in defining who we are as individuals. As our personalities and decisions are strongly influenced by our past experiences, the ability to remember the past reflects an integral component of our lives. Perhaps for this reason, memory has long been a central focus of cognitive research.

One of the first studies undertaken to systematically probe the properties of memory processing was that of Hermann Ebbinghaus in his work learning and remembering nonsense syllables (Ebbinghaus, 1913). By teaching himself a series of artificially constructed strings of letters and then testing his recollection of the learning set after varying temporal delays, Ebbinghaus was able to systematically evaluate his memory processing across such parameters as the number of syllables remembered, the time to recall each one, and the nature of forgetting past

information. Subsequently, a wide variety of researchers attacked the question memory and its role in behavior across an array of different approaches (James, 1890; Pavlov, 1927; Skinner, 1938; Thorndike, 1898; Tolman, 1948). But it was Karl Lashly that can likely be attributed to be the first to employ a directly neurobiological approach. Concerned primarily with the question of how and where memories are stored, Lashly sought to uncover the location in the brain where particular experiences were represented long-term, commonly referred to as a memory's "engram" (Lashley, 1950). After training rats to successfully navigate through a maze, Lashly performed localized surgical lesions of the brain, attempting to determine what areas were necessary for the rats to remember the path through the maze and successfully complete the task. In a somewhat disappointing set of results, he found that no individual region led to impaired behavioral performance, but rather that performance was a function of the total volume of brain that had been removed. As such, he concluded that there is no single region of the brain where memory was stored, but instead that it is distributed across the entirety.

Less than 10 years after the publication of Lashly's studies our understanding of the neurobiology of memory systems fundamentally changed. Work by Brenda Milner with a patient referred to as H.M. revealed that the medial temporal lobe (MTL) is critical for supporting episodic memory, the memory for autobiographical events (Scoville and Milner, 1957). As a treatment for a severe case of epilepsy, H.M. underwent surgery to bilaterally remove large portions of his MTL, including the majority of the hippocampus as well as part of the parahippocampal gyrus and the amygdala. While the surgery could be considered successful in treating H.M.'s epilepsy, it had a profound impact on his ability to form new memories, while leaving other cognitive functions largely intact. Building on the work by Milner, subsequent study of memory has utilized additional human patients with damage localized to portions of the MTL, as well as directed lesioning of specific brain areas in non-human primate and rodent

models. Collectively, these studies have served to refine our understating of the MTL, both the hippocampus and its main input structure the entorhinal cortex (EC), and its role in episodic memory processing.

One of the clearest outcomes of memory research has been the finding that multiple memory systems exist throughout the brain. Habitual learning, emotional memory, skilled motor learning, and priming behaviors all represent cognitive capacities that remain intact in human amnesic patients and animal models of MTL damage (Eichenbaum, 2000; Squire, 1982; Squire and Zola-Morgan, 1991). Instead it is the encoding, storage, and retrieval of specific, detailed experiences, or episodic memory, that has been linked to the hippocampus and EC. In follow-up work to that of Milner, human amnesia patients with more restricted damage confirmed that the hippocampal CA1 region is critical for episodic memory (Squire and Zola-Morgan, 1991; Victor and Agamanolis, 1990; Zola-Morgan et al., 1986). Informed by findings from these patients, directed lesions to the MTL of monkeys produced dramatic deficits in delayed match-to-sample tasks in which a subject must retain information about a presented stimulus in order to subsequently make a correct response. Yet other forms of learning remained intact, highlighting a restricted role of the hippocampus and adjacent EC in episodic memory (Mishkin, 1978; Squire and Zola-Morgan, 1983; Squire and Zola-Morgan, 1991; Zola-Morgan and Squire, 1986). Comparable results have since been obtained from rats performing various behavioral tasks that require an animal to learn and remember information about a specific odor, object, or locational stimulus (Aggleton et al., 1986; Bunsey and Eichenbaum, 1995; Clark et al., 2000; Dusek and Eichenbaum, 1997; Eichenbaum, 2000; Morris et al., 1982). Collectively, the behavioral deficits observed in these cases following damage to the MTL highlight the importance of the hippocampus and EC in the processing and storage of information about specific experiences.

While the significance of the hippocampus and EC to memory processing has become clear, an important question has remained: What information is actually represented by the activity of neurons in these regions? In pursuit of this question John O'Keefe implanted electrodes into the hippocampi of rats to record the electrical activity of individual cells as the rat interacted with the world. O'Keefe's hope was that the firing of hippocampal cells would correlate to some behaviorally relevant stimulus or action such that a cell could be inferred to be representing that information, much in the same way as cells in the visual cortex respond to specific patterns of light. Quite surprising, O'Keefe discovered that individual hippocampal pyramidal cells fired action potentials in a spatially selective manner, robustly spiking when, and only when, the rat was in a specific location (O'Keefe, 1976; O'Keefe and Dostrovsky, 1971). Owing to their unique firing pattern, O'Keefe termed these cells "place cells" with the location in space that led a cell to fire, its receptive field so to speak, referred to as the cell's "place field". Subsequent study of hippocampal physiology has revealed two additional points to consider in drawing meaning from the spiking activity of individual cells. First, while not every hippocampal cell will fire spikes as a rat travels around space, virtually all hippocampal pyramidal cells that do fire spikes will fire in a spatially restricted manner (Thompson and Best, 1989). Thus, spatially modulated activity is a physiological property common to all principal cells across the hippocampus. Second, if multiple hippocampal cells are recorded simultaneously, it can be observed that each cell will represent its own specific spatial location, developing a place field whose location is completely independent of the activity of other cells (Redish et al., 2001; Wilson and McNaughton, 1993). When considering the many thousands of cells that make up the hippocampus, it becomes clear that each and every spatial location in the outside world will be preferentially represented by a set of unique place cells. As such, the collective activity of the hippocampus forms a complete spatial representation of an explored area, in effect an internally

generated map of the space. In the idea of O'Keefe, the formation of this "cognitive map" serves to provide the rest of the brain with an internal representation of the external world to be used for any cognitive processes that may be required (O'Keefe and Nadel, 1978).

Arising largely from the discovery of place cells, study of the hippocampus, as well as the MTL in general, has expanded to include a role in navigation and spatial memory. Behavioral work on memory has routinely utilized tasks requiring an animal to remember and return to a specific location, or to establish and recall an association between spatial information and a task relevant stimulus. Perhaps the most common example of behavioral tests for spatial memory is the Morris water maze (Morris, 1984; Morris, 1981). In this task an animal is made to explore a large pool of opaque water searching for a small escape platform submerged just below the water line. Each trial, the animal's goal is to find the platform as quickly as possible, allowing it to end the unpleasant experience of swimming. By leaving the platform in the same location across trials, animals gradually learn its spatial location and are able to utilize this knowledge to swim directly to the platform and escape quickly. Such a behavior requires an accurate memory of the spatial location of the hidden platform and appropriate navigation to reach it, and has been well documented to rely on hippocampal processing (D'Hooge and De Deyn, 2001; McDonald and White, 1994; Morris et al., 1982; Sutherland et al., 1982). In addition to the water maze, a number of other behavioral tasks have linked hippocampal processing to spatial memory including the novel object location task, radial arm tasks, and spatial alternation tasks, across all of which animals must remember the spatial location of a given stimulus and adapt their subsequent behavior according to this memory (Eichenbaum and Cohen, 2001; Ennaceur et al., 1997; Kesner et al., 1993; O'Keefe et al., 1975; Parkinson et al., 1988; Racine and Kimble, 1965; Save et al., 1992). Between the clear physiological signature of space apparent from place cell activity, and its necessity for successful performance in spatial memory tasks, the hippocampus then has come

to be attributed a substantial role in spatial processing (Burgess et al., 2002; Buzsaki and Moser, 2013; Eichenbaum and Cohen, 2001; O'Keefe and Nadel, 1978).

In evaluating our current understanding of the hippocampus, it appears as though this structure is involved in two seemingly independent cognitive processes. On the one hand, it is critical for episodic memory and the encoding, storing, and recalling of specific pieces of information, even in the absence of any spatial content. On the other hand, a wide array of memories have substantial spatial components that must be encoded and coupled with the strong physiological representation of an animal's physical location. A logical question then becomes how these two roles could be supported by the cells and network interactions within the hippocampus. Do these reflect two distinct and parallel functions of the hippocampus, or instead are there properties of hippocampal place cells that allow for concurrent representations of both spatial content and episodic memory?

Hippocampal place cells: Multimodal representations and remapping

Collectively, the activity of place cells provides a spatial representation, or map, of an explored environment. Most commonly the activity of place cells is evaluated through a random foraging task in a two dimensional open field arena. Rats are allowed to freely explore the 2D space with an experimenter periodically delivering a food reward at random locations to encourage exploration. By having the path of the rat through the arena be random (or at least close to random) the goal is to dissociate the physical location of the animal with as many other behavioral or cognitive variables as possible (Muller et al., 1987). The firing of hippocampal cells can then be associated with the rat traversing a particular region of space, a cell's place field, with high rates of activity occurring when the animal is in the center of the region of interest and

progressively lower firing rates at farther distances, either as the rat moves into or out of the place field.

As described above, the fact that each and every location across an explored environment can be represented by the firing activity of a subset of place cells has given rise to the theory that the role of the hippocampus is to provide the brain with an internal spatial metric which could then be used for navigation or other forms of spatial processing (O'Keefe and Nadel, 1978). In line with this idea, early work on place cells revealed that by simultaneously recording only a few dozen cells it became possible to use hippocampal network activity to predict in real time, with very high accuracy, where a rat actually was in space (Wilson and McNaughton, 1993). In effect, this meant that hippocampus activity could be directly read out by downstream brain regions to provide information as to an animal's position with respect to the world around. Relatedly, two network level hippocampal processes, sharp-wave ripple (SWR) replay and theta sequences (Foster and Wilson, 2006, 2007; Gupta et al., 2012; Lee and Wilson, 2002), have supported the idea that the spatial firing of place cells can be directly utilized by the brain for cognitive planning of behavioral trajectories through space. When animals move through an environment, a series of place cells will fire in sequence according to the physical trajectory of the animal. Yet, during periods in which an animal remains stationary, such as when they pause to make a decision as to the proper path to take to reach a reward, these same series of place cells can become active during SWRs or theta sequences and fire in the sequential pattern corresponding to movement through their firing fields in the real world. The interpretation of these results is that the activation of place cell sequences during these stationary periods reflects a cognitive process by the animal of imagined movement through the world with the activation of each place cell corresponding to thoughts of a particular spatial location (Buzsaki, 2015; Lisman and Redish, 2009). Such a process could be used for mentally planning routes to specific goal locations, or for

evaluating between two different trajectory options by vicariously exploring both, possibilities that have been supported by experimental reconstruction of the spatial trajectories represented by place cell activation during these network processes (Johnson and Redish, 2007; Pfeiffer and Foster, 2013; Wikenheiser and Redish, 2015).

While the role of place cells in representing spatial information has been a primary driver of study of the hippocampus, physiological recordings have indicated that an animal's physical location in space is not the only factor that contributes to the activity of hippocampal cells. In addition to the allocentric representation of an environment, a large body of work has shown that the firing of place cells can be strongly influenced by a variety of other factors. Salient spatial signals can play a role in orienting and anchoring the spatial firing locations of place cells and the non-spatial content of an experience can serve a strong modulatory role in the cognitive map formed by hippocampal network activity. Early recordings of hippocampal cells first revealed the impact of these additional factors with the introduction and systematic relocation of prominent landmark signals (Muller and Kubie, 1987). If a single prominent cue card is placed on the interior wall of an open field arena, place cells will fire normally. But, if the position of the cue is then changed, moved from one wall to another, the locations of hippocampal place fields will change accordingly, maintaining the same geometric relationship between the hippocampal spatial map and the cue.

In conjunction with this response of place cells to the spatial location of prominent landmarks, a host of studies have investigated the modulatory nature that non-spatial factors can have on place cell firing. Spatial modulation can be influenced by local visual and tactile cues, features of an explored space, the identity or valance of nearby objects, an animal's upcoming behavioral responses, or even the internal metabolic state (Anderson and Jeffery, 2003; Bostock et al., 1991; Kennedy and Shapiro, 2009; Knierim, 2002; Leutgeb et al., 2005b; Moita et al.,

2004; Shapiro et al., 1997; Wood et al., 1999; Wood et al., 2000). In some cases where spatial content becomes irrelevant, representation of non-spatial information can even become the dominant coding mode of hippocampal cells. In particular, hippocampal cells have been found to reliably represent specific time points during a delay period, cumulative distance run along a treadmill, or auditory tones, with little residual representation of the animal's spatial location (Aronov et al., 2017; Kraus et al., 2013; MacDonald et al., 2013; MacDonald et al., 2011; Pastalkova et al., 2008). Taken together, it is clear that place cell firing conveys more than just allocentric space, expanding to incorporate information about any relevant stimuli, either spatial or non-spatial. Accordingly, it is perhaps more appropriate to expand the understanding of the hippocampal representations beyond simply establishing the spatial map of an environment to representations that include information about the non-spatial characteristics as well. Thus at the network level, the collective activity of hippocampal place cells provides a compressive, multimodal neural representation of an entire experience.

Given that hippocampal place cells are able to represent not just spatial information but non-spatial content as well, it becomes relevant to consider how such a network representation could support episodic memory processing. In order to act as a mechanism for memory, neural activity must fulfill two main functions. First, the hippocampal representation must be reliable. Episodic memory requires that a cognitive representation of an experience be stored in the brain with the ability to be faithfully recalled. In examining the activity of place cells this need appears to be met. Developing relatively quickly when an animal first enters a new environment (Wilson and McNaughton, 1993), the spatial map of the area remains stable, with each place cell exhibiting the same spatially restricted firing field each time the animal returns to the same location (Mankin et al., 2012; O'Keefe and Dostrovsky, 1971). As revealed by hippocampal calcium imaging, this same spatial representation remains reliable over at least a month (Rubin et

al., 2015; Ziv et al., 2013), indicating that the information is retained in the brain long-term. Similarly, non-spatial modulation of place cell firing is reliable across multiple exposures to the same conditions with the same stimuli eliciting the same response in the hippocampal network (Mankin et al., 2012; Rubin et al., 2015).

Second, to support episodic memory the hippocampal representation must be selective. In order to prove useful for memory, it is necessary for different experiences to be differentially represented by the brain, allowing for a degree of discrimination between them. The phenomenon of place cell remapping seems to fulfill this requirement, providing a viable neural mechanism to support differentiation of experiences (Colgin et al., 2008; Muller and Kubie, 1987). In a general sense, remapping is the idea that changes in the extremal world can lead to changes in the internal cognitive map produced by place cell firing. To explore remapping experimentally, one can record from the hippocampus while rats perform random foraging in an open field enclosure with the exploration of the space considered to be the experience or episode that is represented internally by place cells. By then manipulating the sensory components of that experience it becomes possible to determine how the hippocampus responds to these changes. For example, relocation of a prominent cue as described above will elicit a rotation of the overall place cell map. In this case, movement of the cue elicits a "remapping" of hippocampal activity in order to maintain constancy between the cue and the spatial map. Broadly, remapping can be grouped into two categories: "global remapping" in which large differences between experiences, most often to the spatial content, are accompanied by a complete reorganization in the spatial firing patterns of place cells, and "rate remapping" in which more subtle differences to non-spatial content elicit modulation of place cell firing rates while their spatial signal remains unchanged (Leutgeb et al., 2005b).

While almost any specific alteration to the sensory aspects of an experience can elicit remapping in hippocampal place cells, the exact nature of the change in the place cell network is highly dependent on the nature of the alteration. One way an experience can be altered is by changing the broad location at which it occurs. Experimentally, this involves relocating an explored environment from one room to another while leaving all other components identical. In this case, the alteration of the spatial content is associated with a complete reorganization of the spatial locations of place fields and the generation of a new hippocampal map; a process termed global remapping (Leutgeb et al., 2005b). In essence, a given hippocampal map is able to provide reliable spatial information as an animal explores a given location. But if the animal moves to a new location, the old map is no longer informative and a new one must be generated. Global remapping can also be elicited in situations in which the spatial content remains unchanged but many other components of the experience are all substantially altered, leading to a completely different contextual environment (Fyhn et al., 2007). In these cases, while the spatial information remains the same, in theory meaning that the same spatial map could be useful, the dramatic level of change to other aspects of the experience seem to necessitate the generation of a new spatial signal. This change in the spatial map may reflect a cognitive evaluation by the animal that spatial information is no longer in and of itself a reliable indicator of the experience, or could indicate that the large contextual changes have made them confused and led them to perceive that their location has been altered.

In contrast, two experiences could vary only subtly in their non-spatial content, consistent in their broad location and spatial content, and differing only across a single feature of the explored environment such as the wall color or environment shape. In this circumstance, because the overall location across the two experiences remains unchanged, the same spatial map remains informative and the spatial location of place cell firing is preserved. Instead, these subtle changes

in the non-spatial content are accompanied by systematic modulation of the overall firing rates of place fields; a process termed rate remapping (Leutgeb et al., 2005b). Through rate remapping, hippocampal place cells are able to maintain a reliable metric of the spatial environment via the location of place fields, and concurrently represent its non-spatial aspects according to the rates at which these cells are active.

By adapting the spatial map thorough global remapping, place cells account for changes to broad locations, both in varying the map required to navigate and in allowing for memory encoding of similar events that occur at different locations. As a complement, the place cell network can utilize rate remapping to maintain a single spatial signal across multiple experiences that occur in close proximity, but concurrently maintain an ability to distinguish between them. Thus, through network activity hippocampal place cells are able to encode a spatial map that can be used for navigational purposes, and reliably represent and distinguish between different experiences as would be necessary to support episodic memory.

A role for the medial entorhinal cortex: Spatial processing upstream of hippocampus

The hippocampal network provides the brain with a multimodal representation of the outside world, providing information about both spatial and non-spatial components. By maintaining its spatial representation and adapting place cell activity according to external changes the hippocampus provides a neural mechanism to support both spatial navigation and episodic memory. But how does the necessary information to support these two cognitive processes come to be in the hippocampus in the first place? Do spatial representation and remapping emerge as a result of hippocampal processing or are they inherited from upstream inputs? The hippocampus has commonly been thought of as sitting at the apex of a neural

processing hierarchy, with sensory information progressing through primary and association cortices to ultimately arrive at the hippocampus where various content streams can be combined into a single multimodal signal and fed back to the rest of the brain (Felleman and Van Essen, 1991; Squire and Zola-Morgan, 1991). Immediately upstream in this flow of information, the entorhinal cortex (EC) provides the main source of cortical and processed sensory content to the hippocampus (van Strien et al., 2009; Witter and Amaral, 2004). Thus, what may be the role of the entorhinal cortex in supporting hippocampal spatial and memory processing? What information is represented upstream and how could these signals be integrated by the hippocampus?

The entorhinal cortex is typically divided into two anatomical divisions, the lateral entorhinal cortex (lEC) and the medial entorhinal cortex (mEC). In broad terms, lEC and mEC seem to differ both in their cytoarchitectural character, and in their connectivity with the rest of the MTL (Burwell, 2000; van Strien et al., 2009; Witter and Amaral, 2004; Witter et al., 1989). Information arrives into the lEC predominantly from the perirhinal cortex whereas mEC receives input from the postrhinal cortex. In their projections to hippocampus, lEC and mEC seem again to be anatomically segregated, exhibiting largely non-overlapping regions of output in the dentate gyrus (DG), CA3, and CA1 regions. Whereas for DG and CA3 this division appears to be largely across the deep vs superficial axis of the hippocampal lamina, in CA1 projections from mEC and lEC are restricted along the proximo-distal axis. Thus anatomically, good reason exists to consider differential functional roles of lEC and mEC.

Much in the same way as has been done for hippocampus, a major approach in the study of the entorhinal cortex has been recording from single EC neurons in behaving animals and attempting to determine what stimuli are relevant for eliciting or modulating spiking. In stark contrast to hippocampal place cells, neurons in the lateral entorhinal cortex exhibit little if any

spatially modulated firing patterns as rats explore an open field environment (Hargreaves et al., 2005). Individual cells spike randomly throughout the environment, with any spatially localized firing behaving inconsistently across multiple explorations of the same place. Even in situations in which the distal surroundings are highly enriched with visual cues, where spatial patterns could be formed based on associations to salient landmarks, firing within lEC remains largely independent of spatial location (Yoganarasimha et al., 2011). Instead, for cells in the lEC the important stimuli appear to be objects. If a series of objects are placed into an open field, the firing of lEC cells becomes dramatically more selective (Deshmukh and Knierim, 2011). Reliability of spatial firing within lEC increases and a large proportion of lEC cells are directly responsive to the presence of the objects, exhibiting an increase in firing that is spatially restricted around the object or a change in firing location if an object is moved. For a subset of lEC cells, the response to objects does not occur immediately but instead emerges after an object has been removed, firing specifically at the location at which the object had previously been, its "trace location" (Tsao et al., 2013).

In the medial entorhinal cortex, the influence of spatial location on firing of individual cells is much more substantial. Curious as to how such precise spatial firing fields could be generated by hippocampal place cells, the lab of Edvard and May-Britt Moser performed single unit recordings from the dorso-caudal pole of mEC as rats explored an open field environment. Looking specifically at the region that projects downstream to dorsal hippocampus, the area with the most robust spatial coding by place cells, they found the firing of individual mEC principal cells to be strongly modulated by an animal's spatial location (Fyhn et al., 2004). Over the subsequent 15 years, researchers have discovered that the mEC network is likely not a homogenous population, but rather composed of several subclasses of cells that vary in their functional firing properties, but which all appear highly specialized for navigational processing

and all send projections downstream to hippocampus (Moser et al., 2017; Zhang et al., 2013). To gain an appropriate understanding of the role of mEC firing then it becomes necessary to evaluate each of these classes in turn.

The first of the mEC functional subclasses to be identified, and subsequently the most well studied, was the grid cells (Hafting et al., 2005). While early data suggested as many as half of mEC cells may be grid cells (Boccara et al., 2010), more recent estimates are closer to 10 – 20 % of the total population (Kropff et al., 2015; Latuske et al., 2015; Sun et al., 2015; Tang et al., 2014; Zhang et al., 2013). Characterized by multiple highly precise firing fields that tessellate an explored environment in a regular hexagonal "grid" pattern, grid cells represent one of the most striking examples of complex receptive fields outside of primary sensory systems. Owing to their highly ordered firing patterns, grid cells have commonly been thought of as the brain's primary metric of space and the main source of spatial input relayed from mEC to hippocampus (Moser et al., 2014). After their initial discovery, research into grid cells has broadly fallen into three main categories: 1) What are other properties of grid cells beyond their hexagonal firing pattern? 2) How is the periodic spatial pattern of grid cells influenced by the environment? 3) What components are necessary to elicit the unique periodicity of grid cells?

Often clearly identifiable by eye, grid cell firing is quantified through the calculation of a "grid score", or a measure of the degree of 60º rotational symmetry within the spatial firing pattern, with the hexagonal layout of grid fields yielding a high value (Sargolini et al., 2006). In addition to their grid score, grid cell firing can be described according to the size of their fields and the spacing between them or their "grid scale", the rotation of their fields or "grid orientation", and the spatial offset of the fields or "grid phase" (Hafting et al., 2005). With orientation and phase varying between individual cells, collectively the spatial firing patterns of a population of grid cells cover the entire extent of a large environment, much in the same way as

for hippocampal place cells. While the spacing between grid fields of an individual cell is highly consistent, giving rise to the periodic organization, this spacing varies systematically according to anatomical position along the dorso-ventral (DV) axis of mEC with smaller spacing for grid cells in dorsal mEC and larger spacing for grid cells more ventral (Brun et al., 2008b; Hafting et al., 2005; Stensola et al., 2012). As a result, the spatial resolution of grid cell maps varies along the DV axis, allowing for robust spatial representation across a range of behaviorally relevant scales. Interestingly, this increase in grid scale does not occur along a continuous gradient, but rather through a series of discreet steps or "modules" (Stensola et al., 2012), with grid cells that are members of the same module tending to respond coherently to experimental stimuli (Stensola et al., 2012; Stensola et al., 2015) suggesting each grid cell module may function as a collective unit. In parallel with the progressive increase in grid scale, several intrinsic cellular properties follow a similar gradient along the mEC's DV axis (Garden et al., 2008; Giocomo and Hasselmo, 2008; Giocomo et al., 2007). In particular, expression of the hyperpolarization-activated cyclic nucleotide gated (HCN1) channel has been directly linked to the spatial scale of grid cells (Giocomo et al., 2011a; Mallory et al., 2018) suggesting that the temporal integration of network input is important for establishing grid spacing.

In order to gain a more complete understanding of the role of grid cells in providing a fundamental spatial signal, a second body of literature has focused on how the spatial representations of grid cells are influenced by environmental factors such as novelty, environment expansion, fracturing and merging of environments, and interactions with environment edges. When an animal is first placed in an open field environment, the spatial firing fields of grid cells develop quickly over the first minutes (Hafting et al., 2005), but over the course of several exposures the firing pattern changes in two ways. While initially large, grid spacing gradually decreases, finally stabilizing at the appropriate distance according to the grid cell's anatomical

DV location (Barry et al., 2012). Additionally, the perfect hexagonal field layout begins to shear along the environment walls and rotate slightly leading to a final grid pattern that exhibits a degree of elipticity (squishing of the regular hexagonal layout), particularly near the edges of an environment, and whose orientation tends to be rotated about 7° from square (Stensola et al., 2015). If an open field environment is rapidly expanded along a single axis, grid cells often exhibit a similar novelty type effect, scaling proportionally along the expanded axis to fill the new space at the expense of the regular arrangement of grid fields (Barry et al., 2007). However, over the course of several exposures the grid fields gradually shift back into a regular pattern, returning to the spacing characteristic of the given cell. Interestingly this rescaling occurs independently between grid cell modules with different modules behaving differently but with a uniform response across all the grid cells that belong to a given module (Stensola et al., 2012).

The spatial firing of grid cells also exhibits adaptation when rats are presented with multiple environments in close proximity. If rats are allowed to freely explore a maze composed of two compartmentalized areas joined by a corridor, initially, identical grid patterns develop in each compartment. But, after experience, an integrated grid map develops across the entire maze with grid fields situated not with respect to individual compartments but rather to the entire space (Carpenter et al., 2015). Similarly, rats can be exposed to two adjacent open field arenas and if kept distinct, two independent grid maps develop. If the two arenas are then merged into a single large environment, grid fields across the two arenas will shift such that the grid maps likewise merge into a single coherent spatial pattern (Wernle et al., 2018). In both cases, these results are consistent with grid cell maps prioritizing the establishment of a single, global representation of space.

A final pair of instances in which the spatial firing of grid cells is somewhat unexpected occur for animals exploring what can be thought of as non-conventional environments. When

animals run along a 1D linear track grid cells exhibit multiple firing fields (Hafting et al., 2008) in patterns hypothesized to reflect slices through a standard 2D grid map (Yoon et al., 2016). However, when rats run along a linear track that has been repeatedly folded back upon itself into a hairpin maze, instead of treating the track as either a continuous 1D path or as trajectories thorough 2D space as might be predicted, the grid map resets at each juncture along the hairpin (Derdikman et al., 2009). Thus, grid cell firing along each segment of the hairpin is identical, providing only a single spatial representation of the track that is simply repeated as many times as there are loops. In this way, grid cell firing simplifies the spatial landscape into its most basic component, perhaps as a means of minimizing the degree of information that must be represented. Grid cell firing is also interesting when open field environments deviate from the typical geometrically regular shapes of squares or circles. During exploration of a trapezoidal open field, the spacing and layout of individual grid fields becomes highly distorted from their typical hexagonal configuration (Krupic et al., 2015). In more square regions of the arena grid spacing remains regular, but in more triangular regions the grid fields appear to shift toward walls, leading to substantial deviation from the ideal layout and illustrating a clear influence of environment geometry on the overall spatial firing pattern of grid cells. To date, the implications of such distortions in the overall grid map are not clear, but they do represent an important consideration in evaluating the spatial signal that originates in mEC.

Motivated by a desire to understand the role of grid cells, both in the generation of downstream place cell firing patterns and in their relevance to behavior, the third focus of grid cell research has attempted to determine the necessary input components to support periodic grid firing. Overwhelmingly, grid cells are hypothesized to arise from a neural path integration (PI) calculation (Burak and Fiete, 2009; Burgess et al., 2007; Fuhs and Touretzky, 2006; Giocomo et al., 2011b; McNaughton et al., 2006) in which speed and directional input are combined in some

fashion to produce real time information about where an animal is in space, the read out of which would be the grid fields. Informed by these models, studies have attempted to remove single components of the path integration calculation and disrupt the periodic spatial firing of grid cells. One hypothesized source of the necessary speed input is the local field potential theta rhythm, a speed modulated oscillation of 6-10 Hz that is believed to be paced by the medial septal area (MSA) in the midbrain (McFarland et al., 1975; Slawinska and Kasicki, 1998; Stewart and Fox, 1990). Indeed, pharmacological inactivations of the MSA provided the first example of disruption of the periodic spatial firing pattern of grid cells (Brandon et al., 2011; Koenig et al., 2011), consistent with a removal of speed information into the path integrator. Periodic grid firing has also been abolished when a rat was passively driven around an open field in a remote-controlled car (Winter et al., 2015b), presumably again due to disruptions in an animal's ability to compute its movement speed. To disrupt the directional signal, lesions or inactivations of the anterior thalamic nuclei have been performed which abolish coding for an animal's heading direction in the mEC and most other parts of the brain (Goodridge and Taube, 1997; Winter et al., 2015a). Predictably, these manipulations reliably eliminated the spatial firing pattern of grid cells (Winter et al., 2015a), consistent with the necessity of a directional signal for PI calculations.

Another pair of manipulations that have been found to impact grid cell firing are removal of the GluA1 receptor subunit, either locally in mEC or across the whole brain, and inactivation of local mEC parvalbumin expressing (Pvalb) interneurons. In both cases the overall grid structure was largely preserved, but the reliability and fine scale spatial precision of grid cells was diminished (Allen et al., 2014; Gil et al., 2018; Miao et al., 2017). In evaluating grid cells from the stand point of PI calculations, it is reasonable to think that in addition to raw speed and direction information the brain would need some form of integrative and plastic network system to appropriately tune the PI output. Accordingly, removal of GluA1 subunits or Pvalb

interneurons could impact such network level integrations, perhaps leading to mild impairments in grid cell firing without a complete breakdown of the overall PI calculation.

Beyond the focus on path integration calculations, two final manipulations have been found to impact grid cells. Inactivations of the hippocampus abolished periodic firing in grid cells (Bonnevie et al., 2013), suggesting that spatial feedback from place cells somehow contributes. One potential explanation of this result is that the spatial processing of grid cells does not exist in isolation but instead involves a degree of feedback from spatially modulated place cells, perhaps acting as an internal reference signal analogous to the efference copy observed in the motor system (Wolpert and Flanagan, 2001). Additionally, systemic administration of the muscarinic antagonist scopolamine has been found to disrupt the spatial firing of grid cells (Newman et al., 2014). Unfortunately, the implications of scopolamine are unclear as one effect is a flattening of the normally observed relationship between theta frequency and running speed (Newman et al., 2013), a potential mechanism for providing grid cells with speed information. Thus, grid cell disruption may arise from a loss of speed information, or rather from the generalized loss of cholinergic input to the mEC network.

A second subclass of mEC cells is the border cells (Savelli et al., 2008; Solstad et al., 2008), also referred to as boundary or boundary vector cells, which likely make up about 10 % of the mEC population (Kropff et al., 2015; Latuske et al., 2015; Tang et al., 2014; Zhang et al., 2013). Whereas grid cells have many firing fields systematically organized across an entire environment, border cells tend to have only one or two spatially restricted fields which are located along the wall or edge of an environment. The length and width of fields varies between cells, with some occupying only a small portion of the wall and others spanning the entire extent, but in all cases border cells are defied according to a high “border score”, a calculated ratio between firing along the exterior of an environment and its interior (Solstad et al., 2008). In

addition to a high border score, true border cells will respond to introduction of a new environmental "border" with the development of an additional firing field, parallel to its original border field (Solstad et al., 2008). Unfortunately, not all studies confirm this second criterion, relying only on a high border score to identify putative border cells, somewhat muddying our understanding of this subclass of mEC cells. Overall, border cell activity patterns have appeared to be quite robust. While a variety of manipulations have been described that disrupt the firing of other mEC cells types, in each case the properties of border cells have remained intact (Bonnevie et al., 2013; Gil et al., 2018; Koenig et al., 2011; Miao et al., 2017), though it should be noted that as of yet there have been no experiments designed to specifically perturb border cells.

Unlike grid cells which represent space across an entire two-dimensional environment, the firing of border cells is localized to salient features, specifically its borders. As such, one idea is that border cells provide a more landmark based signal which could be utilized on its own for navigational processing (Barry et al., 2006; Bush et al., 2014; Buzsaki and Moser, 2013). However, theories have also posited that the main function of border cells is to provide a direct neural readout of when an animal is interacting with an environmental edge. This landmark information can then be fed into the computation of grid cells, providing a kind of anchoring signal that could correct gradual error in the spatial firing of grid cells that is expected to accumulate over time via path integration calculations (Burak and Fiete, 2009; Burgess et al., 2007; Fuhs and Touretzky, 2006; Hardcastle et al., 2015; Solstad et al., 2008). In line with this conceptual framework of border cells acting to relay information about environment edges, if an open field environment is expanded, border fields also expand to match the new environment and maintain a consistent representation of their boundary (Savelli et al., 2008; Solstad et al., 2008). Additionally, a true border cell should be "context invariant" (Solstad et al., 2008), maintaining a

firing field along the edge of any and all environments regardless of manipulations to the environment, behavioral factors, or other components that may influence the overall context.

The next two classes of mEC cells, head direction (HD) cells and speed cells, are identified based on more navigational firing properties as opposed to strictly spatial firing patterns. Together, these two cell classes are thought to provide the direction and speed information necessary to compute path integration for grid cells. In general, membership in these classes is often taken to not be mutually exclusive with that of grid or border cells, yielding a proportion of the mEC population that is designated as conjunctive cells (e.g. conjunctive grid x HD firing).

Prior to the discovery of grid cells in the mEC, work by Jeffrey Taube and James Ranck uncovered that a subset of cells in the rodent presubiculum, a major input to the mEC, would preferentially fire according to the angle of an animal's trajectory (Taube et al., 1990). In the most extreme cases, presubicular cells would fire only when a rat's head was facing in a single direction with an error of only a few radial degrees. Accordingly, these cells were named head direction cells, and collectively a population of HD cells could provide an animal with a kind of internal compass, conveying relevant navigational information as they explored an environment (Taube, 2007). Subsequent study has revealed the presence of HD cells in a host of brain regions including the retrosplenial cortex, anterior thalamic nucleus (ATN), lateral mammillary nucleus, striatum, and mEC. Interestingly, HD content appears to be passed directly from one brain region to the next, with information originating in the ATN based on vestibular inputs, and ultimately arriving in mEC as the last region with a pure HD signal (Sargolini et al., 2006).

Because of the direct relay of information, mEC HD cells are vulnerable to disruptions of the HD system at any preceding point along the chain, such as via a lesion of the ATN

(Goodridge and Taube, 1997; Winter et al., 2015a). However, beyond their direct dependence on the rest of the brain's HD system, mEC HD cells appear highly resistant to manipulations. In all cases in which firing of grid, border, or other mEC cells have been disrupted, HD firing remained intact (Allen et al., 2014; Brandon et al., 2011; Gil et al., 2018; Koenig et al., 2011; Miao et al., 2017; Newman et al., 2014). For some manipulations, the loss of periodic grid fields was even accompanied by a marked increase in the radial selectivity of HD signaling (Bonnevie et al., 2013; Winter et al., 2015b), suggesting a strongly interconnected network of HD cells within mEC. The prospect of robust connectivity across mEC HD cells is further supported by recordings from developing rats which show that even before the age of eye opening a subset of mEC cells display clear, though unstable, directional preferences and that this HD coding remain coherent across the mEC population (Bjerknes et al., 2015).

The most recently described category of mEC cell classes is that of speed cells (Kropff et al., 2015). Shortly after the discovery of grid cells, it was found that for at least a subset of mEC grid cells, overall firing rate varied linearly with an animal's running speed (Sargolini et al., 2006), velocity acting as a form of gain control with faster running epochs associated with higher firing rates. More directed studies of the impact of running speed on mEC firing revealed that speed modulation is not exclusive to grid cell firing, but reflects a broader coding scheme across the mEC population. Modulation of mEC cells by running speed can be observed for rats running along a linear track under controlled velocity conditions or during periods of random foraging in a 2D environment, and much like the spatial firing of border cells this speed modulation is context independent (Kropff et al., 2015).

Though still a relatively simple concept, two recent studies have added nuance to our understanding of mEC speed modulation, expanding beyond a simple positive linear relationship. Work by Hinman et al. (2016) showed that while most mEC cells exhibit a positive relationship

between running speed and firing rate, a small subset instead have an inverse relationship, a phenomenon that had been noted previously but not explored (Kropff et al., 2015). Additionally, this work described an alternative form of speed modulation in which the relationship between running speed and firing rate saturates at high velocity, providing no additional information after an animal reaches a certain threshold. Work by Hardcastle et al. (2017) expanded upon this concept of non-linear relationships between running speed and firing rate, utilizing an alternative classification method to identify speed modulation. This work found that for a large portion of mEC cells, running speed can be estimated based on firing rates, but that the relationship between the two variables could not be well predicted by any presupposed tuning curve.

Like most mEC cell types, studies involving manipulations of speed cells are scarce. What is known is that mEC speed cell coding is disrupted upon pharmacogenetic inactivation of local Pvalb interneurons but not following inactivation of somatostatin expressing (SOM) interneurons (Miao et al., 2017), suggesting specialized integration within the interneuron network. Additionally, much like HD cells, speed cells show increased tuning following the inactivations of the MSA that disrupt grid cells (Hinman et al., 2016).

Whereas grid cells and border cells have well organized firing fields, either periodic or along an environment edge, many cells in mEC have firing fields that, while spatially selective and consistent across experience, are much less well defined, often looking more like a Rorschach test than the clean Gaussian fields of place cells or grid cells (Fyhn et al., 2004). Identifiable based on a spatial firing pattern with high spatial information content, that is similar between the first and second half of an open field foraging session, and not in a grid or border pattern, we refer to this subclass of mEC cells as non-grid spatial cells (NGS), though they have also been called non-periodic or irregular spatial cells. Beyond having a quantifiable degree of spatial content, firing of NGS cells can vary widely in number of spatial fields, and these fields' size,

shape, and layout with respect to each other and the environment itself. Importantly though, the spatial firing pattern is reliably recalled upon an animal's return to the same environment (Investigated in chapters 1 and 3 of this dissertation), indicating that while less precise, the spatial signal conveyed by NGS cells can provide useful information. Overall, the firing of NGS cells appears to be relatively robust, remaining unaffected by manipulations that disrupt grid cell firing including inactivation of the MSA or local Pvalb interneurons (Koenig et al., 2011; Miao et al., 2017). Work has demonstrated that the spatial information content and reliability of NGS cells mildly decreases following genetic knockout of GulA1 receptors (Allen et al., 2014; Gil et al., 2018) or inactivation of local SOM interneurons (Miao et al., 2017), though even in these cases NGS cells retain a significant level of spatial firing.

The last class of mEC cells, non-spatial cells, are perhaps unsatisfyingly defined based on a perceived lack of any measurable spatial or navigational coding properties (Zhang et al., 2013). These cells have low spatial specificity in their firing pattern across an open field, any spatial selectivity is unreliable over the course of an experience, and their firing is unrelated to HD or running speed. Because most single unit studies of mEC cells in behaving rodents focus on the spatial domain, little is known about non-spatial cells which are often simply grouped into a kind of "other" category or largely ignored.

Taken collectively, the cells of the mEC appear well suited to provide the hippocampus with the requisite spatial and navigational information to support the generation of a place cell map. In general, grid cells are thought of as providing the primary spatial metric with non-grid cells fulfilling more supporting roles: HD and speed cells providing the requisite information to support PI calculations and border cells acting as a mechanism for error correction. Looking to explain how spatial selectivity arises in hippocampus, numerous computational models have proposed how the firing of mEC cells could be integrated to yield place field activity. In line with

their proposed role as the central spatial component of the mEC population, a large majority of these models have focused on mechanisms by which a collection of grid cells could summate into place cells (Blair et al., 2008; Cheng and Frank, 2011; de Almeida et al., 2009; Fuhs and Touretzky, 2006; McNaughton et al., 2006; Rolls et al., 2006; Solstad et al., 2006), though alternative mechanisms by which border cell activity could produce place fields have also been proposed (Barry et al., 2006; Hartley et al., 2000; O'Keefe and Burgess, 1996). Unfortunately, NGS and non-spatial cells have been largely overlooked in this work, leaving any hypotheses of their roles in hippocampal processing severely lacking. In an effort to better understand the potential role of NGS and non-spatial cells, a central focus of chapter 1 of this dissertation is the spatial firing properties of NGS cells. This work is followed up in chapter 3 where the activity of NGS and non-spatial cells is monitored over time.

Memory coding in the hippocampus: An integration of entorhinal signals

In general, study of EC activity has focused on the spatial firing properties of individual cells with the goal of understanding how spatial coding in mEC may relate to the downstream formation of place fields. However as described above, place cell networks complement their spatial map with information about the non-spatial components of an experience and adapt their representations through remapping according to changes in an experience, a potential mechanism to support episodic memory (Colgin et al., 2008). Thus, what role does the EC have in supporting hippocampal encoding of episodic memory via remapping? Does the combined place cell coding for space and memory reflect an integration of independent EC signals, or rather could mEC input provide more than just a spatial map?

In response to large changes to an experiences, in particular modifications to the spatial content, place cells undergo global remapping, completely changing their spatial firing patterns and leading to the generation of a different hippocampal map (Fyhn et al., 2007; Leutgeb et al., 2005b). If the spatial firing of hippocampal place cells were generated through an integration of upstream mEC signals as has been proposed, one would expect that changes to the hippocampal map would be accompanied by changes to mEC spatial firing patterns. Alterations to an experience's spatial content would elicit changes in the spatial firing of mEC cells that are in turn passed down to hippocampus with the maps of mEC and hippocampus behaving in parallel. In fact, that is exactly what has been observed. Just as place cells follow the movement of prominent local cues, so to do the spatial firing or HD modulation of mEC cells, with hippocampus and mEC similarly reorienting their spatial maps according to the cue (Hargreaves et al., 2007; Neunuebel et al., 2013; Savelli et al., 2017; Yoganarasimha and Knierim, 2005). Similarly, recordings from grid cells revealed that in response to movement of an environment between rooms or dramatic changes to its overall context, two manipulations that produce global remapping in hippocampus, grid cells too undergo a spatial reorganization (Fyhn et al., 2007). While the periodic grid pattern of individual cells is maintained across conditions, the entire grid map becomes realigned, leading to a shift in grid phase and the formation of a distinct spatial map. Examining mEC cells more generally, several works have observed similar relationships between the spatial firing of place cells and the activity of upstream mEC. Manipulations that would be expected to elicit changes in place field locations were found to also lead to large changes in the spatial firing patterning or overall levels of calcium activity in mEC cells (Keene et al., 2016; Kitamura et al., 2015; Marozzi et al., 2015). As a complement, several studies have performed manipulations of mEC firing, either increasing or decreasing overall activity, and in each case these artificial changes to mEC resulted in a global remap of downstream place cells

(Kanter et al., 2017; Miao et al., 2015; Rueckemann et al., 2016). Thus, recordings from mEC are consistent with the theory that the hippocampal map is driven by upstream mEC spatial firing patterns, and that changes to the spatial content of an experience elicit changes in mEC firing, which in turn lead to changes in the spatial firing of place cells.

Alternatively, when spatial content remains consistent and the differences between experiences are more subtle, restricted to non-spatial features of an environment, place cells respond through modulation of their firing rates while maintaining their same spatial signal (Leutgeb et al., 2005b). Under these conditions, past work has shown that firing of grid cells and border cells remains unchanged (Fyhn et al., 2007; Solstad et al., 2008). The spatial firing of both cell types remains highly stable, presumably because the spatial landscape to be represented has remained the same. Furthermore, whereas place cells modulate their firing rates, the firing of individual grid fields have been found to not vary systematically according to environmental conditions (Fyhn et al., 2007). As such, these results have been taken as evidence that in situations in which experiences differ only in their non-spatial content, the information necessary for the hippocampus to distinguish between them via rate remapping is not provided by the mEC (Eichenbaum et al., 2012; Knierim et al., 2014).

Instead, evidence has suggested that lEC may support rate coding by downstream place cells. As individual lEC cells exhibit no real spatial firing patterns but robust responses to objects (Deshmukh and Knierim, 2013; Hargreaves et al., 2005; Tsao et al., 2013; Yoganarasimha et al., 2011), lEC seems particularly well tuned to provide non-spatial input to hippocampus as a complement to the spatial input provided by mEC cells. In line with this suggestion, lesions of the lEC were found to reduce the degree of firing rate modulation observed in place cells when an environment's features were altered (Lu et al., 2013). Yet, individual lEC cells themselves do not exhibit any clear change in their firing properties in response to alterations of an environment's

wall color, suggesting that the relay of non-spatial input necessary to support hippocampal rate coding occurs in lEC as a network level process (Lu et al., 2013).

Together, the lack of physiological changes in grid and border cells in response to non-spatial manipulations and the impairment of hippocampal rate coding in response to lEC lesions have been taken as evidence that mEC and lEC reflect parallel input pathways to the hippocampus (Deshmukh, 2014; Eichenbaum et al., 2012; Knierim et al., 2006; Knierim et al., 2014). MEC cells would collectively provide the requisite spatial input to define the specific location of place fields, while lEC network input would provide the non-spatial input necessary to establish appropriate firing rates. This segregation of information would mean that hippocampal place cells reflects the first point in the brain in which spatial and non-spatial content are integrated into a single, multimodal representation. In support of this parallel processing theory, computational modeling has appropriately reproduced both global and rate remapping behavior by place cells by way of dedicated inputs streams of spatial and non-spatial information originating in mEC and lEC respectively (Renno-Costa et al., 2010).

However, the notion that spatial and non-spatial information are restricted to parallel input streams into the hippocampus, with mEC producing the spatial location of place cells and rate coding supported entirely by lEC input relies on three important considerations. First, while lEC lesions did reduce the degree of hippocampal rate coding, it was not completely eliminated, even in the most extreme cases of lEC damage. Rather, about 70 % of firing rate modulation in place cells remained intact, indicating that an alternative input must contribute to rate remapping (Lu et al., 2013). Second, while the representation of spatial information by mEC cells is relatively clear, recent work has shown that mEC firing can encode non-spatial information as well. On various behavioral discrimination tasks firing of mEC cells can be modulated by the identity of explored objects or by contextual aspects of the task, two prominent non-spatial

factors (Keene et al., 2016; Kitamura et al., 2015; Lipton et al., 2007). Tone discrimination tasks appear to transition hippocampus and mEC from a spatial processing domain into one centered on representation of an auditory landscape with mEC cells now exhibiting reliable coding for specific auditory frequencies (Aronov et al., 2017). And if a rat is required to run along a treadmill during a delay period mEC grid cells no longer represent the animal's spatial location but instead respond to the elapsed time through the delay (Kraus et al., 2015), much like the behavior of hippocampal time cells under similar conditions (Eichenbaum, 2014). These examples of non-spatial coding indicate that at least in certain circumstances mEC cells are capable of expanding beyond spatial processing and can provide a multimodal representation of an experience. Accordingly, these findings would suggest the existence of a mechanism to distinguish between experiences that share the same spatial content and have only subtle differences in a non-spatial domain, as is required for hippocampal rate remapping. Third, the broad conclusion that mEC cells do not respond to subtle change in the non-spatial features of an environment was based on the activity of grid and border cells, yet together these two classes of mEC cells represent less than a third of the total population (Kropff et al., 2015; Latuske et al., 2015; Tang et al., 2014; Zhang et al., 2013). The response of NGS and non-spatial cells to alterations in the non-spatial aspects of an experience remain unknown and may in fact represent an important contribution to hippocampal processing.

In light of these considerations, chapter 1 of this dissertation seeks to investigate the firing of NGS cells in response to changes in the spatial content of an experience associated with global remapping in the hippocampus and to more subtle changes in the non-spatial features of an environment associated with rate remapping. If it is true that mEC firing is involved only in relaying spatial information downstream to hippocampus, we would expect to see changes in NGS cell firing only in instances in which the spatial content of an experience were changed.

However, if we were to observe that change to the non-spatial features of an environment, to its wall color or its shape, elicit changes in the firing patterns of NGS cells, it would indicate that in conjunction with a representation of spatial content mEC is able to concurrently represent differences in non-spatial aspects of an experience as would been need to support episodic memory.

Reliability of neural representations across time: Implications for spatial coding and episodic memory

Extensive research has highlighted the role of the hippocampus in spatial navigation and episodic memory, and described physiological mechanisms by which hippocampal cells can support these two processes. Across a collection of place cells, the hippocampal network is able to construct a cognitive map of the outside world, and alter this map through remapping whenever an animal's spatial environment changes. In conjunction with this spatial representation, modulation of place field firing rates allows the hippocampus to distinguish between experiences that vary only in their non-spatial content, reflecting a mechanism for the brain to encode and distinguish between specific events as is necessary to support episodic memory. Yet for both of these cognitive processes, navigation and memory, an important consideration is the relative stability, or variability, of the network representation over time. In the case of navigation, the usefulness of a spatial representation is directly related to its reliability. If a map were to change rapidly, either through degradation or systematic alteration, the locations of landmarks and the relationships between points in the map would no longer match with the real world and the map would lose its utility. However, in the case of episodic memory, variation over time can prove beneficial. An often overlooked component of episodic memory is memory for how long ago an

event occurred (Tulving, 1972). Not only do we remember the details of specific events, but we also have an intuitive sense of when they happened and how to relate multiple experiences to each other in order across time. Remapping of place cells allows for the encoding and differentiation of individual experiences but provides no information as to the temporal aspects of an event. One mechanism that has been proposed and gained wide support, both theoretically and physiologically, for encoding temporal recency is gradual drift in a representation over time.

If a representation were to change systematically over time at a known rate, it would be possible to compute the elapsed time based on the total degree of change. One proposal that has been put forth by computational models is to combine such a temporally varying signal with one that is stable across time (Estes, 1955; Howard and Kahana, 2002; Polyn et al., 2009). By maintaining both signals in parallel it becomes possible to determine the total degree of change as simply the difference between the two signals. If one were to assume that at the point of initially encoding an event the brain stored two identical copies of the information, after which one copy changed systematically over time while the other did not, then the difference between the two copies becomes a function of the rate of temporal change of the variable signal and the elapsed time since it was first encoded.

While the exact nature of the temporally variable signal can vary considerably, the underlying principal remains the same. In support of this model of temporal coding, drifting network representations have been repeatedly observed in the hippocampus of both rats and humans. In an odor discrimination task in which rats were presented with a series of odors and had to report on their temporal ordering, physiological representations of the odors in CA1 became more dissimilar the farther apart in time the odors were presented (Manns et al., 2007). Reflecting the utility of such a change over time, the increase in dissimilarity was only observed in instances in which the rat made an accurate response regarding the temporal ordering of the

presented odors. During error trials, the increased dissimilarity between temporally remote stimuli was absent, reflecting a loss in the ability to compute temporal ordering from the neural signals. Similar results have also been observed in the spatial responses of CA1 cells over periods of hours to days. While the spatial selectivity of individual cells remains consistent, the network level representation of an explored environment changes gradually over time (Mankin et al., 2012; Rubin et al., 2015; Ziv et al., 2013). Individual cells exhibit large changes in firing rate, even having extended periods of no firing at all, leading to systematic changes in the ensemble representation. In human subjects, temporal drift has been observed in physiological recordings from patients with epilepsy and from functional imaging studies. Across these studies, the similarity of neural representations between two presented stimuli was again directly related to the temporal delay between them, indicating that the network representation was undergoing a gradual drift over time (Ezzyat and Davachi, 2014; Hsieh et al., 2014; Jenkins and Ranganath, 2016; Manning et al., 2011; Nielson et al., 2015). Much like in the case of rats performing odor discriminations, this systematic drift in humans was shown to relate to performance or subjective evaluations in temporal encoding tasks (Ezzyat and Davachi, 2014; Hsieh et al., 2014; Jenkins and Ranganath, 2016).

In the rodent hippocampus, the variable representation in CA1 appears to be complemented by a highly stable representation in CA3. The spatial firing patterns of CA3 cells remain consistent and the firing rates of individual place cells do not systematically change over time (Lu et al., 2015; Mankin et al., 2012). As a result, the collective representation of an experience within the CA3 network remains highly similar over the course of many hours, providing the necessary complement to a temporally drifting representation. Thus one model would be that CA1 and CA3 collectively provide the requisite time varying and stable information to support a neural signature for elapsed time (Mankin et al., 2012).

However this understanding of the roles and interactions of hippocampal subregions fails to account for the CA2 region, a small area anatomically located between CA3 and CA1 (Lorente De Nó, 1934). Overall, the study of CA2 has been limited with the area often considered to be simply a transition zone between CA1 and CA3. Yet the work that has been done has uncovered CA2 as a highly unique region, with anatomical connections, physiological and plasticity properties, and a gene expression profile unlike that of CA1 or CA3 (Dudek et al., 2016; Jones and McHugh, 2011). Unlike CA1 and CA3 which each receive input from only one of the two superficial layers of upstream mEC, CA2 cells appear to receive input from both mEC layer II and layer III (Chevaleyre and Siegelbaum, 2010; but see Kohara et al., 2014). Additionally, while in CA1 and CA3 mEC input generally produces weak depolarizations as compared to local hippocampal connections, for CA2 mEC input is quite strong, in excess of signals arriving from CA3 (Chevaleyre and Siegelbaum, 2010). Furthermore, whereas CA3 projections to CA1 exhibit robust long-term potentiation, the same is not true of CA2. Under control conditions, CA3 inputs to CA2 cells do not appear to potentiate and only after application of modulatory factors can any change of the CA3 to CA2 synapse be observed (Chevaleyre and Siegelbaum, 2010; Lee et al., 2010; Simons et al., 2011; Simons et al., 2009; Zhao et al., 2007).

More recently, efforts have been made to uncover a functional role of the CA2 region. Inactivation or lesion of CA2 has been linked to deficits in social memory, or an ability to accurately recall having interacted with a conspecific (Hitti and Siegelbaum, 2014; Stevenson and Caldwell, 2014). Gene expression and single unit recordings have suggested that CA2 cells can be modulated by experiences of novelty (Alexander et al., 2016; Wintzer et al., 2014). Finally, study of interactions of CA2 with the broader hippocampal network have suggested a potential role of CA2 cells in initiating sharp-wave ripples (Oliva et al., 2016), as well as in maintaining an internal representation of the spatial location of an animal during periods in which they remain

stationary and canonical place cells in CA1 and CA3 do not fire (Kay et al., 2016). Yet across these behavioral and physiological results, the development of a comprehensive understanding of the role of CA2 in hippocampal processing remains in progress.

Physiologically, CA2 cells do exhibit spatially defined place fields (Martig and Mizumori, 2011), but many of the properties of these place cells remain unknown. In particular it is unknown if CA2 cells exhibit remapping or how their firing may change over time, two characteristics directly relevant to a potential role of the CA2 region in memory processing. Chapter 2 of this dissertation seeks to investigate *in vivo* firing properties of CA2 place cells, in particular looking at how CA2 activity behaves over time and thus how activity in this often overlooked region may relate to CA1 and CA3 representation of temporal recency. Overall this work revealed that CA2 representations are even more variable than those observed in CA1. As such, a model of temporal coding emerged in which CA1 receives and integrates a stable signal arriving from CA3 and a temporally variable signal from CA2, allowing the CA1 network to simultaneously maintain information about space, memory, and elapsed time.

While considerable processing occurs within the hippocampal network, an important question remains what information is provided by upstream EC cells. In particular, how does EC activity relate to the ability of hippocampal place cells to maintain a reliable spatial signal to be used for navigation, while also undergoing variation over time as could be used to compute the temporal recency of an event?

By its very nature, the spatial firing of place cells is thought of as being relatively consistent. The precise spatial selectivity arises due to stability in the representation, and the ability to reconstruct an animal's position based on place cell activity is contingent on the spatial signal being reliable. Even over long intervals in which the CA1 network varies as a potential

mechanism for representing elapsed time, the variation occurs largely through changes in firing rates, not in place field locations as evidenced by the ability to accurately decode an animal's position using a 30 day old place cell map (Ziv et al., 2013). Does this stability in the hippocampal spatial signal result from computations internal to the hippocampus, perhaps relying on CA3 recurrency, or is it contingent on upstream EC input?

As described above, individual cells in the lEC exhibit little to no spatial firing patterns as animals explore open field environments (Hargreaves et al., 2005; Yoganarasimha et al., 2011). Thus, for the same reasons that lEC is not attributed to support *de novo* generation of spatial firing in hippocampal place cells, it seems unlikely that lEC is fundamentally involved in the long-term stability of the hippocampal map. On the other hand, mEC firing is broadly implicated in the spatial firing of place cells. In addition to the theoretical work suggesting how various mEC firing patterns could be integrated to yield place cells, manipulations of mEC have produced changes in the size and stability of downstream hippocampal place fields. Inactivations of the dorsal mEC as well as mEC lesions, either restricted to the hippocampal CA1 projecting layer III or covering the entire mEC expanse, lead to increases in the size of downstream CA1 place fields (Brun et al., 2008a; Hales et al., 2014; Ormond and McNaughton, 2015). Complete mEC lesions also result in a dramatic decrease in the spatial stability of CA1 place fields over time, both within a single 10-minute behavioral session and over the course of several hours (Hales et al., 2014; Schlesiger et al., 2018; Schlesiger et al., 2015). One hypothesis then is that mEC acts to provide the hippocampus with a rigid and stable spatial representation, helping to restrict the spatial extent of place cell firing, and serving to anchor the downstream spatial map over time. Indeed, some evidence supports the idea that mEC firing patterns could provide a stable spatial signal. In particular, grid cells continue to exhibit the same spatial firing fields across multiple exposures to the same environment even when separated by a 24-hour period (Hafting et al., 2005; Mallory et

al., 2018). However, given that grid cells compose only a small fraction of the total mEC population, it is important to also consider the behavior of non-grid cells, a population whose long-term stability has not been systematically examined.

On the other side of the coin, network activity in CA1 and CA2 gradually drift over time (Mankin et al., 2012; Chapter 2 of this dissertation), presenting a good candidate for encoding information about the temporal recency of an event. Yet the original source of such a temporal drift remains unclear. One possibility is that the signal is generated *do novo* in hippocampal CA2 as a result of the unique connectivity and cellular characteristics of this region. The time varying signal could then be relayed downstream to CA1, where it is integrated together with temporally stable input from CA3 in order to calculate the recency of an experience. Alternatively, the time varying signal that has been observed in both CA1 and CA2 may arise upstream in mEC. While the spatial firing of grid cells has been reported to remain similar across days, grid cell activity has never been examined systematically over time to determine if their firing patterns undergo any variation. As illustrated by CA1 activity, it is possible to maintain a strong spatial signal over long periods while still undergoing systematic changes, such as to firing rates. Likewise, no attempts have been made to examine the activity of non-grid cells over time, leaving no real understanding of how the large population of non-grid cells may contribute to downstream activity.

Currently, it remains largely unknown how mEC cells behave over extended periods and what information this population could provide downstream to hippocampus. MEC may provide hippocampus with a temporally stable signal that functions to maintain the spatial precision of place cells and support long-term navigational processes. However, mEC could also provide hippocampal CA1 and CA2 with a temporally varying signal that facilitates drift and can be utilized for encoding elapsed time. Still a third alternative exists in which mEC activity fulfills

both roles with a subset of the population remaining stable and supporting navigation while a different subset changes over time in order to encode the recency of an event. Chapter 3 of this dissertation will investigate this question, examining how the firing of mEC grid and non-grid cells respond as rats repeatedly explore the same environment at the same location in space over the course of six hours.

Preview of the dissertation

A broad collection of behavioral work focused on the MTL has uncovered a central role in episodic memory processing. Concurrently, physiological recordings have strongly implicated both the hippocampus and the mEC in representations of spatial information and an ability for animals to navigate through the world. Yet hippocampal place cells are not exclusive in their encoding of spatial information. Non-spatial content is also robustly represented, indicating that the collective hippocampal network provides a comprehensive, multimodal picture of experiences. Through this multimodal coding, and remapping in response to changes in experiences, the hippocampus is able to form a reliable and comprehensive representation of a given experience and simultaneously distinguish between multiple events, the two characteristics necessary to support episodic memory.

Historically, such a multimodal representation has been believed to be exclusive to hippocampus, with upstream mEC providing only spatial content and having no ability to encode non-spatial information or remap as a means of differentiating between experiences. Yet such an interpretation has several important caveats, most notably that it is informed almost exclusively by the behavior of mEC grid cells, discounting any role of the large fraction of non-grid cells. Thus, in chapter 1 we recorded the activity of the entire mEC population, both grid and non-grid

cells, as an animal explored an open field environment in which specific features, either the environment shape or the color, were altered. As previously described, spatial selectivity was abundant across the mEC population, with many cells exhibiting grid, border, HD, or NGS patterns. Though interestingly these recordings revealed a fundamental flaw in the quantification of spatial firing. Past work has described spatial firing to exist in only about half of mEC cells, but by correcting this flaw, our results found some degree of spatial firing in virtually all mEC cells. Furthermore, in evaluating the ability of mEC cells to remap in response to changes in environmental features, we observed distinct, but complementary, coding schemes in grid and NGS cells. For grid cells, feature changes were represented through a coordinated redistribution of firing rates across spatially stable grid fields. In contrast, NGS cells responded to feature changes with a complete reorganization of their spatial firing pattern, foregoing any need to provide a useful map for navigation.

In chapters 2 and 3, spatial representations and episodic memory coding is explored in the context of representations over time. In evaluating episodic memory, a reliable representation of an experience must be combined with an ability to determine its temporal recency, or how long ago the experience occurred. Within the hippocampus, CA1 network representations gradually change over time, presenting a theoretical mechanism to support calculation of elapsed time. This drifting representation is complemented by a stable network code in the CA3 region. However the activity of CA2 remains unknown. In chapter 2 we investigate CA2 cells as rats repeatedly explore the same environment over the course of a 30-hour period. Surprisingly, activity in CA2 was quite variable over even relatively short time periods of tens of minutes, with individual CA2 place fields exhibiting dramatic variation in firing rates well in excess of that observed in CA1. Within the broader hippocampal network these results suggest that CA1 activity may occur as a result of integration of a temporally stable CA3 signal, and highly time varying CA2 signal,

allowing the CA1 network representation to reside in a middle ground, providing a collective representation of both space and time.

Chapter 3 expands on our findings from the CA2 region seeking to determine how such a temporal drift may originally come about. Does the variation observed in CA2 emerge *de novo* as a result of the unique characteristics of CA2, or is it inherited from upstream mEC activity? To address this question, we recorded the activity of individual mEC cells across repeated explorations of the same environment across a period of six hours. Collectively we found that all grid cells and the majority of non-grid cells in mEC exhibited no systematic change over time. Yet for a small subset of non-grid cells, elapsed time was represented with dramatic changes in the spatial firing pattern or overall firing rate. Thus, it appears as though a primary role of mEC activity is to provide a reliable spatial signal downstream to anchor hippocampal place cells. But at the same time a small subset of the mEC population may provide the necessary time varying information to the CA2 region to be further integrated into a neural signal for elapsed time.

Finally, chapter 4 will attempt to integrate these finding, along with those of others, to provide thoughts as to how activity in mEC directly relates to hippocampal firing patterns and what conclusions can be drawn regarding how these coding schemes may be utilized.

CHAPTER 1: GRID AND NON-GRID CELLS IN MEDIAL ENTORHINAL CORTEX REPRESENT SPATIAL LOCATION AND ENVIRONMENTAL FEATURES WITH COMPLEMENTARY CODING SCHEMES

Abstract

The medial entorhinal cortex (mEC) has been identified as a hub for spatial information processing by the discovery of grid, border, and head-direction cells. Here we find that in addition to these well characterized classes, nearly all of the remaining two thirds of mEC cells can be categorized as spatially selective. We refer to these cells as non-grid spatial cells and confirmed that their spatial firing patterns were unrelated to running speed and highly reproducible within the same environment. However, in response to manipulations of environmental features, such as box shape or box color, non-grid spatial cells completely reorganized their spatial firing patterns. At the same time, grid cells retained their spatial alignment and predominantly responded with redistributed firing rates across their grid fields. Thus, mEC contains a joint representation of both spatial and environmental feature content, with specialized cell types showing different types of integrated coding of multimodal information.

Introduction

The medial entorhinal cortex (mEC) is specialized for spatial information processing with many neurons in the superficial layers displaying spatially and directionally selective firing (Hafting et al., 2005; Sargolini et al., 2006; Solstad et al., 2008). Among mEC cell types, grid cells show the most well defined spatial firing fields and, similar to place fields in the hippocampus (O'Keefe and Nadel, 1978), the spatial firing locations of these fields are reliably

reproduced when animals repeatedly explore the same environment (Hafting et al., 2005). Moreover, grid cells respond to exploration of distinct environments with profound shifting of their spatial firing patterns and, concurrently, orthogonal hippocampal place cell maps are formed ('global remapping') (Fyhn et al., 2007; Leutgeb et al., 2005b). The parallel reorganization of activity patterns between mEC and hippocampus (Fyhn et al., 2007; Hargreaves et al., 2007) suggests that grid and place cells each provide a stable spatial representation of a particular environment, but reconfigure their spatial firing to distinguish between environments at distinct locations (Buzsaki and Moser, 2013; O'Keefe and Nadel, 1978). In addition, aspects of an experience other than the location, such as timing, reward contingencies, or the appearance of an environment, are also discriminated by neuronal activity in mEC (Kraus et al., 2015; Lipton et al., 2007; Marozzi et al., 2015; Quirk et al., 1992).

When examining the different types of spatial and non-spatial coding in mEC, past work has largely focused on the cell population as a whole, on anatomically defined cell types such as layer II stellate and pyramidal cells, or on only grid cells. For the entire mEC cell population the reorganization of firing patterns is generally more pronounced in response to larger differences [with the exception of layer II pyramidal cells (Kitamura et al., 2015)], but more limited in response to minor differences between environments (Hargreaves et al., 2007; Keene et al., 2016; Kitamura et al., 2015; Perez-Escobar et al., 2016). This pattern is consistent with findings from only grid cells, for which large contextual changes elicit distinct spatial firing patterns and for which more minor manipulations of environmental features, such as the shape of its exterior or the color of its walls, do not alter the spatial firing patterns (Fyhn et al., 2007). Yet, less is known about the responses of non-grid mEC cells to manipulations of environments. It is feasible that non-grid cells show major reorganization along with the realignment of grid cells, but only minor responses when the grid pattern is stable. In the latter case, discrimination between environmental

features could thus be predominantly performed by the hippocampus in response to lateral entorhinal cortex (lEC) input (Lu et al., 2013). Alternatively, it is possible that mEC cells other than grid cells contribute to distinguishing between environmental features. To examine this possibility, we performed single-unit recordings from the superficial layers of dorsal mEC without biasing our sampling for a particular cell type. By subsequently classifying all recorded entorhinal cells and analyzing cell classes separately, we could identify whether feature discrimination was performed by distributed mEC networks, irrespective of functional cell type, or whether spatial location information and environmental feature information were preferentially represented by particular functional cell types.

Results

Nearly all mEC cells expressed reliable spatial firing patterns in the open field.

Using 10-min sessions of random foraging, we sorted all recorded mEC cells (n = 345 cells in 7 rats; Figure 1S.1) into distinct functional cell classes including grid, border, non-grid spatial (reliable spatial firing but not in a grid pattern or along a border), pure head direction (HD; heading modulated firing but no spatial firing), and non-spatial cells (otherwise uncategorized). For mEC recordings, classification has previously been performed by first calculating descriptive values for each cell class (grid score, border score, spatial information, HD mean resultant length) and by then comparing the values to those calculated from the shuffled data of all recorded mEC cells pooled together (Figure 1S.2A) (Barry et al., 2012; Bjerknes et al., 2015; Boccara et al., 2010; Koenig et al., 2011; Kropff et al., 2015; Krupic et al., 2015; Langston et al., 2010; Latuske et al., 2015; Perez-Escobar et al., 2016; Stensola et al., 2012; Tang et al., 2014; Wills et al., 2010; Winter et al., 2015b; Zhang et al., 2013). However, pooling shuffled data across all cells fails to account for the firing statistics of individual cells, most notably the relationship between a cell's

firing rate and its spatial information (Figure 1S.2B) (Rolls et al., 1997). Thus, to consider the characteristics of individual cells and more closely follow methods that have been used to define hippocampal place cells as spatially precise and consistent (Aghajan et al., 2015; Lee et al., 2015; Muller et al., 1987), we generated shuffled data for each cell independently. For identifying cells as spatial we then required that a cell's spatial information as well as its correlation between the first and second halves of a recording session were both above the 95th percentile of the corresponding measurements taken from the same cell's shuffled data. Using these criteria, a large majority (~95 %) of mEC cells was classified as spatial (Figure 1.1A), including numerous cells which would previously have been identified as non-spatial (Figure 1S.2C). The proportions of cells with specialized spatial firing patterns were comparable to previous reports (grid cells: 17.7 %; border cells: 9.3 %) (Kropff et al., 2015; Latuske et al., 2015; Tang et al., 2014; Zhang et al., 2013) (Figure 1S.2D), but also included a substantial fraction of spatial cells (67.5 %) that lacked any grid or border pattern. We refer to the latter type as non-grid spatial cells (Figure 1.1B, C and Table 1S.1) and confirmed that their spatial firing patterns did not arise from systematic variation in running speed. First, all non-grid spatial cells remained classified as non-grid spatial when using firing rate maps that excluded periods of low running speed (< 5 cm/s). Second, we found no relation between running speed patterns and cells' firing rate patterns (Figure 1S.1).

Grid alignment remained stable for manipulations of environment shape or color. Given that non-grid spatial cells were the most numerous cell type in mEC, we sought to determine whether they responded coherently with or distinctly from grid cells to manipulations of box shape, box color, and box location. We began by reproducing previously reported results for grid cells which showed retained grid alignment across manipulations of environmental features (i.e., box shape and box color), but major shifts across different box locations (Fyhn et al., 2007; Hafting et al., 2005). Our experiments thus repeated these paradigms (Figure 1.2A). For

Figure 1.1: Approximately 95 % of cells in mEC superficial layers were identified as spatial. (**A)** Each cell's spatial information (top) and within-session spatial correlation (bottom) is plotted against the respective 95th percentile value from the same cell's shuffled data ('cutoff'). Approximately 95 % of mEC cells were above the cutoffs for both spatial information and spatial correlation. **(B)** Of the spatial cells, 17.7 % had significant grid scores and 9.3 % had significant border scores. The remaining 67.5 % did not have either of these specialized firing patterns and are thus referred to as 'non-grid spatial cells'. **(C)** Rate maps of four cells that were identified as non-grid spatial. Firing rates are color-coded according to the scale bar on the right. For each rate map, the peak rate is noted above and the spatial information (SI) value is noted below. In the box marked by the stippled line, rate maps from the four cells are shown separately for the first and second half of the 10-min behavioral session. The within-session correlation (WSC) between the two half-session rate maps is noted below each pair of rate maps. See Figure 1S.1 for histology and cluster quality metrics and Figure 1S.2 for comparison to previously used classification criteria for mEC cells. Table 1S.1 shows that all cell types were identified in similar proportions across animals.

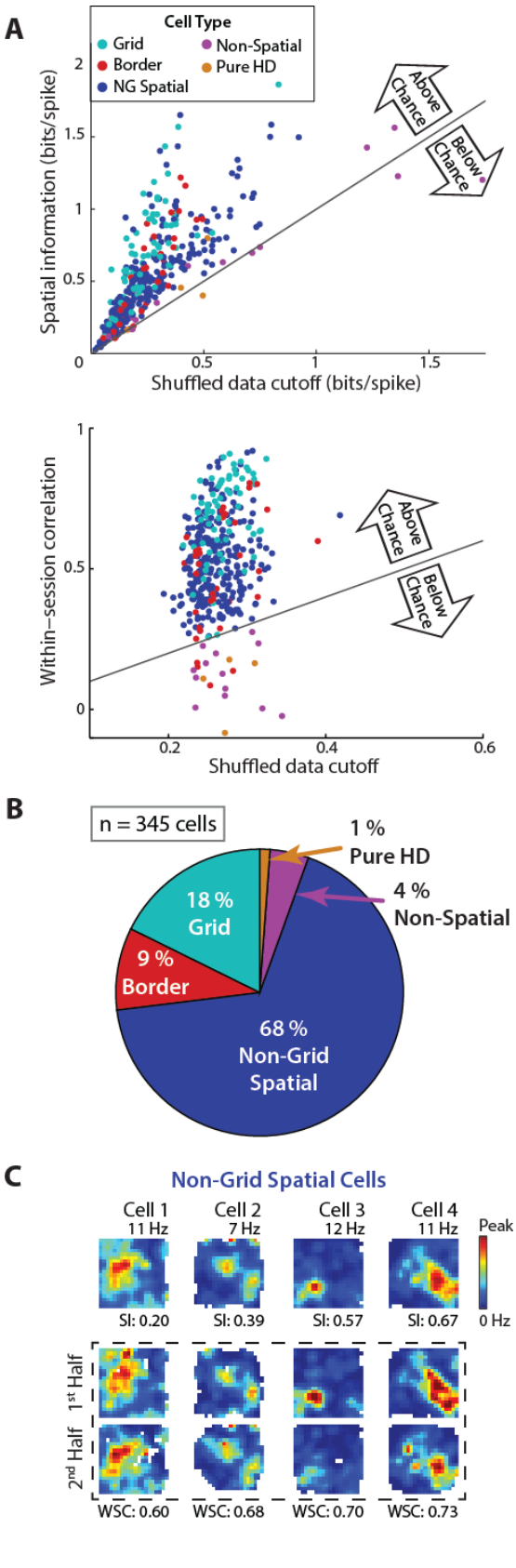
A
Cell Type
Grid
Border
NG Spatial
Non-Spatial
Pure HD
Above Chance
Below Chance
Spatial information (bits/spike)
Shuffled data cutoff (bits/spike)
Within−session correlation
Shuffled data cutoff
B
n = 345 cells
1 %
Pure HD
4 %
Non-Spatial
18 %
Grid
9 %
Border
68 %
Non-Grid
Spatial
C
Non-Grid Spatial Cells
Cell 1
11 Hz
Cell 2
7 Hz
Cell 3
12 Hz
Cell 4
11 Hz
Peak
0 Hz
SI: 0.20
SI: 0.39
SI: 0.57
SI: 0.67
1st Half
2nd Half
WSC: 0.60
WSC: 0.68
WSC: 0.70
WSC: 0.73

the shape-change manipulation, recordings consisted of four 10-min sessions during which rats randomly foraged in an enclosure that remained at a fixed location within a room. Using flexible walls, the enclosure was shaped as a circle during two sessions and as a square during two sessions. For the color-change manipulation, recordings were performed in a second, different room using a square enclosure. The enclosure again remained at a fixed location within the room, and its walls were black for two sessions and white for two sessions. Because the shape-change and color-change manipulations were performed in separate rooms, cells that were recorded in both rooms were used to evaluate the response of mEC cells to changes in box location.

We first confirmed that ensembles of grid cells retained stable spatial maps within the shape-change and color-change paradigms. For each rat and paradigm we generated the population vector (PV) for the set of recorded grid cells (shape-change: 2-7 grid cells from 6 rats; color-change: 2-21 grid cells from 3 rats) and calculated the PV cross-correlation between pairs of sessions. For the color-change paradigm in 1 additional rat, only one grid cell was recorded, and we thus used the cell's spatial cross-correlation. In the resulting correlation matrices, the displacement of the most central peak from the origin was used to measure the spatial alignment of the grid patterns (Figure 1S.3A, B). As previously reported for feature manipulations (Fyhn et al., 2007), the spatial firing of grid cell ensembles remained stable across manipulations of either box shape or color in the majority of rats (shape-change: 6 of 6 rats; color-change: 3 of 4 rats).

Because we were specifically interested in mEC firing patterns under conditions when the spatial coding of grid cells remained stable, we further analyzed individual grid cells from datasets with stable grid maps (Figure 1.2B). We calculated spatial cross-correlations for each cell separately and again measured the displacement of the central peak (Figure 1.2C). As a baseline for the analysis across different box features or locations, we compared repeated recording sessions in matching environments. Across sessions in matching environments, grid

Figure 1.2: For manipulations of box shape or box color, grid cell maps showed only minor shifts in their spatial location, but substantial redistributions of firing rates. (A) Schematic of the experimental paradigms. **(B)** Firing rate maps of an example grid cell that was recorded across all conditions. The peak rate of the cell across each set of four sessions is indicated to the right. **(C)** To measure the spatial stability between sessions, spatial cross-correlations were computed for the rate maps of each grid cell. For the example cell in (B), spatial cross-correlation maps are shown across matching conditions (left column) and across different shapes (right, top), colors (right, middle), and locations (right, bottom). Cross-correlation matrices are scaled from the minimum to the maximum correlation coefficient (noted to the right, blue to red). The displacement of the central peak from the origin measures the extent of the shift in the grid pattern. **(D)** Displacement from the origin when manipulating box shape, color, or location. For each comparison, the shift between repetitions of matching conditions was subtracted from the shift between sessions in different conditions (Δ displacement). Grid cells exhibited a significant displacement for shape, color, and location changes (Wilcoxon signed-rank matching vs different shape: $z = 3.8$, $p < 0.001$; different color: $z = 3.3$, $p < 0.01$; different location: $z = 2.5$, $p < 0.05$), although the median increase was only 1.3 cm for the shape change and 2.8 cm for the color change. **(E)** To further evaluate the overall firing profile of grid fields, we considered coordinated rate changes across grid fields and, for each grid cell, generated firing rate vectors (RVs) in which each element is the mean rate of a grid field. Rate maps and the resulting RVs (row vectors and bar graphs) are shown for two example grid cells in the shape-change and color-change paradigms. The average Spearman correlation of RVs across matching and different conditions is noted for both examples. Note that the vector is similar between matching conditions but changes across different conditions. **(F)** For grid cells with at least three fields (shape: $n = 27$; color: $n = 14$), rate vector correlation coefficients between matching environments and different environments are shown, along with the mean ± SEM. In addition, the Δ between the correlation coefficient in matching and different environments is plotted. RVs are more correlated between matching boxes compared to boxes with different shapes or different colors (Wilcoxon signed-rank matching vs different shape: $z = -2.4$, $p < 0.05$; different color: $z = -2.0$, $p < 0.05$). **(G)** Cumulative density functions (CDFs) of the spatial correlation between pairs of grid cell rate maps. Pairs were from recordings of the same cell in either matching or in different environments, and cell identity was permutated to generate chance correlations. Compared to correlations between rate maps in matching environments, spatial correlations decreased in response to manipulations of environment shape or color (Wilcoxon signed-rank matching vs different shape: $z = -4.7$, $p < 0.001$; different color: $z = -3.6$, $p < 0.001$). When comparing across different locations, spatial correlations were not different from shuffled values (Mann-Whitney U different location vs shuffled: $z = -1.4$, n.s.). * $p < 0.05$, ** $p < 0.01$, *** $p < 0.001$. See Figure 1S.3 for corresponding data from individual animals and Figure 1S.4 for corresponding hippocampal CA1 place cell data.

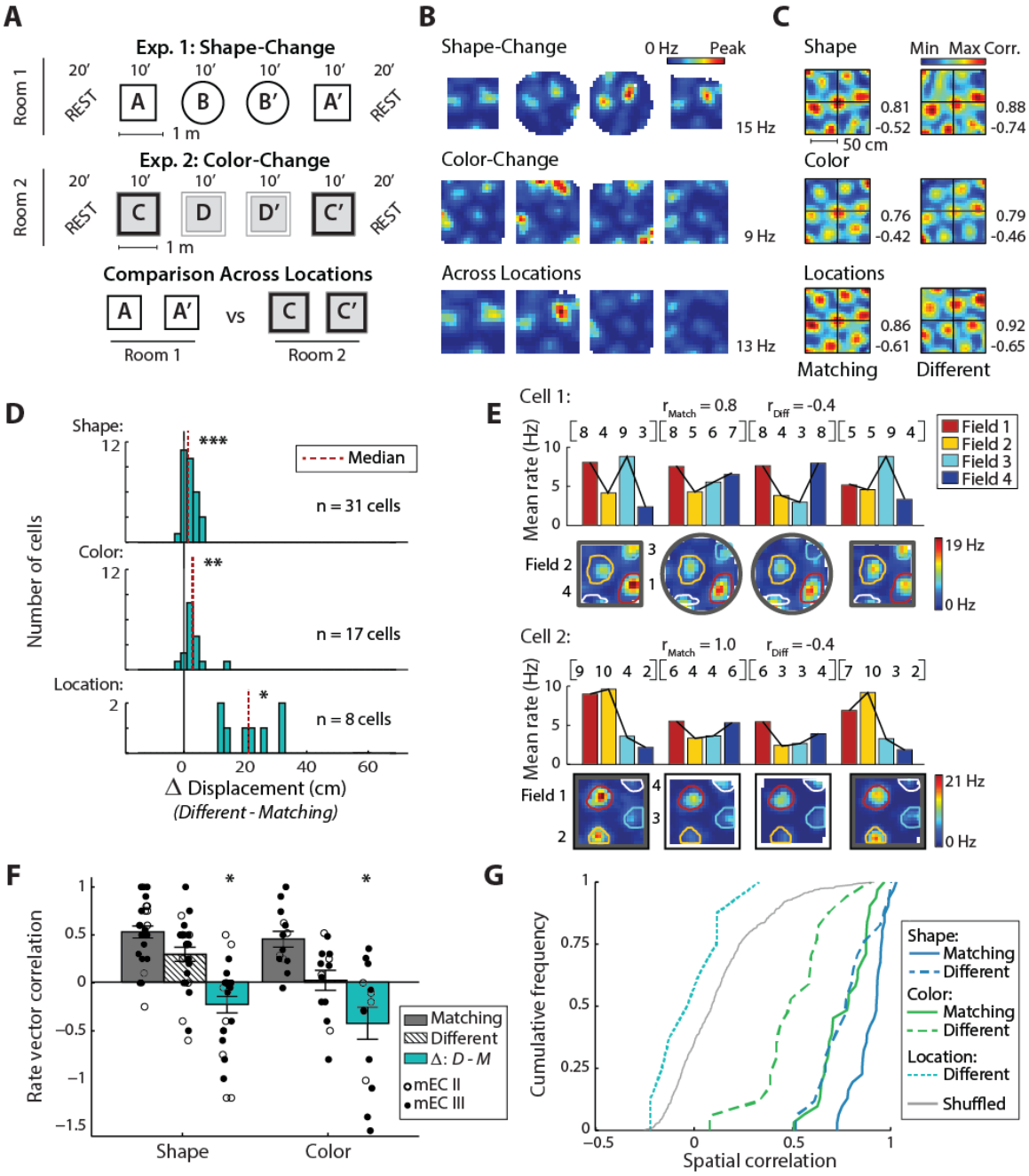
A
Exp. 1: Shape-Change
Room 1
20′ REST 10′ A 10′ B 10′ B′ 10′ A′ 20′ REST
1 m
Exp. 2: Color-Change
Room 2
20′ REST 10′ C 10′ D 10′ D′ 10′ C′ 20′ REST
1 m
Comparison Across Locations
A A′ vs C C′
Room 1
Room 2
B
Shape-Change
0 Hz Peak
15 Hz
Color-Change
9 Hz
Across Locations
13 Hz
C
Shape
Min Max Corr.
0.81 -0.52
0.88 -0.74
50 cm
Color
0.76 -0.42
0.79 -0.46
Locations
0.86 -0.61
0.92 -0.65
Matching
Different
D
Shape:
Color:
Location:
***
**
*
Median
n = 31 cells
n = 17 cells
n = 8 cells
Number of cells
Δ Displacement (cm)
(Different - Matching)
E
Cell 1:
r Match = 0.8
r Diff = -0.4
[8 4 9 3][8 5 6 7][8 4 3 8][5 5 9 4]
Field 1
Field 2
Field 3
Field 4
Mean rate (Hz)
19 Hz
0 Hz
Cell 2:
r Match = 1.0
r Diff = -0.4
[9 10 4 2][6 4 4 6][6 3 3 4][7 10 3 2]
21 Hz
0 Hz
F
Rate vector correlation
Matching
Different
Δ: D - M
mEC II
mEC III
Shape
Color
G
Cumulative frequency
Spatial correlation
Shape:
Matching
Different
Color:
Matching
Different
Location:
Different
Shuffled

cell displacement was minor (median displacement: 2.4 cm and 2.6 cm for matching box shape and color, respectively). Across different box shapes or box colors, we detected a small increase in displacement relative to matching conditions (median increase: 1.3 cm and 2.8 cm, $p < 0.001$ and $p < 0.01$, respectively; Figure 1.2D). These increases were well below those that were detected across environments located in different rooms (median increase: 20.9 cm; Kruskal-Wallis comparing box shape, color, and location: Chi-square (2) = 21.1, $p < 0.001$; post-hoc location vs shape, $p < 0.001$; location vs color $p < 0.01$).

Manipulations of box shape or color resulted in a firing rate redistribution across grid fields. While we observed only minimal changes in the spatial firing patterns of grid cells in response to our manipulations, it is possible that the environmental change is instead represented by grid fields using a distributed rate code. Consistent with previous reports, we found only minor fluctuations in the firing rates within individual grid fields (Figure 1S.3C) as opposed to the large rate changes characteristic of place fields (Fyhn et al., 2007; Leutgeb et al., 2005b; Perez-Escobar et al., 2016). Yet, small differences in firing rates of individual grid nodes could be indicative of a coordinated rate redistribution across the fields of individual grid cells. We therefore performed two analyses that are well suited to detect rate differences across multiple firing fields. First, we calculated the mean firing rate within each grid field and entered these values into a rate vector for each grid cell and each 10-min session. By comparing the rate vectors across sessions (Figure 1.2E, F), we confirmed that the firing rates of a cell's grid fields were similar between sessions in matching box shapes or colors (median Spearman's rank correlation: 0.50 and 0.43 respectively). However, when comparing across different box shapes or colors we found a significantly lower correlation of grid rate vectors (median correlation: 0.40 and 0.13; both $p < 0.05$ vs matching; Figure 1.2F), indicating that grid cell rate patterns became redistributed, in particular for manipulations of environment color where the correlation across different conditions was at

chance levels (Mann-Whitney U different color vs shuffled field identity: $z = 1.22$, n.s.). Second, we evaluated the overall similarity of the spatial maps of grid cells by calculating the spatial correlation between rate maps (Figure 1.2G). Although spatial correlation has frequently been used for confirming the spatial stability of cells' firing patterns, it is also highly sensitive to a redistribution of firing rates across multiple fields. For grid cells, spatial correlations were high between repeated recordings with matching box shapes or colors (median spatial correlation: 0.85 and 0.70 respectively), but lower across different box shapes or colors (median correlation: 0.72 and 0.42 respectively; both $p < 0.001$ vs matching), again indicating that grid cell firing rates became redistributed in response to feature manipulations.

Non-grid spatial cells responded to feature manipulations with pronounced changes in their spatial firing patterns. After establishing that grid cells showed relatively stable spatial firing patterns along with a rate redistribution across grid fields, we proceeded to test whether non-grid spatial cells would show corresponding responses to feature manipulations (Figure 1.3A-E). Non-grid spatial cells were defined based on stable spatial firing within a 10-min behavioral session (see Figure 1.1). We therefore expected that their spatial firing would also be reproducible over repeated 10-min recording sessions in matching environments. To confirm reproducible firing, we calculated the cross-correlation displacement and the spatial correlation between rate maps of each cell. For matching box shapes or colors we found that cross-correlation displacements were small (median displacement: 4.4 cm and 4.7 cm respectively) and that spatial correlations were high (median spatial correlation: 0.62 and 0.62 respectively). The firing patterns of mEC non-grid spatial cells were therefore reliable across repeated exploration of the same environment, though measurably below the values for grid cells (Mann-Whitney U grid vs non-grid spatial cells, displacement across matching shapes: $z = -4.5$, $p < 0.001$; colors: $z =$

Figure 1.3: For manipulations of box shape or box color, non-grid spatial cells exhibited profound changes in their spatial firing patterns. (A) Schematic of the experimental paradigms (redrawn from Figure 1.2). **(B)** Firing rate maps of an example non-grid spatial cell across all three conditions. **(C)** Spatial cross-correlation maps for the example cell in (B) indicate that the predominant firing has shifted to a different location. **(D)** Displacement of the cross-correlation central peak for manipulations of box shape, color, or location (Δ displacement between different and matching conditions). Manipulations of box shape or box color resulted in pronounced shifts in the predominant firing location (matching vs different shape: median displacement increase of 13.1 cm, Wilcoxon signed-rank, $z = 8.1$, $p < 0.001$; different color: median increase of 15.3 cm, $z = 9.1$, $p < 0.001$), but which was less than the more complete reorganization of the spatial maps across different locations (matching vs different location: median increase of 28.9 cm, $z = 5.6$, $p < 0.001$). **(E)** CDFs of the spatial correlation between pairs of rate maps. Pairs were from recordings of the same cell in either matching or in different environments, and cell identity was permutated to generate chance correlations. Spatial correlations decreased in response to manipulations of environment shape or color (Wilcoxon signed-rank matching vs different shape: $z = -8.7$, $p < 0.001$; different color: $z = -10.0$, $p < 0.001$) but less than across different locations where correspondence between maps was not different from shuffled values (Mann-Whitney U different location vs shuffled: $z = 1.0$, n.s.). **(F)** Comparison of the median cross-correlation displacement (left) and the median spatial correlation (right) between grid cells and non-grid spatial cells. Horizontal lines: medians of all cells; circles: medians of individual animals for matching (M, filled) and different conditions (D, open). *** $p < 0.001$. See Figure 1S.4 for corresponding hippocampal place cell data.

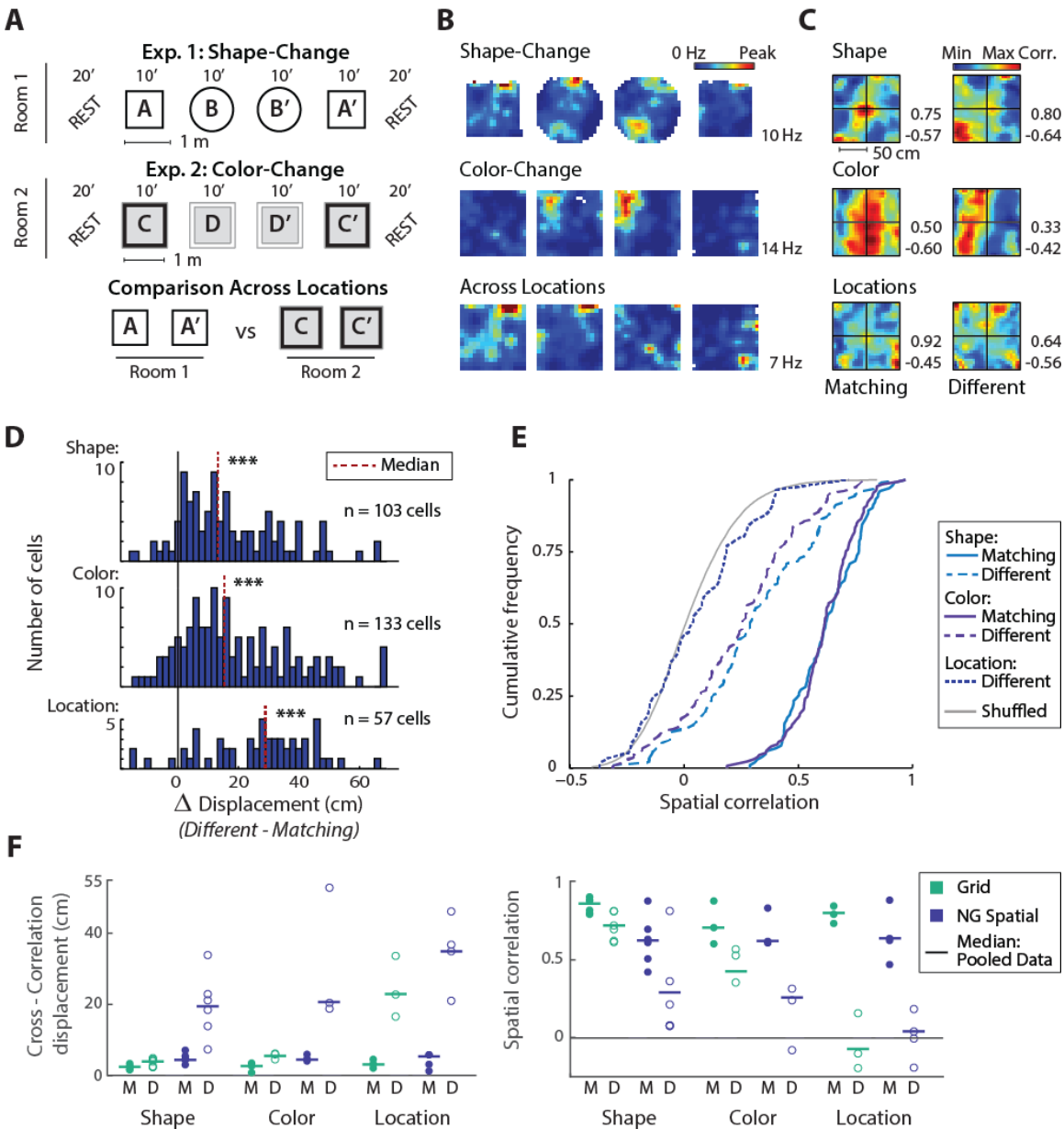
A
Exp. 1: Shape-Change
Room 1
20′ REST 10′ A 10′ B 10′ B′ 10′ A′ 20′ REST
1 m
Exp. 2: Color-Change
Room 2
20′ REST 10′ C 10′ D 10′ D′ 10′ C′ 20′ REST
1 m
Comparison Across Locations
A A′ vs C C′
Room 1
Room 2
B
Shape-Change
0 Hz Peak
10 Hz
Color-Change
14 Hz
Across Locations
7 Hz
C
Shape
Min Max Corr.
0.75 -0.57
0.80 -0.64
50 cm
Color
0.50 -0.60
0.33 -0.42
Locations
0.92 -0.45
0.64 -0.56
Matching
Different
D
Shape:
Color:
Location:
Median
n = 103 cells
n = 133 cells
n = 57 cells
***
Number of cells
Δ Displacement (cm)
(Different - Matching)
E
Cumulative frequency
Spatial correlation
Shape: Matching Different
Color: Matching Different
Location: Different
Shuffled
F
Cross - Correlation displacement (cm)
Spatial correlation
Grid
NG Spatial
Median: Pooled Data
M D M D
Shape
Color
Location

-3.2, $p < 0.01$; spatial correlation across matching shapes: $z = -6.5$, $p < 0.001$; colors: $z = -2.4$, $p < 0.05$).

We then examined the consistency of the firing patterns of non-grid spatial cells across different environment shapes or colors. Compared to sessions in matching conditions, non-grid spatial cells showed a median increase in displacement of 13.1 cm and 15.3 cm for shape and color change respectively (both $p < 0.001$ vs matching) indicating a profound change in spatial firing location, but not reaching the level of displacement observed across rooms (median increase: 28.9 cm; Kruskal-Wallis comparing box shape, color, and location: Chi-square (2) = 11.9, $p < 0.01$; post-hoc location vs shape, $p < 0.01$; location vs color $p < 0.05$). Measuring the spatial correlation yielded corresponding results with much lower correlations across different box shapes or colors (median spatial correlation: 0.29 and 0.26, respectively) compared to matching conditions (both $p < 0.001$). In fact, the degree of change elicited by feature manipulations was so substantial that response magnitudes overlapped with those produced by changing locations, limiting the ability of an ROC analysis to discriminate between these two highly distinct manipulations (Figure 1S.3D).

Responses were consistent across animals and in simultaneous recordings of grid and non-grid spatial cells. After finding in our full dataset that manipulations of environmental shape or color resulted in largely stable grid cell maps, but a pronounced reorganization of the firing patterns of non-grid spatial cells, we examined whether this pattern could also be observed in individual animals and in simultaneous recordings of grid and non-grid spatial cells. We found that grid cells responded less than non-grid spatial cells to feature manipulations in each subject (Figure 1.3F) and found that the differences between cell types were comparable to the full data set when only analyzing simultaneously recorded ensembles of grid and non-grid spatial cells (Figure 1.4, Table 1S.2). Furthermore, differences between grid and non-grid cells were also

Figure 1.4: Analysis of only simultaneous recordings of grid and non-grid spatial cells confirmed the results from the full dataset. Across all sessions, 38 of 48 grid cells were recorded with non-grid spatial cells (NGS) and 109 of 236 NGS cells were recorded with grid cells. **(A)** Rate maps of simultaneously recorded cell ensembles during manipulations of environment shape (left), color (middle), and location (right). Different ensembles are presented for each of the three manipulations. **(B)** Cross-correlation displacement (top row) and spatial correlation (bottom row) of subsets of grid and NGS cells across matching or different box shapes (left), colors (middle), and locations (right). Data are first presented for all recorded grid and NGS cells (All, same data as in Figs. 1.2 and 1.3) and then divided into subsets: grid cells with at least one NGS cell (w/NGS), NGS cells with at least one grid cell (w/Gr), and either cell type recorded simultaneously without cells from the opposing category (w/out). For each subset, the number of cells is noted in parenthesis. See Table 1S.2 for additional quantification of simultaneous recordings of grid and non-grid spatial cells.

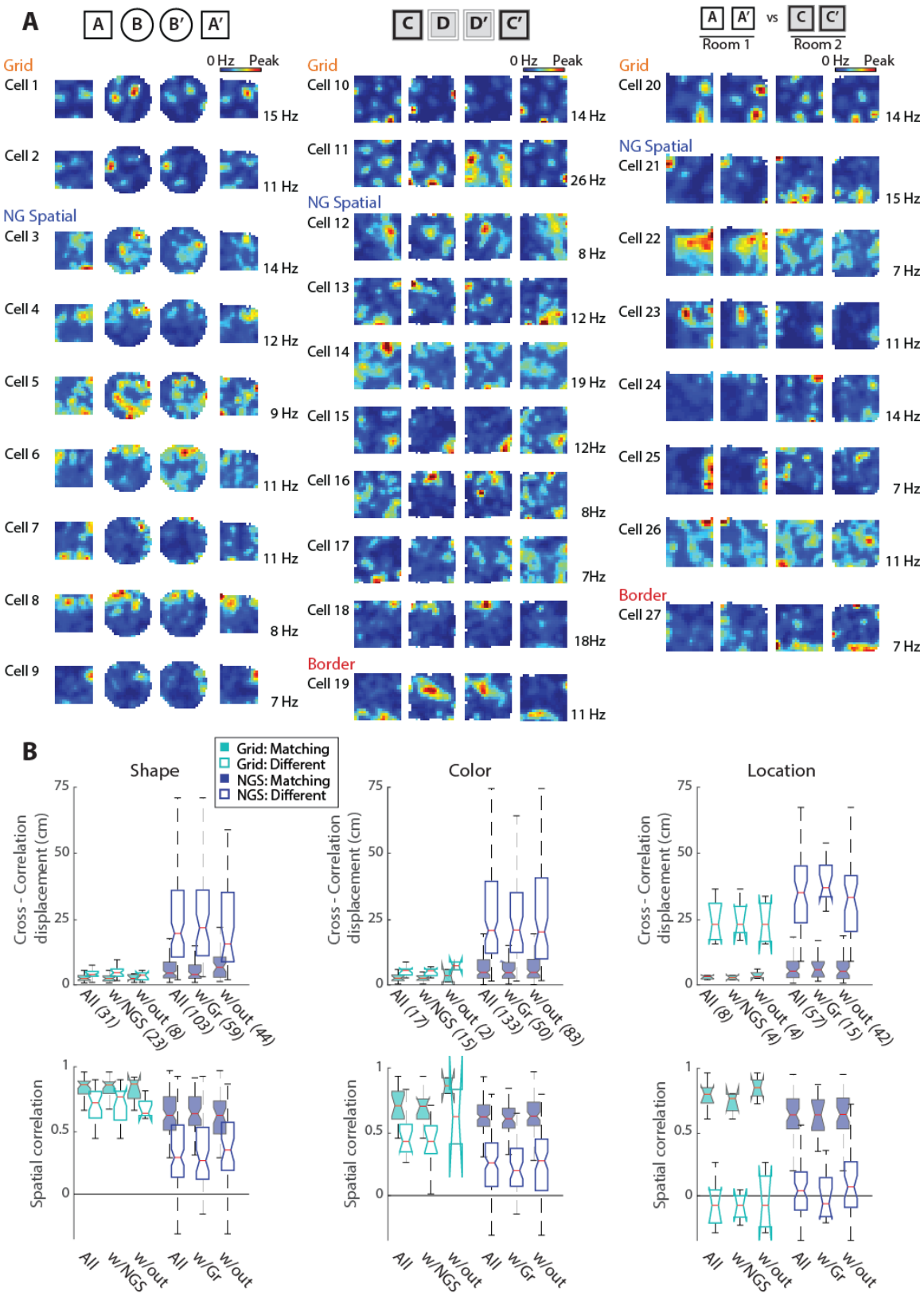
A
A
B
B′
A′
C
D
D′
C′
A
A′
vs
C
C′
Room 1
Room 2
0 Hz
Peak
Grid
Cell 1
15 Hz
Cell 2
11 Hz
NG Spatial
Cell 3
14 Hz
Cell 4
12 Hz
Cell 5
9 Hz
Cell 6
11 Hz
Cell 7
11 Hz
Cell 8
8 Hz
Cell 9
7 Hz
Grid
Cell 10
14 Hz
Cell 11
26 Hz
NG Spatial
Cell 12
8 Hz
Cell 13
12 Hz
Cell 14
19 Hz
Cell 15
12Hz
Cell 16
8Hz
Cell 17
7Hz
Cell 18
18Hz
Border
Cell 19
11 Hz
Grid
Cell 20
14 Hz
NG Spatial
Cell 21
15 Hz
Cell 22
7 Hz
Cell 23
11 Hz
Cell 24
14 Hz
Cell 25
7 Hz
Cell 26
11 Hz
Border
Cell 27
7 Hz
B
Grid: Matching
Grid: Different
NGS: Matching
NGS: Different
Shape
Color
Location
Cross - Correlation displacement (cm)
75
50
25
0
All (31)
w/NGS (23)
w/out (8)
All (103)
w/Gr (59)
w/out (44)
All (17)
w/NGS (15)
w/out (2)
All (133)
w/Gr (50)
w/out (83)
All (8)
w/NGS (4)
w/out (4)
All (57)
w/Gr (15)
w/out (42)
Spatial correlation
1
0.5
0
All
w/NGS
w/out
All
w/Gr
w/out

apparent when analyzing either layer II or III separately (Figure 1S.1E). Taken together, the distinct responses of mEC grid and non-grid spatial cells to manipulations of environmental features occurred consistently across animals and in both superficial cell layers.

Discussion

In comprehensive recordings from mEC superficial layers, we found that ~95 % of mEC cells exhibited spatial firing patterns. Of these spatially selective cells, ~20 % were grid cells and ~10 % were border cells, while the remaining two thirds ('non-grid spatial cells') had less specialized, yet consistent spatial firing patterns. The classification of a much larger proportion of mEC cells as spatial compared to previous reports is based on applying criteria that have been widely used for hippocampal place cells. As for hippocampus (Aghajan et al., 2015; Lee et al., 2015; Rolls et al., 1997), we shuffled the spiking data of each individual mEC cell to generate cell-specific cutoffs that account for the variability of an animal's behavior as well as the spiking statistics of individual cells. After identifying a major proportion of mEC non-grid cells as spatial, we asked whether these cells responded in parallel to grid cells to manipulations of environmental features. While grid cells predominantly exhibited a firing rate redistribution across spatially stable grid fields, non-grid spatial cells underwent a profound reorganization of their spatial firing patterns in response to the same environmental manipulations. The qualitative difference in the response pattern between grid and non-grid spatial cells also makes it unlikely that a sizeable fraction of non-grid spatial cells are in fact single fields of grid cells at a larger spacing. Grid fields would be expected to have stable spatial firing fields across our recording conditions, contrary to our findings for non-grid spatial cells. In addition, recordings of grid and non-grid spatial cells were highly intermixed along the dorso-ventral axis. Our experiments therefore identified mEC cell-type selective response patterns, which have not been observed in previous

studies that either evaluated only grid cells, did not distinguish between functional cell types, or reported changes that were consistent across mEC cell types (Fyhn et al., 2007; Hargreaves et al., 2007; Keene et al., 2016; Kitamura et al., 2015; Lipton et al., 2007; Marozzi et al., 2015; Perez-Escobar et al., 2016; Quirk et al., 1992).

Notably, the response pattern that we describe for grid cells resembles the mechanism by which place cell reorganization represents environmental features. In the hippocampus, firing rates are modulated while the spatial locations of place fields remain fixed in response to changes in environment shape or color ('rate remapping') (Anderson and Jeffery, 2003; Leutgeb et al., 2005b). We confirmed that hippocampal cells showed rate modulation while their spatial firing was stable using the same experimental paradigms in which spatial firing patterns of grid cells were retained (10 rats in our laboratory, including one rat with simultaneous recordings of hippocampal and mEC cells; Figure 1S.4). The stability of spatial firing patterns of grid cells and place cells in these conditions is in contrast to substantially reorganized spatial firing patterns of mEC non-grid spatial cells. Such reorganization of spatial firing of non-grid cells in response to cue manipulations illustrates that spatially distinct patterns are used to represent more than just allocentric space. Related joint coding of environmental features by combined spatial and rate responses has also been reported for hippocampal place cell populations, where it is referred to as partial remapping (Quirk et al., 1990). While we found a similar coding scheme for mEC, our findings differ from the hippocampal data in that the type of response (spatial or rate) to a manipulation is dependent on functional cell type (non-grid or grid).

Furthermore, we show that integration of feature and spatial coding occurs within mEC and that mEC cells can serve as a source for the emergence of feature coding by the hippocampus, in addition to direct inputs from lEC (Deshmukh, 2014; Knierim et al., 2006; Renno-Costa et al., 2010). LEC lesions were found to produce a 30 % impairment in

hippocampal rate coding (Lu et al., 2013), which indicates that remaining entorhinal inputs may provide a major contribution to rate coding. Although our data are thus consistent with the general notion that hippocampal coding patterns emerge from joint inputs from the two EC divisions (Eichenbaum et al., 2012; Keene et al., 2016; Knierim et al., 2014), they also show that joint representations of spatial and feature information are already present in the mEC inputs to hippocampus. Information streams could thus be integrated in parallel within hippocampus and mEC indicating that the rodent mEC is not predominantly specialized for only spatial or sequence representations (Buzsaki and Moser, 2013; Kraus et al., 2015), but may instead show similar integration of multimodal coding features as the primate entorhinal cortex (Bellgowan et al., 2009; Killian et al., 2012; Quian Quiroga et al., 2009; Wirth et al., 2003).

Appendix 1.1: Supplemental Figures

Figure 1S.1: Grid and non-grid cells were recorded from the superficial layers of mEC. (A) Tetrode locations in mEC are shown in representative sagittal brain sections, one for each of the seven rats in which mEC data were recorded. The superficial layers (II & III) of mEC are delineated with a black line, and the most ventral position of each tetrode track is marked with a red dot. (Bottom right panel) In rat G, cells were recorded simultaneously from both mEC and hippocampus, and hippocampal tracks are shown in a sagittal section through the hippocampal recording site. Scale bars = 500 µm. **(B)** Examples of cluster isolation. Spikes were considered to be from a single mEC cell when their waveform distribution across the four tetrode channels showed clearly identifiable clusters. In the examples either the peak spike amplitude or the spike energy (i.e., area under the waveform curve) on one tetrode channel is plotted against the amplitude or energy on a second channel. The three scatterplots are from different pairs of channels of the same tetrode, and each recorded spike is plotted as a dot with all spikes that were assigned to a given cell in the same color. Four different cells are shown, three non-grid spatial cells (cells 1, 3, 4) and one grid cell (cell 2). Each cell is already clearly isolated in the displayed scatterplots but cluster isolation was confirmed by comparing multiple spike waveform parameters across all pairs of tetrode channels. For illustration purposes spikes were downsampled to 40 % of the total number of spikes in the recording session. Behavioral trajectories and spatial firing patterns of the four cells are shown in the bottom right quadrant. The animal's path through the environment is shown as a gray line with a red dot at the location of each spike. The cell's spatial firing pattern is also shown in a color-coded rate map with the peak firing rate of each cell noted in the top row to the right of each map. There is no resemblance between the spatial maps of cells that were recorded from the same tetrode, which confirms that the spatial firing patterns of non-grid spatial cells are not a result of contamination by spikes from other cells. Possible contributions of speed-related firing to spatial selectivity were also examined. The speed score (SS) of each cell is noted in the middle row to the right of each rate map. The firing of cell 3 is highly modulated by speed whereas cells 1, 2 and 4 are not. Below the four rate maps, the speed map for the behavioral session is shown in which the average running speed at each spatial location is color coded from low running speeds in orange to high running speeds in white. The peak bin and mean running speeds are noted to the right. To determine whether localized running speed differences influenced the spatial firing of individual cells the firing rate maps were correlated to the speed map. The correlation between the rate map and speed map (rate-speed correlation: RSC) is noted in the bottom row to the right of each rate map. Note that even though cell 3 is highly speed modulated, there is a low correlation between the rate map and speed map relative to the correlation of cells 1, 2, and 4 which are not modulated by speed and thus reflect chance level correlation. **(C)** To quantify the quality of our clusters we calculated L-ratio and isolation distance which are presented as mean ± SEM of all mEC cells that were included in the analysis. For both metrics, there was no difference in the cluster quality between grid, non-grid spatial, and border cells (Kruskal-Wallis comparing grid, non-grid spatial, and border cells, L-Ratio: Chi-square (2) = 0.3, n.s.; Isolation distance: Chi-square (2) = 2.2, n.s.). Our clusters had isolation distances comparable to a previous study (Latuske et al., 2015), and over 99.5 % of our cells would pass the minimum isolation distance thresholds used by others (Newman and Hasselmo, 2014; Perez-Escobar et al., 2016).

(Figure 1S.1 Continued)

(D) To confirm that our pattern of results was not biased by poor clustering we segregated our grid and non-grid spatial cells into those above (high isolation) or below (low isolation) their respective median isolation distance. Spatial correlations are presented as mean ± SEM across matching environments (matching shape and matching color grouped), different shapes or colors (both paradigms grouped), and across rooms. There was no difference for any of the spatial correlation measurements between cells in the upper or lower half of isolation distances (Mann-Whitney U high vs low isolation, grid cells matching: $z = -1.2$; different: $z = -1.8$; across rooms: $z = -0.1$, all n.s.; non-grid spatial cells matching: $z = 0.8$; different: $z = 0.8$; across rooms: $z = -1.8$, all n.s.). **(E)** To determine whether our observed changes in spatial firing patterns were consistent across mEC layers II and III, particularly in light of their differential projection patterns to the hippocampus (van Strien et al., 2009), we segregated our data based on the anatomical reconstruction of our recording sites into putative layer II and layer III cells (See Table 1S.1). Spatial correlations are presented as mean ± SEM across matching environments (matching shape and matching color grouped), different shapes or colors (both paradigms grouped), and across rooms. For both grid and non-grid spatial cells there were no differences in spatial correlation measurements across cell layers (Mann-Whitney U layer II vs layer III, grid cells matching: $z = 1.3$; different: $z = 0.7$; across rooms: $z = -0.2$, all n.s.; non-grid spatial cells matching: $z = -1.9$; different: $z = -1.1$; across rooms: $z = -0.2$, all n.s.). **(F)** To determine whether spatial firing of mEC cells may be influenced by a bias to run faster in certain parts of the arena, we calculated speed scores for each cell in each session and compared them to the spatial information of the corresponding rate map. We found no relationship between the speed score and the spatial information of individual cells (n.s.) suggesting that any observed spatial firing was not the result of localized running speed variations. Cells are color coded as for Figure 1.1, according to the legend. Thresholds for identification of cells as 'highly speed modulated' (± 0.15) are shown as vertical dashed lines. **(G)** Distribution of speed scores across all recorded cells. Thresholds for identification of cells as 'highly speed modulated' (± 0.15) are shown as vertical dashed lines with the region designated as 'low speed modulation' shaded gray. **(H)** Cells that were identified as highly speed modulated, either positively or negatively, were further analyzed by comparing the spatial information of each cell's firing rate map to the spatial information of its respective speed map. **(I)** As in (H), but for the reliability of spatial firing, which was calculated by splitting the behavioral sessions in half and calculating the spatial correlation between maps from the first and from the second half of a session. Cells are color coded as in (F). For comparisons of spatial information and reliability, there were no correlations between the values calculated from the rate map and from the speed map (both n.s.), further indicating that the spatial firing of mEC cells is not driven by localized variations in running speed.

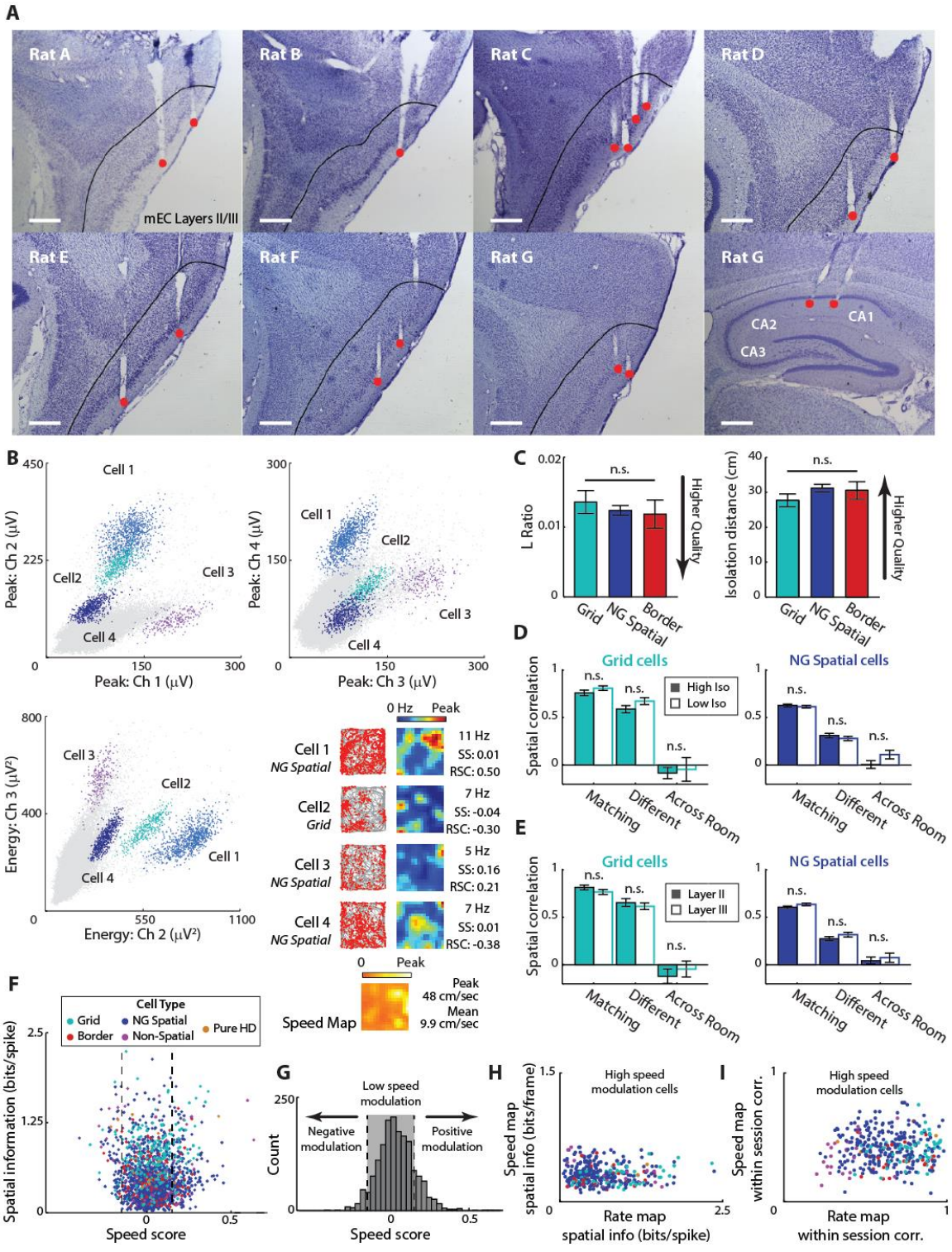
A
Rat A
Rat B
Rat C
Rat D
mEC Layers II/III
Rat E
Rat F
Rat G
Rat G
CA2
CA1
CA3
B
Cell 1
Cell2
Cell 3
Cell 4
Peak: Ch 2 (μV)
Peak: Ch 1 (μV)
Peak: Ch 4 (μV)
Peak: Ch 3 (μV)
Energy: Ch 3 (μV²)
Energy: Ch 2 (μV²)
0 Hz
Peak
Cell 1 NG Spatial
11 Hz
SS: 0.01
RSC: 0.50
Cell2 Grid
7 Hz
SS: -0.04
RSC: -0.30
Cell 3 NG Spatial
5 Hz
SS: 0.16
RSC: 0.21
Cell 4 NG Spatial
7 Hz
SS: 0.01
RSC: -0.38
Speed Map
Peak
48 cm/sec
Mean
9.9 cm/sec
C
L Ratio
Higher Quality
Isolation distance (cm)
n.s.
Grid
NG Spatial
Border
D
Grid cells
NG Spatial cells
Spatial correlation
High Iso
Low Iso
Matching
Different
Across Room
E
Layer II
Layer III
F
Cell Type
Grid
NG Spatial
Pure HD
Border
Non-Spatial
Spatial information (bits/spike)
Speed score
G
Low speed modulation
Negative modulation
Positive modulation
Count
H
High speed modulation cells
Speed map spatial info (bits/frame)
Rate map spatial info (bits/spike)
I
Speed map within session corr.
Rate map within session corr.

Figure 1S.2: Using the pooled spatial information scores from the shuffled datasets of all recorded mEC cells as criteria for classification is biased toward defining cells with low firing rates as spatial. (A) Histograms of grid, border, information, and head direction scores that were calculated from shuffled data of all mEC cells (red: data from the shape-change paradigm; blue: data from the color-change paradigm). Vertical lines indicate the 95th percentile cutoff from each set of scores, which resemble those that were reported by other studies using the pooled method (Kropff et al., 2015; Langston et al., 2010; Latuske et al., 2015; Zhang et al., 2013). **(B)** (Left) The spatial information scores of all cells in all sessions are plotted against the cells' average firing rates. The spatial information population cutoff values from the pooled method are shown as horizontal stippled lines (top line: shape-change paradigm; bottom line: color-change paradigm). Spatial information scores are higher for low rate cells (r^2: 0.28, $p = 1.1x10^{-119}$), such that low rate cells would be preferentially classified as spatial (i.e., those above the horizontal lines when using the pooled method). For comparison, cells are shown as classified by the single-cell method in Fig. 1.1 (i.e., with the color code that is indicated in the legend). (Right) For the same cells for which the actual spatial information is shown in the panel to the left, the 95th percentile of each cell's information scores from shuffled data (i.e., the single-cell shuffled cutoff) is plotted against the cell's average firing rate. This reveals that the single-cell cutoff values for spatial information (colored dots) differ substantially from the pooled cutoff values (horizontal stippled lines). Similar to the actual information scores, single-cell cutoff values are higher for cells with lower rates (r^2: 0.49, $p = 7.2x10^{-246}$), and the use of single-cell cutoff values thus eliminates the bias of preferentially selecting low-rate cells as spatial. **(C)** For four example cells, histograms with the spatial information scores from the shuffled data of each cell are shown. Cells 1 and 2 are taken from the shape-change paradigm, and cells 3 and 4 are taken from the color-change paradigm. The pooled cutoff value is shown as a red or blue vertical line, the single-cell cutoff value is shown as a black line, and the cell's actual information score is indicated by the dashed line. The rate map for each cell is shown in the inset, with the peak firing rate, the spatial information score (SI), and the within session correlation (WSC) noted to the right. For each of the four depicted cases the single-cell cutoff was substantially lower than the pooled cutoff, yet the spatial information of the recorded cell is still well above the single-cell cutoff, indicating that the cell's spatial firing is more precise than chance. The observation that these cells code for space was confirmed by finding that their within session correlation values are also above chance. Cells 1 and 2 in Fig. 1.1D are additional examples of cells with spatial information values above the single-cell cutoff, but which would be identified as non-spatial by the pooled shuffling method. **(D)** Classification of all recorded mEC cells using the pooled cutoff and the single-cell cutoff methods. (Top) We classify cells identically to previous methods, using pooled shuffling procedures and spatial information for identification of non-grid spatial cells. (Bottom) We use single-cell shuffling procedures but, in contrast to Fig. 1.1, use exclusively the spatial information as a criterion for identifying non-grid spatial cells. This identified > 99 % of cells as spatial (grid, border, or non-grid spatial). Adding the within-session correlations as a criterion (see Fig. 1.1) identified ~95 % of mEC cells as spatial.

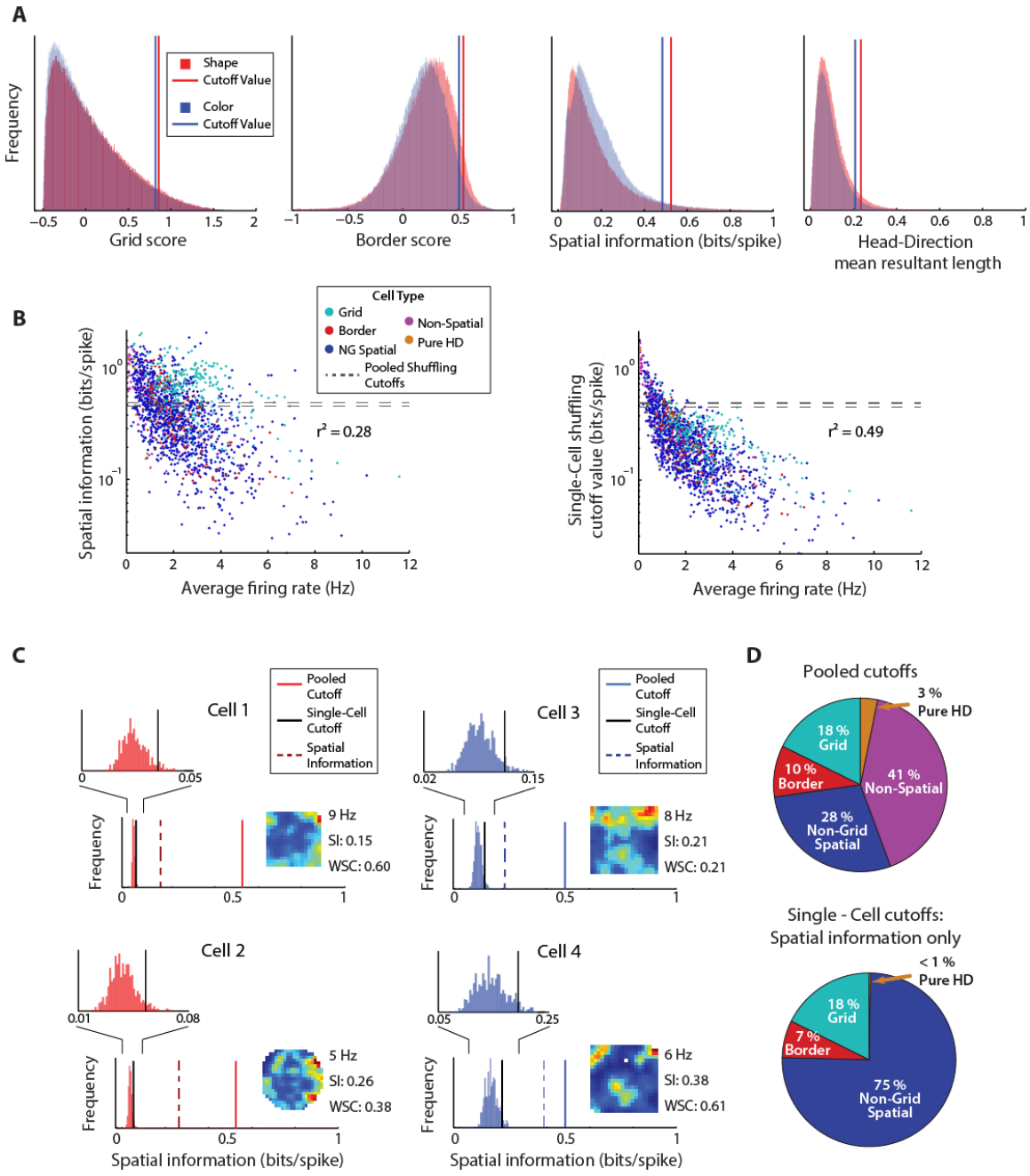
A
Frequency
Shape
Cutoff Value
Color
Cutoff Value
Grid score
Border score
Spatial information (bits/spike)
Head-Direction
mean resultant length
B
Cell Type
Grid
Border
NG Spatial
Non-Spatial
Pure HD
Pooled Shuffling
Cutoffs
Spatial information (bits/spike)
r² = 0.28
Average firing rate (Hz)
Single-Cell shuffling
cutoff value (bits/spike)
r² = 0.49
Average firing rate (Hz)
C
Cell 1
Pooled
Cutoff
Single-Cell
Cutoff
Spatial
Information
9 Hz
SI: 0.15
WSC: 0.60
Cell 3
8 Hz
SI: 0.21
WSC: 0.21
Cell 2
5 Hz
SI: 0.26
WSC: 0.38
Cell 4
6 Hz
SI: 0.38
WSC: 0.61
Frequency
Spatial information (bits/spike)
D
Pooled cutoffs
3 %
Pure HD
18 %
Grid
10 %
Border
41 %
Non-Spatial
28 %
Non-Grid
Spatial
Single - Cell cutoffs:
Spatial information only
< 1 %
Pure HD
18 %
Grid
7 %
Border
75 %
Non-Grid
Spatial

Figure 1S.3: Grid maps were stable in response to manipulations of environmental features. **(A)** (Pair of color-coded matrices on left of each panel) For each type of recording session (e.g., A, B, B', and A') and animal, the rate maps of all recorded grid cells were stacked to generate population vectors for each *x*-*y* pixel. Population vector (PV) cross-correlations were then calculated by shifting the stacked maps of two separate recording sessions with respect to each other along the *x* and *y* dimension. The resulting matrices of correlation coefficients at each *x*-*y* offset indicate whether the spatial firing of grid cell ensembles showed stable spatial firing patterns or spatial shifts across recording sessions. A comparison between recordings in matching conditions is shown to the left (e.g., A vs. A'), and a comparison across manipulated environments (as indicated in the schematics on top) are shown to the right (e.g., A vs. B). Cross-correlations are scaled from the minimum correlation coefficient in blue to the maximal correlation coefficient in red (listed to the right of each correlogram), and the number of cells that make up each population is noted below each set of cross-correlation matrices. If maps remained aligned, the central most peak of the correlogram was close to the origin, whereas if the map shifted, the central peak was displaced. Cross-correlations showed a central peak close to the origin for changes in box shape or color, which is indicative of a stable grid map, as previously reported (Fyhn et al., 2007). (Right of each panel, polar plots) Cross correlations were also calculated for each grid cell individually and the resulting displacements for individual grid cells are shown for each animal and manipulation. Each line in the polar plot is the cross-correlation displacement of one grid cell across matching conditions (e.g., A vs. A'; black lines) or different conditions (e.g. A vs. B; red lines). For comparison, the median displacement of grid cells across rooms is shown as the circular blue dashed line in each plot. Taken together, recorded grid cells in most rats showed appreciable spatial stability for manipulations of environmental features (box shape and box color, see also Fig. 1.2D) with the exception of rat F for the box color manipulation (highlighted by the red box). **(B)** Quantification of the displacement of the PV cross-correlation peak for each animal. Manipulations of box shape, color, and location are compared to repeated sessions in matching conditions. Displacement for rat F for the change in box color is shown as the filled circle, and this value was identified as an outlier compared to the other values for manipulations of environmental features (Tukey's outlier test). Data from the box color manipulation in rat F were therefore excluded from subsequent analysis of environmental manipulations. In addition, no grid cells were recorded from rat D in the shape-change paradigm, and because we could therefore not assess the response of grid cells, we also excluded data from this case from subsequent analysis. **(C)** Similarity scores for the mean firing rates within individual grid fields. A rate overlap close to 1 indicates that the firing rate was approximately equal across the two compared conditions. Some variability in firing rates is already observed for recordings in matching conditions, and we thus measured whether shape and color manipulations resulted in increased variability (Δ overlap; inset). Grid field firing rate similarity was not altered by the shape manipulation (median Δ overlap: 0.0012; Wilcoxon signed-rank matching vs different: $z = -1.0$, n.s.) but exhibited a minor decrease in response to the color manipulation (median Δ overlap: 0.0092; matching vs different: $z = -3.2$, $p < 0.01$). **(D)** To evaluate how profoundly changes in environment shape or color altered the spatial firing pattern of mEC cells, we used ROC analysis of the cross correlation displacement (left) and of the spatial correlation values (right). Using both measurements, we compared the cells' response to manipulations of environmental features with the cells' response to moving between rooms.

(Figure 1S.3 Continued)

More substantial reorganization in response to feature manipulations is expected to result in reduced discriminability from the complete reorganization of firing patterns that is produced by moving between rooms. For grid cells, ROC discrimination between feature manipulations within a room as opposed to moving between rooms was near perfect using either the cross-correlation displacement (accuracy and d' for shape vs location change: 100 % and -3.2; color vs location change: 99 % and -2.9) or the spatial correlation (accuracy and d' for shape vs location change: 100 % and -4.1; color vs location change: 96 % and -2.7). In contrast, the large changes in spatial firing of non-grid spatial cells for feature manipulations within a rooms resulted in poor ROC discrimination from moving between rooms using either displacement (accuracy and d' for shape vs location change: 69 % and -0.4; color vs location change: 68 % and -0.3) or spatial correlation (accuracy and d' for shape vs location change: 76 % and -1.1; color vs location change: 71 % and -0.7).

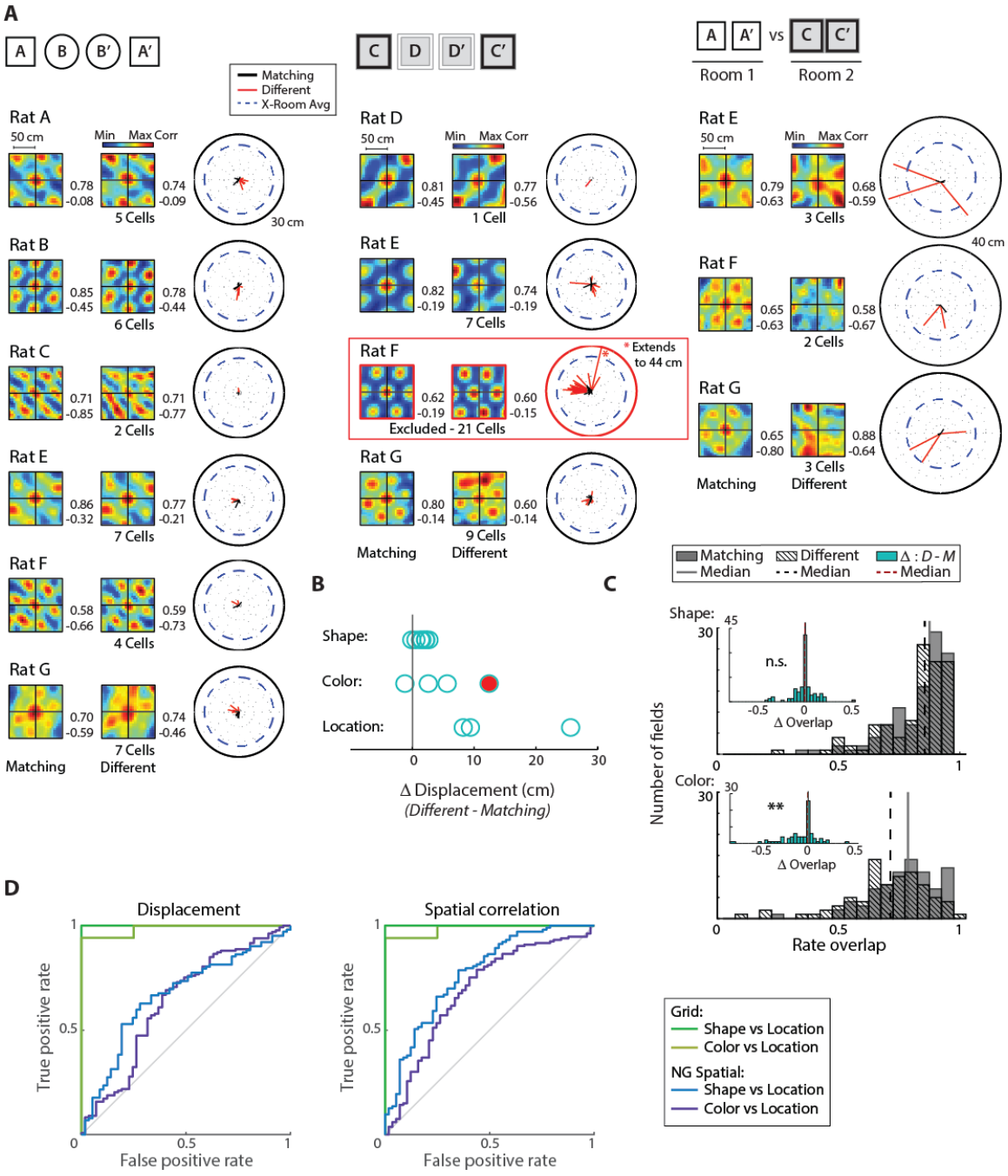
A
A
B
B′
A′
C
D
D′
C′
A
A′
vs
C
C′
Room 1
Room 2
Matching
Different
X-Room Avg
Rat A
50 cm
Min
Max Corr
0.78
-0.08
0.74
-0.09
5 Cells
30 cm
Rat B
0.85
-0.45
0.78
-0.44
6 Cells
Rat C
0.71
-0.85
0.71
-0.77
2 Cells
Rat E
0.86
-0.32
0.77
-0.21
7 Cells
Rat F
0.58
-0.66
0.59
-0.73
4 Cells
Rat G
0.70
-0.59
0.74
-0.46
7 Cells
Matching
Different
Rat D
0.81
-0.45
0.77
-0.56
1 Cell
Rat E
0.82
-0.19
0.74
-0.19
7 Cells
Rat F
* Extends to 44 cm
0.62
-0.19
0.60
-0.15
Excluded - 21 Cells
Rat G
0.80
-0.14
0.60
-0.14
9 Cells
Matching
Different
Rat E
0.79
-0.63
0.68
-0.59
3 Cells
40 cm
Rat F
0.65
-0.63
0.58
-0.67
2 Cells
Rat G
0.65
-0.80
0.88
-0.64
3 Cells
Matching
Different
B
Shape:
Color:
Location:
0
10
20
30
Δ Displacement (cm)
(Different - Matching)
C
Matching
Median
Different
Median
Δ : D - M
Median
Shape:
30
45
n.s.
-0.5
0
0.5
Δ Overlap
0
0.5
1
Color:
30
**
Number of fields
Rate overlap
D
Displacement
Spatial correlation
True positive rate
False positive rate
1
0.5
0
Grid:
Shape vs Location
Color vs Location
NG Spatial:
Shape vs Location
Color vs Location

Figure 1S.4: Hippocampal CA1 place cells undergo rate-remapping in response to feature manipulations. In a previously published study from our laboratory, we recorded CA1 and CA3 cells from six rats and observed robust rate-remapping in response to changes in box shape (Mankin et al., 2012). In the current study, we recorded hippocampal CA1 cells from four additional rats (including one rat with simultaneous recordings of hippocampus and mEC grid and non-grid cells) while manipulating box shape or color. These additional CA1 data are presented here and confirm that rate-remapping is the predominant response to our manipulations of environment features. **(A-C)** Example place cell recordings for manipulations of environmental shape (A), color (B), and location (C). For manipulations of shape and color, all of the active cells recorded from one tetrode (TT) are shown. For manipulation of location, cells from two tetrodes are shown. Rate maps are scaled to the peak firing rate across the four sessions, noted to the right. The two rate maps from the condition with a lower peak rate are then rescaled to the right, with the rescaled peak rate noted. For clarity, the rate maps for which rescaled versions are depicted are marked by a star in the top-right corner of the original maps. Below each ensemble of place cells, a simultaneously recorded mEC grid cell is shown along with its respective spatial cross-correlation. **(D)** A population vector (PV) cross-correlation was calculated for the ensemble of all place cells that were recorded from all animals across manipulations of environment shape, color, and location. Hippocampal PV cross-correlation maps are all scaled from 0 to 1 to illustrate the change in PV correlation maxima generated by rate remapping. Collectively, the hippocampal map remained stable during manipulations of environmental features (evident by the retention of the central peak at the origin) but changes in the firing rates of individual place fields resulted in a lower peak PV correlation (indicated below each correlogram). When comparing maps between boxes in separate rooms (i.e., location manipulation), the spatial firing completely reorganized, as indicated by a displacement of the central peak from the origin. **(E)** Spatial cross-correlations were calculated for each place cell individually and the displacement of the central peak was calculated for manipulations of box shape, color, and location. For each comparison, the shift between repetitions of matching conditions (e.g., A vs. A') was subtracted from the shift between sessions in different conditions (e.g., A vs. B). Place cells exhibited a small but significant increase in displacement for manipulations of box shape (median displacement increase: 6.3 cm; Wilcoxon signed-rank matching vs different shape: $z = 4.5$, $p < 0.001$) and box color (median displacement increase: 4.9 cm; matching vs. different: $z = 4.3$, $p < 0.001$), and a much larger displacement for comparisons between separate box locations (median displacement increase: 36.7 cm; matching vs different: $z = 5.7$, $p < 0.001$). **(F)** Comparison of mean firing rates of individual place fields were performed by calculating the overlap score (i.e., 1 – rate difference/rate sum). Histograms of the overlap scores for comparisons between matching and different environments are shown. The pairwise delta in the overlap score (different minus matching environments) for each place field is plotted in the inset. Place field firing rates changed substantially in response to manipulations of environment shape (median Δ overlap: 0.24; Wilcoxon signed-rank matching vs different: $z = -4.8$, $p < 0.001$) or color (median Δ overlap: 0.07; matching vs different: $z = -4.6$, $p < 0.001$), as previously reported (Leutgeb et al., 2005b). **(G)** CDFs of the spatial correlation of place cells for matching environments or across environments that differed in box shape, box color, or box location. A shuffling procedure was also performed in which cell identity was permutated to generate chance correlations.

(Figure 1S.4 Continued)

Spatial correlation coefficients decreased moderately in response to manipulations of environment shape or color (Wilcoxon signed-rank matching vs different shape: $z = -5.8$, $p < 0.001$; different color: $z = -5.1$, $p < 0.001$). Place cells were even somewhat less correlated than shuffled rate maps across different box locations (Mann-Whitney U different location vs shuffled: $z = -2.0$, $p < 0.05$). *** $p < 0.001$.

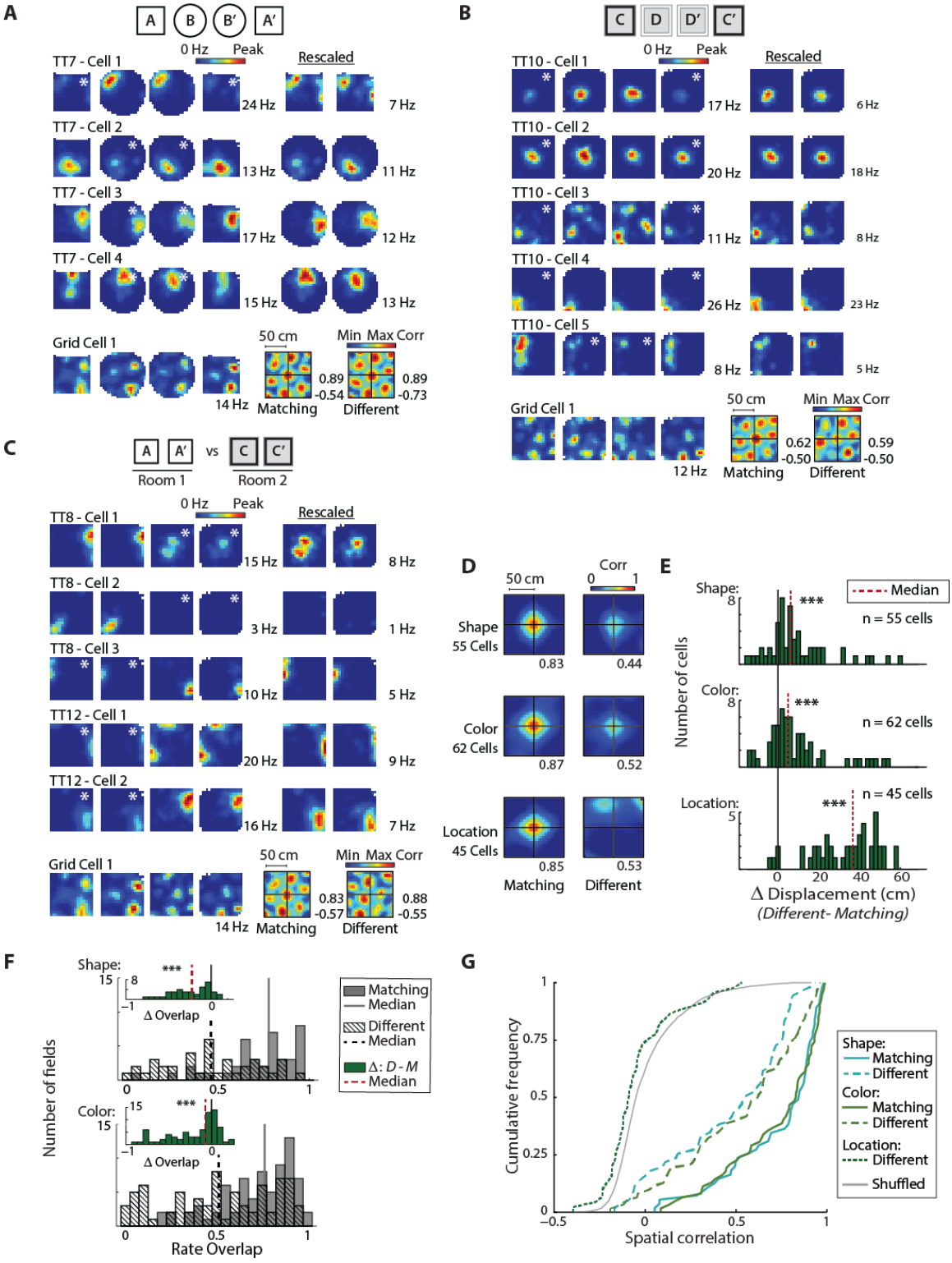
A
A
B
B′
A′
0 Hz
Peak
Rescaled
TT7 - Cell 1
24 Hz
7 Hz
TT7 - Cell 2
13 Hz
11 Hz
TT7 - Cell 3
17 Hz
12 Hz
TT7 - Cell 4
15 Hz
13 Hz
Grid Cell 1
50 cm
Min Max Corr
14 Hz
0.89
-0.54
Matching
0.89
-0.73
Different
B
C
D
D′
C′
0 Hz
Peak
Rescaled
TT10 - Cell 1
17 Hz
6 Hz
TT10 - Cell 2
20 Hz
18 Hz
TT10 - Cell 3
11 Hz
8 Hz
TT10 - Cell 4
26 Hz
23 Hz
TT10 - Cell 5
8 Hz
5 Hz
Grid Cell 1
50 cm
Min Max Corr
12 Hz
0.62
-0.50
Matching
0.59
-0.50
Different
C
A
A′
vs
C
C′
Room 1
Room 2
0 Hz
Peak
Rescaled
TT8 - Cell 1
15 Hz
8 Hz
TT8 - Cell 2
3 Hz
1 Hz
TT8 - Cell 3
10 Hz
5 Hz
TT12 - Cell 1
20 Hz
9 Hz
TT12 - Cell 2
16 Hz
7 Hz
Grid Cell 1
50 cm
Min Max Corr
14 Hz
0.83
-0.57
Matching
0.88
-0.55
Different
D
50 cm
Corr
0
1
Shape
55 Cells
0.83
0.44
Color
62 Cells
0.87
0.52
Location
45 Cells
0.85
0.53
Matching
Different
E
Shape:
8
***
Median
n = 55 cells
Color:
8
***
n = 62 cells
Location:
5
***
n = 45 cells
Number of cells
0
20
40
60
Δ Displacement (cm)
(Different- Matching)
F
Shape:
15
8
***
−1
0
Δ Overlap
0
0.5
1
Color:
15
15
***
−1
0
Δ Overlap
0
0.5
1
Rate Overlap
Number of fields
Matching
Median
Different
Median
Δ: D - M
Median
G
Cumulative frequency
1
0.75
0.5
0.25
0
−0.5
0
0.5
1
Spatial correlation
Shape:
Matching
Different
Color:
Matching
Different
Location:
Different
Shuffled

Appendix 1.2: Supplemental Tables

Table 1S.1: Distribution of mEC cell types across animals. The total number of well-isolated mEC cells recorded from each animal in each paradigm, and number of cells of each functional type. (Top of each box) Total number of cells in the superficial layers. (Bottom of each box) Number of layer II/ layer III cells. Data that were excluded from analysis of the effects of environmental manipulation (i.e., not included in Figs. 2-4) are shaded in red (See methods for details).

Rat ID		A	B	C	D	E	F	G	Total
Total Cells Recorded	Box Shape	32 8/24	14 9/5	8 8/0	31 18/13	15 4/11	10 0/10	78 36/42	**188** **83/105**
	Box Color	---	---	---	74 49/25	16 4/12	61 29/32	76 38/38	**227** **120/107**
	Box Location	---	---	---	17 12/5	9 3/6	5 0/5	39 20/19	**70** **35/35**
Grid Cells	Box Shape	5 1/4	6 3/3	2 2/0	0 0/0	7 2/5	4 0/4	7 3/4	**31** **11/20**
	Box Color	---	---	---	1 1/0	7 1/6	21 9/12	9 3/6	**38** **14/24**
	Box Location	---	---	---	0 0/0	3 1/2	2 0/2	3 1/2	**8** **2/6**
Border Cells	Box Shape	3 1/2	2 2/0	0 0/0	4 2/2	0 0/0	2 0/2	7 3/4	**18** **8/10**
	Box Color	---	---	---	7 6/1	1 0/1	7 4/3	3 2/1	**18** **12/6**
	Box Location	---	---	---	2 2/0	0 0/0	1 0/1	1 1/0	**4** **3/1**
Non-Grid Spatial Cells	Box Shape	20 6/14	4 2/2	5 5/0	26 15/11	8 2/6	2 0/2	64 30/34	**129** **60/69**
	Box Color	---	---	---	62 39/23	8 3/5	28 15/13	63 33/30	**161** **90/71**
	Box Location	---	---	---	15 10/5	6 2/4	1 0/1	35 18/17	**57** **30/27**
Non-Spatial Cells	Box Shape	3 0/3	2 2/0	1 1/0	0 0/0	0 0/0	2 0/2	0 0/0	**8** **3/5**
	Box Color	---	---	---	3 2/1	0 0/0	5 1/4	0 0/0	**8** **3/5**
	Box Location	---	---	---	0 0/0	0 0/0	1 0/1	0 0/0	**1** **0/1**
Head Direction Cells	Box Shape	1 0/1	0 0/0	0 0/0	1 1/0	0 0/0	0 0/0	0 0/0	**2** **1/1**
	Box Color	---	---	---	1 1/0	0 0/0	0 0/0	1 0/1	**2** **1/1**
	Box Location	---	---	---	0 0/0	0 0/0	0 0/0	0 0/0	**0** **0/0**

Table 1S.2: Simultaneous ensemble recordings of grid and non-grid spatial cells. For each of the three conditions (shape, color, and location change), each ensemble that includes at least one grid cell that was recorded simultaneously with at least one non-grid spatial cell is shown. Each row lists one ensemble, and ensembles are grouped by animal. If one cell of a type was recorded, the table lists the measurement for that cell. If more than one cell of a type was recorded, the median is listed. Firing rate maps of the ensembles shaded blue are shown in Fig. 1.4A. (Bottom) For each paradigm, the mean and SEM of each column is calculated. Statistical comparisons between the mean for matching environments and the mean for different environments yielded the same pattern of results as for the pooled data (Displacement: Grid cells, Wilcoxon signed-rank matching vs different shape: $z = -3.5$, $p < 0.001$; different color: $z = -2.5$, $p < 0.05$; Non-grid spatial cells, matching vs different shape: $z = -3.5$, $p < 0.001$; different color: $z = -2.5$, $p < 0.05$; Spatial correlation: Grid cells, matching vs different shape: $z = -3.6$, $p < 0.001$; different color: $z = -2.5$, $p < 0.05$; Non-grid spatial cells, matching vs different shape: $z = -3.6$, $p < 0.001$; different color: $z = -2.5$, $p < 0.05$), with more minor differences for grid cells than for non-grid cells for both the shape and color manipulation.

Box Shape	Number of Cells		Median Displacement: Matching (cm)		Median Displacement: Different (cm)		Median Spatial Correlation: Matching		Median Spatial Correlation: Different	
	Grid	Non-Grid Spatial	Grid	Non-Grid Spatial	Grid	Non-Grid Spatial	Grid	Non-Grid Spatial	Grid	Non-Grid Spatial
Rat A	1	2	1.2	15.4	7.3	11.2	0.71	0.53	0.49	0.06
	1	3	3.2	4.8	6.3	43.1	0.79	0.61	0.61	0.36
	1	3	5.4	2.7	4.9	35.9	0.68	0.54	0.58	0.26
	1	5	2.7	6.6	4.6	17.5	0.88	0.68	0.82	0.30
	1	1	1.8	4.5	3.1	33.9	0.86	0.49	0.81	0.09
Rat B	1	1	1.2	3.1	6.5	8.3	0.89	0.77	0.58	0.05
	1	1	3.7	6.2	9.5	53.9	0.86	0.77	0.59	-0.06
Rat C	1	1	1.7	1.3	3.2	22.8	0.86	0.59	0.64	0.08
Rat E	1	1	1.4	4.8	3.4	53.5	0.83	0.81	0.78	0.18
	2	2	1.4	10.1	2.7	26.4	0.92	0.64	0.84	0.37
	3	3	1.6	2.6	5.1	6.4	0.92	0.90	0.81	0.78
Rat F	2	1	2.3	7.5	2.5	32.4	0.86	0.40	0.84	-0.06
Rat G	1	7	3.4	6.5	7.5	11.1	0.88	0.61	0.72	0.29
	2	7	3.3	3.9	5.7	22.7	0.80	0.62	0.57	0.36
	2	6	2.7	2.7	3.4	29.3	0.70	0.59	0.60	0.22
	1	8	3.4	7.6	3.4	19.1	0.79	0.64	0.76	0.28
	1	7	2.9	3.5	3.4	15.3	0.86	0.65	0.81	0.23
Mean	1.4	3.5	2.5	5.5	4.9	26.0	0.83	0.64	0.70	0.22
SEM	0.1	0.6	0.3	0.8	0.5	3.6	0.02	0.03	0.03	0.05

(Table 1S.2 Continued)

Box Color	Number of Cells		Median Displacement: Matching (cm)		Median Displacement: Different (cm)		Median Spatial Correlation: Matching		Median Spatial Correlation: Different	
	Grid	Non-Grid Spatial	Grid	Non-Grid Spatial	Grid	Non-Grid Spatial	Grid	Non-Grid Spatial	Grid	Non-Grid Spatial
Rat D	1	8	0.8	7.5	6.1	30.6	0.70	0.55	0.56	0.15
Rat E	2	1	2.4	18.4	9.9	50.7	0.78	0.41	0.52	0.05
	3	1	4.5	13.0	5.9	53.1	0.87	0.83	0.62	-0.15
Rat G	1	8	4.9	6.1	5.6	17.3	0.54	0.64	0.32	0.23
	3	8	2.8	1.8	4.8	14.9	0.70	0.64	0.36	0.25
	2	6	1.4	3.8	4.6	25.2	0.60	0.68	0.54	0.30
	2	7	1.9	7.3	3.8	20.5	0.62	0.55	0.31	0.20
	1	11	2.2	2.6	3.3	16.9	0.60	0.55	0.35	0.25
Mean	1.9	6.3	2.6	7.6	5.5	28.6	0.68	0.61	0.45	0.16
SEM	0.3	1.3	0.5	2.0	0.7	5.4	0.04	0.04	0.04	0.05

Box Location	Number of Cells		Median Displacement: Matching (cm)		Median Displacement: Different (cm)		Median Spatial Correlation: Matching		Median Spatial Correlation: Different	
	Grid	Non-Grid Spatial	Grid	Non-Grid Spatial	Grid	Non-Grid Spatial	Grid	Non-Grid Spatial	Grid	Non-Grid Spatial
Rat E	1	1	3.5	8.9	36.3	33.9	0.80	0.43	0.05	-0.02
Rat G	1	5	2.0	6.6	23.1	45.4	0.73	0.65	-0.23	0.15
	1	3	3.6	9.2	16.9	36.8	0.60	0.60	-0.10	-0.09
	1	6	1.9	2.8	22.7	40.6	0.79	0.68	-0.05	-0.11
Mean	1.0	3.8	2.8	6.9	24.8	39.2	0.73	0.59	-0.08	-0.02
SEM	0.0	1.1	0.5	1.5	4.1	2.5	0.05	0.06	0.06	0.06

Appendix 1.3: Supplemental Methods

Experimental model and subject details. Data from the dorsal medial entorhinal cortex (mEC) were collected from seven adult male, experimentally naïve, Long Evans rats (Rats A-G) with a preoperative weight of 300-400 g. In one rat (Rat G), mEC data were collected simultaneous with data from the hippocampal CA1 region. In an additional group of three rats (Rats H-J), tetrodes were aimed at mEC and hippocampus but only hippocampal CA1 cells were successfully recorded. In one rat (Rat J), a cannula was also directed at the medial septal area (MSA) for use in a different study, however all data included here were collected prior to any drug infusions. Rats were housed individually and maintained on a 12-h light/dark schedule with lights off at 7:00 am. All behavioral testing occurred during the dark phase and was performed in dim light in dedicated behavioral testing rooms within the laboratory. All experimental procedures were performed as approved by the Institutional Animal Care and Use Committee at the University of California, San Diego and according to National Institutes of Health and institutional guidelines.

Method details. *Surgery:* At the time of surgery, rats were anesthetized with isoflurane (1.5-2.5 % in O_2) and buprenorphine (0.02 mg/kg, S.C.) was administered as an analgesic. A craniotomy was drilled above the right mEC exposing the transverse sinus. A 'hyperdrive' consisting of 14 independently movable tetrodes was implanted 0.5-1.0 mm anterior to the transverse sinus and 4.6-5.2 mm lateral to the midline. In rats G-J, half of the tetrodes were directed towards mEC with the remaining tetrodes directed towards the right hippocampus, and implanted at approximately 4.2 mm posterior and 3.2 mm lateral to bregma, at an angle of approximately 15° anterior. Tetrodes were constructed from 17 µm platinum-iridium (90/10 %)

wire and were plated with a 1.5 % platinum solution to lower impedances to 125-325 kΩ at 1 kHz prior to surgery. In rat J, a stainless steel guide cannula (23 gauge), was directed to the MSA and implanted at 0.6 mm anterior and 1.1 mm lateral to bregma, 4.3 mm ventral to dura, at an angle of 10° lateral (Koenig et al., 2011). The guide cannula was filled with a stainless steel dummy wire (32 gauge) that extended 0.5 mm beyond the cannula.

Behavioral procedures: After one week of recovery from surgery, rats were partially food-deprived to 85 % of free feeding weight and trained to forage for randomly scattered cereal crumbs in an open field enclosure with flexible black walls that could be shaped either as a square (80 x 80 cm) or as a 16-sided polygon (50 cm radius, referred to as a 'circle'). A polarizing white cue card (20 cm wide) was placed on one interior wall. Seven rats (rats D-J) also foraged in a larger square enclosure (100 x 100 cm), located in a second room, with reversible walls colored black on one side and white on the other. A polarizing black and white checkerboard pattern (25 cm wide) was placed on the interior of one wall. Environments were always centered in the same place in the room, and the position of the cue card was kept constant. The recording system, experimenter, and all other external cues within the room were readily visible to the rats.

Rats were trained in blocks of four 10-minute sessions. In the smaller enclosure with flexible walls the box shape was manipulated. Two sessions were conducted with the enclosure shaped as a square and two sessions with the enclosure shaped as a circle ('shape-change paradigm'). For three rats (rats A-C) the order of squares and circles was varied randomly in each block of four sessions and two training blocks of the box shape-change paradigm were conducted each day, separated by six hours. When single units were recorded in both blocks, they were only analyzed for the block in which a larger number of well-isolated clusters were identified. For the remaining seven rats (rats D-J), each block of four sessions was ordered in an ABB'A' design, with the identity of the first session randomized for each block. In addition, these seven rats (rats

D-J) were also trained in a second paradigm, the color-change paradigm. The box appearance was manipulated by conducting two sessions with four black walls facing the inside of the box and two sessions with four white walls facing the inside of the box. The rats that were trained in both paradigms would often perform two blocks in a single day, one in each paradigm. The order of paradigms varied from day to day. As the two paradigms were conducted in different rooms, a comparison across the two was used to evaluate the effect of changing box location. Each of the training paradigms was flanked by 20-minute sleep periods, and rats were given five minutes between sessions to rest in a pot away from the foraging enclosure. Between sessions the floor of the enclosure was cleaned with water. Prior to any electrophysiological recordings, all enclosures were made highly familiar over at least six training days, and rats performing both paradigms had approximately equal exposure to each. Behavioral procedures while recording mEC units were identical to training procedures.

Recordings and single unit identification: Following surgery, tetrodes were gradually advanced towards the superficial layers of mEC. One tetrode remained in the visual cortex and was used as a reference for all recordings. A second tetrode was rapidly advanced through the brain to identify the beginning of mEC, which was marked by the presence of clear theta oscillations in the local field potential (LFP) and strong theta modulation in unit activity. The same tetrode was later advanced through mEC to identify the transition from layer II to layer I, marked by a clear inversion of the phase of LFP theta. The remaining 12 tetrodes were advanced 25 to 160 μm per day through mEC to record single unit activity. Recordings were performed when well-isolated cells could be observed. At the end of each day of recording, tetrodes were advanced so as to avoid multiple recordings of the same cell. All advancements of tetrodes and recordings were performed blind to cell identity, ensuring an unbiased sampling of the functional cell types within mEC. We continued to record units and to advance tetrodes through mEC until

all tetrodes reached layer I. MEC data were collected over 3-12 recording days (mean: 7.1) per animal for the shape-change paradigm and 7-16 recording days (mean: 10.5) per animal for the color-change paradigm. For rats G-J, one of the tetrodes that were implanted above hippocampus remained in the cortex to serve as a local reference. The remaining tetrodes were advanced to the CA1 cell layer. Recordings began when well-isolated cells were simultaneously observed in mEC and CA1. All analyzed CA1 data were collected on a single recording day for each rat.

For recording spikes and local field potentials, hyperdrives were connected through a multichannel, head-mounted preamplifier to a digital Neuralynx recording system. Unit activity was amplified and band-pass filtered between 0.6 kHz and 6 kHz. Spike waveforms above a trigger threshold (35-55 μV) were time-stamped and digitized at 32 kHz for 1 ms. Continuous LFP was recorded from each tetrode, filtered between 0.1 Hz and 900 Hz, and sampled at 2000 Hz. Position data of a red and a green LED located on either side of the head-mounted preamplifier were tracked at 30 Hz by a video camera mounted above the experimental area to determine the rat's *x*-*y* position and head-direction.

Spike sorting was manually performed offline using a customized version of MClust (Redish, A.D. MClust. http://redishlab.neuroscience.umn.edu/MClust/MClust.html) (Mankin et al., 2012). Sleep periods before and after behavioral sessions were used to ensure stability of recorded cells. Only clusters that were deemed by the experimenter as well separated were included in analysis. To quantify the quality of analyzed clusters we calculated the L-Ratio and isolation distance of each (Schmitzer-Torbert et al., 2005). While we did not establish an exclusion threshold for either metric, others have set minimum isolation distances of 5 or 10 cm (Newman and Hasselmo, 2014; Perez-Escobar et al., 2016). Of those clusters that we accepted for analysis, 99.5 % had isolation distances of at least 10 cm. Putative interneurons were identified

and removed from the data set based on an average firing rate above 10 Hz and a peak to valley ratio of the average spike waveform below 1.

Histological analysis of tetrode locations: At the completion of all experiments, rats were given an overdose of sodium pentobarbital and were perfused transcardially with saline and 4 % formaldehyde. Brains were extracted and post fixed for 24 hours before being transferred to a 30 % sucrose solution and allowed to sink. Sagital sections (40 µm) were cut on a freezing microtome and sections through the right mEC and hippocampus were mounted on slides and stained with cresyl violet. Tetrode trajectories through mEC or hippocampus were determined through 3D reconstruction of the sectioned tissue. Based on records of the systematic movement of tetrodes through the brain and the trajectory information, complemented by records of LFP profiles, tetrode locations on each recording day were assigned to either the deep or superficial layers of mEC and to a dorsoventral distance from the parasubiculum border. Any recordings from the deep mEC layers or from the pre- or parasubiculum were removed from the dataset. Along the dorsoventral axis, recording locations of mEC grid and non-grid cells were intermixed with numerous instances of simultaneous recordings of grid and non-grid spatial cells on the same tetrode (69 grid and 71 non-grid spatial cells across 55 recordings). In each rat we also identified the most ventral recording location with an identified grid cell and found that over 85% of the data was recorded from more dorsal regions of mEC. This anatomical intermixing, coupled with the discretized increase in grid spacing from dorsal to ventral (Stensola et al., 2012), suggests that no more than a minor fraction of non-grid spatial cells could be grid cells with spacing large enough to exceed our detection limits.

Data Analysis: *Rate maps.* We constructed firing rate maps in the standard manner by summing the total number of spikes that occurred in a given location bin (5 x 5 cm), dividing by

the total amount of time that the rat occupied the bin, and smoothing with a 5 x 5 bin Gaussian filter with a standard deviation of approximately 1 bin (Koenig et al., 2011):

```
[0.0025  0.0125  0.0200  0.0125  0.0025;
 0.0125  0.0625  0.1000  0.0625  0.0125;
 0.0200  0.1000  0.1600  0.1000  0.0200;
 0.0125  0.0625  0.1000  0.0625  0.0125;
 0.0025  0.0125  0.0200  0.0125  0.0025].
```

Bins that were never within a distance of less than 2.5 cm from the tracked path or with total occupancy of less than 150 ms were regarded as unvisited and were not included in the rate map. To control for possible influences of stationary periods, rate maps were also constructed with periods below a minimum running speed of 5 cm/s excluded. The selection of only high running speed epochs did not result in the reclassification of any mEC cells. Furthermore, the spatial correlation between unthresholded and thresholded maps was high (median correlation: > 0.96), and spatial information values of thresholded maps were 6.8% higher than for unthresholded maps. Thus, we retained the maps with the more conservative estimate of spatial information (i.e., the untresholded maps) for all subsequent analyses. Unless otherwise noted, rate maps for a given cell are shown scaled to the peak firing rate across all four sessions in a recording block. To avoid errors associated with low sampling, cells with a peak rate below 2 Hz in all bins of the four sessions of a block were considered 'silent' and excluded from subsequent analysis (5 of 59 hippocampal cells from the shape-change paradigm and 7 of 69 hippocampal cells from the color-change paradigm).

Speed maps. To identify any local variations in the average running speed we constructed speed maps for each behavioral session. Speed maps were calculated corresponding to rate maps, except that running speed values within each bin were summed and divided by the time spent in each bin.

Firing field boundaries. Firing field boundaries for mEC grid cells and hippocampal place cells were calculated by first generating a reference map for the four sessions of a recording block. The reference map was built by averaging the rate maps of the four 10-min sessions. For recordings from the shape-change paradigm, only the area common to the two shapes (80 x 80 cm) was used to build the reference map. The minimum peak rate to identify a field was 2 Hz for grid cells and 1 Hz for place cells, with a minimum field size of 250 cm^2. A lower minimum peak rate was used for place cells to correct for the fact that some place fields are active in one environmental condition but silent in another, yielding a reduced average firing rate in the reference map (Leutgeb et al., 2005b). Starting from the peak bin, field bounds were defined on the reference map by building contours iteratively outwards until a threshold value of 0.3 times that peak rate was reached. If any peaks above the minimum rate remained, the procedure was repeated. For cells with multiple fields, contours were then recalculated simultaneously for all fields, and the edge of each field was defined as the contour at which the threshold value was reached or where two fields met, whichever came first. These field boundaries from the reference map were then applied to each of the four sessions, and firing statistics were calculated for each identified field in each session. For each field, the mean field rate was taken as the average of all in-field bin rates and the field center was taken as the center of mass (COM) of all firing within the field bound.

Spatial correlation, rate overlap, and population vector correlation. We calculated the spatial similarity between two rate maps (or between a rate map and a speed map) using Pearson's correlation between the firing rates of bins at corresponding locations. Any bins that were unvisited in either map were excluded from the calculation. Firing rate overlap was calculated for each grid or place field as: $1 - \frac{|R1-R2|}{R1+R2}$ where *R1* is the mean in-field firing rate from map 1 and *R2* is the mean in-field firing rate from map 2.

For population vector (PV) correlations, the rate maps of individual cells were stacked into a three-dimensional matrix in which the *x* and *y* axes correspond to spatial location in the environment, and the *z* axis corresponds to cell identity (Leutgeb et al., 2005b). PV correlations were then obtained by calculating, for each *x*-*y* location, the Pearson correlation coefficient for firing rates along the *z*-dimension between pairs of sessions. The correlation coefficients of all spatial bins were then averaged to estimate the population vector correlation for a pair-wise comparison between sessions.

Spatial cross-correlation and population vector cross-correlation. To generate a spatial cross-correlation matrix we calculated the spatial correlation between two rate maps while shifting one of the maps in the *x* and *y* directions for all the combinations of *x*-*y* offsets to generate a matrix of correlation values. When evaluating cell ensembles, a population vector (PV) cross-correlation was performed in which the entire ensemble was shifted together and a PV correlation was calculated for each *x*-*y* offset. For grid cells, ensembles were composed of all grid cells recorded within a single animal. For place cells, ensembles were composed of place cell data pooled across all animals. If an ensemble contained only a single cell a spatial cross-correlation was performed. For displacement calculations, the cross-correlation matrix was normalized to the maximal correlation value and peaks were identified as described above for firing fields, using a minimum peak value of 0.8, a threshold of 0.3, and a minimum size of 250 cm^2. From the identified cross-correlation peaks, map displacement was calculated as the offset of COM of the central most peak from the origin (Fyhn et al., 2007). Whenever displaying PV cross-correlations the total number of cells in the ensemble is noted. If the number of cells is not given adjacent to a cross-correlation matrix, the cross-correlation was performed on the rate maps of a single cell.

Comparisons across sessions. For each manipulation (shape, color, or location) we evaluated the effect on mEC cells relative to a baseline value obtained by taking the

corresponding measurements across repeated recordings in matching boxes. For each block of four sessions (ABB'A'), we compared each condition to its repetition (A to A', B to B'), and averaged the resulting values to yield a single baseline measurement. To measure the effect of shape and color manipulations, we compared across the two pairs of non-adjacent, contrasting conditions (A to B', B to A'), and then averaged these values to yield a single measurement for the effect of the manipulation. For all analyses, rate maps were only compared if at least one of the two maps had a peak rate of at least 2 Hz. For the shape-change paradigm, only the area common to both shapes (80 x 80 cm) was used for calculations. For comparisons of boxes across locations, the square environment from the shape-change paradigm and the black environment from the color-change paradigm were used. Since the color-change box was larger, only the central 80 x 80 cm was used for calculations. As a control for any effects of removing edge firing, an alternative comparison was also made in which rate maps from the color change box were shrunk to 80 x 80 cm in order to maintain firing throughout. Shrinking maps yielded comparable results to cutting out the central 80 x 80 cm so the cutout method was used in all analysis so as to maintain proper spacing of grid fields. When comparing across locations, all rate maps from a given animal were rotated in 90° steps between rooms to determine which rotation of the population yielded the highest average spatial correlation across all cells. For each animal, the ideal rotation across the two rooms was then applied to all rate maps for all analysis between rooms. To determine chance level spatial correlation across distinct box locations, cell identities were permutated such that the rate map of each cell was correlated against the rate map of every other cell, but never against itself. Chance distributions were generated independently for each cell classification (i.e. grid cell rate maps were only permuted with those of other grid cells).

ROC discrimination. To compare the degree of change produced by environmental manipulations to that produced by moving across distinct locations we performed a

discrimination between changes in shape vs location and between changes in color vs location using receiver operating characteristics analysis (ROC). Analyses were performed in Matlab (2015b) using the built in functions 'patternnet' and 'roc'. For each ROC, the area under the curve (accuracy) and d' metric were used to evaluate discrimination quality. To account for stochasticity in training the neural network, ROC was performed 100 times for each comparison and the median accuracy value was used.

Grid score and spatial auto-correlation. To identify grid cells we evaluated the degree of six-fold rotational symmetry in each cell's spatial auto-correlation by calculating a grid score as described previously (Koenig et al., 2011). For each cell, we calculated rate maps as above (Data analysis: *Rate Maps*) but based on a bin size of 2.5 cm. To then generate the spatial auto-correlation matrix we used the same procedure as for the spatial cross-correlation, but now shifted each cell's rate map with respect to itself. From this spatial auto-correlation matrix an annulus that contained the first hexagon of peaks around the center, but excluded the central peak, was extracted. The average correlation value of bins in the annulus was then taken at each angle from the center (i.e., along a 'ray'). These values were rotated in 30 degree steps and correlated to the un-rotated average values. If six-fold symmetry exists, the correlations at 30, 90, and 150 degrees are expected to be low while the correlations at 60 and 120 degrees are expected to be high. A cell's grid score was thus taken as the average difference between the latter and former sets of correlation values.

Border score. To identify border cells we calculated a border score for each rate map, which is a measure of the proportion of firing localized to the edges of an environment as compared to the firing within the middle of the environment (Solstad et al., 2008). We identified firing fields as described above (Data analysis: *Firing field boundaries*) using a minimum firing rate of 2 Hz, a threshold value of 0.3 times the peak field rate, and a minimum field size of 250

cm^2. We then determined the proportion of each wall that was adjacent to a firing field and the value C_M was taken as the maximal extent of a single field along any wall. The mean firing distance d_m was calculated as the average distance to the nearest wall of each bin in the map, weighted by its firing rate and normalized by half of the length of the shortest side of the environment to obtain a fraction between 0 and 1. Border score was calculated as: $b = \frac{C_M - d_m}{C_M + d_m}$ and ranged from -1 for cells with central firing to 1 for cells with firing aligned to walls. Any rate map in which a firing field could not be identified was not assigned a border score.

Spatial information score. To identify cells as spatial we calculated the spatial information per spike for each firing rate map as: $I = \sum_i P_i \frac{R_i}{R} log_2 \frac{R_i}{R}$, where *i* indexes the spatial bins, P_i is the probability of occupancy in each bin, R_i is the mean firing rate in each bin, and R is the mean firing rate across the spatial map (Skaggs et al., 1993). For calculating spatial information of speed maps, the mean running speed was substituted for the mean firing rate.

Within-session correlation. As a secondary metric for identifying cells as spatial we determined the reliability of spatial firing of each cell by calculating a within-session correlation. For each cell in each session, the 10-mins of trajectory and spiking data was cut in half into the first 5 minutes and the second 5 minutes. Firing rate maps were then generated independently for each half of the behavioral session and the two half-session rate maps were correlated. Within-session correlations for speed maps were calculated using identical procedures.

Head-direction mean resultant length. To identify head-direction cells we calculated the mean resultant length (MRL) of the polar plot generated by comparing cell spiking to angular direction of the animal's head. Using angular bins with one degree resolution, the number of spikes was divided by the amount of time spent at each bin. These values were used to generate

polar plots from which the mean angle and MRL of head-direction modulated firing were calculated.

Speed score. To identify cells with speed-related firing rates, we calculated a speed score for each cell. As previously described (Kropff et al., 2015), the speed score for each cell was the Pearson's correlation between the instantaneous running speed and the instantaneous firing rate. Instantaneous running speed was calculated for each camera frame by passing trajectory data through a Kalman filter. Instantaneous firing rate was calculated across all frames in a session by summing the number of spikes that occurred between subsequent frames, dividing by the time between frames, and smoothing with a 250-ms wide Gaussian filter with a standard deviation of 90-ms. Periods below an instantaneous running speed of 2 cm/sec and in the top 5 % of running speeds were excluded from the correlation. Cells with a speed score above 0.15 or below -0.15 were selected as highly speed modulated.

Shuffled distributions. To generate shuffled distributions we drew a single random value from a uniform distribution between 20 and 580 seconds. For each cell in each session we added this value to the timestamp of each individual spike. This shuffling procedure serves to dissociate neuronal spiking from *x-y* position while maintaining any variation in the animal's behavior and any internal spiking statistics. As such, any biases associated with either will be retained in the shuffled data and accounted for. Spike times exceeding the total duration of a session (~600 sec) were wrapped around to the beginning of the session. We then constructed firing rate maps based on the shuffled spike times, and calculated grid scores, border scores, spatial information scores, within-session correlations, and head-direction MRLs as described above. Shuffling was repeated 1000 times for each cell in each session. For the historical, pooled shuffling method of cell identification, the values for each type of score (grid, border, spatial information, and head direction MRL) were pooled over all recordings of all cells to generate each of the score's

shuffled distribution (Langston et al., 2010; Wills et al., 2010). To account for differences in environment size, data were pooled independently for the shape-change and color-change paradigms. The 95th percentile of each score's distribution was taken as the cutoff for the metric and was applied to all cells. For the pooled shuffling method, only information score was used for determining the identity of non-grid spatial cells. Note that this method for identifying mEC cells was only used in Figure 1S.2D. For the single-cell method of cell identification, shuffled values were not pooled across all cells but instead the 95th percentile cutoff for each type of score (grid, border, spatial information, within-session correlation, and head direction MRL) was taken from the distribution of 1000 scores that were obtained from the same cell's shuffled data (see also Figure 1S.2). The single-cell shuffling procedure was used for cell classification throughout the manuscript, with the exception of Figure 1S.2D.

Cell type identification. For each cell we first defined cell identity in each session hierarchically from grid > border > non-grid spatial > head-direction > non-spatial if the corresponding firing metric was above its respective 'cutoff score'. Thus, if a cell's grid score was above the grid score cutoff it was identified as a grid cell for the session. Otherwise, its border score was compared to the border score cutoff and so on until the cell was classified, or it passed no cutoff values and was identified as a non-spatial cell. For identification of non-grid spatial cells, a two-fold criterion was used in which both the cell's spatial information and its within-session correlation had to pass their respective cutoff scores. Note that as a result of the hierarchy, the classification of 'head-direction' signifies a pure head-direction cell (Pure HD), that is, a cell with head-direction specific firing but no conjunctive representation of space (grid, border, or non-grid spatial). We then determined the overall classification for each cell as the category to which the majority of 10-min sessions were assigned. In the event of a tie (e.g. border cell classification in two sessions and non-grid spatial cell classification in two sessions), cells

were assigned as grid > border > non-grid spatial > head-direction > non-spatial. The majority classification was then used for all recordings of a given cell (i.e., a 'grid cell' was classified as a 'grid cell' in every recording session of the same cell). For cells recorded in both the shape-change and color-change paradigms, all eight sessions were considered for classification.

Rate vector comparisons. To compare the firing rate profile of grid fields of a grid cell we determined the mean firing rate of each identified field and collected these values into a vector. The correspondence between fields was maintained across all four sessions in a given block. For grid cells with at least 3 fields, rate vectors were then compared across sessions using Spearman's rank correlation. To compare rate vectors to chance, shuffled firing rate vectors were generated by permuting grid fields across all grid cells such that rate vectors of each grid cell were populated by randomly selected firing rates from the entire population of mean field rates.

Excluded Data. We sought to evaluate the response of mEC cells to manipulations associated with hippocampal rate remapping (Fyhn et al., 2007; Leutgeb et al., 2005b; Lu et al., 2013; Mankin et al., 2012), specifically looking at the behavior of non-grid cells when the grid map remained stable. In one rat we recorded no grid cells during the shape-change paradigm. In another rat the shift in the spatial firing pattern of grid cells during the color-change paradigm was identified as an outlier from the other recordings during manipulations of environmental features based on Tukey's test for outliers. The PV displacement for this rat exceeded a distance of 3*IQR beyond the third quartile of the data set. As we were not able to verify for either of these cases that the grid map remained stable, we excluded these data from analysis of the effects of manipulations of environmental features (Rat D in shape-change: 0 grid cells and 31 non-grid cells; Rat F in color-change: 21 grid cells and 40 non-grid cells).

Quantification and statistical analysis. Evaluation of the effects of box shape, box color, or box location manipulations were made by comparing the effects of each manipulation vs repeated recordings in matching conditions using the Wilcoxon signed-rank test. Spatial correlations across locations were compared to chance distributions using a Mann-Whitney U test. Comparison across mEC cell types (Grid vs Border vs Non-Grid Spatial) or between box manipulations (Shape vs Color vs Location) were made using the Kruskal-Wallis test with Tukey's honestly significant difference (HSD) criterion for post-hoc analysis. If only two cell types were compared, a Mann-Whitney U test was used. Comparison between ensemble averages and the pooled data set were made using a Mann-Whitney U test. Evaluation of the differences between cells with high and low isolation distances and between mEC layer II and layer III subpopulations was made using a Mann-Whitney U test. For statistical comparisons n represents the number of mEC cells, except when evaluating the firing rate of individual grid or place fields where n represents the number of fields. Data centers are presented as medians or as means ± SEM when noted in the figure legend. Statistical comparisons were significant at $p < 0.05$ for two tailed distributions.

Acknowledgements

We thank B. Boublil and M. Wong for technical assistance. Research was supported by National Institute of Health grants MH-100349, MH-102841, the Whitehall Foundation 20130571, and a Walter F. Heiligenberg Professorship to J.K.L, and National Institute of Health grants MH-100354, NS-084324, and NS-086947 to S.L.

Chapter 1, in full, is material as it appears in *Neuron*, 2017, Diehl, Geoffrey W., Hon, Olivia J., Leutgeb, Stefan, and Leutgeb, Jill K. The dissertation author was the primary researcher and author of this paper.

CHAPTER 2: HIPPOCAMPAL CA2 ACTIVITY PATTERNS CHANGE OVER TIME TO A LARGER EXTENT THAN BETWEEN SPATIAL CONTEXTS

Abstract

The hippocampal CA2 subregion has a different anatomical connectivity pattern within the entorhino-hippocampal circuit than either the CA1 or CA3 subregion. Yet major differences in the neuronal activity patterns of CA2 compared to the other CA subregions have not been reported. We show that standard spatial and temporal firing patterns of individual hippocampal principal neurons in behaving rats, such as place fields, theta modulation, and phase precession, are also present in CA2, but that the CA2 subregion differs substantially from the other CA subregions in its population coding. CA2 ensembles do not show a persistent code for space or for differences in context. Rather, CA2 activity patterns become progressively dissimilar over time periods of hours to days. The weak coding for a particular context is consistent with recent behavioral evidence that CA2 circuits preferentially support social, emotional, and temporal rather than spatial aspects of memory.

Introduction

The hippocampal CA fields are subdivided into the CA3, CA2, and CA1 subregions based on unique cytoarchitecture, connectivity, physiology, and gene expression patterns (Kjonigsen et al., 2011; Lein et al., 2005; Lorente De Nó, 1934; Woodhams et al., 1993; Zhao et al., 2001). Standard circuit diagrams of the hippocampal formation include a trisynaptic loop from the entorhinal cortex to the dentate gyrus, from the dentate gyrus to CA3, and from CA3 to CA1, as well as additional direct connections from entorhinal cortex to the dentate gyrus, the

CA3 subregion, and the CA1 subregion. Although it has long been recognized that the hippocampal CA2 subregion is distinct from the other CA subregions in that it receives inputs from the supramammillary nucleus (Cui et al., 2013; Jones and McHugh, 2011; Magloczky et al., 1994; Pan and McNaughton, 2004; Woodhams et al., 1993), it has primarily been considered as a transition zone between CA1 and CA3. However, major differences from CA3 and CA1 in CA2 connectivity within the hippocampal circuit and with entorhinal cortex have recently been described (Cui et al., 2013; Hitti and Siegelbaum, 2014; Kohara et al., 2014; Rowland et al., 2013). Notably, CA2 neurons are strongly excited by distal dendritic inputs from the entorhinal cortex and only weakly activated by CA3 inputs (Bartesaghi and Gessi, 2004; Bartesaghi et al., 2006; Chevaleyre and Siegelbaum, 2010; Kohara et al., 2014; Zhao et al., 2007). Thus, entorhinal information arrives in CA1 via the CA2 pathway in parallel to the direct pathway to CA1 and the indirect pathway through the dentate/CA3 subregions (Figure 2.1A).

In addition to these major differences in connectivity, CA2 is unique among hippocampal subregions in its mechanisms for long-term plasticity and in the baseline membrane properties of its principal cells (Caruana et al., 2012; Chevaleyre and Siegelbaum, 2010; Jones and McHugh, 2011; Pagani et al., 2015; Zhao et al., 2007). Furthermore, behavioral studies support a potentially unique functional role for CA2 in memory by demonstrating that the vasopressin 1b receptor, which is selectively enriched in CA2 neurons (Young et al., 2006), is necessary for social recognition and for discriminating the recency of an event (DeVito et al., 2009; Wersinger et al., 2002). In addition, CA2 has been directly found to be necessary for aggression towards intruders and for social memory (Hitti and Siegelbaum, 2014; Pagani et al., 2015). Neither vasopression 1b receptor knockout nor genetic silencing of CA2, however, affects spatial or contextual memory (DeVito et al., 2009; Hitti and Siegelbaum, 2014; Wersinger et al., 2002).

Major differences in anatomical and functional characteristics between hippocampal subregions do not *a priori* enable predictions of whether or how neural network firing patterns will differ in behaving animals. For example, standard spatial and temporal firing patterns of hippocampal principal cells, such as place fields, theta modulation, and phase precession, are remarkably similar between CA1 and CA3, despite the substantial differences in connectivity and function between these subregions. Differences in neuronal activity patterns between these subregions only become apparent when considering how activity across the entire population of neurons responds to different behavioral situations. For example, when conflicting cues are presented, CA1 cells show a heterogeneous response, with different subpopulations responding to each aspect of an environment or memory task, while the cell population in the CA3 subregion more coherently follows one set of cues (Lee et al., 2004; Leutgeb et al., 2007; Leutgeb et al., 2004; Vazdarjanova and Guzowski, 2004). Additionally, firing patterns change over time in the CA1 population (Ludvig, 1999; Mankin et al., 2012; Manns et al., 2007; Ziv et al., 2013) while they remain more consistent within the CA3 network (Mankin et al., 2012). These differences in population responses indicate that each hippocampal subregion performs specialized computations that, in concert, can support the acquisition and retrieval of the different aspects of episodic memories (Marr, 1971; McNaughton and Morris, 1987; Rolls, 1989; Treves and Rolls, 1994). We thus asked whether the CA2 network might show neuronal coding at the population level that is distinct from CA1 and CA3 and, consistent with behavioral studies (DeVito et al., 2009; Hitti and Siegelbaum, 2014; Wersinger et al., 2002), may show less specialized network coding for spatial compared to temporal aspects of memories.

Results

To examine how time and contextual change effect firing patterns in CA2, we obtained single unit and local field potential recordings in an experimental design in which rats randomly foraged in highly familiar environments in the morning and again, after an interval of 6 hours, in the afternoon (Figure 2.1). Each morning and afternoon block consisted of four 10-min sessions, two in a square and two in a circular enclosure, and the enclosure shapes were presented in random order within each testing block. The identity of hippocampal CA2 cells (n = 62 cells in 5 rats) was tracked for a total of sixteen sessions (Figure 2S.1) from the morning block of one recording day through the afternoon block of the next recording day (i.e., 4 recording blocks with 4 sessions each). The recordings from the CA2 region were simultaneous with recordings from tracked CA1 cells (n = 43 in 4 rats) and/or tracked CA3 cells (n = 42 in 3 rats) (see Table 2S.1 for the number of cells per rat). For the comparisons with CA1 and CA3, we also included additional simultaneous recordings from these two subregions in the same experimental design (n = 46 CA1 cells and 29 CA3 cells in 3 rats; Mankin et al., 2012). Recording locations were confirmed using anatomical criteria and immunohistochemical markers specific for CA2 neurons (Figures 2.1B–C; Figure 2S.2).

We first analyzed the spatial firing patterns of hippocampal cells within each of the sixteen 10-min sessions and, for each cell, averaged across the sixteen sessions. CA2 cells had a higher mean firing rate than either CA1 or CA3 cells (Mann-Whitney U: CA1 vs. CA2, $z = -2.96$, $P = 0.0062$; CA1 vs. CA3, $z = 1.51$, $P = 0.13$; CA2 vs. CA3, $z = 3.43$, $P = 0.0018$; see Table 2S.2 and 2S.3 for detailed statistics for all Mann-Whitney U tests) (Figure 2.2A and 2.2B). However, when considering the peak firing among all spatial locations in the enclosure, there were no differences between subregions (Mann-Whitney U: CA1 vs. CA2, $z = -0.30$, $P = 0.77$; CA1 vs. CA3, $z = 2.09$, $P = 0.087$; CA2 vs. CA3, $z = 2.19$, $P = 0.087$) (Figure 2.2C). A higher

Figure 2.1: Behavioral paradigm and the identification of recording sites in CA1, CA2, and CA3. (A) Schematic of the entorhino-hippocampal circuitry. Dotted lines denote CA2 connections that have recently been described but have not been confirmed in additional anatomical studies (Cui et al., 2013; Hitti and Siegelbaum, 2014; Kohara et al., 2014; Rowland et al., 2013). EC, entorhinal cortex; DG, dentate gyrus; S, subiculum; pp, perforant path; ta, temporoammonic path. **(B)** The hippocampal CA2 area (demarcated by yellow lines) is defined by positive α-actinin-2 immunoreactivity (brown), and cell bodies that are larger and less densely packed than in CA1, as indicated with a cresyl violet counterstain (purple). The locations of all recording tetrode positions along the A–P axis are projected onto a representative section according to their proximal to distal position within each subregion, but note that tetrode placement spans up to 1 mm along the A–P axis. Tetrodes that were more anterolateral were targeted to either CA2 or CA3 while tetrodes that were more posteromedial were targeted to CA1 or CA2. Because the orientation of the dorsal hippocampus is from anteromedial to posterolateral, this strategy resulted in electrode positions in CA1/CA2 and CA3 that were approximately matched for the longitudinal position within the hippocampus. Along the transverse axis, most recordings were in proximal CA1 while few recordings were in distal CA3 (i.e., close to CA2). Although this increased our confidence that CA3 recordings could not have been misassigned to CA2, this resulted in recording sites that were not precisely matched for connectivity between CA3 and CA1, which is strongest from distal CA3 to proximal CA1 (Witter, 2007). **(C)** Tetrode tracks in a section with α-actinin-2 and cresyl violet staining. Overview (left, scale bar = 500 µm) shows tetrode tracks (red oval, CA1; teal oval, CA2) with areas shown at high magnification to the right (red and teal boxes). In CA1 (middle), cell bodies are small, the cell layer is compact, and there is minor co-staining for α-actinin-2 (scale bar = 50 µm). In CA2 (right), cell bodies are larger and less densely packed, and there is strong α-actinin-2 staining in cell bodies and proximal dendrites (white arrowheads; scale bar = 50 µm). See Figure 2S.2 for further illustration. **(D)** Behavioral design. A series of four 10-min random foraging sessions were performed in the morning and again in the afternoon, over multiple days. Each time block consisted of a random sequence of 2 sessions with the recording enclosure in a square configuration and 2 sessions in a circle configuration. Twenty-min rest sessions flanked the behavioral sequence. Single unit recordings commenced after 9–20 days of pretraining (‘Day 1’ indicates the first day of electrophysiological recording).

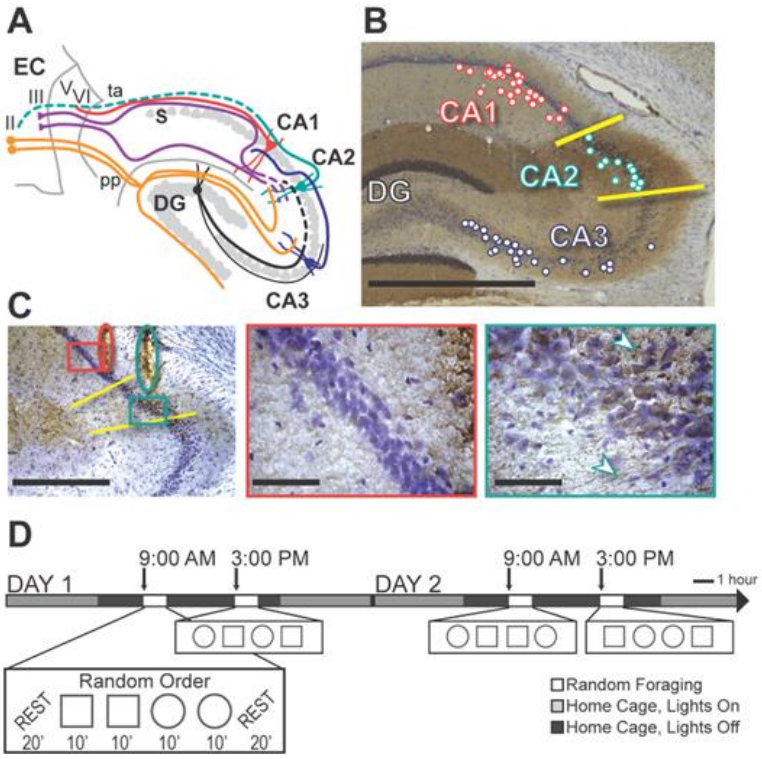
A
EC
III
V
VI
ta
II
S
CA1
CA2
pp
DG
CA3
B
CA1
CA2
DG
CA3
C
D
9:00 AM
3:00 PM
DAY 1
9:00 AM
3:00 PM
DAY 2
1 hour
Random Order
REST
20'
10'
10'
10'
10'
REST
20'
Random Foraging
Home Cage, Lights On
Home Cage, Lights Off

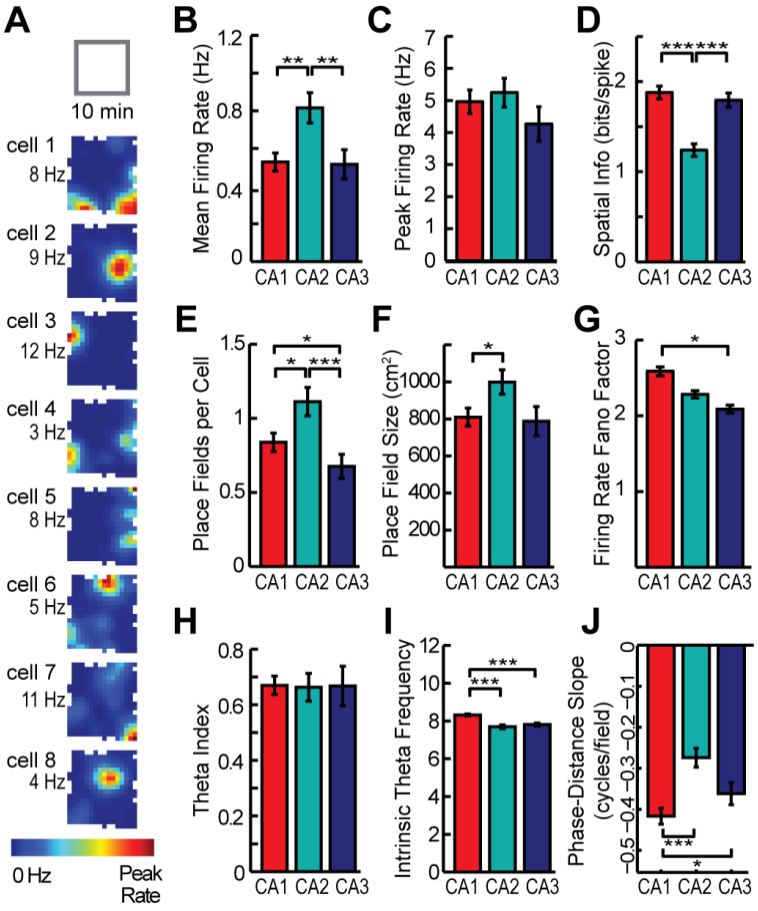

Figure 2.2: The spatial and temporal firing patterns of individual hippocampal CA2 principal neurons in 10-min sessions are largely consistent with those of CA1 and CA3, but with quantitative differences. (A) The firing rate maps of eight CA2 cells that were recorded simultaneously during a 10-min random foraging session in a square-shaped box. Average firing rate in each spatial location is represented from 0 Hz (dark blue) to the peak rate for the cell (red, noted to the left of each map). **(B–F)** Rates were higher and spatial tuning in CA2 was broader than in CA1 and CA3. The broader spatial tuning resulted from an increase in place field size and place field number per cell. **(G)** The variability in firing rate during individual passes through each place field did not differ between CA2 and the other CA subregions. **(H, I)** CA2 cells are modulated by the hippocampal theta rhythm to a similar extent as CA1 and CA2 cells and show intrinsic theta frequency comparable to CA3. **(J)** Place fields in CA2 showed phase precession, but to a lesser degree than in CA1. * $P < 0.05$, ** $P < 0.01$, *** $P < 0.001$ (Mann-Whitney U test). Bars are the mean ± SEM. See Table 2S.2 and text for detailed statistics and Figure 2S.3 for examples of phase precession.

mean rate without a difference in peak rate could emerge from broader spatial firing in CA2 compared to the other hippocampal subregions. Consistent with this notion, the amount of spatial information per cell was lower in CA2 compared to CA1 and CA3 (Mann-Whitney U: CA1 vs. CA2, $z = 5.85$, $P < 0.001$; CA1 vs. CA3, $z = 0.93$, $P = 0.35$; CA2 vs. CA3, $z = -4.95$, $P < 0.001$) (Figure 2.2D). We then asked whether the lower spatial information in the CA2 cell population indicated that many of the CA2 cells were somewhat less spatially tuned or whether the lower average may have emerged from a heterogeneous population of CA2 cells in which some cells remained spatially tuned while others had extremely weak spatial tuning. Of the CA2 principal neurons that were active during any of the recorded 10-min sessions (n = 54 of 62), we found that all had a spatial information score that was higher than 0.75 and place fields smaller than 25 % of the recording enclosure in at least one session, which indicates that each cell showed at least moderate spatial tuning.

To further characterize the spatial firing of CA2 cells, we calculated the number of place fields per cell and the size of each place field. The number of place fields per cell was higher in CA2 compared to the other subregions (Mann-Whitney U: CA1 vs. CA2, $z = -2.37$, $P = 0.035$; CA1 vs. CA3, $z = 2.30$, $P = 0.035$; CA2 vs. CA3, $z = 3.73$, $P < 0.001$) (Figure 2.2E). Because many cells in CA1 and CA3 were either silent during behavior and hence did not have a place field or had only one place field during behavior, this resulted in an average of less than one field per cell in CA1 and CA3. To examine whether a higher proportion of active cells per session in CA2 (CA1, 59.2 %; CA2, 68.2 %; CA3, 48.1 %) may have resulted in the larger number of fields, we restricted the analysis to cells that had at least one place field. Even when considering only cells with at least one field, CA2 had more fields per cell than the other hippocampal subregions (Table 2S.2) (Mann-Whitney U: CA1 vs CA2, $z = -2.85$, $P = 0.0088$; CA1 vs. CA3, $z = 1.49$, $P = 0.14$; CA2 vs. CA3, $z = 3.28$, $P = 0.0032$). When measuring field size, we found that the fields of

CA2 cells were 24.5 % larger than those of CA1 cells (Mann-Whitney U: CA1 vs. CA2, z = −2.54, P = 0.034) (Figure 2.2F). The difference between CA2 and CA3 did not reach statistical significance (Mann-Whitney U: CA2 vs. CA3, z = 2.2, P = 0.053). The less pronounced difference in field size compared to spatial information can be explained by the fact that the reduction of spatial information in CA2 is caused by the combination of a larger number of fields per neuron and an increase in field size. Because field size in CA2 was moderately larger than in CA1, we considered whether the increased field size in CA2 might be a result of slow spatial drift throughout the 10-min recording session. To examine this possibility, we first calculated field size using spatial maps that were obtained from either the first or the second 5-min half of the session. CA2 had larger fields than either CA1 or CA3 even over 5-min periods (Mann-Whitney U: CA1 vs. CA2, z = −2.31, P = 0.042; CA1 vs. CA3, z = 1.94, P = 0.052; CA2 vs. CA3, z = 3.62, P < 0.001). To then directly examine whether fields became larger by drift, we constructed spatial maps from 5 minutes of recording data that were sampled by including either only the odd or only the even minutes of the 10-min recording session. We then compared the field sizes from the continuous 5-min periods with the field size from the interleaved samples over 10 minutes and found no difference (Mann Whitney U: CA1, z = 0.38, P = 0.71; CA2, z = 0.78, P = 0.44; CA3, z = −0.64, P = 0.52). This is evidence that spatial drift on a time scale of minutes does not account for the larger fields in CA2.

After confirming that CA2 fields showed no evidence of greater spatial variability within a 10-min recording session than those in CA1 or CA3, we also examined the variability of the firing rates throughout the session. The variability in the firing rates between passes through the field did not differ between CA2 and the other subregions (Mann-Whitney U: CA1 vs. CA2, z = 1.90, P = 0.11; CA1 vs. CA3, z = 2.85, P = 0.013; CA2 vs. CA3, z = 1.20, P = 0.23) (Figure 2.2G). The standard measurement of variability is not sensitive to a systematic drift in firing rate

throughout the 10-min recording session. We therefore estimated by how much the firing rate within each place field changed between the beginning and the end of a 10-min session, and found that the change was smallest in CA2 (Mann-Whitney U: CA1 vs. CA2, $z = 3.5$, $P = 0.0016$; CA1 vs. CA3, $z = 0.57$, $P = 0.57$; CA2 vs. CA3, $z = -2.4$, $P = 0.033$). Taken together, we found no evidence that place field location or firing rate in CA2 is less stable than in CA1 or CA3 cells during a single 10-minute random foraging session.

We also examined the relationship between firing in CA2 cells and the hippocampal theta rhythm and found that the depth of theta modulation of CA2 cells was not different from CA1 and CA3 (Mann-Whitney U: CA1 vs. CA2, $z = 0.79$, $P = 0.85$; CA1 vs. CA3, $z = 1.28$, $P = 0.60$; CA2 vs. CA3, $z = 0.65$, $P = 0.85$) and that the intrinsic theta frequency of CA2 cells was not different from CA3 (Mann-Whitney U: CA2 vs. CA3, $z = -0.36$, $P = 0.72$) though slower than in CA1 (Mann-Whitney U: CA1 vs. CA2, $z = 4.75$, $P < 0.001$). To determine to what extent the phase at which cells fire within the theta cycle precesses during running through the place field, we calculated the slope of the phase-distance relationship for each place field (O'Keefe and Recce, 1993). The slopes of CA2 fields were significantly less than 0 (sign test: $n = 53$, sign = 4, $P < 0.001$), indicating that the majority of CA2 place cells phase precessed, although the magnitude of the precession was less than in CA1 (Mann-Whitney U: CA1 vs. CA2, $z = -4.97$, $P < 0.001$). This difference is consistent with the well-established relation between a larger field size and a less pronounced phase precession (Shen et al., 1997). The difference in phase precession between CA2 and CA3 did not reach statistical significance (Mann-Whitney U: CA2 vs. CA3, $z = 1.84$, $P = 0.066$) (Figure 2.2H–J and Table 2S.2; see Figure 2S.3 for examples of phase precession plots from individual CA2 fields).

After finding that CA2 cells had the basic firing characteristics of hippocampal place cells with only minor quantitative differences during single 10-min random foraging sessions, we

asked whether CA2 ensembles exhibited additional population coding features that are typical of neural networks in CA1 and CA3 and next analyzed neuronal activity patterns during the four recording sessions within a block, two in a square enclosure and two in a circular enclosure (Figure 2.3A). As expected (Leutgeb et al., 2005c; Lever et al., 2002; Muller and Kubie, 1987), the activity patterns of CA1 and CA3 cells were distinct between these contexts. However, the shape preference of CA2 cells was considerably lower than in the other CA regions (Mann-Whitney U: CA1 vs. CA2, $z = 7.59$, $P < 0.001$; CA1 vs. CA3, $z = 0.62$, $P = 0.54$; CA2 vs. CA3, $z = -4.53$, $P < 0.001$) (Figure 2.3B–C; see also Figure 2S.4 for a description of the shape preference score accompanied by individual CA2 examples). Weak discrimination between spatial contexts by hippocampal network activity would typically be a result of unchanged network representations for different box shapes, but could also emerge when there is low baseline reproducibility of activity patterns for repetitions of the same shape. To distinguish between these alternatives, we computed population vector correlations between pairs of sessions (Figure 2.3D). We first tested whether spatial firing patterns were consistent between repeated visits to the same box shape. When selecting two consecutive sessions in the same box shape, CA2 showed activity patterns that were as consistent as in CA1 or CA3 [Mann-Whitney U: CA1 vs. CA2, $U(n1 = 7, n2 = 5) = 4$, $P = 0.091$; CA1 vs. CA3, $U(n1 = 7, n2 = 8) = 26$, $P = 0.87$; CA2 vs. CA3, $U(n1 = 5, n2 = 8) = 13$, $P = 0.71$] (Figure 2.3D–E). However, for repeated sessions in the same box shape that were separated by an intervening session of the other shape, CA2 was less consistent than CA1 or CA3 [Mann-Whitney U, CA1 vs. CA2, $U(n1 = 6, n2 = 4) = 1$, $P = 0.038$; CA1 vs. CA3, $U(n1 = 6, n2 = 4) = 0$, $P = 0.029$; CA2 vs. CA3, $U(n1 = 4, n2 = 4) = 0$, $P = 0.038$]. In fact, at this lag, the coding differences between repetitions of the same context were as pronounced as the coding differences between sessions in different contexts in CA2 [Mann-Whitney U: same shape vs different shape at lag 2, $U(n1 = 4, n2 = 8) = 10$, $P = 0.37$]. This

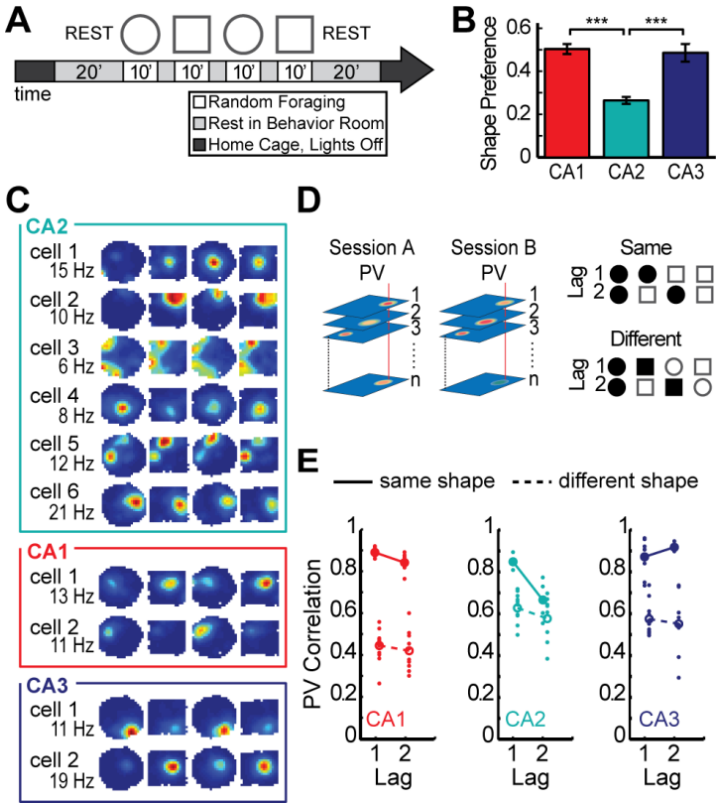

Figure 2.3: Place fields in CA2 are weakly modulated by spatial context. (A) Experimental timeline. Four 10-min sessions of random foraging in a square and a circle-shaped box. **(B)** Place fields in CA2 had lower shape preference scores than fields in CA1 or CA3. See Figure 2S.4 for a description of the shape preference score and individual examples. **(C)** Spatial firing rate maps for six representative CA2 cells and, for comparison, two CA1 cells and two CA3 cells. Maps are color coded as described in Figure 2.2A. CA2 cells 1–4 were recorded simultaneously with CA1 cells 1–2, and CA2 cells 5–6 were recorded simultaneously with CA3 cells 1–2. The changes in the spatial firing patterns of CA2 cells were not correlated with the switching between box shapes. **(D)** The schematic on the left shows how population vectors (PVs) were calculated. The spatial maps of all cells in corresponding sessions were arranged into *x*–*y*–*z* stacks, where *x* and *y* represent the two spatial dimensions and z represents the cell identity. In each stack, the distribution of firing rates along the *z* axis for a given *x*–*y* location represents the population vector for that spatial bin (examples are denoted by the red vertical lines in each stack). To compare two recording sessions, the Pearson correlation coefficient was calculated between each pair of population vectors at corresponding locations, and the correlation coefficients of all spatial bins were averaged. A PV correlation of 1 indicates identical activity patterns and 0 indicates independent patterns. The schematic to the right gives examples of comparisons between pairs of sessions (filled shape symbols) for each time lag in either the same-shape or different-shape category. **(E)** Each pairwise population vector correlation is shown as a dot, and the mean correlation for each lag is shown as a circle (filled, same-shape; open, different-shape). These measures revealed that same-shape comparisons in CA2 were as stable as in CA1 or CA3 only for adjacent sessions (lag 1). *** $P < 0.001$. Symbols and error bars are the mean ± SEM.

suggests that any contextual coding that may be present in CA2 would be masked by temporal changes in network activity, even for intervals as short as 20 minutes.

To examine how time and contextual changes affect firing patterns in CA2 over longer time intervals, we analyzed the full experimental design in which rats randomly foraged in highly familiar environments in the morning and afternoon over 2 days (Figure 2.4A). The similarity between the CA2 population representations in identical enclosure shapes decreased monotonically as a function of the temporal distance between exposures for time intervals up to 18 h and then reached an asymptote of approximately 0.35 [ANOVA: $F(4) = 103.8$, $P < 0.001$; Tukey's HSD: all P-values < 0.001, except 18, 24, and 30 hour time points were not significantly different from each other]. The asymptotic value is larger than the correlation when cell identity was shuffled (> 99.9% of shuffled values for each time point were smaller than the mean of the actual values) (Figure 2.4B–C; see Figure 2S.5 for timescales of up to 60 hours and Figure 2S.6 for example cells from each rat). The time-dependent effect in CA2 was sufficiently pronounced that the amount of change due to time after six hours already exceeded the amount of change produced by distinct spatial contexts without a time lag (see Figure 2.4C). There were no circadian fluctuations in CA2 population similarity (Figure 2.4C) or in normalized firing rates (Figure 2S.5), although there was a significant increase of firing rates within each recording block [two-way ANOVA: between blocks, $F(3) = 1.53$, $P = 0.21$; session number within blocks, $F(3) = 5.23$, $P = 0.0014$; Tukey's HSD between session 1 and session 4, $P < 0.01$; all other comparisons, n.s.].

Next, we compared the pattern of population similarity in CA2 with that of CA1 and CA3 in the same behavioral paradigm. The change in neuronal activity as a function of time was more pronounced in CA2 than in either the CA1 or CA3 cell populations [two-way ANOVA: brain region, $F(2) = 1061.1$, $P < 0.001$; time difference, $F(4) = 184.8$, $P < 0.001$; interaction, $F(8) =$

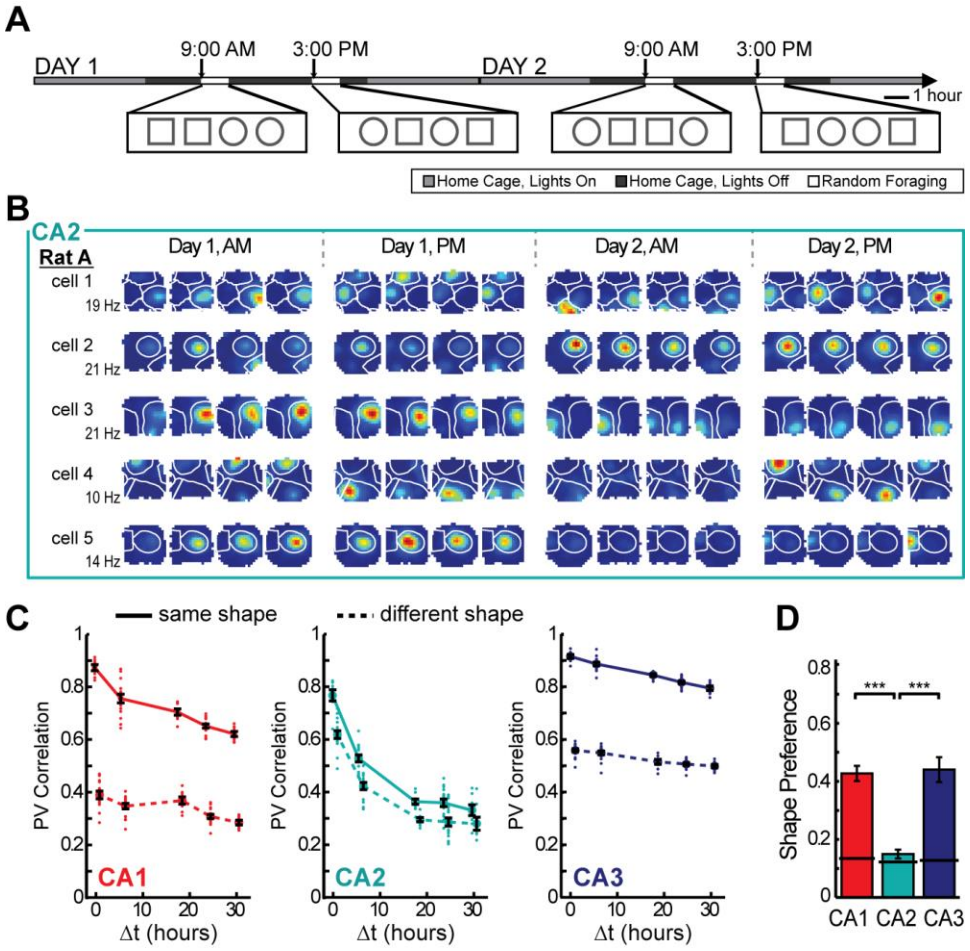

Figure 2.4: Of the three hippocampal CA areas, CA2 is the only one that shows more pronounced change over time than between spatial contexts. (A) To examine the effect of temporal distance on spatial firing patterns in CA2, we recorded CA2 ensembles across two days during four blocks of four 10-min sessions. **(B)** Spatial firing rate maps for five simultaneously recorded CA2 cells. Place field boundaries, calculated from the average of the 16 spatial maps for each cell, are superimposed in white. Note that individual place fields can be off for several sessions before reappearing at the same location and that the firing rates of individual place fields from single cells are modulated independently (see Figure 2S.8). **(C)** The population vector correlation was calculated between pairs of sessions of either the same or different shape, and the comparisons were grouped by the time interval between sessions (Δt). Each dot represents a pairwise comparison, and symbols and error bars represent the mean ± SEM for each time lag. The mean correlations for same shape comparisons are connected by a solid line, while the mean correlations for comparisons between square and circle are connected by a dotted line. **(D)** Place fields in CA2 had lower shape preference scores than fields in CA1 or CA3, and their scores were not different from a shuffled distribution across all 16 sessions (solid black line). See Table 2S.3 and text for detailed statistics, Figure 2S.1 for cluster stability, Figure 2S.5 for additional analysis, and Figure 2S.6 for examples from each rat. *** $P < 0.001$.

24.6, $P < 0.001$; Tukey's HSD between brain regions, $P < 0.001$]. We confirmed that the larger difference in firing patterns with time in CA2 compared to the other hippocampal subregions could not be attributed to the quality of the isolation of single units (Figure 2S.1) and that it was found in all but one single rat (Figures 2S.5 and 2S.6). We also confirmed that the decrease in correlation over time was found irrespective of the number of intervening recording blocks (Figure 2S.5). The passage of time rather than the amount of exposure to the recording environment therefore best explained the difference in the CA2 firing patterns. Finally, we calculated shape preference for each field across all 16 recording sessions, of which eight were in the square and eight were in the circular enclosure. CA2 showed much lower shape preferences than either CA1 or CA3 (Mann-Whitney U: CA1 vs. CA2, $z = 8.16$, $P < 0.001$; CA1 vs. CA3, $z = -0.23$, $P = 0.82$; CA2 vs. CA3, $z = -6.09$, $P < 0.001$), and the shape preference scores in CA2 were not significantly different than scores after randomly shuffling shape identity (only 67.9% of shuffled scores were lower than the actual mean score) (Figure 2.4D; see Figure 2S.4 for individual examples). CA2 is therefore the only hippocampal subregion in which the population code more prominently differs between highly similar experiences at different time points than between different spatial contexts in close temporal proximity.

To determine whether the emergence of inconsistency in coding for the same box shape in CA2 required the intervening experience in a different box shape, we also performed recordings in a paradigm in which all 10-minute random foraging sessions were performed in the same box shape (n = 62 CA1 cells in 4 rats, 34 CA2 cells in 2 rats, and 70 CA3 cells in 2 rats; Figure 2.5A–B, Table 2S.1). In this paradigm, we found that the population vector correlation between sessions within a block was generally lower in CA2 than in the other subregions, but that the correlation decreased in all three hippocampal subregions with an increasing lag [Two-way ANOVA: brain region, $F(2) = 19.8$, $P < 0.001$; lag, $F(2) = 40.1$, $P < 0.001$; interaction, $F(4) =$

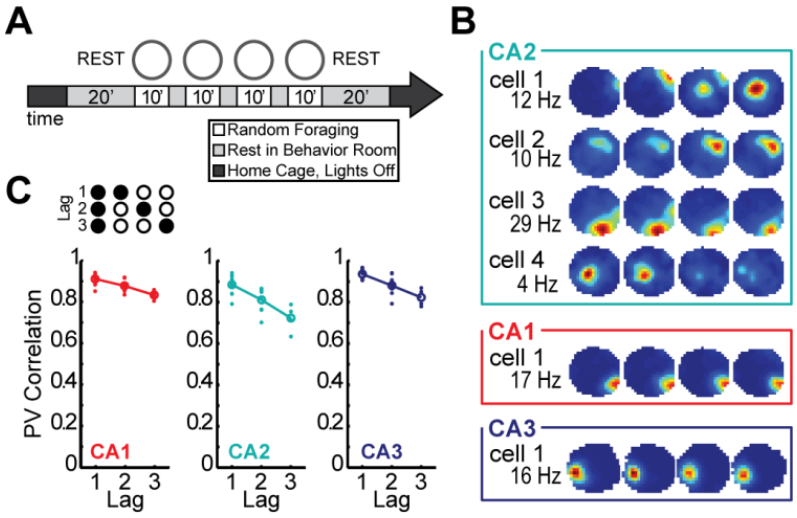

Figure 2.5: In the single-shape paradigm all hippocampal subregions are characterized by a short-term decrease in the correlation of population activity. (A) To determine whether the inconsistency in coding for the same box shape in CA2 required the intervening experience in a different box shape, we performed recordings in a paradigm in which all 10-min random foraging sessions were in the same box shape. **(B)** Spatial firing rate maps for four representative CA2 cells are shown and, for comparison, one representative CA1 and CA3 cell. Maps are color coded as described in Figure 2.2A. Variability in spatial firing patters of CA2 cells occurred despite the consistent repetition of the same box shape over time. **(C)** An increase in the temporal distance between sessions within a block was accompanied by a decrease in the PV correlation in all three subregions, but the overall PV correlation was lowest in CA2. Symbols and error bars represent the mean ± SEM for each time lag. See text for statistics and Figure 2S.7 for additional analysis.

1.73; P = 0.15; Tukey's HSD between CA2 and CA1 and between CA2 and CA3, P < 0.001] (Figure 2.5C). The similar trend for CA1 and CA3 as for CA2 within a block of four recording sessions raised the question whether the more pronounced decline in CA2 compared to the other CA subregions, which we had observed in the two-shape paradigm, would at longer time intervals also emerge in the single-shape paradigm (Figure 2.6A). When comparing CA2 population vectors between blocks of recordings in a single shape, the similarity decreased as a function of the temporal distance between recording sessions for time intervals up to 18 h [ANOVA: F(4) = 202.6, P < 0.001; Tukey's HSD, P-values < 0.001 for all comparisons except comparisons between the 18, 24, and 30 hour time points were n.s.] (Figures 2.6B–D), and the decrease over time was more pronounced in CA2 than in either CA1 or CA3 [Two-way ANOVA: region, F(2) = 1204.2, P < 0.001; time difference, F(4) = 263.5, P < 0.001; interaction, F(8) = 79.5, P < 0.001; Tukey's HSD between brain regions, P < 0.001]. By charting the PV correlations between the first session of each block and all the other sessions within the two-day recording sequence, we could directly compare the population vector correlation within a block with the correlation between blocks (Figure 2S.7). All CA subregions showed a short-term decrease in their correlation within a block. Between blocks, the correlation reset to a higher value in CA3 while it typically continued to decrease in CA2. CA1 was intermediate between CA2 and CA3. The recordings with only a single shape therefore confirmed that CA2 is the hippocampal subregion in which the change of the population code over time periods of hours is most pronounced.

Differences in the CA2 population code over time may result from various sources of variability in the firing patterns, such as from a loss or gain of firing fields, from a drift in place field location, or from rate changes within single firing fields. These possibilities can be distinguished by measuring the number and location of place fields over different time periods (Figure 2.7A). We compared the number of active firing fields of CA2 cells with those of CA1

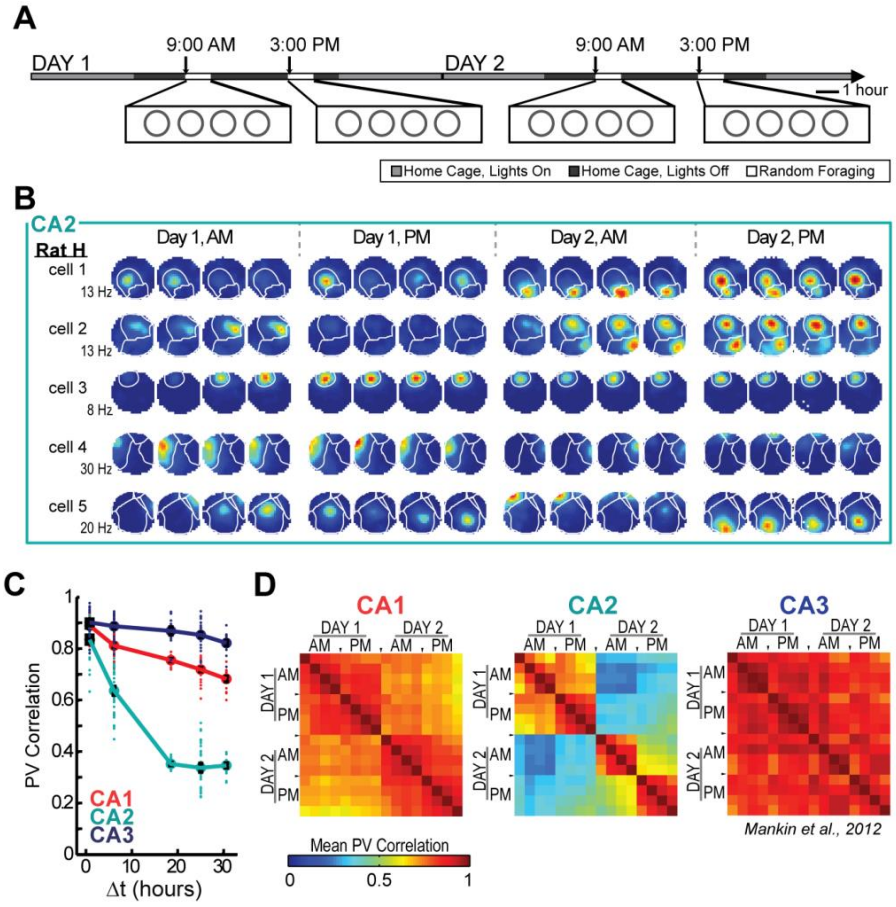

Figure 2.6: The change in population activity over extended time periods was most pronounced in CA2 even when box shape was held constant. (A) To test whether the change in CA2 representations required two spatial contexts or would also be observed during testing in a single context, we recorded cells in only a single environment shape over two days. **(B)** Spatial firing rate maps for five simultaneously recorded cells in CA2 during the single-shape behavioral paradigm, with place field boundaries superimposed (white lines). As in the two-shape paradigm, place fields in CA2 cells appeared, vanished, and could reappear. **(C)** In CA2, the decrease in PV correlation over time reached the same asymptotic level in the single-shape paradigm as in the two-shape paradigm, indicating that the change was predominantly a function of temporal distance and did not require switching between box shapes. In contrast, representations in CA3 have previously been shown to remain highly correlated over longer time intervals. In this paradigm, the CA2 and CA3 recordings are from different animals, and the CA3 recordings correspond to those reported in Mankin et al. (2012). Each dot is a pairwise comparison, and symbols and error bars represent the mean ± SEM for each time interval. **(D)** Pairwise PV correlation matrices for repeated recordings in the same enclosure shape. Correlation matrices depict all possible comparisons between each of the sixteen recording sessions. Comparisons between the same sessions are shown along the diagonal, and their correlation coefficient is, by definition, 1. The lowest correlation coefficients were observed in the CA2 population for comparisons at intervals of at least 18 hours (see Figure 2S.7 for additional plots).

and CA3 cells when averaging over an increasing number of sessions (i.e. one session, a block of four sessions, the eight sessions in a single day, and sixteen sessions over two days). CA1 and CA3 showed no difference in the number of fields over different time periods, whereas in CA2, the mean number of place fields per cell increased for increasingly longer analysis periods [Two-way ANOVA: brain region, $F(2) = 214.1$, $P < 0.001$; time scale, $F(3) = 13.7$, $P < 0.001$; interaction: $F(6) = 4.24$, $P < 0.001$; Tukey's HSD between brain regions, $P < 0.001$] (Figure 2.7B). Furthermore, we found that place fields from a single cell modulated their firing rates independently (Figure 2S.8). Thus, the transient presence and independent modulation of each of the multiple firing fields of CA2 neurons is a source of the decorrelation within the CA2 network over time. In addition, changes in field locations could also cause decorrelation. To test this directly, we estimated the center of each place field in each session and traced the trajectory of the centers across the sixteen 10-min recording sessions in the single-shape experiment. CA2 place field centers drifted considerably more than those in CA1 and in CA3 (Mann-Whitney U: CA1 vs. CA2, $z = -4.61$, $P < 0.001$; CA1 vs. CA3, $z = 1.74$, $P = 0.073$; CA2 vs. CA3, $z = 4.52$, $P < 0.001$) (Figure 2.7C). We therefore detected that both spatial drift and firing rate variability were much higher in CA2 than in the other subregions over long time intervals but not over short time intervals. These findings indicate that a combination of loss or gain of firing fields, changes in firing rate, and moderate drift in precise firing location of CA2 place cells resulted in the substantial change in neuronal activity patterns in the CA2 network over time.

Discussion

The distinct connectivity, gene expression profiles, and cellular plasticity of CA2 (Caruana et al., 2012; Chevaleyre and Siegelbaum, 2010; Cui et al., 2013; Kohara et al., 2014;

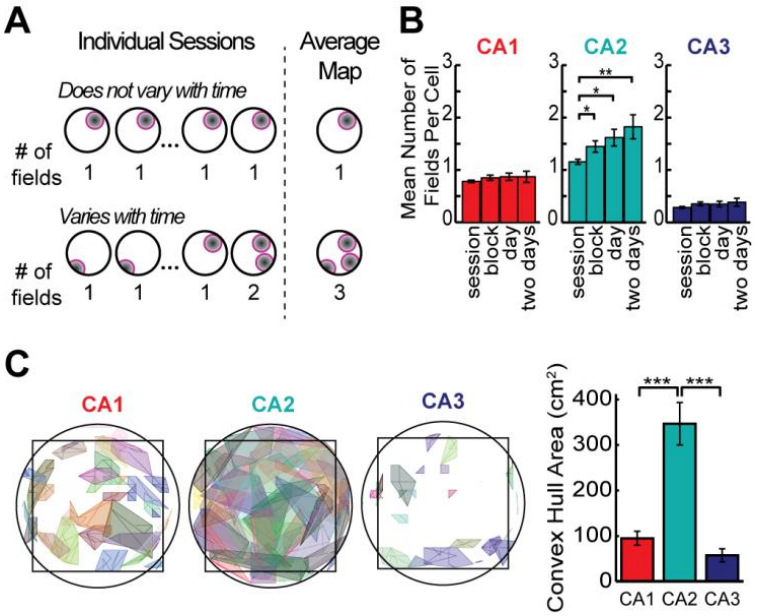

Figure 2.7: Dissimilarity in spatial firing patterns in CA2 emerges from transiently silent firing fields accompanied by a drift in the center of each place field location. (A) The schematic shows that the number of fields in the average firing rate map remains constant over a series of sessions when cells have a consistent place field, but that the number increases when the firing rate switches on and off at multiple place field locations. See Figure 2S.8 for additional analysis of firing rates. **(B)** Number of fields per cell in the single-shape paradigm after averaging over different time periods. In CA2, the number of fields per cell increased when including longer time periods, consistent with the idea that each cell can be transiently active at multiple firing locations (see Figures 2.4, 2.6, and 2S.6 for examples). **(C)** To evaluate the degree to which firing within a place field was retained at a consistent location, place field boundaries were calculated from the average map (over 16 sessions). For each place field, the trajectory of the field center was then tracked across sessions, and the convex hull of the trajectory is shown. The bar graph to the right shows the average area of the fields' convex hulls, which was largest in CA2, indicating that the exact firing distribution within the field varied from session to session. See text for detailed statistics. * $P < 0.05$, ** $P < 0.01$, *** $P < 0.001$. Bars represent the mean ± SEM.

Lein et al., 2005; Pagani et al., 2015; Rowland et al., 2013; Woodhams et al., 1993; Zhao et al., 2007) suggest that its neuronal computations differ from the other hippocampal subregions. To test for specialized neural network activity, we recorded activity patterns from CA2 cells in behaving animals. We found that standard spatial and temporal firing patterns in CA2 at the level of single neurons, such as place fields, theta modulation, and phase precession, are comparable to the other CA fields, with only minor quantitative differences. This confirms a previous report in which differences in location-selective firing between CA2 and CA1 cells were not detected (Martig and Mizumori, 2011). However, when comparing activity patterns during repeated visits to the same environment over extended time periods, major differences in the CA2 firing patterns emerged. Rather than faithfully coding for features of an environment and for differences between environments, as is characteristic of CA1 and CA3, our data show pronounced variability in the spatial firing patterns of CA2 cells over hours and days. The major time dependent differences were a consequence of the fact that CA2 cells could exhibit place fields at multiple locations, of which only a subset was selectively active at any point in time. The firing rates within each of the fields of a CA2 cell varied independently, and each field showed drift around its central firing position. Through these combined changes in the firing patterns of each cell, the population coding of CA2 changed over time, and the amount of change after 6 hours already exceeded the amount of change as a consequence of presenting different environments. Together with behavioral evidence that neither silencing of CA2 nor ablating vasopressin 1b receptors, which are selectively enriched in CA2, impacts performance on spatial and contextual tasks (DeVito et al., 2009; Hitti and Siegelbaum, 2014), this suggests that CA2 is less specialized for representing space and for distinguishing between spatial contexts than the other hippocampal subfields.

The generation of distinct neuronal codes for different contexts is a prominent feature of hippocampal neuronal activity patterns in CA1 and CA3 (Anderson and Jeffery, 2003; Leutgeb et al., 2004; Lever et al., 2002; Muller and Kubie, 1987; Vazdarjanova and Guzowski, 2004). A study using immediate early gene labeling as a marker for neuronal activity in the mouse recently reported that the CA2 region is similar to CA1 and CA3 in that it generates distinct neural codes for two different environments that are presented with an interval of 20 minutes (Wintzer et al., 2014). At temporal distances on the order of minutes and without any intervening experiences, we also found that two different contexts resulted in a more distinct CA2 firing pattern than a repetition of the same context (see Figure 2.3E). However, when we extended our recordings to longer time intervals, the changes in firing patterns with time were much more pronounced than the component of the decorrelation that was context dependent. These major changes over time rather than in response to distinct contexts are contrary to what we observed in the same paradigm in the CA1 and CA3 networks, where network similarity for repeated presentations of the same environment, even over intervals of 30 hours, is higher than for distinct contexts at close temporal proximity (Mankin et al., 2012; see also Figure 2.4C).

The lower stability of CA2 firing patterns could originate from the unique connectivity and physiology of this hippocampal subregion. For example, long-term potentiation (LTP) at the synapses between CA3 and CA2 is not inducible by standard protocols in hippocampal slices while these synapses can be potentiated by neuropeptides (Caruana et al., 2012; Chevaleyre and Siegelbaum, 2010; Pagani et al., 2015; Zhao et al., 2007). In CA1, pharmacological blockade of LTP reduces place field stability while conditions that enhance LTP result in more stable CA1 place fields (Kentros et al., 1998; Kentros et al., 2004). Thus, one source of place field instability in CA2 could potentially be the more limited LTP of inputs from CA3, and stability may increase by peptide release during behaviors that depend on vasopressin 1b receptor activation (DeVito et

al., 2009; Pagani et al., 2015; Wersinger et al., 2002). However, it is currently unknown whether plasticity in CA2 can be modulated during behavior and, because CA3 inputs to CA2 are at baseline already weaker than entorhinal inputs (Chevaleyre and Siegelbaum, 2010), it is uncertain whether modulating plasticity at the CA3 inputs to CA2 would have major effects on CA2 firing patterns. Rather, from the findings that entorhinal inputs to CA2 are strong and that the resting membrane potential of CA2 cells is lower than in other hippocampal subregions (Chevaleyre and Siegelbaum, 2010; Zhao et al., 2007), it appears that CA2 activity may be more directly dependent on the convergence of inputs from entorhinal subdivisions. Medial entorhinal inputs to the hippocampus consist of grid cells, head direction cells, border cells, and nonspatial cells (Hafting et al., 2005; Sargolini et al., 2006; Zhang et al., 2013) while lateral entorhinal inputs are generally less modulated by spatial features than those from the medial entorhinal cortex (Deshmukh and Knierim, 2011; Hargreaves et al., 2005; Tsao et al., 2013). Furthermore, grid cells were found to not be context selective (Fyhn et al., 2007). Taken together, this raises the possibility that the reduced context selectivity and high variability of CA2 firing patterns results from the convergence of spatial and nonspatial entorhinal inputs, which have not been processed by the dentate gyrus and/or CA3. We also observed that CA2 cells can become silent within a particular firing field to only later reemerge at the same location. This observation suggests a stable spatial input over time from either the entorhinal cortex or, alternatively, from CA3, which has weaker input to CA2 (Chevaleyre and Siegelbaum, 2010) but has previously been found to retain consistent spatial representations in the same experimental paradigm (Mankin et al., 2012).

The observation that there is a strong time-varying signal in the CA2 network compared to other hippocampal subregions raises questions about the function of neuronal firing patterns that vary over time within a brain structure that is required for long-term memory. It has been found that noise or variability over time can be used as a neural coding mechanism. For example,

a time-varying signal in memory circuitry has been shown to be necessary in brain circuits for motor learning (Stepanek and Doupe, 2010; Wu et al., 2014). Furthermore, findings in rats and human subjects demonstrate that a time-varying code in the hippocampus and medial temporal lobe can predict subjective estimates of elapsed time, as well as performance on temporal order and sequence memory tasks (Ezzyat and Davachi, 2014; Hsieh et al., 2014; Manning et al., 2011; Manns et al., 2007). These experiments demonstrate that neural drift on a time scale of up to minutes is informative and that gradually changing activity patterns in the hippocampus can be integrated into a neural code that contains memory for temporal context. A particularly clear manifestation of a temporal code are the recently discovered sequence and time cells in the hippocampus, which fire in a stereotyped order while animals are stationary over periods of up to tens of seconds during each delay period (MacDonald et al., 2011; Pastalkova et al., 2008). Here we find a pronounced gradual change in CA2 ensemble activity over intervals of hours, but it remains to be determined whether neuronal firing patterns that fluctuate over this time scale could become repeated. Although there is no theoretical reason why temporal coding with repeated sequences would be limited to a particular time scale, it is likely that sequential neuronal activity on a much longer time scale would require different underlying cellular and circuit mechanisms than the sequential activation of CA1 cells over much shorter intervals. In contrast to a mechanism that relies on fixed sequences to be informative about elapsed time, it is also feasible that the time-varying neuronal firing patterns do not become informative by direct repetition during memory recall, but that it is rather a transition from changing to fixed neuronal firing patterns that supports memory, as has been suggested for neuronal activity in the mouse CA1 subregion (Kentros et al., 2004; Wang et al., 2012).

Alternatively, the CA2 cell population may contribute to memory coding neither by showing a sequence code nor by becoming stable, but by continuing to fluctuate and by thus

providing a unique input pattern to CA1 at different time points. In this coding scheme, the variability over time in CA2 would be a prerequisite for providing temporal context, but it would not by itself constitute the temporal code. Rather, the unique inputs from CA2 would be associated with other stable inputs to CA1, such that CA1 activity patterns at one time differ somewhat from the activity patterns at a later time point. Such convergence of time-varying and stable inputs would provide a time-stamped neural code that differs between similar events at different times while it has higher overlap for events that occurred in close temporal proximity (Estes, 1955; Howard and Kahana, 2002; Raaijmakers and Mensink, 1988). In support of such combinatorial coding, the neural population code in CA1 has previously been identified to gradually vary over intervals of hours to weeks (Mankin et al., 2012; Manns et al., 2007; Ziv et al., 2013) while also faithfully continuing to discriminate between spatial contexts (Mankin et al., 2012). Yet it has not been apparent how reliable representations of different environments could be retained in CA1 while also allowing the network activity in the same cell population to drift over time. We now show that the dissimilarity in CA1 population activity over time is intermediate between CA2 and CA3, and it is known that CA1 receives strong excitatory inputs from both the CA3 and the CA2 subregion (Bartesaghi and Gessi, 2004; Bartesaghi et al., 2006; Chevaleyre and Siegelbaum, 2010; Kohara et al., 2014). This suggests that the CA1 network can integrate and/or compare the consistently precise information about spatial context it receives from CA3 with the slowly changing firing patterns we characterized in CA2 (Figure 2.8). The intermediate response of CA1 could thus indicate that the final processing stage of the hippocampus integrates information from not only CA3 and entorhinal cortex, but also from CA2 such that the stability of the CA1 firing patterns is dynamically regulated to determine the persistence and temporal context of hippocampal memory signals.

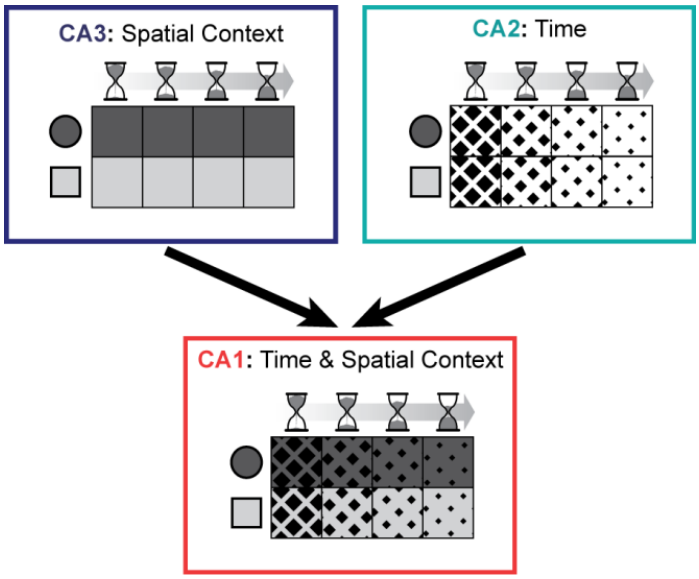

Figure 2.8: A schematic of the coding in CA1, CA2, and CA3 for context and space at different times and how inputs from CA2 and CA3 could be combined to jointly reflect this information in CA1. The two-by-four grid for each hippocampal subregion depicts a population representation for events at different times (left to right) and in different spatial contexts (top and bottom). Firing patterns in CA3 differ depending on context (shades of gray) and firing patterns in CA2 differ depending on elapsed time (diamond size). CA1 shows coding for both aspects, possibly by integrating or comparing inputs from the other hippocampal subregions.

Experimental Procedures

Subjects and surgical procedures. Eight male Long-Evans rats (400–510 g) were implanted with a mulitetrode drive assembly ('hyperdrive') aimed at the right hippocampus (AP 3.9–4.0 mm posterior to bregma, ML 3.0–3.5 mm). Tetrodes were prepared as described previously (Leutgeb et al., 2007) and were placed in the hippocampal cell layer using techniques optimized for recording stability across days (Mankin et al., 2012).

Behavioral procedures. After one week of recovery from surgery, rats were partially food-deprived and trained to forage for randomly scattered cereal crumbs in an enclosure with walls that could be shaped either as a square (80 cm by 80 cm) or as a 16-sided polygon (50 cm radius; referred to as a 'circular enclosure'). Training was performed in two daily blocks. The first block started at approximately 9:00 am and the second block at approximately 3:00 pm. Rats were trained to run for four 10-minute sessions during each block, with two sessions in the square enclosure and two sessions in the circular enclosure, presented in random order. The recording phase of the experiment began after 9 to 20 days of behavioral training. Recordings were first conducted for 2 days in the standard training paradigm (referred to as two-shape, day 1 and day 2). Additionally, a subset of animals was tested in a paradigm in which all random foraging sessions were conducted in a single enclosure shape (single-shape, day 1 and day 2).

Cell-tracking. Because our study depended on tracking the same set of principal neurons over an extended time period, we developed a customized version of MClust (Redish, A.D., http://redishlab.neuroscience.umn.edu/MClust/MClust.html) with added functions that allowed for the comparison of the cluster boundaries of each cell throughout a series of recording sessions. Clusters that persisted in the same region of parameter space throughout two days were

accepted as single cells for further analysis. Care was taken to accept only cells that could be precisely followed from the beginning to the end of the data analysis (Figure 2S.1).

Data Analysis. For tracked cells, we calculated spatial maps and identified place fields. For each place cell and field, we determined standard characteristics (e.g., mean rate, peak rate, spatial information, phase precession), and we analyzed the firing during individual passes through the place field. From the firing rate distribution within the place field in each enclosure shape, we derived a shape preference score (see Figure 2S.4). For the entire population of cells recorded in each subregion, we calculated all pairwise population vector correlations between 10-minute sessions, and grouped them by the elapsed time between sessions and by comparisons between either different shapes or the same shape.

Statistical Analysis. Comparisons between the firing characteristics of hippocampal subregions were performed using the Mann-Whitney U test. Holm-Bonferroni corrections for multiple comparisons were applied to the P-values. Comparisons between population vector correlations over different time intervals were performed using the Mann Whitney U test when there were two conditions and using ANOVA when there were three or more time intervals. If comparisons were between multiple time intervals as well as between brain regions, two-way ANOVA was used. Tukey's HSD method was used for all post-hoc comparisons.

Histology. Tetrode locations were confirmed postmortem in histological material. Immunostaining for α-actinin-2 (i.e., a CA2 marker) (Ratzliff and Soltesz, 2001; Wyszynski et al., 1998) and cresyl violet were used to determine whether the final recording site for each tetrode was in or near the principal cell layers of the CA3, CA2, or CA1 subregion (see Figure 2S.2). Detailed descriptions on cell tracking, data analysis, and histology can be found in Appendix 2.3: Supplemental Methods.

Approvals. All experimental procedures were performed as approved by the Institutional Animal Care and Use Committee at the University of California, San Diego and according to National Institutes of Health and institutional guidelines.

Appendix 2.1: Supplemental Figures

Figure 2S.1: Changes in CA2 activity are not a result of tetrode recording instability over time. (A) Complete experimental timeline. The gray boxes mark sessions that are highlighted in (B-D). **(B)** In each panel, the peak spike amplitude recorded on one channel of a tetrode is plotted against the peak spike amplitude recorded on another channel of the same tetrode. The same two tetrode channels are used for each plot, and different plots correspond to different time points in the experimental timeline as indicated by the gray boxes in (A). Each dot represents one sampled spike, and each dot color represents spikes that were assigned to a cluster. In amplitude plots, clusters are known to be generated by the regularity of the amplitude distribution of extracellular spikes from single cells. After defining clusters for all the recording sessions from one day, the cluster boundaries were applied to data recorded from the same tetrode on subsequent days. If clusters persisted in the same region of parameter space where they had been identified on the previous day, boundaries were adjusted to assure that all spikes that were determined to correspond to a cell were included within the boundaries. If the spikes for the set of clusters of a tetrode could be included with minor adjustments of the boundaries from the day before, the clusters were considered to correspond to the same set of cells as on the previous day, and the cells were included in analysis. Because we occasionally found that cells appeared to turn their spiking activity on or off during a subset of the recorded sessions, it was imperative to confirm that these effects were not simply a consequence of instability in the tetrode location. We thus only included cells in the analysis for which clusters could be identified within the same amplitude space at the beginning of the day (in the first sleep session or the first behavioral session in either shape) and at the end of the day (during the last sleep session or the last behavioral session in either shape). The cluster plots that are depicted correspond to cells 1-4 in Figure 2.4B. **(C)** Average waveforms from the clusters in (B). The color of the waveform matches the color of the corresponding spike cluster. The mean waveform (± standard deviation) is shown for the first behavioral session on the first day (left) and the last behavioral session on the second day (right). **(D)** Spatial maps from the same cells as in (B). The average firing rate in each 5 × 5 cm pixel is color-coded with a color scale from 0 Hz (blue) to the peak rate within the day (red). The peak firing rate for each cell is indicated to the left of the maps. Although spatial maps from tracked cells were not used to determine whether clusters were the same from one day to the next, we visually inspected spatial maps from tracked cells. In CA2, place fields frequently changed over the course of two days, but also reappeared at former locations after extended time intervals. For example, white arrowheads on the maps of Cell 1 indicate one location where a place field was often but not consistently present, including during the first and last behavioral session. This can be taken as further confirmation that the same cell was recorded across both days, even though a different spatial firing pattern appeared during intervening periods. **(E)** For each cell with more than 13 spikes per block, we measured cluster quality with two metrics: L-Ratio and isolation distance. Lower L-Ratios indicate better cluster quality, while higher isolation distances indicate better cluster quality. There was no statistical difference between regions for L-Ratio [Mann-Whitney U: CA1 (n=71 cells) vs. CA2 (n = 50 cells): z = 0.67, P = 1; CA1 vs. CA3 (49 cells): z = 0.74, P = 1; CA2 vs. CA3: z = 0.13, P = 1]. CA2 had moderately lower mean isolation distance compared to CA1 [Mann-Whitney U: CA1 (n=71 cells) vs. CA2 (n = 50 cells): z = 2.54, P = 0.033; CA1 vs. CA3 (n = 49 cells): z = 1.09, P = 0.52; CA2 vs. CA3: z = -1.12, P = 0.52].

(Figure 2.S1 Continued)

(F) (Left) To confirm that differences in population coding between hippocampal subregions could not be attributed to differences in the isolation distance between spike clusters, we separated the cell sample into two groups based on whether each cell's isolation distance was greater than or less than the median isolation distance in that subregion (CA1, 40.6; CA2, 28.9; CA3, 34.5). There was no difference between regions when comparing the mean isolation distance for cell clusters in the lower isolation distance group [Mann-Whitney U: CA1 (n=36 cells) vs. CA2 (n=25 cells): $z = 1.49$, $P = 0.41$; CA1 vs. CA3 (n = 25 cells), $z = 1.40$, $P = 0.41$; CA2 vs. CA3: $z = -0.33$, $P = 0.74$], while CA2 had lower mean isolation distances than the other regions when comparing cells included in the higher isolation distance group [Mann-Whitney U: CA1 (n = 35 cells) vs. CA2 (n = 25 cells): $z = 4.53$, $P < 0.001$; CA1 vs. CA3 (n = 24 cells) $z = 1.10$, $P = 0.27$; CA2 vs. CA3: $z = -2.55$, $P = 0.022$]. These results indicate that CA2 clusters were not considerably less isolated than those in the other subregions, but rather that CA2 had fewer exceptionally well-separated clusters. (Right) Population vector correlations for the same box shape across time (as in Figure 2.4C) are plotted for cells from each group of cluster quality (high quality, connected by solid lines; lower quality, connected by dashed lines) for each region. The PV correlation declined to the greatest extent across time in CA2 regardless of whether we included only the cells with the lowest isolation distances or only the cells with the highest isolation distances [two-way ANOVA for lower isolation distance: brain region: $F(2) = 473.2$, $P < 0.001$; elapsed time: $F(4) = 107.2$, $P < 0.001$; interaction: $F(8) = 21.1$, $P < 0.001$; Tukey's HSD for all comparisons between regions, $P < 0.001$; two-way ANOVA for higher isolation distance: brain region: $F(2) = 631.4$, $P < 0.001$; elapsed time: $F(4) = 67.1$, $P < 0.001$; interaction: $F(8) = 6.9$, $P < 0.001$; Tukey's HSD for all comparisons between regions, $P < 0.001$]. Although the two curves for CA2 differ [two-way ANOVA: cluster quality group, $F(1) = 48.4$, $P < 0.001$; elapsed time, $F(4) = 78.1$, $P < 0.001$; interaction, $F(4) = 1.3$, $P = 0.28$], PV correlation values were lower in the higher isolation distance group than in the lower isolation distance group. Taken together, these findings indicate that the larger change in CA2 population activity over time could not be attributed to poorer cluster quality.

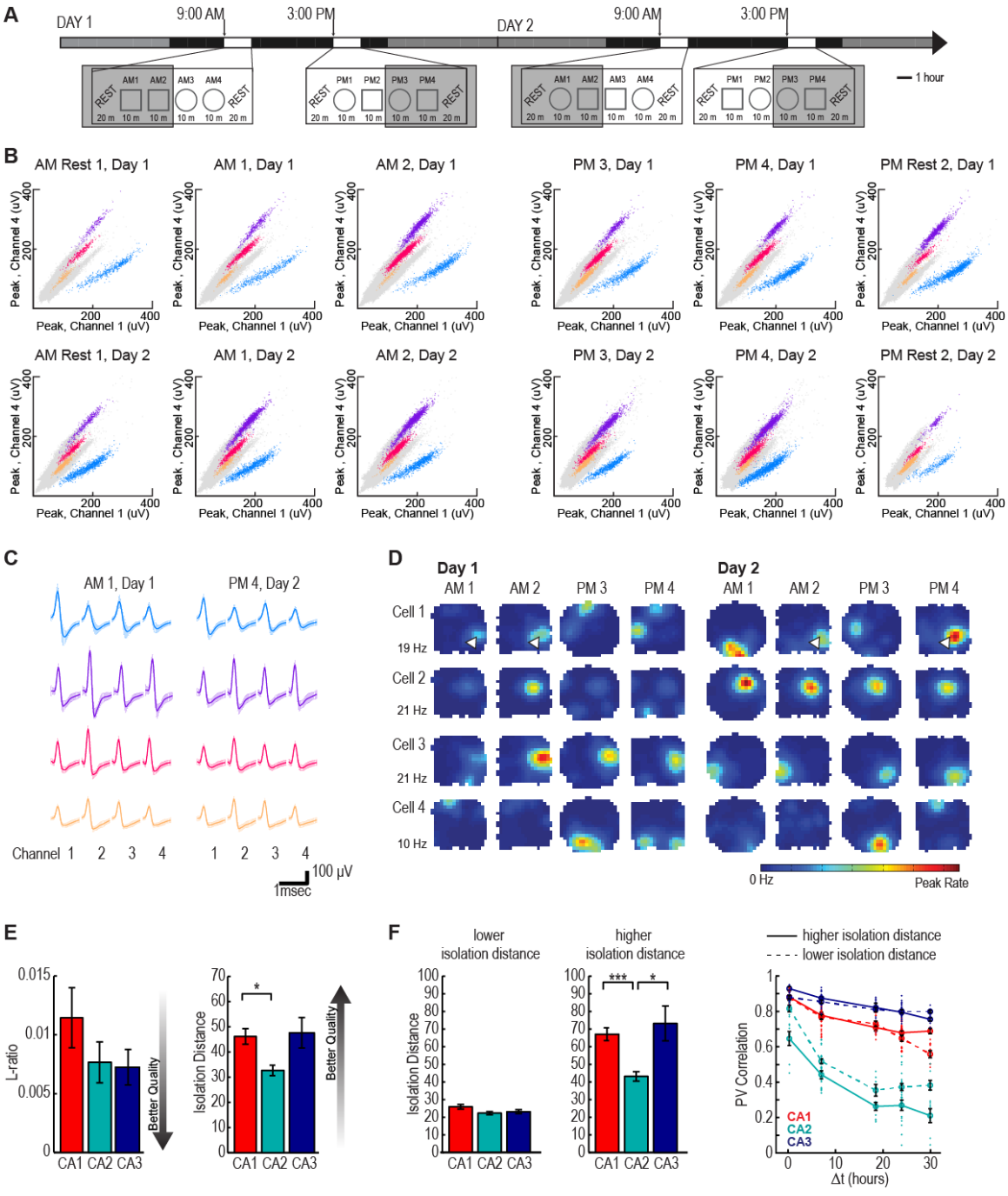
A
DAY 1
9:00 AM
3:00 PM
DAY 2
9:00 AM
3:00 PM
1 hour
REST
AM1
AM2
AM3
AM4
PM1
PM2
PM3
PM4
20 m
10 m
B
AM Rest 1, Day 1
AM 1, Day 1
AM 2, Day 1
PM 3, Day 1
PM 4, Day 1
PM Rest 2, Day 1
AM Rest 1, Day 2
AM 1, Day 2
AM 2, Day 2
PM 3, Day 2
PM 4, Day 2
PM Rest 2, Day 2
Peak , Channel 4 (uV)
Peak, Channel 1 (uV)
C
AM 1, Day 1
PM 4, Day 2
Channel 1 2 3 4
1 2 3 4
100 µV
1msec
D
Day 1
Day 2
AM 1
AM 2
PM 3
PM 4
Cell 1
19 Hz
Cell 2
21 Hz
Cell 3
21 Hz
Cell 4
10 Hz
0 Hz
Peak Rate
E
L-ratio
Better Quality
Isolation Distance
CA1 CA2 CA3
F
lower
isolation distance
higher
isolation distance
Isolation Distance
***
*
higher isolation distance
lower isolation distance
PV Correlation
CA1
CA2
CA3
Δt (hours)

Figure 2S.2: Confirmation of recording sites in each of the hippocampal subregions by using cytoarchitectural and immunohistochemical criteria. (A) Sections were immunostained for α-actinin-2 and counterstained with cresyl violet to compare the boundaries that were defined by each of the methods. Example images were taken along the hippocampal cell layer (20x, scale bar = 200 μm) and were stitched together throughout the region of interest to determine the boundaries between subregions (top: CA1 to CA2; bottom: CA2 to CA3). Through the region of interest delineated by dashed lines, additional images of the CA1 to CA2 cell border are shown at higher magnification (63x, scale bar = 50 μm). The CA2 area (demarcated by teal lines) was defined as the region with the most dense α-actinin-2 immunostaining (brown; see Wyszynski et al., 1998) of cell bodies and proximal dendrites (teal arrows). CA1 and CA3 (demarcated by white lines) were defined as the adjacent areas with weak immunolabeling. In addition, CA1 is characterized by smaller, densely packed cell bodies while CA3 shows larger cell bodies and a large fraction of cells outside of a densely packed inner sublayer. A transition zone between CA1 and CA2 (between the white and teal line) was defined as the area in which the cells were almost as densely packed as in CA1 and in which there was only sparse immunolabeling of cell bodies and dendrites. A transition zone between CA3 and CA2 (between the teal and white line) was defined as the area with larger cell bodies, but few cell bodies outside of the densely packed inner sublayer. **(B)** Cytoarchitectural criteria that matched the criteria from the α-actinin-2/cresyl violet co-staining were used in cresyl violet stained tissue to identify the hippocampal subregions and the transition zones. Only recordings from tetrode tracks (circled in color) that could be confidently assigned to a hippocampal subregion outside of transition zones were used in the analysis, and those in transition zones were excluded (see Figure 2.1B for the final recording locations of cells included in analysis).

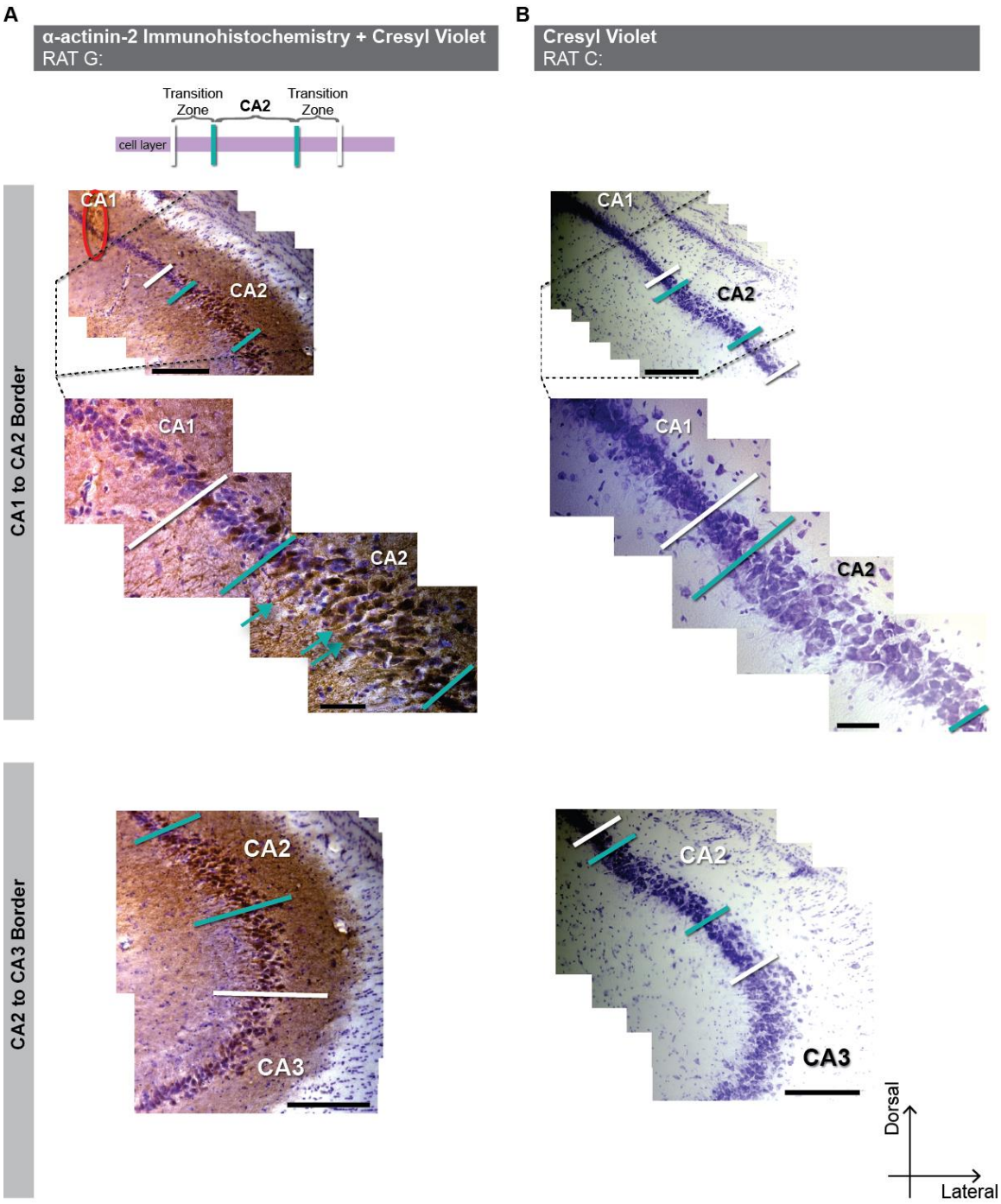
A
α-actinin-2 Immunohistochemistry + Cresyl Violet
RAT G:
B
Cresyl Violet
RAT C:
Transition Zone
CA2
Transition Zone
cell layer
CA1 to CA2 Border
CA2 to CA3 Border
CA1
CA2
CA3
Dorsal
Lateral

Figure 2S.3: Examples of phase precession in CA2 place fields. (A) For each rat, the activity pattern is shown for 2-3 CA2 cells. (Upper left of each panel) Color-coded firing rate map (0 Hz, blue; peak rate, red) with the field boundary superimposed in white. The cell number and session number correspond to cell numbers and session numbers in Figure 2S.6. (Lower left) Spikes within the place field (red dots) superimposed on the rat's trajectories through the field (gray lines). The field boundary is superimposed in black. (Right panel) Scatter plot of the normalized run distance against the theta phase at which each spike occurred. For better visualization, each spike is replotted in a second cycle with the beginning and end of each plotted cycle (0, 1, and 2) representing the trough of the theta cycle recorded in the hippocampal fissure. The regression line is superimposed in blue when the slope is significantly different from 0 ($P < 0.05$) and in gray when n.s., and its slope (in theta cycles/normalized run distance) is reported above each scatterplot. As common for the firing patterns of CA2 cells (Figure 2.2), Cell 2 from Rat H fired action potentials in multiple spatial locations within the environment. Phase precession was found in each of the three fields. Each regression line has a y-intercept between 1.0 and 1.1, which indicates that the phase precession cycle did not continue between fields but rather began at the boundary of each field. **(B)** For comparison, one example cell per rat is shown from either CA3 (rats A-C) or CA1 (rats G-H). Panels are arranged as described in A. Cell number is not indicated, as these cells do not correspond to those in other supplemental figures.

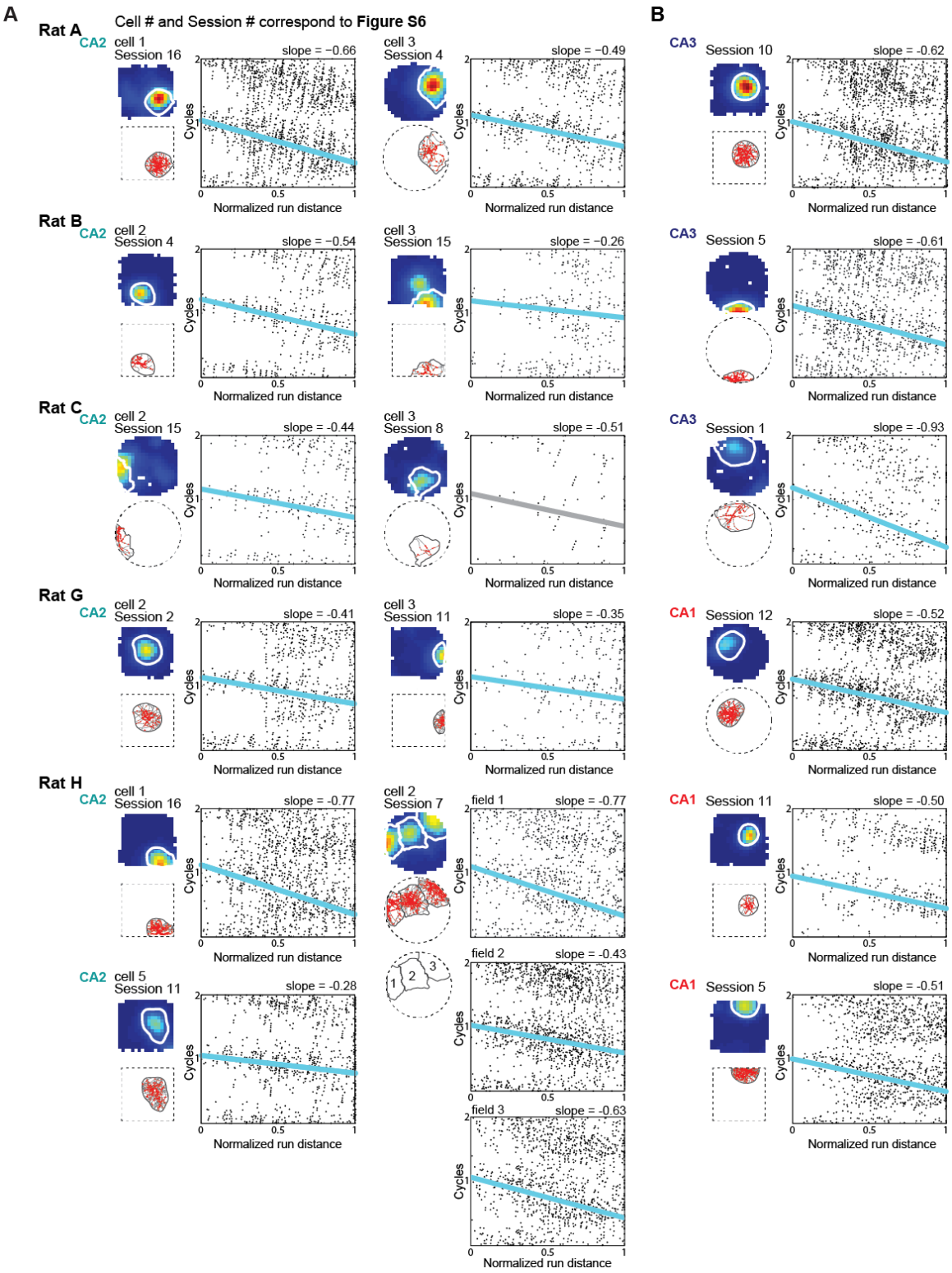
A
Cell # and Session # correspond to Figure S6
Rat A
CA2 cell 1 Session 16 slope = −0.66
cell 3 Session 4 slope = −0.49
Rat B
CA2 cell 2 Session 4 slope = −0.54
cell 3 Session 15 slope = −0.26
Rat C
CA2 cell 2 Session 15 slope = -0.44
cell 3 Session 8 slope = -0.51
Rat G
CA2 cell 2 Session 2 slope = -0.41
cell 3 Session 11 slope = -0.35
Rat H
CA2 cell 1 Session 16 slope = -0.77
cell 2 Session 7 field 1 slope = -0.77
field 2 slope = -0.43
field 3 slope = -0.63
CA2 cell 5 Session 11 slope = -0.28
B
CA3 Session 10 slope = -0.62
CA3 Session 5 slope = -0.61
CA3 Session 1 slope = -0.93
CA1 Session 12 slope = -0.52
CA1 Session 11 slope = -0.50
CA1 Session 5 slope = -0.51
Cycles
Normalized run distance

Figure 2S.4: CA2 cells with low shape preference scores are found in all rats. (A-D) Calculation of shape-preference scores. **(A)** The activity pattern of two example cells (top, CA1; bottom, CA3) are shown for the 16 sessions of the two-day different-shape experiment. For each cell, color-coded firing rate maps (0 Hz, dark blue; peak rate, red) are shown for each 10-minute random foraging session, and the place field boundaries that were calculated from the average of the 16 spatial maps for each cell are superimposed in white. Below each rate map, the firing rate for each pass of the rat through the place field is shown in purple when the enclosure was in the circle configuration and in green when the enclosure was in the square configuration. The running velocity during each pass is plotted downwards in light blue. The presence of a velocity bar without a corresponding firing rate bar indicates passes without spikes. The CA1 cell was silent during the morning of the first day and became active in subsequent sessions, but only when the enclosure was shaped as a square. The CA3 cell exhibited higher firing rates in the circular shape than in the square shape throughout the entire recording sequence. Each cell demonstrated a clear firing rate preference for one of the box shapes, which resulted in a high shape preference score as described in B-D. **(B)** The firing rate distribution for passes through the place field when the box was in a square configuration (left, green) and for passes when the box was in a circle configuration (right, purple). The horizontal axes begin at -2 Hz in order to clearly visualize values at 0. **(C)** Cumulative distribution plots for the firing rates in B. Lines that are farther to the right indicate distributions in which higher rates were more frequent. **(D)** For each pair of firing rate distributions in C, the Receiver Operant Characteristic (ROC) curve was calculated (thick gray line) and the difference between the area under the ROC curve and area under the identity line was calculated (shaded in gray). This value was multiplied by 2, which results in a shape preference score that equals -1 for firing in only the circle, 1 for firing in only the square, and 0 for equal firing in the square and circle. The absolute value of the score measures the magnitude of the preference for either shape. The absolute shape preference score for the example cells is indicated in bold script. The same procedure was followed to calculate within-block absolute shape preference scores, except that only firing rates from sessions within a single block were used and that the scores for each of the four blocks were averaged. **(E)** Firing rate histograms, firing rate distributions, and shape preference scores for three CA2 place fields from each rat (A-G) and for six place fields from rat H. The firing rates correspond to those in the fields in Figure 2S.6 where the rate maps for all 16 sessions are depicted. The color scheme and layout of all plots is as described in A-D. Note that CA2 fields frequently have similar CDFs for each of the shapes, yielding shape preference scores close to 0.

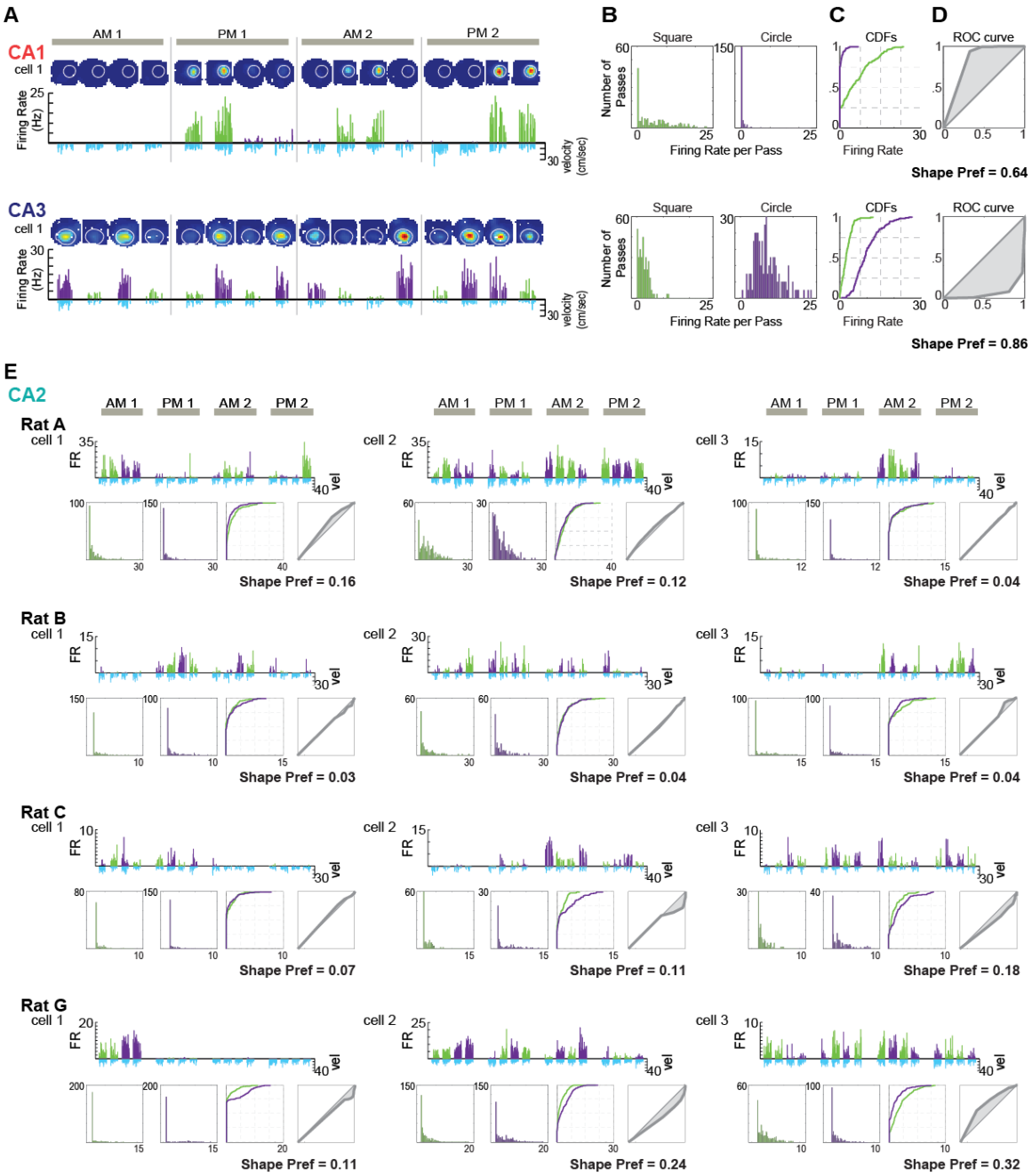
A
AM 1
PM 1
AM 2
PM 2
CA1
cell 1
Firing Rate (Hz)
velocity (cm/sec)
CA3
cell 1
B
Square
Circle
Number of Passes
Firing Rate per Pass
C
CDFs
Firing Rate
D
ROC curve
Shape Pref = 0.64
Shape Pref = 0.86
E
CA2
Rat A
cell 1
cell 2
cell 3
FR
vel
Shape Pref = 0.16
Shape Pref = 0.12
Shape Pref = 0.04
Rat B
Shape Pref = 0.03
Shape Pref = 0.04
Shape Pref = 0.04
Rat C
Shape Pref = 0.07
Shape Pref = 0.11
Shape Pref = 0.18
Rat G
Shape Pref = 0.11
Shape Pref = 0.24
Shape Pref = 0.32

(Figure 2.S4 Continued)

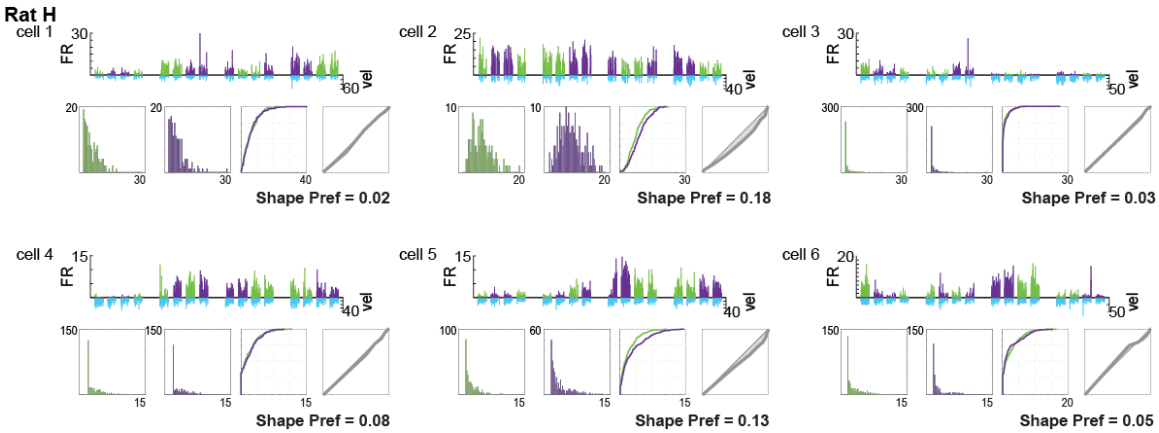

Figure 2S.5: Additional analysis of the similarity in hippocampal firing patterns over time. **(A)** To confirm that an asymptote had been reached in CA2 after approximately one day, we extended hippocampal recordings across three days (see Appendix 2.3: Supplemental Methods). On the third day, all behavioral sessions were shifted by six hours, which makes comparisons for up to 60 hours possible for the population of cells that were tracked across all three days (n = 57 CA1 cells from 5 rats; n = 32 CA2 cells from 2 of 5 rats). **(B)** Population vector correlations between pairs of recordings in the same enclosure shape are shown as dots. Each dot corresponds to a pairwise comparison at the interval that is indicated on the horizontal axis. Symbols and error bars correspond to the mean ± SEM for all comparisons at a particular time interval. Solid black lines represent best exponential fits to the data, and dotted black lines represent best linear fits. The explained variance was higher for the exponential compared to the linear fits in CA1 (R^2 exponential = 0.83, and R^2 linear = 0.81) and CA2 (R^2 exponential = 0.84, R^2 linear = 0.73). For the exponential fit, the time constant for the decay of the PV correlation is 76.3 hours in CA1 and 20.96 hours in CA2. **(C)** A two-way ANOVA on brain region and elapsed time revealed main effects of brain region [$F(1) = 662.1$, $P < 0.001$] and elapsed time [$F(8) = 172.7$, $P < 0.001$], as well as a significant interaction [$F(8) = 9.97$; $P < 0.001$] indicating that the way in which correlation changed with time varied between regions. For each region, a grid of Tukey's HSD comparisons is shown, and darker colors indicate more highly significant differences. Correlation levels in CA2 reached an asymptote by 30 hours. The slower change in CA1 compared to CA2 could be explained by proposing that CA1 integrates the continually changing signal from CA2 with a stable signal from CA3, which would presumably result in an intermediate level of place field stability in CA1 (see Figure 2.8). **(D-E)** Hippocampal CA2 and CA1 population patterns become decorrelated over time irrespective of intervening experience. To determine the possible role of intervening blocks on the population vector decorrelation, we analyzed hippocampal recordings on the third recording day. The 6-hour shift on the third day resulted in blocks between the second and third day that are separated by 24 hours without intervening behavioral testing and by 30 hours with one intervening block. **(D)** Population vector (PV) correlations for comparisons between recordings in the same enclosure shape at intervals of 24 hours or 30 hours (left, CA1; right, CA2). Each comparison between two sessions is shown as a dot, and the symbols and error bars are the mean ± SEM for a time interval. Different numbers of intervening blocks did not result in differences in the degree of decorrelation [comparisons between 0 and 1 intervening blocks at the 24-hour interval: CA1, $t(22) = -2.11$, $P = 0.094$; CA2, $t(22) = -1.07$, $P = 0.60$; comparisons between 1 and 2 intervening block at the 30-hour intervals: CA1, $t(22) = -0.49$, $P = 0.63$; CA2, $t(22) = -0.052$, $P = 0.96$]. **(E)** PV correlations between pairs of recordings in the same enclosure shape. Only comparisons without intervening recording blocks are included. Each comparison between two sessions is shown as a dot, and the symbols and error bars are the mean ± SEM for a time interval. A stronger decorrelation of CA2 population activity compared to CA1 population activity with time was also observed when there were no intervening recording blocks [Two-way ANOVA: brain region, $F(1) = 203.0$, $P < 0.001$; time difference, $F(3) = 125.2$, $P < 0.001$; interaction, $F(3) = 10.9$, $P < 0.001$]. **(F)** The population of neurons that were recorded in CA2 over three days reached asymptote after 30 hours (see B and C) compared to 18 hours in the larger dataset in Figure 2.4C. To test whether this was a result of including a behavioral session that was shifted by 6 hours on Day 3, we analyzed the same population of cells that was used for the analysis in (B) and (C) but only included comparisons for sessions that were recorded on Days 1 and 2. When comparing both data sets, the same level of decorrelation was reached at 30 hours. This result indicates that the variability in the time interval when asymptote was reached in CA2 was due to selecting a different set of animals for the analysis rather than due to selecting a different set of recording days for the analysis.

(Figure 2S.5 Continued)

(G) To further test the variability between individual animals in the two-day, two-shape condition (Figure 2.4), we performed a jackknife procedure in which PV correlations were calculated for sets of cells while leaving out one animal at a time. The mean correlation values for these reduced datasets are shown. In each case, there was a much more substantial decrease in coding similarity with time in CA2 compared to CA1 and CA3, although the decorrelation levels in CA2 after one day (18 to 30 hour intervals) varied from approximately 0.5 to 0.3. Despite the variability in the exact time course and decorrelation level, the full effect size in CA2 was reached within approximately one day (18-30 hrs) for all data sets. **(H)** Because one rat performed the experimental sequence twice with two different sets of independent cells, we also checked whether the observed results would differ substantially if the rat had been excluded (solid lines), or if the set of cells from one or the other repetition had been removed (dashed lines). In each case the decorrelation progressed much more rapidly in CA2 than in CA1, and reached a level between 0.3 and 0.4 in CA2 by 30 hours. **(I)** Finally, we only included CA1 and CA3 ensembles that were recorded simultaneously with CA2 ensembles in the analysis and found a pronounced difference in the rate of decorrelation between CA2 and each of the two other hippocampal subregions [Two-way ANOVA: brain region, $F(2) = 1251.0$, $P < 0.001$; time difference, $F(4) = 167.3$, $P < 0.001$, interaction, $F(8) = 29.6$, $P < 0.001$; Tukey's HSD between brain regions, $P < 0.001$ for each comparison]. **(J)** Firing rates in CA2 did not show circadian fluctuations but varied with recording blocks. The mean ± SEM of the normalized firing rate for all active CA1, CA2, and CA3 principal neurons is shown for each ten-minute recording session across the two-day, two-shape experiment. For each cell, the normalized firing rate was calculated by dividing the average firing rate for each session by that cell's average maximum firing rate throughout all 16 sessions. An ANOVA with day and session as factors did not reveal differences between Day 1 and Day 2 for any of the subregions, which is expected because the recording environments were already highly familiar on the first recording day [CA1: $F(1) = 1.56$, $P = 0.21$; CA2: $F(1) = 0.061$, $P = 0.80$; CA3: $F(1) = 0.035$, $P = 0.85$]. An effect of session identity was not found in CA3 [CA3: $F(7) = 0.36$, $P = 0.92$], was close to significance in CA1 [CA1: $F(7) = 1.97$, $P = 0.055$], and was found in CA2 [$F(7) = 2.41$, $P = 0.019$, Tukey's HSD revealed that the significant differences ($P < 0.05$) were between session 5 and sessions 4 and 8]. This result suggests that the effect was not circadian but that there were firing rate differences between the beginning and the end of recording blocks. An ANOVA with block and session within a block as factors confirmed that normalized firing rates did not vary between blocks in any region [CA1: $F(3) = 1.04$, $P = 0.37$; CA2: $F(3) = 1.53$, $P = 0.21$; CA3: $F(3) = 0.53$, $P = 0.65$] but varied within blocks in CA1 and CA2, but not CA3 [CA1: $F(3) = 3.82$, $P = 0.0097$; CA2: $F(3) = 5.23$, $P = 0.0014$; CA3: $F(3) = 0.21$; $P = 0.89$]. In CA1, sessions 1 and 2 had lower firing rates than session 4 (Tukey's HSD, $P < 0.05$), and in CA2 session 1 had lower rates than session 4 (Tukey's HSD, $P < 0.01$).

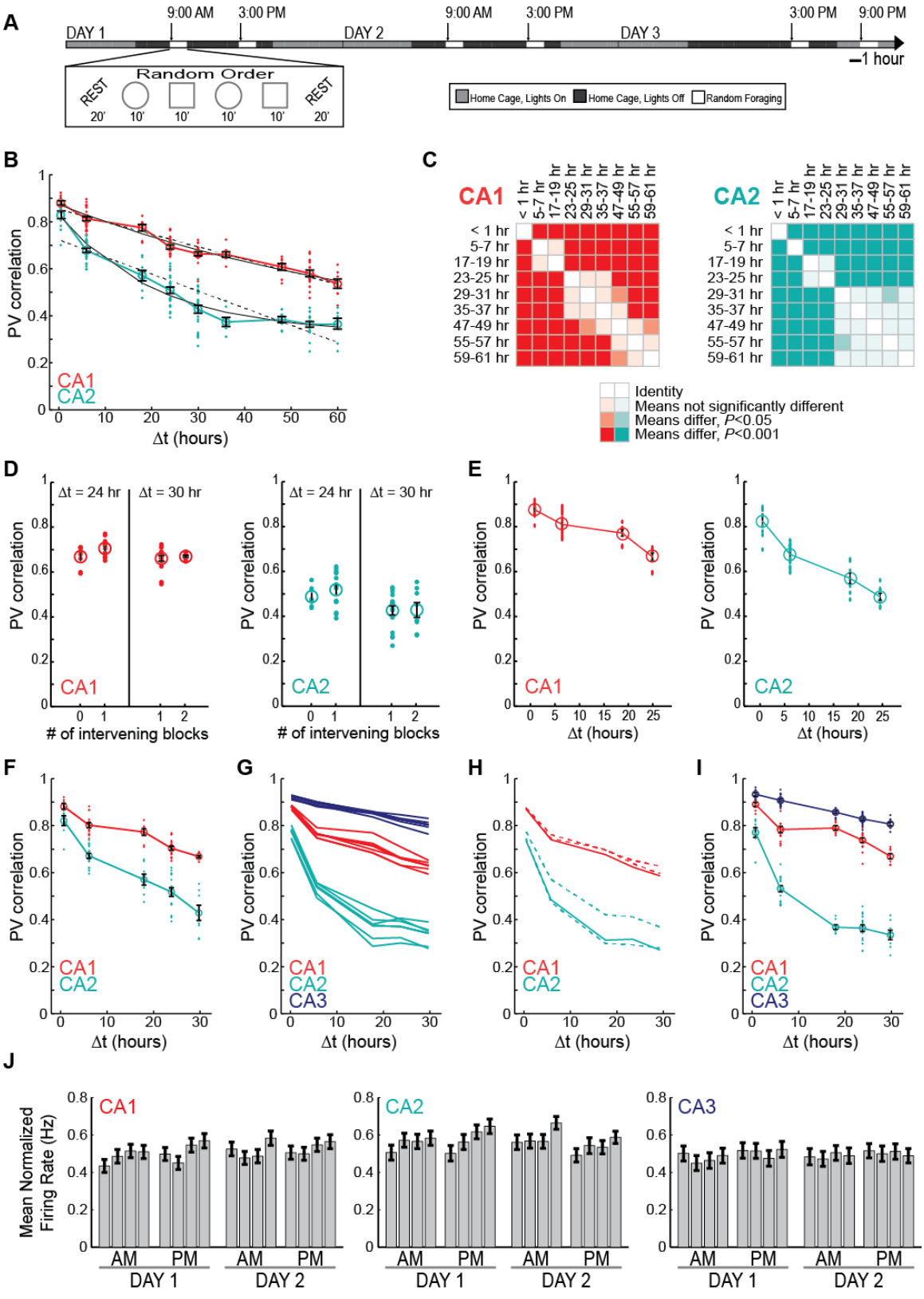
A
DAY 1
9:00 AM
3:00 PM
DAY 2
9:00 AM
3:00 PM
DAY 3
3:00 PM
9:00 PM
1 hour
Random Order
REST
20'
10'
10'
10'
10'
REST
20'
Home Cage, Lights On
Home Cage, Lights Off
Random Foraging
B
PV correlation
Δt (hours)
CA1
CA2
C
CA1
CA2
< 1 hr
5-7 hr
17-19 hr
23-25 hr
29-31 hr
35-37 hr
47-49 hr
55-57 hr
59-61 hr
Identity
Means not significantly different
Means differ, P<0.05
Means differ, P<0.001
D
Δt = 24 hr
Δt = 30 hr
PV correlation
# of intervening blocks
CA1
CA2
E
PV correlation
Δt (hours)
CA1
CA2
F
PV correlation
Δt (hours)
CA1
CA2
G
PV correlation
Δt (hours)
CA1
CA2
CA3
H
PV correlation
Δt (hours)
CA1
CA2
I
PV correlation
Δt (hours)
CA1
CA2
CA3
J
Mean Normalized Firing Rate (Hz)
CA1
CA2
CA3
AM
PM
DAY 1
DAY 2

Figure 2S.6: CA2 cells with profound changes in spatial firing patterns over time were found in each rat. (A) Three example CA2 cells are shown from each animal. (Each row) Color-coded firing rate maps of one cell that was recorded for 16 behavioral sessions throughout the course of the two day experiment. The color scale is from 0 Hz (blue) to peak rate within the entire testing sequence (red, indicated to the left) with pixels not visited in white. For each cell, the place field boundaries were computed on the average map of all 16 sessions in square and circular enclosures. The field boundary for one place field from each cell is highlighted in white. Rat H performed the experimental sequence twice with a unique set of cells during each repetition; cells 1-3 are from the first repetition and cells 4-6 are from the second repetition. **(B)** Mean population vector correlations (as described in Figure 2.4C) for simultaneously recorded cell ensembles from each rat. Pairs of recordings in the same enclosure shape at different time points were compared. The number of cells in the analysis is indicated at the lower left corner of each plot (in parentheses). Red, CA1; teal green, CA2; dark blue, CA3. Brain regions with fewer than 5 cells were not analyzed. The smallest difference between CA1 and CA2 in the population measure was observed in Rat G and cell set 1 of Rat H, nonetheless these recordings had clear examples of multiple cells that changed over time.

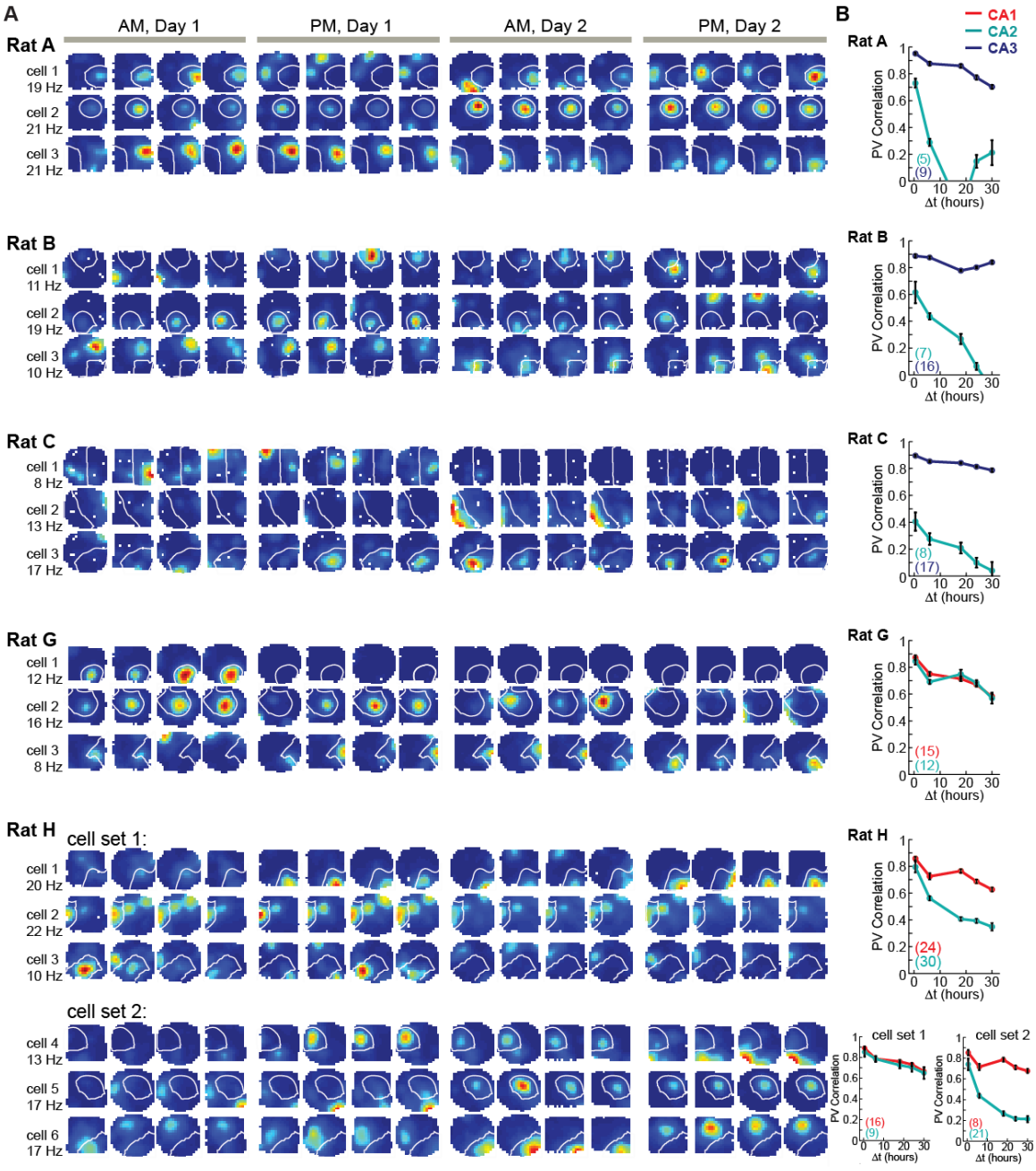
A
AM, Day 1
PM, Day 1
AM, Day 2
PM, Day 2
Rat A
cell 1
19 Hz
cell 2
21 Hz
cell 3
21 Hz
Rat B
cell 1
11 Hz
cell 2
19 Hz
cell 3
10 Hz
Rat C
cell 1
8 Hz
cell 2
13 Hz
cell 3
17 Hz
Rat G
cell 1
12 Hz
cell 2
16 Hz
cell 3
8 Hz
Rat H
cell set 1:
cell 1
20 Hz
cell 2
22 Hz
cell 3
10 Hz
cell set 2:
cell 4
13 Hz
cell 5
17 Hz
cell 6
17 Hz
B
CA1
CA2
CA3
Rat A
Rat B
Rat C
Rat G
Rat H
PV Correlation
Δt (hours)
cell set 1
cell set 2

Figure 2S.7: In the two-day, single-shape paradigm, all three hippocampal subregions show a moderate decorrelation within a recording block, but major differences between subregions emerge over longer time intervals. (A) In the timeline for the two-day single-shape experiment, the first 10-minute session of each AM or PM block is denoted with a lower case letter. **(B)** The complete correlation matrix for each hippocampal subregion is redrawn from Figure 2.6D. Correlation coefficients between sessions are represented on a color scale (0 to 1, dark blue to red). The pixel in the i^{th} row and j^{th} column in the correlation matrix represents the mean Population Vector (PV) correlation between the i^{th} and j^{th} sessions. Consequently, the matrix is symmetric with comparisons between the same sessions along the diagonal (their correlation coefficient is, by definition, 1). The four rows that consist of comparisons with the first session of each block (a-d, see A) are highlighted on the CA3 matrix (black box). **(C)** PV correlations between the first session of each block (a-d) and all other sessions. Each hippocampal subregion is shown in a column (CA3, left; CA2, middle; CA1, right). The time axis represents elapsed time from the beginning of the experiment. In CA2, correlation falls off sharply in either direction from the reference point. In CA3, the PV correlations decrease within a block but reset at the beginning of each block. CA1 is intermediate between CA2 and CA3.

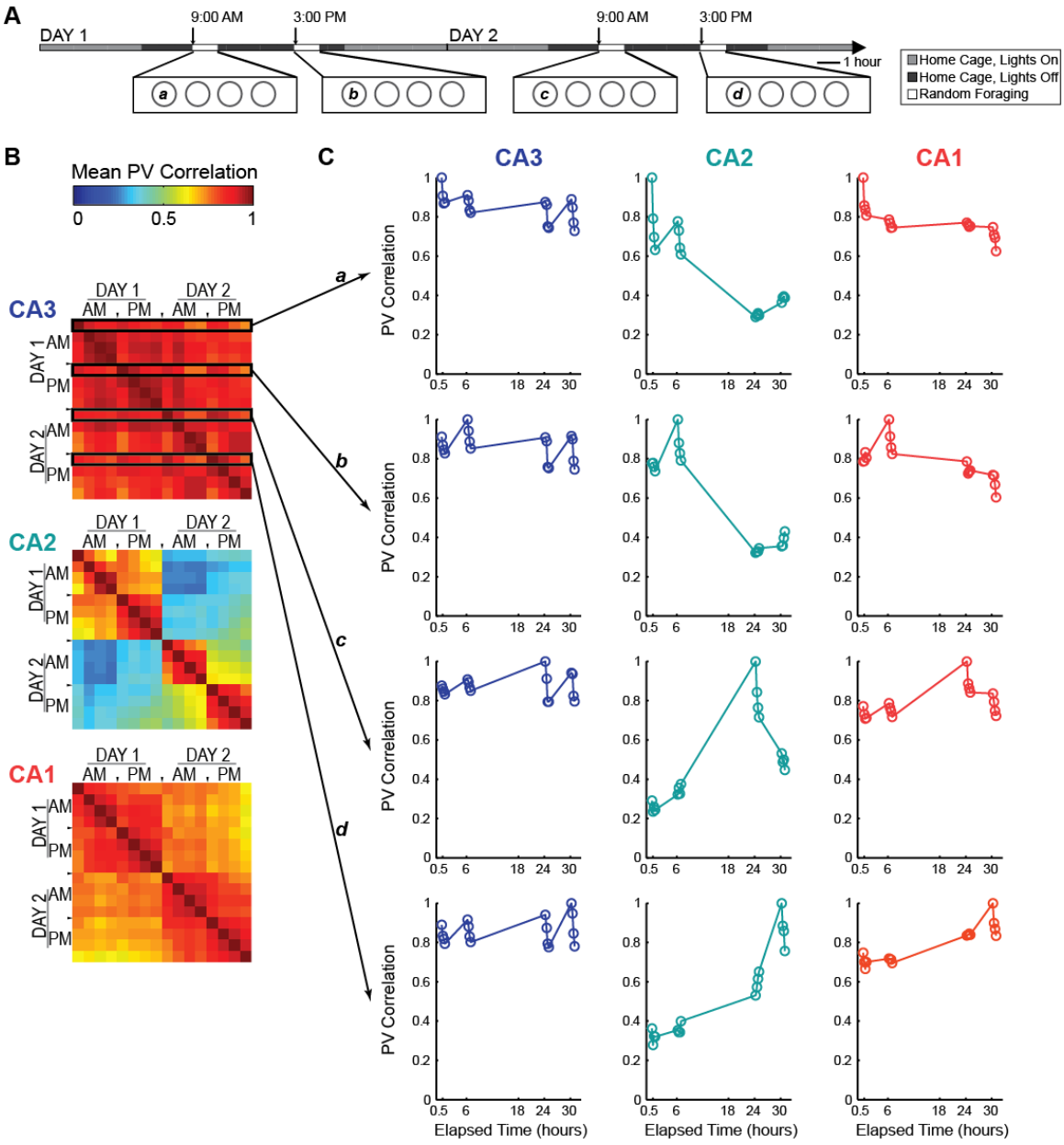
A
DAY 1
9:00 AM
3:00 PM
DAY 2
9:00 AM
3:00 PM
1 hour
a
b
c
d
Home Cage, Lights On
Home Cage, Lights Off
Random Foraging
B
Mean PV Correlation
0
0.5
1
CA3
CA2
CA1
DAY 1
DAY 2
AM
PM
C
CA3
CA2
CA1
PV Correlation
Elapsed Time (hours)
0.5
6
18
24
30

Figure 2S.8: Peak firing rates in place fields of multi-peaked CA2 cells are modulated independently. (A) Five representative CA2 cells with multiple place fields are shown. For each cell, the place field boundaries were computed on the average map of all 16 sessions in square and circular enclosures. In the overview image on the left, the place field with the highest overall peak rate is shown in blue, the place field with the next highest rate is shown in green, and if present, a third place field is shown in red. To the right of the overview image, the firing rate maps of all 16 sessions over 2 days are depicted. Maps are ordered by time, but squares and circles are segregated into separate panels. Thus, sessions that are labeled 1-2 in the line graph were recorded on the morning of day 1, 3-4 were recorded on the afternoon of day 1, 5-6 were recorded on the morning of day 2, and 7-8 were recorded on the afternoon of day 2. For each cell, the peak rate of each place field in each behavioral session is plotted below the corresponding map. Line colors correspond to the place field depicted in the overview. **(B)** The set of 8 firing rates from a single field in each enclosure shape, ordered by time, constitutes a firing rate trajectory. For pairs of fields from the same cell, the Spearman correlation coefficient between firing rate trajectories was calculated. The same calculation was performed for pairs of fields from separate cells within the same subregion. To test whether firing rates in fields of single cells were modulated independently, we compared the distribution of correlation coefficients from within cell comparisons with the distribution of correlation coefficients from distinct cells. In all three CA regions, the distributions did not differ (Kolmogorov-Smirnov test: CA1, $K = 0.05$, $P = 0.76$; CA2, $K = 0.05$, $P = 0.50$; CA3, $K = 0.08$, $P = 0.54$). This indicates that the firing rates of individual place fields of the same cell are modulated as independently as firing fields from different cells.

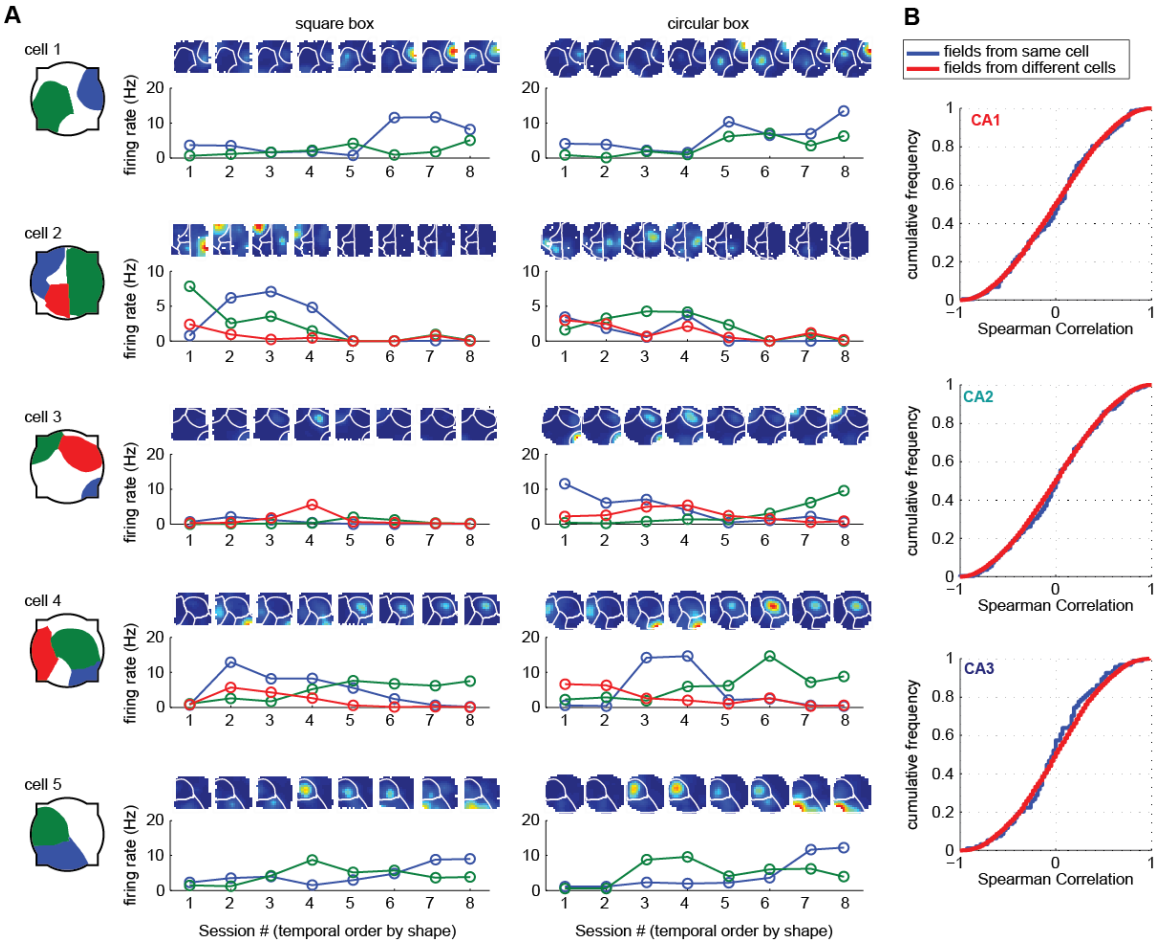
A
square box
circular box
cell 1
cell 2
cell 3
cell 4
cell 5
firing rate (Hz)
Session # (temporal order by shape)
Session # (temporal order by shape)
B
fields from same cell
fields from different cells
CA1
CA2
CA3
cumulative frequency
Spearman Correlation

Appendix 2.3: Supplemental Tables

Table 2S.1: **Number of trackable cells per animal for each experimental condition.** CA1 and CA3 data from rats A-F have been reported previously (Mankin et al., 2012). * Rat H performed the experimental sequence twice, separate sets of unique cells were recorded between the first and second set of experiments. The contribution of cells from each set of experiments is indicated in parentheses (first set/second set). ** Due to the small number of active CA3 place cells across the Third Day of experiments this data was not reported in the analysis.

	Two Shape			Single Shape			Third Day/Shift Day		
	CA1	CA2	CA3	CA1	CA2	CA3	CA1	CA2	CA3
Rat A	3	5	9	0	0	0	0	0	0
Rat B	0	7	16	0	0	0	0	0	0
Rat C	1	8	17	0	0	0	0	0	0
Rat D	30	0	10	0	0	0	17	0	8
Rat E	3	0	11	9	0	23	2	0	5
Rat F	13	0	8	16	0	47	11	0	5
Rat G	15	12	0	26	6	0	10	7	0
Rat H*	24 (16/8)	30 (9/21)	0	11 (5/6)	28 (6/22)	0	17 (9/8)	25(7/18)	0
Total	**89**	**62**	**71**	**62**	**34**	**70**	**57**	**32**	**18****

Table 2S.2: Descriptive statistics for the spiking properties of CA1, CA2, and CA3 neurons during 10-minute random foraging sessions. All reported statistics were first calculated for each of the sixteen 10-minute sessions (see Figure 2.1D) and were then averaged across sessions to yield a single value per cell or per field. For measures reported in the larger table, comparisons between regions were performed using a Mann-Whitney U Test. The Holm-Bonferroni correction for multiple comparisons was applied to obtain adjusted P values. The measure reported in the smaller table compares two methods of calculating field size, and comparisons were performed within each region using a Mann-Whitney U Test.

Measure	N calculated on	Summary				Mann-Whitney Test					
			N	Mean	SEM		z-value	U	*P*	Adjusted *P*	Significance level
Mean firing rate (Hz)	Number of cells	CA1	89	0.53	0.048	CA1 vs CA2	-3.0	1977	0.0031	0.0062	*P*<0.01
		CA2	62	0.82	0.080	CA1 vs CA3	1.5	2720	0.13	0.13	n.s.
		CA3	71	0.52	0.078	CA2 vs CA3	3.4	1441	6.1 e-4	0.0018	*P*<0.01
Peak firing rate (Hz)	Number of cells	CA1	89	4.9	0.36	CA1 vs CA2	-0.30	2680	0.77	0.77	n.s.
		CA2	62	5.2	0.45	CA1 vs CA3	2.1	2551	0.037	0.087	n.s.
		CA3	71	4.2	0.53	CA2 vs CA3	2.2	1716	0.029	0.087	n.s.
Thresholded peak firing rate (Hz)	Number of cells with at least one session with peak rate > 2 Hz	CA1	76	7.5	0.34	CA1 vs CA2	0.85	1871	0.39	1	n.s.
		CA2	54	7.0	0.39	CA1 vs CA3	0.93	1712	0.35	1	n.s.
		CA3	50	7.4	0.58	CA2 vs CA3	0.22	1316	0.83	1	n.s.
Spatial information (bits/spike)	Number of cells	CA1	89	1.9	0.072	CA1 vs CA2	5.9	1211	4.8 e-9	1.4 e-8	*P*<0.001
		CA2	62	1.3	0.071	CA1 vs CA3	0.93	2888	0.35	0.35	n.s.
		CA3	71	1.8	0.080	CA2 vs CA3	-5.0	1102	7.2 e-7	1.4 e-6	*P*<0.001
Number of fields per cell	Number of cells	CA1	89	0.84	0.062	CA1 vs CA2	-2.4	2132	0.018	0.035	*P*<0.05
		CA2	62	1.1	0.096	CA1 vs CA3	2.3	2494	0.022	0.035	*P*<0.05
		CA3	71	0.68	0.082	CA2 vs CA3	3.7	1378	1.9 e-4	5.7 e-4	*P*<0.001
Number of fields per active cell	Number of cells with at least one field in at least one session	CA1	76	1.3	0.046	CA1 vs CA2	-2.8	1456	0.0044	0.0088	*P*<0.01
		CA2	54	1.5	0.071	CA1 vs CA3	1.5	1608	0.14	0.14	n.s.
		CA3	50	1.3	0.067	CA2 vs CA3	3.3	853	0.0011	0.0032	*P*<0.01
Field size (cm^2)	Number of cells with at least one field in at least one session	CA1	76	803	49	CA1 vs CA2	-2.5	1515	0.011	0.034	*P*<0.05
		CA2	54	1000	64	CA1 vs CA3	0.38	1823	0.70	0.70	n.s.
		CA3	50	788	78	CA2 vs CA3	2.2	1008	0.026	0.053	n.s.
Field size (cm^2), continuous half sessions	Number of cells with at least one field in at least one half-session	CA1	74	677	44	CA1 vs CA2	-2.3	1580	0.021	0.042	*P*<0.05
		CA2	56	839	56	CA1 vs CA3	1.9	1437	0.052	0.052	n.s.
		CA3	49	564	61	CA2 vs CA3	3.6	808	3.0 e-4	8.9 e-4	*P*<0.001
Fano factor of within-session firing rates per pass through field (Hz)	Number of place fields; analyzed in sessions with mean rate > 0.25 Hz	CA1	132	2.6	0.11	CA1 vs CA2	1.9	7590	0.057	0.11	n.s.
		CA2	133	2.3	0.093	CA1 vs CA3	2.8	3769	0.0044	0.013	*P*<0.05
		CA3	75	2.1	0.11	CA2 vs CA3	1.2	4488	0.23	0.23	n.s.
Within-session absolute change in firing rate	Number of place fields; analyzed in sessions with mean rate > 0.25 Hz	CA1	132	2.8	0.16	CA1 vs CA2	4.4	6033	1.1 e-5	0.3.3 e-5	*P*<0.001
		CA2	133	1.9	0.10	CA1 vs CA3	-0.76	4633	0.44	0.44	n.s.
		CA3	75	2.5	0.18	CA2 vs CA3	2.8	3803	0.0047	0.0093	*P*<0.01
Theta index	Number of cells with at least one session with more than 100 spikes	CA1	75	0.67	0.033	CA1 vs CA2	0.79	1858	0.43	0.85	n.s.
		CA2	54	0.66	0.050	CA1 vs CA3	1.3	1586	0.20	0.60	n.s.
		CA3	49	0.67	0.071	CA2 vs CA3	0.65	1224	0.52	0.85	n.s.
Intrinsic theta Frequency (Hz)	Number of cells with at least one session with more than 300 spikes	CA1	69	8.3	0.053	CA1 vs CA2	4.8	886	2.0 e-6	6.0 e-6	*P*<0.001
		CA2	52	7.7	0.10	CA1 vs CA3	4.6	567	5.3 e-6	1.1 e-5	*P*<0.001
		CA3	36	7.8	0.086	CA2 vs CA3	-0.36	892	0.72	0.72	n.s.
Phase-distance Slope (cycles/field)	Number of cells with at least one field with more than 100 spikes and a well-fit phase-distance line	CA1	68	-0.42	0.020	CA1 vs CA2	-5.0	851	6.8 e-7	2.1 e-6	*P*<0.001
		CA2	53	-0.27	0.023	CA1 vs CA3	-2.5	830	0.012	0.025	*P*<0.05
		CA3	35	-0.36	0.027	CA2 vs CA3	1.8	711	0.066	0.066	n.s.

Measure	N calculated on		Continuous Halves			Interleaved Halves			Continuous vs Interleaved			
			N	Mean	SEM	N	Mean	SEM	z-value	U	*P*	Significance level
Field size (cm^2) for half sessions	Number of cells with at least one field in at least one half-session	CA1	74	677	44	77	624	36	0.38	2747	0.71	n.s.
		CA2	56	839	56	55	762	45	0.78	1408	0.44	n.s.
		CA3	49	564	61	52	602	54	-0.64	1179	0.52	n.s.

Table 2S.3: Full statistics for all comparisons using a Mann-Whitney U Test in analysis over time scales longer than 10 minutes. The first segment of the table reports comparisons between regions. The Holm-Bonferroni correction for multiple comparisons was applied to obtain adjusted P values. The second portion of the table compares PV correlations at Lag 2 between sessions recorded in the same box shape and sessions recorded in different box shapes; comparisons were performed within each region. Gray boxes indicate tests for which the sample size was too small to calculate a z-value.

Measure	N calculated on	Summary				Mann-Whitney U Test					
			N	Mean	SEM		z-value	U	*P*	Adjusted *P*	Significance level
Shape preference (within single block)	Place fields with at least 5 passes through the field in each of the 16 sessions	CA1	105	0.50	0.023	CA1 vs CA2	7.6	2372	3.2E-14	9.7E-14	*P* < 0.001
		CA2	112	0.27	0.016	CA1 vs CA3	0.62	2312	0.54	0.54	n.s.
		CA3	47	0.49	0.041	CA2 vs CA3	-4.5	1432	6.0E-06	1.2E-05	*P* < 0.001
PV corr at lag 1 (same box shape)	Comparisons between population vectors with at least 25 cells	CA1	7	0.90	0.0087	CA1 vs CA2		4	0.030	0.091	n.s.
		CA2	5	0.85	0.014	CA1 vs CA3		26	0.87	0.87	n.s.
		CA3	8	0.87	0.031	CA2 vs CA3		13	0.35	0.71	n.s.
PV corr at lag 2 (same box shape)	Comparisons between population vectors with at least 25 cells	CA1	6	0.85	0.019	CA1 vs CA2		1	0.019	0.038	*P* < 0.05
		CA2	4	0.67	0.052	CA1 vs CA3		0	0.010	0.029	*P* < 0.05
		CA3	4	0.92	0.011	CA2 vs CA3		0	0.029	0.038	*P* < 0.05
Shape preference (across two days)	Place fields with at least 5 passes through the field in each of the 16 sessions	CA1	105	0.43	0.026	CA1 vs CA2	8.2	2106	3.2E-16	9.3E-16	*P* < 0.001
		CA2	112	0.15	0.015	CA1 vs CA3	-0.23	2409	0.82	0.82	n.s.
		CA3	47	0.44	0.043	CA2 vs CA3	-6.1	1017	1.1E-09	2.2E-09	*P* < 0.001
Area covered by spatial drift of place field center	Place fields in the single-shape paradigm that were active in at least 3 sessions	CA1	51	95	16	CA1 vs CA2	-4.7	743	3.3E-06	9.8E-06	*P* < 0.001
		CA2	61	350	47	CA1 vs CA3	1.8	475	0.073	0.073	n.s.
		CA3	25	57	15	CA2 vs CA3	4.5	278	5.4E-06	1.1E-05	*P* < 0.001

Measure	N calculated on		Same Box Shape			Different Box Shape			Same vs Different			
			N	Mean	SEM	N	Mean	SEM	z-value	U	*P*	Significance level
PV correlation at lag 2	Comparisons between population vectors with at least 25 cells	CA1	6	0.85	0.019	10	0.43	0.030		0	2.5 e-4	*P* < 0.001
		CA2	4	0.67	0.052	8	0.58	0.039		10	0.37	n.s.
		CA3	4	0.92	0.011	8	0.55	0.054		0	0.0040	*P* < 0.001

Appendix 2.3: Supplemental Methods

Subjects and surgeries. CA2 data were collected from five male, experimentally naïve, Long Evans rats with a preoperative weight of 400-510 g. Animals were housed individually and maintained on a 12-h light/12-h dark schedule with lights off at 6:00 am. All behavioral testing occurred in the dark, except when noted. The data from three of the five animals were recorded simultaneously with previously reported CA1 and CA3 recordings (Mankin et al., 2012). For comparisons of the CA2 data with all available CA1 and CA3 recordings from the same experimental design, previously published data from three additional animals without CA2 recordings were also included (Mankin et al., 2012).

All experimental procedures were performed as approved by the Institutional Animal Care and Use Committee at the University of California, San Diego and according to National Institutes of Health and institutional guidelines. At the time of surgery, rats were anesthetized with isoflurane (2-2.5 % in O2) and buprenorphine was administered as an analgesic. An electrode assembly consisting of fourteen independently movable tetrodes was implanted above the right hippocampus (AP 3.9-4.0 mm posterior to bregma, ML 3.0-3.5 mm). Tetrodes were prepared as described previously (Leutgeb et al., 2007) and were advanced to the hippocampal cell layer using techniques optimized for recording stability across time (Mankin et al., 2012).

Behavioral Procedures. After one week of recovery from surgery, rats were partially food-deprived and trained to forage for randomly scattered cereal crumbs in an enclosure with walls that could be shaped either as a square (80 cm by 80 cm) or as a 16-sided polygon (50 cm radius; referred to as 'circular enclosure'). A polarizing white cue card (20 cm wide) was placed on an inside wall of the enclosure. The center of the enclosure was always located at the same place in the room, and the angle of the cue card compared to external room cues was kept

constant. Training was performed in two daily blocks. For all rats, the first block started between 8:30 and 10:00 am and the second block between 2:30 and 4:00 pm. For each individual rat, the daily start time of each block varied by less than 30 minutes. Rats were returned to the animal housing room between the morning and afternoon training blocks.

Rats were trained to run for four 10-minute sessions during each block, with two sessions in the square enclosure and two sessions in the circular enclosure. The order of the shapes was varied randomly within each training block. The rats were allowed to rest for five minutes between sessions, and training blocks were flanked by 20 minute sleep sessions. The floor of the enclosure was cleaned with water between each session. Following the sleep session at the end of the afternoon training block, rats were screened for single-unit activity. One tetrode remained in the cortex and was used as a reference for all recordings. Another tetrode was lowered to the hippocampal fissure to record hippocampal local field potentials. The remaining twelve tetrodes were slowly advanced towards the hippocampal cell layer. Prior to the implantation of the recording array, the relative spatial arrangement of all tetrodes with respect to each other was noted. This allowed for the targeting of more anterolateral tetrodes towards CA2/CA3 and the more posteromedial tetrodes towards CA1/CA2. The placement of all tetrode recording sites in each of the hippocampal subregions was determined from histological material that was prepared as described below.

Electrophysiological recordings throughout the morning and afternoon sessions were initiated when multiple well-isolated cells (> 300 μV) were observed on most tetrodes. The recording phase of the experiment began after 9 to 20 days of behavioral training. Recordings were first conducted for 2 days in the standard training paradigm that included recordings in the square and circular enclosure (referred to as two-shape, day 1; two-shape, day 2). In five animals (two with CA2 recordings), recordings were also performed on a third day that was identical to

the first two recording days, except that the start times of the blocks were shifted by 6 hours, so that the first block occurred at 3:00 PM and the second at 9:00 PM. The second block was thus during the light phase of the light/dark cycle (Figure 2S.5). Additionally, four animals (two with CA2 recordings) performed two days of behavior in which all sixteen random foraging sessions were conducted in a single enclosure shape (single-shape, day 1; single-shape, day 2). For each animal, we selected the shape in which we identified the larger number of active cells during the recording on the preceding day. This paradigm was otherwise identical to the two-shape paradigm. In one animal, the five-day recording sequence that included the three days in the two-shape paradigm and the two days in the single-shape paradigm was repeated once. In this animal, the first set of recordings began after 16 days of training and the second set began after 22 days of training, and the set of recorded cells during each sequence were from different tetrodes or, when from the same tetrode, determined to be unique by inspecting the clusters. Therefore, the cells that were recorded during each repetition were included as separate cells in the analysis.

Recording procedures. For recording spikes and local field potentials, the electrode assembly was connected to a multichannel head-mounted preamplifier. The *x-y* position of light emitting diodes on the preamplifier was tracked at 30 Hz by processing video images. Unit activity was amplified and band-pass filtered at 600 Hz to 6 kHz. Spike waveforms above a trigger threshold (40-60 μV) were time-stamped and recorded at 32 kHz for 1 ms.

Cell-tracking and single unit isolation. Because our study depended on being able to follow the same set of principal cells over an extended time period, we developed a customized version of MClust (Redish, A.D. MClust. http://redishlab.neuroscience.umn.edu/MClust/MClust.html) with added functions that allowed for the comparison of the cluster boundaries of each cell throughout a series of rest and 10-minute recording sessions. Clusters that persisted in the same region of parameter space

throughout two days were accepted as single cells for further analysis. Rest sessions at the beginning and end of each behavioral session were analyzed to confirm that changes in cell activity patterns in behavior were not a result of tetrode instability. Care was taken to accept only cells that could be precisely followed from the beginning to the end of the data analysis, and all clusters were inspected visually to ensure that rate changes that were observed could not be attributed to clusters drifting outside of defined cluster boundaries (Figure 2S.1).

Postmortem confirmation of recording location. Rats received an overdose of sodium pentobarbital and were perfused transcardially with saline and either 4 % formaldehyde or, when immunohistochemistry was performed, 4 % paraformaldehyde. The brains were extracted and stored in the fixative with 30 % sucrose. Frozen coronal sections (40 μm) were cut, and each section through the part of the hippocampus with electrode tracks was collected and stained with cresyl violet. To confirm our delineation of CA field boundaries, immunohistochemistry using antibodies against α-actinin-2 was performed as previously described (Ratzliff and Soltesz, 2001) on tissue from two recording animals and two additional animals in which recording was not performed. Immunoreactivity for α-actinin-2 has been shown to be high in CA2, in the molecular layer of the dentate gyrus, and in the cell bodies of interneurons scattered throughout the hippocampus (Wyszynski et al., 1998). Free-floating sections were incubated with mouse anti α-actinin-2 antibody (1:50,000; clone EA-53, Sigma) overnight at 4°C. On the following day, the sections were incubated for 2 hours with HRP-conjugated horse anti-mouse secondary antibody (1:1,000; Sigma). The secondary antibody was visualized by reaction with diaminobenzidine, and sections were counterstained with cresyl violet.

The final tetrode positions were determined by three-dimensional reconstruction of the tetrode array in serial sections. Because the brain was cut at a small angle compared to the orientation of the electrode tracks, the path of each electrode through the brain could be

visualized as elongated segments of tissue damage in each section. The tip of each electrode was found by tracking the damage throughout the series of sections that was arranged from anterior to posterior (see Figure S1 in Leutgeb et al., 2007 for the appearance of the tracks in serial sections). Tetrodes were not moved after electrophysiological recordings, and recordings from a tetrode were included in the data analysis if the tetrode's deepest position was in or just below the pyramidal cell layer of CA1, CA2, or CA3. In tissue for which immunohistochemistry was performed, CA2 was defined as the region with dense α-actinin-2 staining in cell bodies and proximal dendrites. We confirmed that this definition coincided with morphological criteria, so that the boundaries of CA2 could also be identified in tissue in which we did not stain for α-actinin-2. The boundary between CA1 and CA2 was drawn at the transition where the cell layer thickens and where cell bodies increase in size and become less densely packed (Lorente De Nó, 1934; Woodhams et al., 1993). The boundary between CA2 and CA3 was drawn at the transition where the cell layer becomes less compact and where large cell bodies are scattered outside the continuous cell layer (Figure 2S.2).

To further increase confidence that tetrodes were correctly assigned, we excluded tetrodes that were at transitions between CA regions. The transition zone between CA1 and CA2 was defined as the area in which there was only a minor decrease in packing density compared to CA1. This zone corresponded to an area in which the immunolabeling of cell bodies and dendrites was sparse in the α-actinin-2 stained section. The transition zone between CA3 and CA2 was defined as the area with larger cell bodies, but with few cell bodies outside of the densely packed inner sublayer. Because the CA2/CA3 border shows a more gradual transition than the CA1/CA2 border, we obtained further confirmation of tetrode assignment to CA2 by measuring the distance of all CA2 tetrodes from the CA1/CA2 border. At the anteroposterior level where the majority of recording tetrodes was located, the proximal to distal extent of the

principal cell layer within the CA2 region, as defined by α-actinin-2 staining in proximal dendrites, ranged from approximately 350 μm to 425 μm. All tetrodes assigned to the CA2 region were less than 350 μm from the CA1/CA2 border. We also confirmed that tetrodes that were assigned to CA3 were well beyond the CA2/CA3 border, and the nearest tetrode was at a distance of more than 700 μm.

Spatial tuning and correlation. For each well-isolated neuron, a spatial firing rate distribution was constructed in the standard manner, by summing the total number of spikes that occurred in a given location bin (5 cm by 5 cm), dividing by the amount of time that the animal spent in that location, and smoothing with a Gaussian centered on each bin (Leutgeb et al., 2007). Spatial information per spike was calculated for each spatial firing rate map as

$$I = \sum_i P_i \frac{R_i}{R} log_2 \frac{R_i}{R}$$

where i indexes the spatial bins, P_i is the probability of occupancy in each bin, R_i is the mean firing rate in each bin, and R is the mean firing rate across the spatial map (Skaggs et al., 1993).

Place field boundaries, size, number, and stability. Place field boundaries for each cell were calculated as described previously (Mankin et al., 2012) by using maps from either single sessions or the average of 4, 8, or 16 recording sessions. Field boundaries from single sessions were used for the initial analysis to avoid bias that could result from drifting fields (Figure 2.2 and Table 2S.2), and field boundaries from averages across sessions were subsequently used to allow for comparisons over different time intervals. To consider whether short-term spatial drift accounted for differences in field sizes between regions, boundaries were also defined on maps created from 5 minutes of data that were either sampled continuously (the first or second half of each session) or in an interleaved manner (using either the even or the odd minutes of each session). To ensure that broad firing fields were not excluded from the analysis, we used a low

threshold and included all fields with peak firing rates of greater than 2 Hz in a single session. Because this criterion was not stringent, we obtained higher proportions of active cells (59.2 % in CA1, 68.2 % in CA2, and 48.1 % in CA3) than typically reported for CA1 and CA3 in similar recording environments (Leutgeb et al., 2004). To confirm that there was also a higher proportion of active cells in CA2 with a more stringent criterion, we determined the proportion of active cells with peak rates greater than 5 Hz, which resulted in 41.6 % active cells in CA1, 45.8 % active cells in CA2, and 29.5 % active cells in CA3. These values are comparable to those that are typical and confirm that CA2 has more active cells than the other CA subregions irrespective of a particular threshold. In all analysis that averaged maps from recordings in square and in circular shapes, fields with peak firing rates that exceeded 1 Hz were included. The lower threshold for analysis that included the two shapes was used to correct for the fact that fields that were active in only one of the two box shapes would yield a reduced average firing rate in average maps that also include the box shape in which the cell was silent.

After defining field boundaries, the area within the field boundary was taken as the size of the place field, and the bin with the peak firing rate was taken as the field center. For each field that was active in at least three sessions, the area of the convex hull traced out by the field center was used as an estimate for the spatial stability between recording sessions. For each place field, a 'pass' through the field was defined as a trajectory through the place field that included a section through the area of the field in which the firing rate was > 50 % of the maximum firing rate. The mean rate per pass was taken as the number of spikes during the pass divided by the duration of the pass. To estimate the variability of the firing rates, the Fano factor per field was calculated as the variance in firing rate per pass divided by the mean firing rate. Additionally, the change in firing rate throughout a recording session was estimated by calculating the regression for predicting the firing rate from the elapsed time within the session. The absolute value of the slope

of the regression line was taken as the change in firing rate over time, and a slope of 0 indicated that there was no increase or decrease in rate. To avoid that the results reflect variability of cells with very low firing rates or very few passes, sessions during which the mean rate per pass in a field was < 0.25 Hz or during which there were fewer than 5 passes were excluded from the analysis of the Fano factor and the within-session change in firing rate.

Theta index and intrinsic frequency. For each cell and each 10-minute session, we calculated the spike autocorrelogram using a time bin size of 2 ms. For the range between -500 ms and 500 ms, each autocorrelogram was fit with the following equation

$$y(t) = [a(\cos(\omega\tau) + 1) + b]e^{-|t|/\tau_1} + ce^{-t^2/\tau_2^2}$$

where t is the time lag, y is the correlation coefficient at that time lag, and a, b, c, τ_1, τ_2, ω are the fit parameters. The theta index was defined as the ratio a/b (Royer et al., 2010). We also calculated the spectrum of the autocorrelogram using the multi-taper method (http://chronux.org) (Mitra and Bokil, 2008) and defined the intrinsic theta frequency for each cell as the frequency within the 4-11 Hz range with the largest power.

LFP, phase of firing, and phase precession. A local field potential (LFP) was recorded from the hippocampal fissure of each animal and then band-pass filtered in the theta range (4-12 Hz). A Hilbert transform was performed on the theta signal to decompose it into theta phase and amplitude. Periods when theta amplitude fell below two standard deviations of the mean theta amplitude were designated as low-theta-power periods and were not included in the analysis. For each identified firing field in a 10- minute session, the theta phase for each spike within the field was calculated. To analyze phase precession, all spikes from all passes through a field were pooled. For fields with at least 100 spikes, a best-fit line between phase and distance traveled within the place field was found using the circular-linear fit method (Kempter et al., 2012). The

method is iterative, and fields for which the fit did not converge (CA1: 2.75%, CA2: 3.22%, CA3: 1.18%) were excluded from the analysis. The median slope of all fitted fields was compared to zero using the sign test for medians.

Single-Session Firing Properties. To characterize single-session firing properties and compare them between CA regions, we calculated the average firing rate, the spatial information, the number of fields, the theta index, and the intrinsic theta frequency for each cell in each of the 16 sessions recorded across two days. In addition, each cell's firing fields were defined in each session, and the peak rate and field size of each field were measured. If multiple fields were identified, the peak firing rate and field size of all fields within a session were averaged. The statistics for each CA region were calculated after averaging the values for each cell over the 16 recording sessions, and one value per cell was thus used for statistical analysis. To quantify the variability of firing within a field, we calculated the Fano factor for the firing rates during individual passes through the field within each session, and we calculated the slope of the regression line between the firing rate per pass and time when the pass occurred within each recording session. For these calculations, place field boundaries were defined using the average firing map of all 16 behavioral sessions, and the statistics for each CA region were calculated after averaging the values for each field over the 16 recording sessions. Hippocampal CA regions were compared using the Mann-Whitney U test, and the conversion of the U value to the z statistic is reported if the number of observations in each group was greater than 20. If the number of observations was smaller, the conversion to the z statistic is not accurate and the U value is reported in the text. Significance levels were corrected for multiple comparisons by applying the Holm-Bonferroni correction. To find the proportion of active cells, a cell was considered active in a session if its maximum firing rate in any spatial bin exceeded a threshold (2 Hz). The proportion

of active cells in each region was calculated for each session and then averaged across the 16 sessions.

Shape Preference. A shape preference score was calculated for each firing field by measuring the degree to which the distribution of firing rates in one shape was separated from the distribution of firing rates in the other, as previously described (Mankin et al., 2012). Briefly, for every pass through a place field, the average firing rate was computed, and the rates from all passes in each box shape were pooled across either a single block across 16 sessions to yield the firing rate distributions in the square and in the circular enclosure for that place field. The Receiver Operant Characteristic (ROC) curve was computed for these distributions. The area under the ROC curve may take values between 0 and 1 and can be used as a measure of the overlap of two distributions. We scaled this score by subtracting 0.5 to center it at zero and by multiplying it by 2 so that its range was between -1 and 1. We then took the absolute value so that equal firing rate distributions across the two sets of shapes would have a score of zero and that preference for either the square or the circular enclosure would both have a positive score (see Figure 2S.4). For shape preference scores across 16 sessions, chance values were obtained for each CA region by performing random shuffles of shape identity across the 16 recording sessions.

Population Vector Correlations. For each behavioral session and each hippocampal CA region, rate vectors were constructed by arranging the spatial maps of all cells recorded from that region from all animals in an *x*-*y*-*z* stack, where *x* and *y* represent the two spatial dimensions and *z* represents the cell-identity of tracked cells (Leutgeb et al., 2005a; Leutgeb et al., 2005b). To allow for comparisons between the square and circular enclosure shapes, the analysis was restricted to the 16 by 16 bins that were common to both shapes, yielding 256 *x*-*y* locations. Population vector correlations were obtained by calculating, for each *x*-*y* location, the Pearson correlation coefficient for firing rates along the *z*-dimension between pairs of sessions. Cells with

firing below 1 Hz in all *x-y* bins of the two sessions that were compared were excluded from the population vectors before calculating the correlation coefficients. The correlation coefficients of all spatial bins were averaged to estimate the population vector correlation for a pairwise comparison between sessions. For comparisons by time lag within a block, pairs of recording sessions were analyzed based on the number of recording sessions between them (e.g., no intervening session corresponds to lag 1), the experimental paradigm used (two-shape, single-shape), and whether sessions occurred in the same or different shape. Because the sequence of shapes was chosen randomly for each block in the two-shape condition, possible comparisons in a comparison group (e.g., lag 1, same-shape) could include instances in which the shapes were presented at different positions within the recording sequence. For example, same shape comparisons at lag 1 could include instances when the first and second recording session were squares (square 1-square 2), when the second and third recording session were squares (square 2-square 3), or when the third and fourth recording session were squares (square 3-square 4) as well as instances when both of the recordings in a pair were in circles (circle 1-circle 2, circle 2-circle 3, circle 3-circle 4). From each of these possible pairwise comparisons, population vectors were created from cells that were recorded in corresponding shapes over a corresponding lag, and their correlations were included as data points when the vectors consisted of more than 25 cells. Because we only compared lag 1 and lag 2 in the two-shape design, we used Mann-Whitney tests for comparisons that differed by lag. The Holm-Bonferroni method was applied to correct for multiple comparisons. In the single-shape comparisons, three different lags (1, 2, and 3) within a block were compared, and we therefore used a two-way ANOVA by brain region and lag. For comparisons on longer time scales, the population vectors were generated by stacking the cells that were recorded in all animals in each hippocampal subregion in each of the 16 recording sessions. The sessions were sorted by their temporal order after separating squares and circles.

Pairwise comparisons between the 8 stacks in the square and the 8 stacks in the circular enclosure were grouped by time interval between blocks (e.g., 6 hours) and by same/different shape comparison. Population vector correlations were then compared using an ANOVA, with Tukey's Honestly Significant Difference (HSD) criterion for *posthoc* analysis.

Acknowledgements

We thank B. Slayyeh and M. Wong for technical assistance, and C. Varga and I. Soltesz for immunohistochemistry protocols. This research was supported by NIMH (1R01MH-100349), the Ray Thomas Edwards Foundation, Walter F. Heiligenberg Professorship, NSF/BMBF German-US collaboration (CRCNS-IIS-1010463), NIMH Training Grant (T32MH 020002-14), and Alberta Innovates - Health Solutions.

Chapter 2, in full, is material as it appears in *Neuron*, 2015, Mankin, Emily A., Diehl, Geoffrey W., Sparks, Fraser T., Leutgeb, Stefan, and Leutgeb, Jill K. The dissertation author was a primary researcher and author of this paper.

CHAPTER 3: STABILITY OF MEDIAL ENTORHINAL CORTEX REPRESENTATIONS OVER TIME

Abstract

Distinct functional cell types in the medial entorhinal cortex (mEC) have been shown to represent different aspects of experiences, including spatial and non-spatial features of an environment. In order to further characterize activity patterns of mEC neuronal populations that may be critical for memory, we examined whether spatial representations of neurons in the mEC superficial layers depended on environment size and if they changed over extended periods of time. To address these questions, we recorded mEC cells while rats repeatedly foraged in large or small environments and tracked the identity of individual cells across sessions in order to compare activity patterns between sessions separated by time intervals from minutes to hours. When comparing between the environments of different size, we found for grid cells and non-grid cells that the overall precision of the spatial maps was higher in smaller environments. When examining the stability of spatial firing patterns over time, we first established that the majority of mEC neurons retained reliable and consistent spatial firing patterns within a single 10-minute foraging session. For longer temporal intervals, the stability of spatial firing patterns differed across functional cells types. The activity patterns of grid cells were remarkably stable across intervals of hours. A majority of the non-grid cell population was similarly stable over time, while a subset of ~15 % of non-grid cells showed a dramatic change in their spatial firing pattern or firing rate across a six-hour period. Therefore, only a small fraction of the mEC neuron population was characterized by the same spatial map instability that has been previously described for the hippocampal CA2 subregion. The majority of cells exhibited stability levels that

resemble those of the hippocampal CA1 and CA3 regions. Taken together, our data support an essential function of mEC in stabilizing hippocampal maps.

Introduction

The medial entorhinal cortex (mEC) is composed of numerous functional cell types with highly specialized firing patterns that are well suited for supporting computations critical for spatial navigation and spatial memory (Buzsaki and Moser, 2013; Hartley et al., 2014). Subpopulations of entorhinal neurons represent heading direction, speed, and the position of the animal in space (Fyhn et al., 2004; Kropff et al., 2015; Sargolini et al., 2006), with those cells that are specialized for spatial coding often being further subdivided into grid cells, border cells, and non-grid spatial cells (Diehl et al., 2017; Hafting et al., 2005; Savelli et al., 2008; Solstad et al., 2008). In line with a role of mEC providing critical input downstream to hippocampus, subsets of each of these functional classes have been reported to project directly to the hippocampus (Zhang et al., 2013).

Input from spatially selective mEC cells are widely hypothesized to give rise to the highly precise place fields observed in hippocampus, with a wide range of models proposing how such a computation could occur (Blair et al., 2008; Cheng and Frank, 2011; de Almeida et al., 2009; Fuhs and Touretzky, 2006; O'Keefe and Burgess, 1996; Rolls et al., 2006; Solstad et al., 2006). Yet, experimental studies indicate that place coding in hippocampus is at least partially retained after removal or inactivation of mEC (Brun et al., 2008a; Hales et al., 2014; Miao et al., 2015; Ormond and McNaughton, 2015; Robinson et al., 2017; Rueckemann et al., 2016; Schlesiger et al., 2015), suggesting that other inputs to hippocampus can compensate for loss of a spatially precise mEC signal. In contrast, mEC projections were found to be critical for CA1 hippocampal map stability (Hales et al., 2014; Schlesiger et al., 2015), indicating that mEC neural

circuits may instead be particularly important for providing the hippocampus with a rigid and stable spatial representation. However, the stability of the mEC spatial code over time has not been systematically tested.

While the stability of mEC representations over time is not known, it has recently been established that some of the main hippocampal projection targets of mEC cells show place cell firing patterns that vary over time, even when all key aspects of the experience, such as the spatial environment and the behavioral task, are highly familiar and held constant (Lu et al., 2015; Mankin et al., 2015; Mankin et al., 2012; Rubin et al., 2015; Ziv et al., 2013). In particular, the dissimilarity of neuronal coding over time is pronounced in CA2, where place cell representations of an environment are already dissimilar over intervals of minutes. In contrast, the spatial coding of hippocampal CA3 cells exhibits very limited change, even over periods as long as 30 hours (Lu et al., 2015; Mankin et al., 2012). The co-occurence of stable and drifting population codes has been proposed to constitute a potential mechanism for decoding how long ago a particular event occurred (Estes, 1955; Howard and Kahana, 2002), and such temporal coding is thought to constitute a critical component of episodic memory representations (Tulving, 1972). In support of these mechanisms being implemented across mammalian species, drifting network representations have also been observed in the medial temporal lobe of humans (Ezzyat and Davachi, 2014; Hsieh et al., 2014; Jenkins and Ranganath, 2016; Manning et al., 2011; Nielson et al., 2015) and have been shown to relate to behavioral performance or subjective evaluations in temporal encoding tasks (Ezzyat and Davachi, 2014; Hsieh et al., 2014; Jenkins and Ranganath, 2016).

Although it is now well established that hippocampal place cell representations gradually change over time, the neuronal circuit and cellular mechanisms that generate such a drifting code have not been identified. While CA3 projects to both CA1 and CA2 (Dudek et al., 2016; van

Strien et al., 2009), its highly stable representations makes CA3 an unlikely candidate to provide a drifting signal. One possibility is therefore that the rapid change over time observed within the CA2 region is generated de novo locally, perhaps due to the unique anatomical, cellular, and physiological properties of CA2 cells (Dudek et al., 2016; Jones and McHugh, 2011). A stable signal from CA3 and a drifting signal from CA2 could then combine to give rise to the intermediate stability that has been reported for CA1 (Mankin et al., 2015). Alternatively, extra-hippocampal areas, such as the entorhinal cortex, could pass along an either stable or drifting code to one or more hippocampal subregions. Owing to the highly spatial nature of cellular firing within mEC and its strong projections to all hippocampal CA regions, we investigated the stability of mEC firing patterns over extended time periods. To test the stability of mEC spatial representations over extended time, we recorded the activity patterns of the same mEC cell populations while rats explored the same environment at the same location in space over multiple sessions. The temporal intervals between sessions ranged from 5 minutes to six hours. Functional cell types were classified within each session, and for each functional mEC cell type the stability of the spatial representation was examined across sessions.

Materials and Methods

Subjects and Surgery. Experimental procedures were performed as approved by the Institutional Animal Care and Use Committee at the University of California, San Diego and according to National Institutes of Health and institutional guidelines. Data were recorded from eight male Long Evans rats (300 – 400 g) that were housed individually and maintained on a 12-h light/dark schedule with lights off at 7:00 am. Data from three rats (45 out of 313 cells) have been previously reported in a different study (Diehl et al., 2017) and were reanalyzed here. Prior to behavioral testing rats were implanted with a ‘hyperdrive’ recording device consisting of 14

independently movable tetrodes. For drive implantation, rats were anesthetized with isofluorane (1.5-2.5 % in O_2) and given buprenorphine (0.02 mg/kg, S.C.) as an analgesic. After opening a skull window and removing dura, the hyperdrive was implanted above the dorsal mEC 0.5 – 1.0 mm anterior to the transverse sinus and 4.6 – 5.2 mm lateral to the midline. Tetrodes were constructed from 17 µm platinum-iridium (90/10 %) wire and were plated with a 1.5 % platinum solution to lower impedances to 125-325 kΩ at 1 kHz prior to surgery.

Behavioral Procedures. After one week of recovery from surgery, rats were food restricted to 85 % of free feeding weight and were trained to forage for randomly scattered cereal crumbs in open field enclosures (80 cm by 80 cm square, 100 cm diameter circle, 120 cm by 120 cm square). Each open field had a single polarizing cue card (20 or 25 cm wide) placed on an internal wall. Environments were always centered in the same location within the room, the position of the cue card was kept constant, and the recording system, experimenter, and other external room cues were readily visible to the rats.

All rats were trained in blocks of four 10-minute foraging sessions. Two blocks of four 10-minute sessions were conducted each day separated by six hours as described previously (Mankin et al., 2015; Mankin et al., 2012). Training always occurred at the same time of day with the first session starting between 8:00 am and 10:00 am and the second session starting between 2:00 pm and 4:00 pm. Start times varied between rats, but a given rat always ran the morning sessions at the same time and the afternoon sessions six hours later. All recording blocks were flanked by 20-minute sleep periods and rats were given five minutes between sessions to rest in a pot away from the foraging enclosure. Between sessions the floor of the open field was cleaned with water. Single unit recordings in mEC began when the environments were highly familiar (at least 7 days of prior training) to control for neuronal responses to novelty. Behavioral procedures

while recording mEC units were identical to training procedures and continued until cells could no longer be recorded.

For three rats, training and recording sessions were performed in the two smaller boxes (80 cm by 80 cm square enclosure and 100 cm diameter circular enclosure) (Diehl et al., 2017). Within each block of four sessions, two of the sessions were in the square environment and two were in the circular environment, with the two shapes presented in a pseudorandom order. The current analysis focused on the stability of maps, therefore all comparisons were made between sessions of identical shape. For the remaining five rats training and recording sessions were performed in the 120 cm square box with all four recording sessions of each block conducted in the same enclosure.

Electrophysiological recordings. Following surgery, tetrodes were gradually advanced towards the superficial layers of mEC with one tetrode remaining in cortex to serve as a reference. A second tetrode was rapidly advanced through the brain to identify the beginning and end of mEC based on local field potential (LFP) signatures. The remaining 12 recording tetrodes were advanced 25 to 160 μm per day through mEC to record single unit activity. When large amplitude units were observed, tetrodes were not advanced in an effort to record the same cell population multiple times over the course of successive recording sessions, sometimes across multiple days. Advancement of tetrodes and recordings were performed blind to any functional properties of recorded cells ensuring an unbiased sampling of the mEC population. Recordings and advancement of tetrodes continued until LFP criteria indicated that each tetrode had been advanced to layer 1.

For recording single units and LFP, hyperdrives were connected through a multichannel, head-mounted preamplifier to a digital Neuralynx recording system. Unit activity was amplified

and band-pass filtered between 0.6 kHz and 6 kHz. Spike waveforms above a trigger threshold (35-55 μV) were time-stamped and digitized at 32 kHz for 1 ms. Continuous LFP was recorded from each tetrode, filtered between 0.1 Hz and 900 Hz, and sampled at 2000 Hz. Position data of a red and a green LED located on either side of the head-mounted preamplifier were tracked at 30 Hz by a video camera mounted above the experimental area to determine the rat's *x-y* position and head-direction.

Spike sorting was manually performed offline using a customized version of MClust (Redish, A.D. MClust. http://redishlab.neuroscience.umn.edu/MClust/MClust.html) (Mankin et al., 2012). Sleep periods before and after behavioral sessions were used to ensure stability of recorded cells. The identity of individual cells was tracked across recording sessions by comparing the location of clusters in multi-dimensional cluster space. Clusters whose location in cluster space did not change across recording sessions were identified as originating from the same cell. Spiking autocorrelation was occasionally used as a secondary metric for comparing clusters across sessions, but importantly no other firing properties, such as spatial firing pattern, head direction firing, or theta modulation, were used to track cells across sessions. Only clusters that had well-separated boundaries were included in the analysis. To quantify the quality of analyzed clusters we calculated the isolation distance of all recorded cells (Schmitzer-Torbert et al., 2005). While we did not exclude data based on isolation distance, others have set minimum isolation distances of 5 or 10 (Newman and Hasselmo, 2014; Perez-Escobar et al., 2016). Of those clusters that we accepted for analysis, 99.5 % had isolation distances of at least 10. Putative interneurons were identified and removed from the data set based on an average firing rate above 7.5 Hz. Note that this threshold is higher than typically used in the hippocampus because many principal cells in entorhinal cortex fire at intermediate rates.

Histological analysis. At the completion of all experiments, rats were given an overdose of sodium pentobarbital and were perfused transcardially with saline and 4 % formaldehyde. Brains were extracted and post fixed for 24 hours before being transferred to a 30 % sucrose solution and allowed to sink. Sagittal sections (40 µm) were cut on a freezing microtome and sections through the right mEC were mounted on slides and stained with cresyl violet. Tetrode trajectories through mEC were determined by 3D reconstruction of the sectioned tissue. Based on records of the systematic movement of tetrodes through the brain and the trajectory information, complemented by records of LFP profiles, tetrode locations on each recording day were assigned to either the deep or superficial layers of mEC. Cells recorded from the superficial layers were further localized to putative recordings from layer 2 or layer 3. Any recordings from the deep mEC layers or from the pre- or parasubiculum were removed from the dataset.

Rate maps and cell identification. Rate maps were constructed by summing the total number of spikes that occurred in each location bin (5 cm x 5 cm), dividing by the total amount of time that the rat occupied the bin, and smoothing with a 5 x 5 bin Gaussian filter with a standard deviation of approximately 1 bin (Diehl et al., 2017):

```
[0.0025  0.0125  0.0200  0.0125  0.0025;
 0.0125  0.0625  0.1000  0.0625  0.0125;
 0.0200  0.1000  0.1600  0.1000  0.0200;
 0.0125  0.0625  0.1000  0.0625  0.0125;
 0.0025  0.0125  0.0200  0.0125  0.0025].
```

Bins that were never within a distance of less than 2.5 cm from the tracked path or with total occupancy of less than 150 ms were regarded as unvisited and were not included in the rate map. To control for possible influences of stationary episodes, periods below a minimum running speed of 2 cm/sec were excluded from all calculations.

To identify grid cells, we evaluated the degree of six-fold rotational symmetry in each cell's spatial auto-correlation by calculating a grid score and comparing it to a surrogate shuffled

distribution produced by time shifting spike times with respect to an animal's trajectory as described previously (Diehl et al., 2017). For each cell, we calculated rate maps as above but based on a bin size of 2.5 cm. To then generate the spatial auto-correlation matrix we calculated the Pearson's correlation between the firing rates of bins at corresponding locations between the rate map and itself. One map was then shifted in the *x* and *y* dimensions and the correlation was taken at all *x-y* offsets to produce the auto-correlation matrix. From this matrix an annulus that contained the first hexagon of peaks around the center, but excluded the central peak, was extracted. The average correlation value of bins in the annulus was then taken at each angle from the center (i.e., along a 'ray'). These values were rotated in 30 degree steps and correlated to the un-rotated average values. If six-fold symmetry exists, the correlations at 30, 90, and 150 degrees are expected to be low while the correlations at 60 and 120 degrees are expected to be high. A cell's grid score was thus taken as the difference between the average of the latter and the average of the former sets of correlation values. Grid scores were then compared to the 95th percentile of a shuffled distribution of grid scores generated for each individual cell in each session (i.e. chance value), and grid cells were positively identified as those cells for which the majority of sessions had a grid score that exceeded the chance value.

To quantify spatial firing of cells we calculated a spatial information score (SI) and a within session correlation (WSC) as described previously. SI per spike was calculated as: $SI = \sum_i P_i \frac{R_i}{R} log_2 \frac{R_i}{R}$ where i indexes the spatial bins, P_i is the probability of occupancy in each bin, R_i is the mean firing rate in each bin, and R is the mean firing rate across the spatial map (Skaggs et al., 1993). WSC was calculated for each cell in each session by splitting the 10-minute recording into the first and second half. Rate maps were calculated for both 5-minute periods and a Pearson's correlation was taken between the two (Diehl et al., 2017). As for grid scores, chance level SI and WSC were calculated for each cell in each session by shuffling spike times.

Spatial correlation, firing rate overlap, and comparisons across time. We calculated the spatial similarity between two rate maps using Pearson's correlation between the firing rates of bins at corresponding locations. Any bins that were unvisited in either map were excluded from the calculation. Firing rate overlap was calculated for each rate map as: $1 - \frac{|R1-R2|}{R1+R2}$ where *R1* is the mean firing rate from map 1 and *R2* is the mean firing rate from map 2. For grid cells, firing rate overlap was calculated independently for each grid field and the values were averaged across all fields of a given grid cell. For all calculations, only pairs of rate maps from identical configurations of the open field were compared.

Recording the same cell multiple times yields many pairwise comparisons that all share the same temporal delay. For example, across the four recording sessions in a block there are three different pairwise comparisons of adjacent sessions (session 1 vs 2, 2 vs 3, and 3 vs 4). Because some cells were recorded for longer than others, not all cells had an identical number of pairwise comparisons for a given temporal delay. Thus, to make sure that all cells contributed evenly to all analyses, when making any temporal comparison we collected all corresponding pairwise rate maps for a given cell and randomly drew a single pair, meaning that each cell was included in an analysis exactly one time, regardless of the total amount that a cell had been recorded. As this method meant that each individual calculation was influenced by the nature of the random draw, we repeated each calculation 25 times, performing a new random draw each time, to appropriately account for the variation across multiple pairwise comparisons of a cell. Performing such a random draw meant that all cells contributed equally to all calculations regardless of the total number of times that a cell was recorded. For spatial correlations and firing rate overlap calculations, 25 repetitions across corresponding intervals were performed for each cell, which were then averaged to a single value for that cell. Note that in most cases 25 iterations

exceeded all possible pairwise comparisons but that taking the average of randomly repeating comparisons would not bias the final value for the cell.

Statistics. For comparing isolation distances, we used a KS-Test to compare the full data set to the subset of cells that were tracked over at least two recording blocks and to compare the isolation distance between the first and the last recording of those cells that were tracked. All comparisons between groups (WSC, SI, change in spatial correlation, change in rate overlap) were made using either a Mann-Whitney rank-sum test when comparing two groups, or a Kruskal-Wallis test with Tukey's HSD post-hoc when comparing three or more groups. SI and WSC values were corrected by subtracting each cell's chance levels which were obtained by calculating the corresponding values from shuffled data (ΔSI and ΔWSC). Comparisons between median shifted WSC and SI distributions were made using a KS-Test. Comparisons of slope values (change over time) to zero were made using a Wilcoxon signed-rank test. When sample sizes were small ($n < 15$) an exact test statistic was calculated for the rank-sum and signed-rank tests. For data recorded from the small environment, changes between shapes made it such that for some cells and temporal lags it was not possible to make a comparison between identical environments. Therefore, comparisons were made using a Skillings-Mack test for repeated measure with missing data (Skillings and Mack, 1981) with a rank-sum test for post-hoc analysis. For any evaluation of correlation between two variables a Pearson's correlation was performed, though in all cases a Spearman's correlation yielded statistically equivalent results. Comparisons of proportion of cells between layers 2 and 3 were done using Pearson's chi-square test for categorical data. All statistical comparisons were significant at $p < 0.05$ for two tailed distributions.

Results

Principal cells from mEC superficial layers were recorded across multiple sessions within a day. In order to evaluate the stability of mEC spatial firing patterns over time we trained rats to randomly forage in an open field arena for eight 10-minute sessions within a day. Rats were trained to either explore two small enclosures (an 80 cm by 80 cm square or a 100 cm-diameter circle) or to explore one large enclosure (a 120 cm by 120 cm square). In the morning of each day, rats performed a block of four 10-minute foraging sessions that were each separated by 5-minute rest sessions. The morning block was followed by a six hour break, after which rats performed another block of four 10-minute foraging sessions in the afternoon. Between the morning and afternoon blocks rats were returned to their home cage. This design allowed us to evaluate the consistency of mEC firing (n = 313 principal cells; Figure 3.1A, B) within a single 10-minute session, across a series of sessions spanning roughly one hour, and between sessions separated by several hours.

To compare the spatial firing patterns between sessions in the same environment, we used previously published techniques to track the same set of cells across multiple recording sessions (Mankin et al., 2015; Mankin et al., 2012). Briefly, a spike cluster was identified as an individual cell when the cluster remained in the same location in multi-dimensional cluster space over a series of recording sessions and when the cluster was clearly separable from all other clusters in each recording session within the series (Figure 3.1C, D). Identified cells were tracked for as long as possible, ranging from a single block of four sessions to ten recording blocks spanning five days. Cells were tracked until there was no longer a spike cluster remaining in the tracked cluster space for multiple behavioral or sleep sessions. While such a lack of spiking could reflect periods of cellular inactivity during behavior, as has been described in CA1 (Thompson and Best, 1989), we never observed instances in which clusters were only detected in sleep sessions. We also did

Figure 3.1: mEC cells were recorded across multiple sessions in either small or large environments. A) Schematic of the two experimental paradigms. Rats repeatedly randomly foraged in the same open field environment. A block of four sessions in the morning was followed by a block of four sessions six hours later. Each foraging session within a block lasted 10-minutes with five-minute rest periods in between. Individual mEC cells were tracked across sessions and blocks. Three rats explored a small environment with flexible walls that were configured as either a square (80 cm by 80 cm) or a circle (100 cm diameter). Note that for this study all comparisons were between sessions in like-shaped environment configurations. The remaining five rats explored a single large square environment (120 cm by 120 cm). **B)** Example histological sections of mEC tetrode tracks from four rats. The superficial layers are delineated by the black line and the end of each tetrode track is marked with a red dot. Scale bars = 500 μm. **C)** Examples of two well isolated clusters that were tracked across sessions in the morning and afternoon. Each cluster remained in the same location in multi-dimensional cluster space allowing for the determination that each represented a single cell tracked across the day. **D)** Rate maps of the tracked cells from C. Firing rates are color-coded according to the scale bar on the right and the peak rate is noted below each map. Both cells maintain similar spatial firing patterns across the day, but rate maps were never used for cell tracking. **E)** Cluster isolation distance was calculated for all recorded mEC cells and for only those cells that were tracked over multiple recording blocks. Of those cells that were tracked, we also calculated the isolation distance the first and the last time that the cell was recorded. The distribution of isolation distances was comparable across all four conditions. While we did not use any quantitative threshold for our clusters, over 99.5 % of our clusters have an isolation distance in excess of previously published cutoffs (isolation distance of 5 or 10; dashed grey lines).

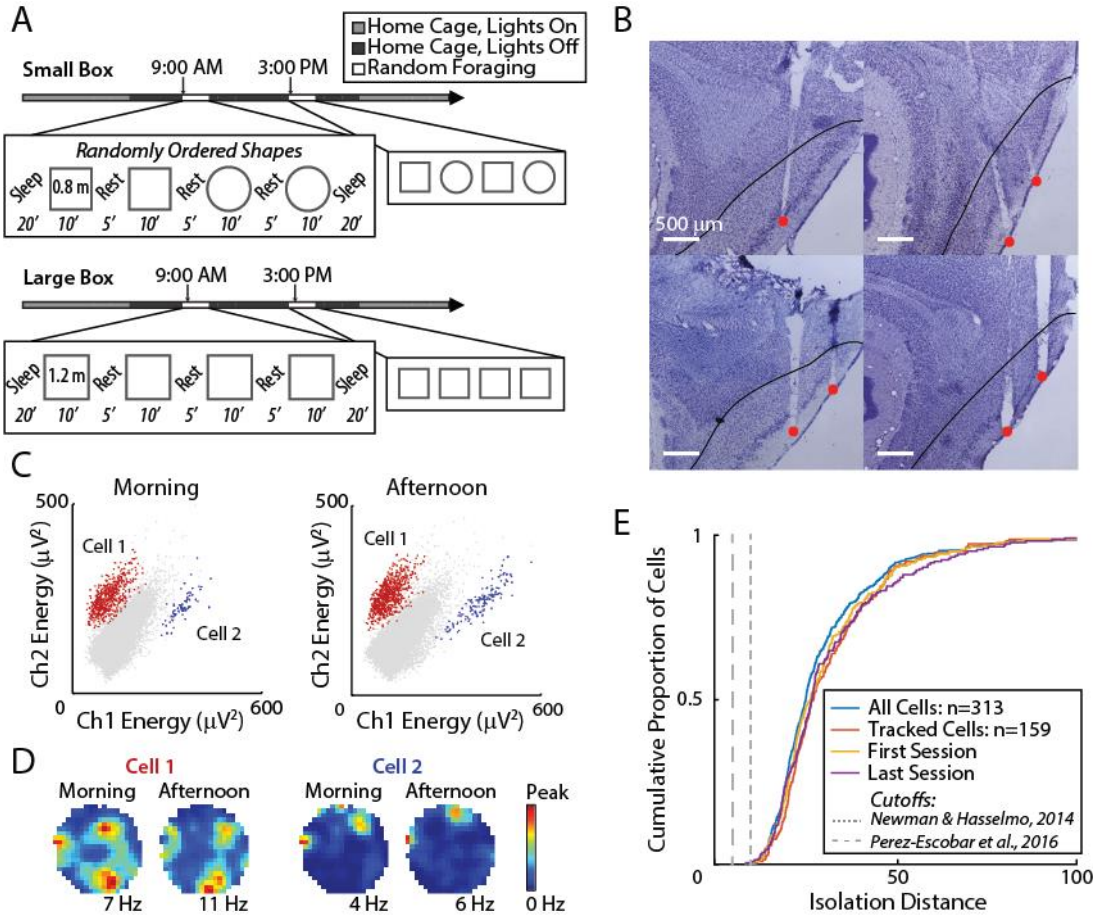
A
Home Cage, Lights On
Home Cage, Lights Off
Random Foraging
Small Box
9:00 AM
3:00 PM
Randomly Ordered Shapes
Sleep
0.8 m
Rest
Sleep
20′ 10′ 5′ 10′ 5′ 10′ 5′ 10′ 20′
Large Box
9:00 AM
3:00 PM
Sleep
1.2 m
Rest
Sleep
20′ 10′ 5′ 10′ 5′ 10′ 5′ 10′ 20′
B
500 µm
C
Morning
Afternoon
500
Ch2 Energy (µV²)
Cell 1
Cell 2
0
Ch1 Energy (µV²)
600
D
Cell 1
Cell 2
Morning
Afternoon
Peak
7 Hz
11 Hz
4 Hz
6 Hz
0 Hz
E
Cumulative Proportion of Cells
1
0.5
0
50
100
Isolation Distance
All Cells: n=313
Tracked Cells: n=159
First Session
Last Session
Cutoffs:
Newman & Hasselmo, 2014
Perez-Escobar et al., 2016

not observe the disappearing and reappearing of clusters during repeated behavioral sessions, contrary to previously described observations for CA1 recordings under similar conditions (Mankin et al., 2012). This observation is consistent with previous reports that the same mEC cells that are active during sleep periods are also active during exploration of an environment (Fyhn et al., 2004).

To quantify the quality of our single-unit clusters we calculated the isolation distance in each session (Figure 3.1E). While we did not exclude data based on isolation distance, 99.5 % of our clusters would be identified as high quality (isolation distance > 10) based on previous criteria for mEC recordings (Newman and Hasselmo, 2014; Perez-Escobar et al., 2016). We compared the isolation distance between the full population of recorded cells and the subset of cells that were tracked across multiple recording blocks and did not find a difference ($ks = 0.098$, $p > 0.05$). We also found no difference in isolation distance between clusters from the first and the last recording session of tracked cells ($ks = 0.069$, $p > 0.05$) (Figure 3.1E).

The spatial content of mEC cells depended on the size of the environment. In both our small and our large environment we identified grid cells as well as a population of non-grid cells with a wide range of spatial firing patterns (Figure 3.2A). Whereas some non-grid cells had highly precise spatial firing patterns, the firing of other non-grid cells was considerably more diffuse. To quantify each cell's spatial firing pattern we calculated the spatial information (SI: a metric of the level of spatial content conveyed by each spike) and the within session correlation (WSC: a metric of the stability of the spatial firing pattern within a single 10-minute session) (Figure 3.2B and 3.2C). These two metrics were adjusted by subtracting each cell's chance activity (ΔSI or ΔWSC).

Figure 3.2: The spatial firing patterns of mEC cells were reliable within a single 10-minute session. A) Rate maps of example grid and non-grid cells recorded from the two environment sizes. Firing rates are color-coded according to the scale bar on the right. For each rate map, the peak rate is noted above and SI is noted below. In the box marked by the stippled line, rate maps from each cell are shown separately for the first and second half of the 10-min behavioral session, and the WSC is noted below each pair. The example cells are identified in the scatter plots in B, C, and D as solid black circles. **B)** Top, average SI of mEC cells in a single 10-minute session as a function of the chance level SI based on shuffling procedures. Bottom, CDFs of the difference between the actual SI and chance-level SI (ΔSI). Data are segregated based on box size and by grid vs non-grid cells. **C)** Top, average WSC of mEC cells in a single 10-minute session as a function of chance level WSC. Bottom, CDFs of the difference between actual WSC and chance-level WSC (ΔWSC). **D)** ΔSI is plotted as a function of ΔWSC for each recorded mEC cell. Despite ΔSI and ΔWSC quantifying different aspects of the spatial firing patterns of a cell, the two were highly correlated ($r = 0.78$, $p = 1.89 \times 10^{-65}$). Cells were identified as spatial if both SI and WSC were above chance (blue quadrant) and as non-spatial if WSC and/or SI was below chance (red quadrants). All grid cells in the small and large environment and most non-grid cells in the small environment were spatial. The few non-spatial cells in the small environment ($n = 5$ of 31, gray circles) were not further analyzed. However, about half of the non-grid cells in the large environment (120 of 257) were non-spatial.

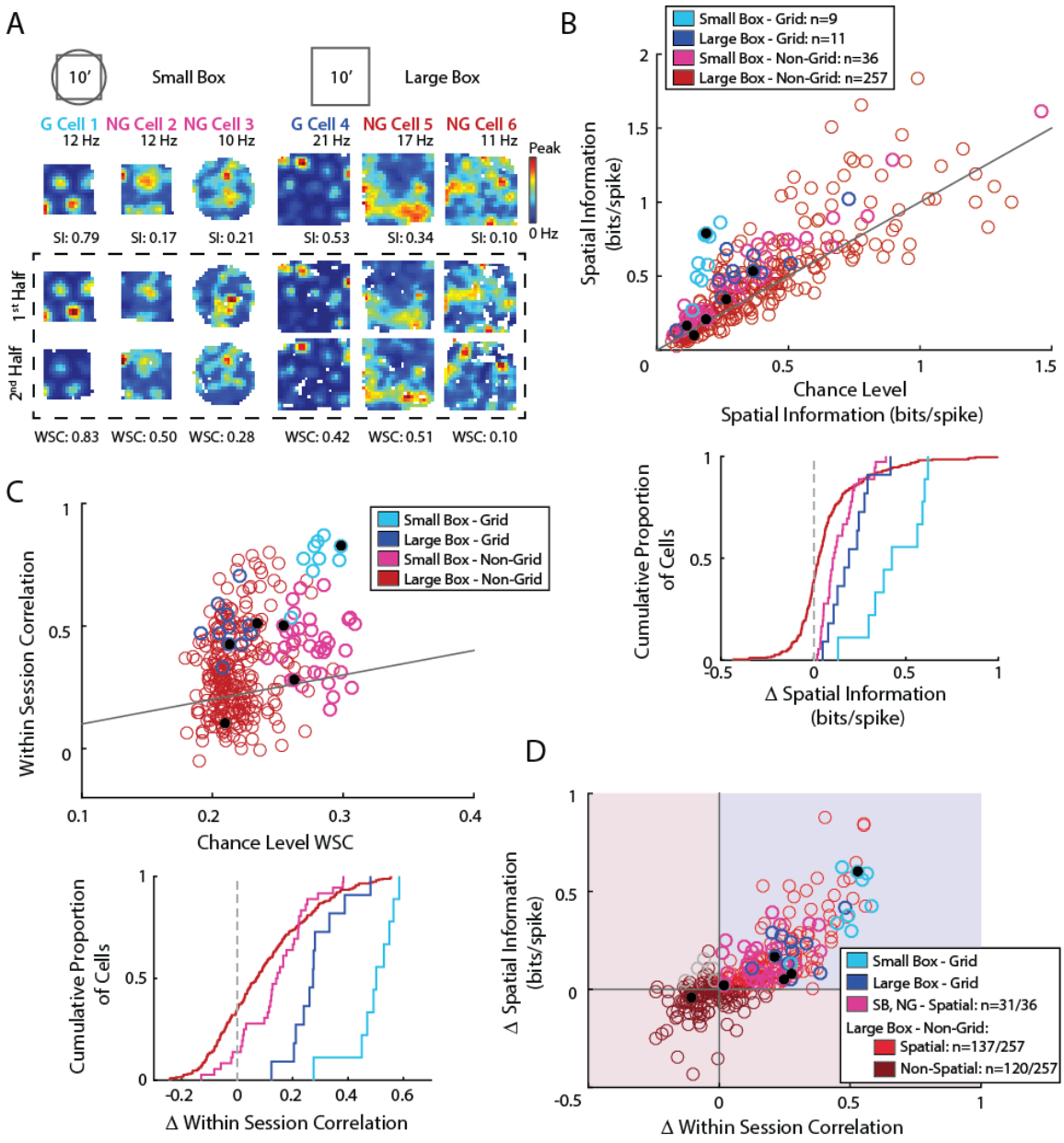
A
10′
Small Box
10′
Large Box
G Cell 1 12 Hz
NG Cell 2 12 Hz
NG Cell 3 10 Hz
G Cell 4 21 Hz
NG Cell 5 17 Hz
NG Cell 6 11 Hz
Peak
0 Hz
SI: 0.79
SI: 0.17
SI: 0.21
SI: 0.53
SI: 0.34
SI: 0.10
1st Half
2nd Half
WSC: 0.83
WSC: 0.50
WSC: 0.28
WSC: 0.42
WSC: 0.51
WSC: 0.10
B
Small Box - Grid: n=9
Large Box - Grid: n=11
Small Box - Non-Grid: n=36
Large Box - Non-Grid: n=257
Spatial Information (bits/spike)
Chance Level Spatial Information (bits/spike)
Cumulative Proportion of Cells
Δ Spatial Information (bits/spike)
C
Small Box - Grid
Large Box - Grid
Small Box - Non-Grid
Large Box - Non-Grid
Within Session Correlation
Chance Level WSC
Cumulative Proportion of Cells
Δ Within Session Correlation
D
Δ Spatial Information (bits/spike)
Small Box - Grid
Large Box - Grid
SB, NG - Spatial: n=31/36
Large Box - Non-Grid:
Spatial: n=137/257
Non-Spatial: n=120/257
Δ Within Session Correlation

Using these metrics for comparisons of spatial firing patterns in single 10-min recording sessions yielded three main results, all of which matched with our subjective observations of the spatial firing properties of mEC cells. First, spatial firing of grid cells was more precise and consistent than that of non-grid cells (ΔSI: Grid vs Non-grid in small box: $z = 3.99$, $p < 0.001$; in large box: $z = 3.45$, $p < 0.001$; ΔWSC: Grid vs Non-grid in small box: $z = 4.47$, $p < 0.001$; in large box: $z = 3.52$, $p < 0.001$). Second, spatial firing patterns of both grid and non-grid cells that were recorded in the small environment were more precise than spatial firing patterns of cells recorded in the large environment (ΔSI: Small vs Large box Grid: $z = 2.96$, $p < 0.01$; Non-grid: $z = 4.44$, $p < 0.001$; ΔWSC: Small vs Large box Grid: $z = 3.27$, $p < 0.01$; Non-grid: $z = 2.03$, $p < 0.05$). Interestingly, the size of the environment did not alter the shape of the SI or WSC distributions, but instead lead to a simple scalar decrease in the level of spatial firing across all mEC cells. After shifting both distributions to a median of 0 there was no difference in the distributions of data recorded in the small and large environments (SI: Small vs Large box Grid: $ks = 0.35$, $p > 0.05$; Non-grid: $ks = 0.20$, $p > 0.05$; WSC: Small vs Large box Grid: $ks = 0.39$, $p > 0.05$; Non-grid: $ks = 0.20$, $p > 0.05$). Due to the fact that data from the two environment sizes were recorded from different rats it is possible that differences in anatomical recording location could explain the difference in spatial firing properties. However, tetrodes were targeted to the same location in all rats, and recordings came from broad, highly overlapping regions across all animals. Furthermore, within each animal there was considerable intermixing of cells with high and low SI and/or WSC, with many instances of simultaneous recordings of high and low values on the same tetrode, making anatomical location an unlikely explanation for the differences between box sizes. Third, whereas about 90 % of mEC cells recorded in our small environment exhibited spatial firing patterns in excess of what would be expected by chance (i.e., ΔSI and ΔWSC > 0), the proportion of significantly spatial cells was reduced to ~55 % for cells recorded

in the large environment. For further examination of the stability of spatial firing of mEC cells, we segregated non-grid cells into two groups: those with SI and WSC above chance levels ('spatial') and those with SI and/or WSC below chance level ('non-spatial') (Figure 3.2D). Taken together, mEC cells were generally less spatial in a larger environment, such that a larger proportion of cells were characterized by spatial firing below chance levels.

Medial entorhinal cortex cells were stable across tens of minutes. After establishing that the majority of mEC cells exhibited spatial firing patterns that were reliable over the course of a single 10-minute recording session, we next asked whether mEC firing patterns were consistent when rats randomly foraged in the same environment repeatedly. As each of our recording blocks consisted of four open field foraging sessions, it was possible to compare the similarity of spatial representations between sessions as a function of the temporal distance between them, which corresponded to either 15, 30 or 45 minutes (Figure 3.3A). Past work has shown that in the hippocampus, CA1 and CA3 place cell representations remain highly stable over the course of an hour, while CA2 cells already begin to exhibit substantial changes after only 15 minutes (Mankin et al., 2015). Thus, we sought to determine whether mEC representations resembled either the stable CA1 and CA3 representations or the time varying CA2 representations.

While we observed that the similarity of spatial firing patterns across sessions was highest in grid cells and lowest in non-grid cells whose spatial firing was below chance ('non-spatial'), both the spatial firing patterns and the overall firing rate of mEC cells were just as similar between sessions separated by 45 minutes as when sessions were separated by only 15 minutes (Figure 3.3B, C). For the subset of cells that were recorded in the small environment, alternating between two shapes meant that it not always possible to compare between identical environments at all three temporal lags. For example, for a recording block with the order [Square, Circle, Circle, Square] it would be possible to evaluate firing with lag 1 (between

Figure 3.3: Medial entorhinal cortex representations were stable across tens of minutes. A) Schematic of potential comparisons for evaluating changes within a block of four sessions, and rate maps of five example cells across the four sessions. Font color for each rate map label corresponds to the legend in C. Firing rate maps were compared between adjacent sessions (Lag 1), between sessions that are two apart (Lag 2), or between sessions that are three apart (Lag 3). **B)** Spatial correlation of mEC cells across lags of 1, 2, or 3 sessions. Data are segregated based on environment size and grid vs non-grid cells. Non-grid cells recorded from the large environment are further segregated into spatial and non-spatial groups (see Figure 3.2D). Left, spatial correlation values of individual cells in the large environment. A random subset of up to 30 cells per group was selected for illustration purposes. As the order of the shape presentation in the small environment was varied, not all lag comparisons were available for each cell. Thus, individual cell data do not include cells from the small environment. Right, group median ± SEM for mEC cell types in the small and large environments. **C)** Firing rate overlaps of mEC cells across lags of 1, 2, or 3 sessions presented as in B with individual cells on the left and group averages on the right. Rate overlap values for grid cells were calculated for each grid field and averaged across all fields of a grid cell. **D)** Changes in spatial correlation and firing rate overlap over time were calculated for each cell by taking the slope of the best fit line of data in B and C. CDFs of the change over time are shown for data recorded from the large environment. For data from the small environment, population average values were used to calculate changes over time and are presented as a single point per group. **E)** Spatial correlation for each cell across sessions separated by lag 1 (top) or lag 3 (bottom) are shown as a function of the average WSC of the cell.

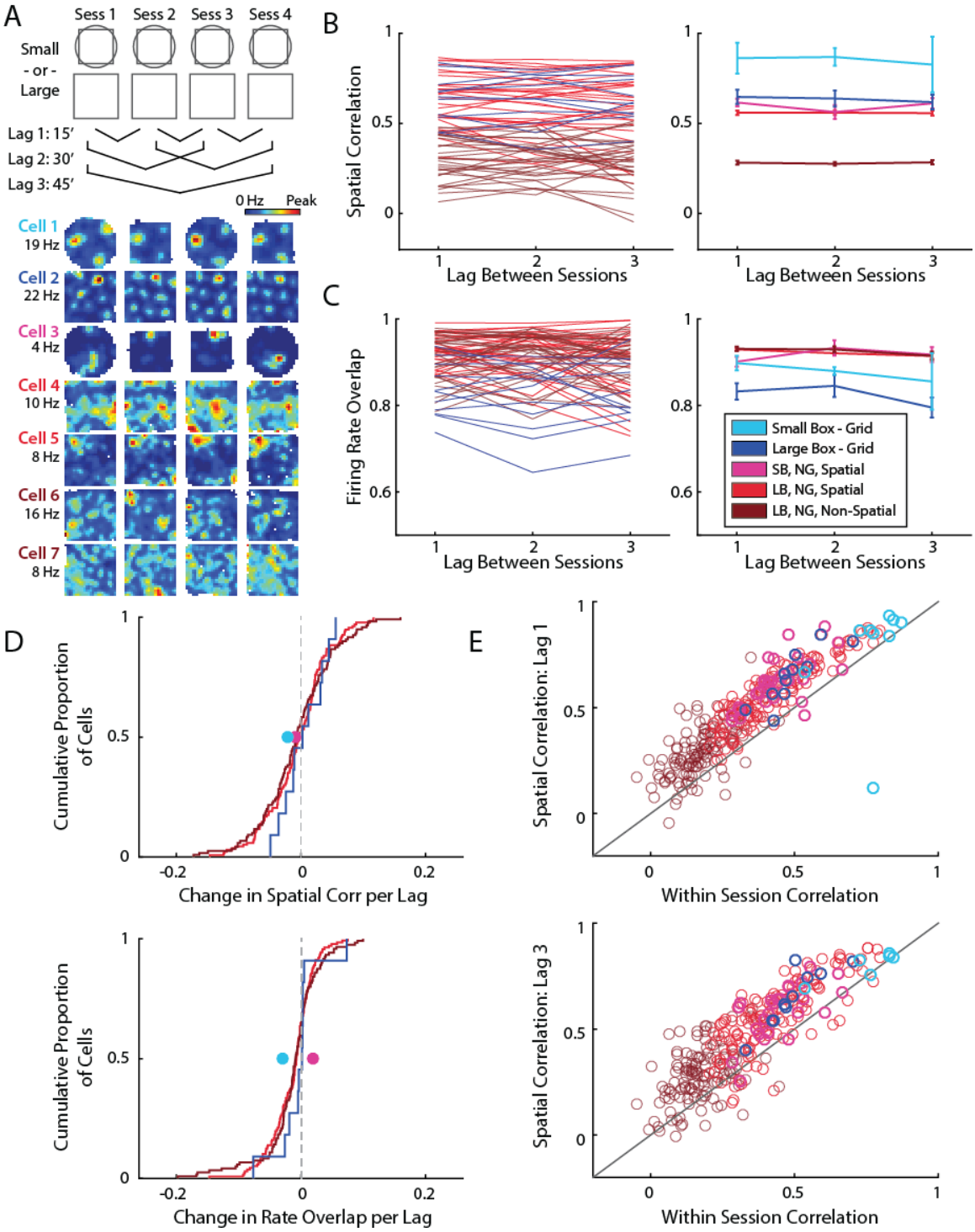
A
Sess 1
Sess 2
Sess 3
Sess 4
Small
- or -
Large
Lag 1: 15′
Lag 2: 30′
Lag 3: 45′
0 Hz
Peak
Cell 1
19 Hz
Cell 2
22 Hz
Cell 3
4 Hz
Cell 4
10 Hz
Cell 5
8 Hz
Cell 6
16 Hz
Cell 7
8 Hz
B
Spatial Correlation
Lag Between Sessions
C
Firing Rate Overlap
Lag Between Sessions
Small Box - Grid
Large Box - Grid
SB, NG, Spatial
LB, NG, Spatial
LB, NG, Non-Spatial
D
Cumulative Proportion of Cells
Change in Spatial Corr per Lag
Change in Rate Overlap per Lag
E
Spatial Correlation: Lag 1
Within Session Correlation
Spatial Correlation: Lag 3
Within Session Correlation

circles) and lag 3 (between squares), but there would be no comparison in which identical environments were separated by lag 2. Thus, for these data only group averages at each lag are presented and statistical considerations were taken to account for missing data points (see methods). For both grid and non-grid spatial cells recorded from the small environment, there was no systematic decrease in spatial correlation or firing rate overlap when comparing the three temporal lags (Spatial Correlation: Grid: $t(2) = 0.88$, $p > 0.05$; Non-grid spatial: $t(2) = 6.92$, $p < 0.05$, lag 1 vs lag 3 $p > 0.05$; Rate Overlap: Grid: $t(2) = 2.49$, $p > 0.05$; Non-grid spatial: $t(2) = 0.45$, $p > 0.05$). As there were only five non-grid cells recorded in the small environment with spatial firing below chance ('non-spatial'), this group was not analyzed.

For mEC cells recorded in the single large environment, comparisons at all three lags were feasible. Thus, to quantify the degree of change in spatial correlation and rate overlap over time we fit the data of each cell across the three time lags with a linear regression and calculated the slope of the fit line (Figure 3.3D). We found that the rate of change in spatial correlation was not different from zero for all three groups of mEC cells (Grid: signed-rank = 28, $p > 0.05$; Non-grid spatial: $z = -1.00$, $p > 0.05$; Non-grid non-spatial: $z = -1.35$, $p > 0.05$) as was the case for the rate of change in firing rate overlap for grid cells (signed-rank = 16, $p > 0.05$). Both groups of non-grid cells had significant decreases in firing rate overlap over time (Non-grid spatial: $z = -4.62$, $P < 0.001$; Non-grid non-spatial: $z = -4.03$, $p < 0.001$), but in both cases the average decrease was less than 5 % over the course of three behavioral sessions. Additionally, we found no differences in slope values between the three mEC cell types recorded in the large box for spatial correlation (Grid vs Non-grid spatial vs Non-grid non-spatial: Chi-Sq(2) = 3.31, $p > 0.05$) or rate overlap (Chi-Sq(2) = 1.00, $p > 0.05$) indicating that all cell types had comparable levels of firing stability over tens of minutes. Lastly, we sought to compare the stability of the spatial firing of mEC cells between sessions to the stability within a single 10-minute session (Figure 3.3E).

WSC and spatial correlation across pairs of rate maps separated by lag 1 were highly correlated ($r = 0.89$, $p = 4.83 \times 10^{-106}$) indicating that those cells that tended to have more consistent spatial firing within a single session also had more consistent firing across repeated exposures to a given environment. A similar pattern was observed when comparing WSC to spatial correlation across lag 3 ($r = 0.80$, $p = 6.75 \times 10^{-69}$), further supporting our finding that the spatial firing of mEC cells did not change systematically over tens of minutes.

Firing patterns of grid cells and the majority of non-grid cells were stable over six hours. After observing that mEC representations did not change across intervals of less than 1 hour, we determined whether representations were stable over the course of several hours. As we were able to track the identity of a subset of our mEC cell population from the morning to the afternoon (159 of 313 cells), it was possible to compare their firing properties between sessions separated by less than one hour (either within the morning or afternoon block) and between sessions that were separated by six hours (between the morning and afternoon block) (Figure 3.4A). In general, mEC cells appeared to be largely consistent in their firing patterns from the morning to the afternoon, exhibiting approximately the same spatial firing patterns at comparable firing rates (Figure 3.4B). To quantify the stability of mEC firing, we compared spatial correlations and firing rate overlap values between rate maps separated by less than one hour and those separated by six hours (Figure 3.4C). We also calculated the change over time (Figure 3.4D), though this was simply the difference between the two time points, as opposed to the slope of a fit line as calculated for Figure 3.3D. Our first observations were that the firing characteristics of mEC grid cells over time were not influenced by the size of the recording environment (Small box vs Large box for change in spatial correlation: rank-sum = 37, $p > 0.05$; change in rate overlap: rank-sum = 36, $p > 0.05$). For non-grid cells, there were neither differences depending on the size of the environment nor depending on whether cells were classified as spatial or non-spatial in the large

Figure 3.4: Medial entorhinal cortex grid cells and most non-grid cells were stable over time but a subset of non-grid cells changed. A) Schematic of comparisons between rate maps separated by less than one hour or with a six-hour delay. **B)** Rate maps of 12 example cells that were tracked from the morning to the afternoon sessions. Font color for each rate map label corresponds to the legend in C. For cells that were recorded in both a square and a circular enclosure, only sessions in identical shapes were compared. In general, the spatial firing patterns of mEC cells remained similar over the course of the day. However, a few cells exhibited major changes in their firing patterns. **C)** Spatial correlation (left) and firing rate overlap (right) for mEC cells. Scatter plots for each of these measurements are between rate maps separated in time by less than one hour and rate maps separated by six hours. Data are color-coded by environment size and by grid vs non-grid cells. Non-grid cells that were recorded in the large environment are further divided into spatial and non-spatial cells. The median values for each group are shown as a filled circle ± standard deviation. **D)** The change in spatial correlation and firing rate overlap over time was calculated for each cell by taking the difference between comparisons across less than an hour and comparisons across six hours. **E)** Top, previously published recordings of hippocampal cells across six hours in a small environment (Mankin et al., 2015) were reanalyzed with the same methods as used here for mEC data. Bottom, mEC data from the small environment are redrawn from panel D. While these plots allow for an approximate comparison between mEC and hippocampal data, direct statistical comparisons were not made due to low mEC cell numbers, lack of any simultaneous recordings between the two regions, and the fundamentally different spatial firing patterns between hippocampal place cells and mEC grid and non-grid cells.

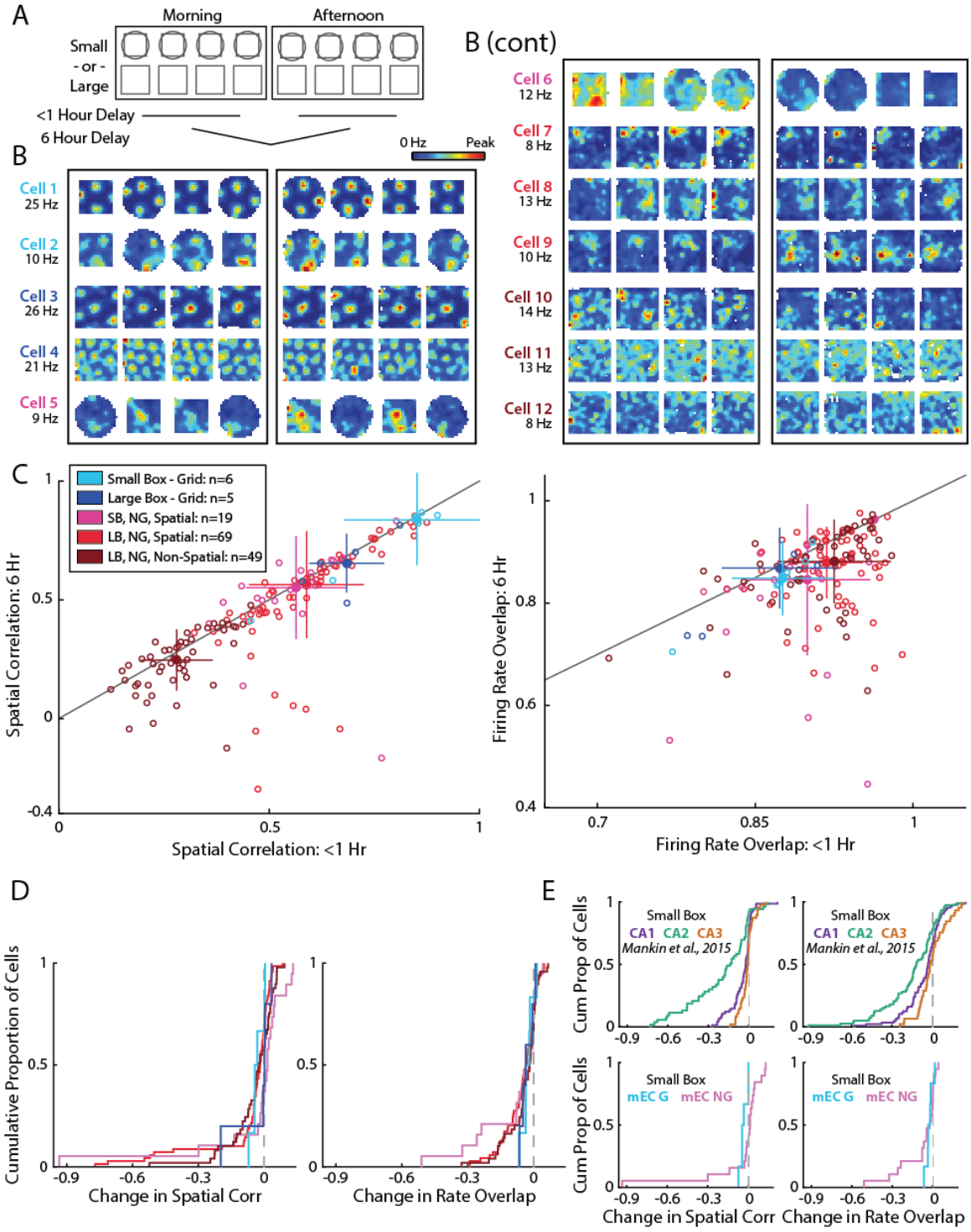
A
Morning
Afternoon
Small
- or -
Large
<1 Hour Delay
6 Hour Delay
B
0 Hz
Peak
Cell 1
25 Hz
Cell 2
10 Hz
Cell 3
26 Hz
Cell 4
21 Hz
Cell 5
9 Hz
B (cont)
Cell 6
12 Hz
Cell 7
8 Hz
Cell 8
13 Hz
Cell 9
10 Hz
Cell 10
14 Hz
Cell 11
13 Hz
Cell 12
8 Hz
C
Small Box - Grid: n=6
Large Box - Grid: n=5
SB, NG, Spatial: n=19
LB, NG, Spatial: n=69
LB, NG, Non-Spatial: n=49
Spatial Correlation: 6 Hr
Spatial Correlation: <1 Hr
Firing Rate Overlap: 6 Hr
Firing Rate Overlap: <1 Hr
D
Cumulative Proportion of Cells
Change in Spatial Corr
Change in Rate Overlap
E
Cum Prop of Cells
Small Box
CA1 CA2 CA3
Mankin et al., 2015
mEC G mEC NG
Change in Spatial Corr
Change in Rate Overlap

box (Non-grid spatial small box vs Non-grid spatial large box vs Non-grid non-spatial large box for change in spatial correlation: Chi-Sq(2) = 0.23, $p > 0.05$; for change in rate overlap: Chi-Sq(2) = 1.93, $p > 0.05$). Thus, for subsequent statistical comparisons we grouped all grid cells together and all non-grid cells together regardless of environment size or degree of spatial firing. In evaluating firing over six hours, we found that the spatial firing pattern and overall firing rate of mEC grid cells was stable over time (change in spatial correlation vs zero: signed-rank = 30, $p > 0.05$; change in rate overlap vs zero: signed-rank = 19, $p > 0.05$). Such high stability is in stark contrast to the rapid decorrelation over time that we previously described for the hippocampal CA2 region (Figure 3.4E; Data reanalyzed from Mankin et al., 2015 and presented for comparison). Yet, whereas the firing of all grid cells remained stable, we observed a clear negative tail in the distribution of non-grid cells for both spatial pattern and firing rate change. As such, the average change in spatial correlation or rate overlap of the non-grid cell population was significantly below zero (change in spatial correlation vs zero: $z = -4.74$, $P < 0.001$; change in rate overlap vs zero: $z = -6.83$, $p < 0.001$). Although the average values fell below zero, it can be appreciated that most non-grid cells maintained their firing patterns over time, and that the effect is driven by a subset of 10–20 % of non-grid cells that exhibited dramatic changes in spatial firing or overall firing rate over the course of a six-hour period.

Non-grid cells that changed over time were preferentially recorded from layer 3 over layer 2. After observing that a subset of mEC non-grid cells exhibited robust changes in their spatial firing or overall firing rate, we sought to gain further insight into this group of cells. We first verified that our observed changes over time were not a consequence of poor single unit cluster cutting procedures. There was no relationship between changes over time and a cell's isolation distance (change in spatial correlation: $r = 0.06$, $p > 0.05$; change in rate overlap: $r = 0.01$, $p > 0.05$) (Figure 3.5A). Next, we sought to determine whether there are any firing

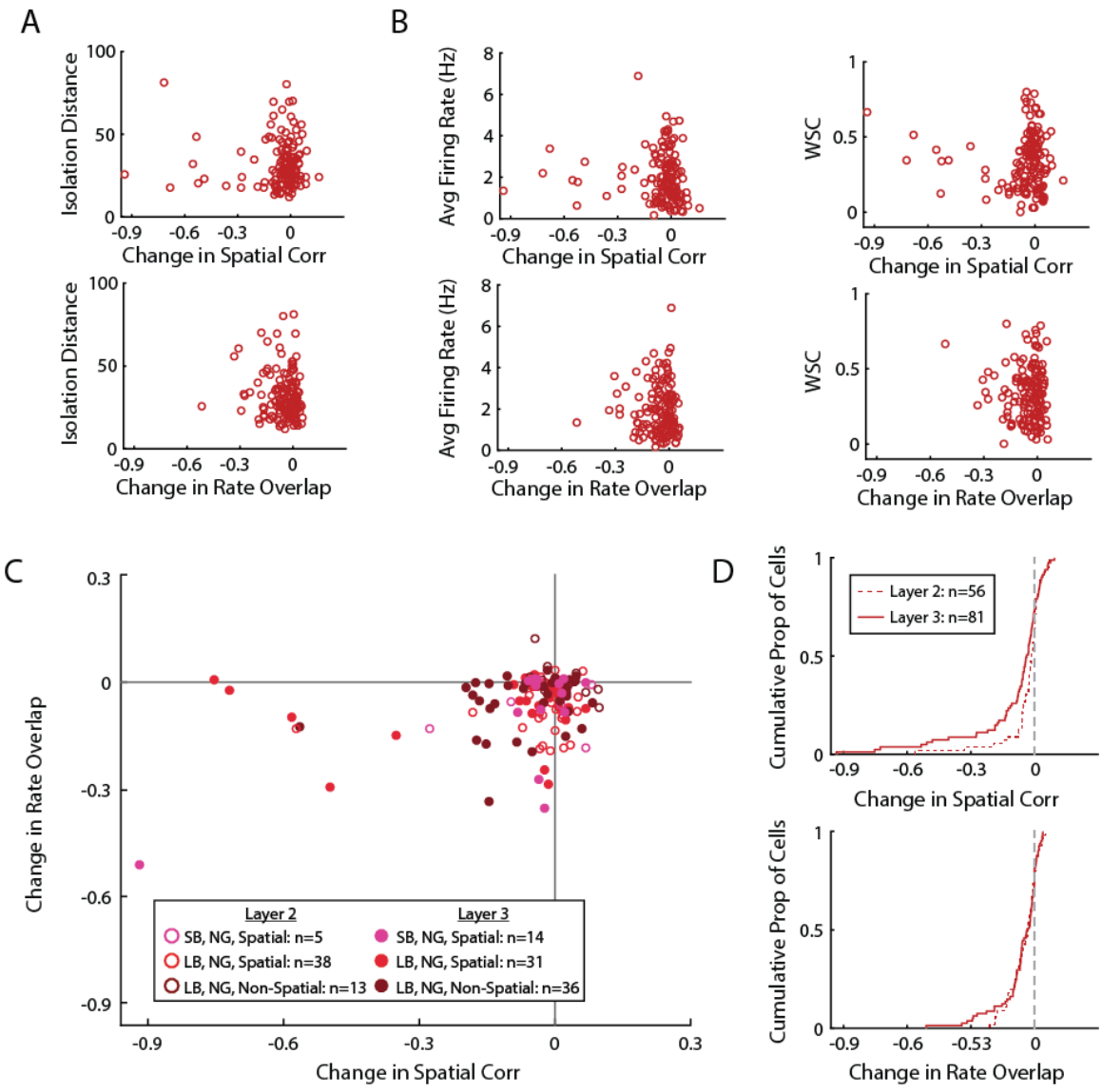

Figure 3.5: Medial entorhinal cortex non-grid cells that change did not represent a distinct subclass. A) Changes in spatial correlation (top) and rate overlap (bottom) over time were unrelated to cluster isolation distance of the cell. **B)** Changes over time were unrelated to cells' average firing rate and WSC. Changes were also unrelated to peak firing rate, SI, head direction modulation, theta modulation, or wave form shape (not shown). **C)** Comparison of the degree of change over time in spatial correlation and firing rate overlap of individual non-grid cells. Data are colored based on experimental paradigm, with non-grid cells recorded in the large environment further divided into spatial and non-spatial cells. Cells are also categorized based on their putative anatomical location within mEC layer 2 or layer 3. **D)** Changes in spatial correlation (top) and firing rate overlap (bottom) are presented separately for non-grid cells recorded from layer 2 and layer 3.

properties that may identify non-grid cells that change over time as a distinct subset of the mEC population. However, we did not observe any clear clustering or any relationship between changes over extended time and a cell's average firing rate, WSC, peak firing rate, SI, head direction modulation, theta modulation, or wave form shape (change in spatial correlation: r ranged from -0.15 to 0.09, all $p > 0.05$; change in rate overlap: r ranged from -0.11 to 0.13, all $p > 0.05$) (Figure 3.5B). Thus, those cells that changed over time did not appear in any way distinct, nor would it have been possible to identify *a priori* which cells would change based on the activity pattern within a single session. As we observed changes over time in both the spatial firing and overall firing rate of a subset of our non-grid cells we sought to determine if there was any relation between the two modalities. There was a weak relationship between changes in space and changes in rate ($r = 0.36$, $p < 0.001$) with a few cells responding in both dimensions, but there were also a large number of cells that altered only their spatial pattern or only their firing rate (Figure 3.5C). Lastly, as mEC superficial layers 2 and 3 have highly differential projection patterns to CA3 and CA1 (van Strien et al., 2009), we asked if there were any anatomical differences between non-grid cells that changed over time and those that did not. For both changes in spatial firing and changes in overall firing rate, we found on average no difference between non-grid cells recorded from layer 2 and from layer 3 (Layer 2 vs Layer 3, change in spatial correlation: $z = 1.62$, $p > 0.05$; change in rate overlap: $z = -0.09$, $p > 0.05$). Yet, further examination of changes in spatial firing patterns over time revealed that the change in spatial correlation of layer 2 non-grid cells was no different than zero (change in spatial correlation vs zero: $z = -1.91$, $p > 0.05$), whereas layer 3 non-grid cells exhibited a significant change in spatial correlation over time (change in spatial correlation vs zero: $z = -3.98$, $p < 0.001$). Additionally, there were fewer layer 2 cells with changes in spatial correlation of at least 0.01 per hour (0.06 over the 6 hour period) as compared to layer 3 non-grid cells (proportion of cells in layer 2 vs

layer 3 with change greater than 0.06: Chi-Sq = 6.96, $p < 0.01$) (Figure 3.5D). Thus, it appears that while layer 3 non-grid cells may be more likely to exhibit large scale changes in their spatial firing pattern over time, there is no clear dichotomy between the average change of mEC layer 2 compared to layer 3 non-grid cells.

Discussion

Hippocampal spatial representations have previously been shown to change over time, and stability of hippocampal representations further decreases when inputs from mEC to hippocampus are damaged (Hales et al., 2014; Schlesiger et al., 2015). We therefore asked whether spatial firing patterns of mEC grid and non-grid cells are stable over extended time periods such that they are in a position to provide a stabilizing signal to the hippocampus. Within a single recording session, we generally found high precision and stability of spatial firing patterns of mEC cells. However, environment size determined the degree of spatial precision. SI and WSC were significantly higher for both grid and non-grid cells in a small box compared to a large box. Furthermore, while almost all non-grid cells had spatial firing patterns above chance levels in the small box, about half of non-grid cells were non-spatial in the large box. We then evaluated the consistency of mEC firing patterns over time. Irrespective of environment size, we observed that grid cell activity was highly consistent across repeated exposures to the same environment both over tens of minutes and over six hours. A majority of the non-grid cell population was similarly stable over time, but for a subset of 10–20 % of non-grid cells, we observed a dramatic change in the spatial firing or overall firing rate across a six-hour period. Further investigation revealed that those non-grid cells that changed over time were preferentially recorded from layer 3, but that we could not predict from the firing characteristics within a 10-

minute recording session whether a cell would show instability over longer time intervals. Taken together, the majority of mEC cells thus showed a high degree of stability, consistent with the possibility that a key function of mEC inputs to the hippocampus is the stabilization of spatial firing patterns over time.

Many previous studies have identified a substantial subset of mEC cells as non-spatial (Kropff et al., 2015; Latuske et al., 2015; Tang et al., 2014; Tang et al., 2015; Zhang et al., 2013). In contrast, recent work utilizing more sophisticated classification criteria found that almost all mEC cells exhibit some degree of spatial firing (Diehl et al., 2017; Hardcastle et al., 2017). Our data add to these findings with two main results. First, our finding that SI and WSC, two metrics for evaluating spatial firing patterns, are both unimodally distributed suggests that spatial firing of mEC cells would be more appropriately described as a continuum, as opposed to discrete classes of spatial and non-spatial cells. For example, we observed no differences in the stability of spatial firing properties over time in non-grid cells with spatial content above and below chance. These findings are consistent with the interpretation that spatial and non-spatial cells are not mEC cell types that can be unambiguously separated. Second, we observed significantly higher SI and WSC values for cells recorded in a smaller compared to a larger box. The size of an environment thus has a substantial impact on the spatial firing properties of mEC cells. Theoretical work has proposed that spatial firing in mEC and hippocampus is strongly influenced by interactions with environmental boundaries or other highly salient spatial landmarks (Barry et al., 2006; Fuhs and Touretzky, 2006; Gothard et al., 1996; Hartley et al., 2000), such that larger environments with more distant boundaries would be predicted to result in poorer spatial representations. Such an idea has gained experimental support by the finding that hippocampal place fields are reliably generated in novel small environments but not in larger ones following pharmacological inactivation of the medial septal area. (Brandon et al., 2014; Wang et al., 2015). Additionally, fine

scale analysis of grid cell firing revealed a gradual accumulation of error in spiking location that was corrected after interactions with a border region (Hardcastle et al., 2015). Larger environments with more distant borders would thus be predicted to lead to greater error accumulation in spatial spiking. Accordingly, we found that the spatial firing of mEC grid and non-grid cells is influenced by environment size.

Along with identifying an effect of environment size on spatial firing of both grid and non-grid cells, we also found that both cell types show a similar degree of stability over periods of less than one hour. Spatial firing patterns of both grid and non-grid cells were highly stable between adjacent sessions as well as when separated by intervening sessions. In comparison to hippocampal place cells, mEC cells thus resemble the stability of CA1 and CA3 rather than the variability of CA2, where changes are already evident over tens of minutes (Mankin et al., 2015). Major differences in the stability of grid cells compared to non-grid cells began to emerge when examining spatial firing patterns over periods of six hours. Consistent with the notion that grid cells may provide a universal spatial signal (Moser et al., 2008; Moser et al., 2014), the stability of the grid signal remained high over extended time periods. While many non-grid cells were also stable, the non-grid population was distinct in that it also included a subset of non-grid cells that changed over time. These observations suggest that a subpopulation of mEC non-grid cells may convey temporal information. Conversely, grid cells and the major population of stable non-grid cells may be a key source of inputs to stabilize hippocampal CA1 and CA3 maps.

Our data therefore suggest that entorhinal cortex can contribute to both stable and drifting network representation across hippocampal subpopulations. By providing a time invariant representation, grid cell input likely provides stability for hippocampal maps. In contrast, non-grid cells present a more complicated picture. The difference in the degree of variability over time between layer 2 and layer 3 cells suggests a possible direct relationship to hippocampal coding,

with the more stable layer 2 population projecting to CA3 and supporting the more stable CA3 region and the more time varying layer 3 population projecting to CA1 and contributing to the more time varying CA1 region (Mankin et al., 2012; van Strien et al., 2009). As CA2 receives input from both mEC layer 2 and layer 3 (Chevaleyre and Siegelbaum, 2010; Cui et al., 2013; Hitti and Siegelbaum, 2014; but see Kohara et al., 2014), a time varying signal could be inherited from the small subpopulation of highly varying mEC cells, though given the large proportion of CA2 cells that change over time and the large degree to which the network changes (Lu et al., 2015; Mankin et al., 2015) other inputs or local integration within the CA2 region are also likely sources of variability over time.

Yet, it must also be recognized that not all mEC layer 3 cells altered their firing properties over time, and that not all mEC cells, either in layer 2 or layer 3, project directly to hippocampus (Tang et al., 2015; Varga et al., 2010; Zhang et al., 2013). An equally feasible situation then is that those non-grid cells which changed over time could project exclusively within mEC, or that the mEC projection downstream to hippocampus is composed of a mixed population of cells that change over time and cells that do not change. While attempts have been made to associate the in vivo firing patterns, genetic and morphological profiles, and anatomical connections of individual mEC cells (Latuske et al., 2015; Sun et al., 2015; Tang et al., 2014; Zhang et al., 2013), there has been limited success in linking different classes of mEC cells and determining a clear, comprehensive wiring diagram of entorhinal-hippocampal interactions. Future studies and new methods are thus required to establish a more direct relation between the inputs to hippocampus and the time-varying firing patterns across hippocampal subregions. Here we find that mEC provides hippocampus with a diverse set of spatially selective inputs of which most are highly stable over time, a necessary feature for establishing reliable spatial maps. Yet hippocampus complements its spatial representation with information about elapsed time, a

feature that we also observe in only a subset of mEC non-grid cells. Thus, our data suggest a possible contribution of mEC to the diversity of temporal coding and the possibility that CA1 and CA2 inherit a time varying signal from mEC layer 3 non-grid cells. Importantly, we also find that the majority of the medial entorhinal projection is highly reliable across time, consistent with findings from lesion studies indicating a major role of mEC in providing hippocampus with a stable spatial code over minutes and hours (Hales et al., 2014; Schlesiger et al., 2015).

Acknowledgements

We thank B. Boublil, A-L. Schlenner, and M. Wong for technical assistance. Research was supported by National Institute of Health grants MH-100349, MH-102841, the Whitehall Foundation 20130571, and a Walter F. Heiligenberg Professorship to J.K.L, and National Institute of Health grants MH-100354, NS-084324, and NS-086947 to S.L.

Chapter 3, in full, is material as it has been submitted to *Hippocampus.* Diehl, Geoffrey W., Hon, Olivia J., Leutgeb, Stefan, and Leutgeb, Jill K. The dissertation author was the primary researcher and author of this paper.

CHAPTER 4 CONCLUDING REMARKS AND FUTURE DIRECTIONS

Episodic memories play an important role in our capacity to adapt our behavior to changing situations. Simultaneously, the ability to localize oneself in space and navigate through the world is critical for an array of behavioral demands including locating and returning to food sources or safety and avoiding dangerous areas. For both of these tasks, episodic memory and spatial navigation, the hippocampus and upstream medial entorhinal cortex play a central role (Eichenbaum, 2000; Squire and Zola-Morgan, 1991). Behavioral work has been essential in this understanding, and physiological recordings have provided insight into what information is important and how it is represented by the brain. In the hippocampus, we have learned how the spatial content of an experience is represented by a network of place cells (O'Keefe and Nadel, 1978), how non-spatial information can be represented in conjunction with this spatial signal (Anderson and Jeffery, 2003; Bostock et al., 1991; Leutgeb et al., 2005b; Wood et al., 1999), how changes to network activity through remapping can serve as a mechanism to support episodic memory (Colgin et al., 2008), and how gradual changes over time can be utilized to encode the temporal recency of an experience (Mankin et al., 2012; Manns et al., 2007). But our understanding of how these various coding schemes emerge is less complete. Within the hippocampus the activity of CA1, CA3, and DG have been well documented but the properties of CA2 and its role in the hippocampal circuit remain uncertain. Upstream in mEC, robust spatial representations have been described and the existence of non-spatial representations is beginning to be revealed (Aronov et al., 2017; Fyhn et al., 2004; Keene et al., 2016; Kraus et al., 2015). But the dynamics of these signals over time are largely unknown and the physiological mechanisms by which the mEC network could support encoding of episodic memory remains unclear. In this dissertation we have sought to address these unknowns, focusing predominantly on the activity of

mEC cells, and sought to understand how their firing patterns may relate to, and support, downstream hippocampal coding.

Overwhelmingly, the spatial firing patterns of downstream hippocampal place cells have been hypothesized and modeled to emerge through integration of mEC input, in particular through that of grid cells (Barry et al., 2006; de Almeida et al., 2009; Fuhs and Touretzky, 2006; McNaughton et al., 2006; Solstad et al., 2006). While initially this viewpoint seemed appropriate given reports of grid cells composing the majority of the mEC signal sent to hippocampus (Boccara et al., 2010), reasons to question it have emerged. Most prominently, we now know that grid cells are not the only players, or even the majority players, in spatial coding by the mEC network. In chapter 1, we highlighted the presence of non-grid spatial cells (NGS) as an important component of mEC activity. While far less precise in their specific spatial firing patterns, the activity of NGS cells is reliable, in many cases even over several hours as described in chapter 3, indicating that the spatial information can be useful. Furthermore, our work revealed that the proportion of mEC cells with a significant degree of spatial firing is substantially greater than previously thought, making up between half and two thirds of the total population. Thus, it appears that if integrated appropriately, input from NGS cells could be sufficient to support the formation of downstream place fields.

However, the hippocampus can also represent episodic memory information in conjunction with its spatial signal, in particular through the process of rate remapping in response to subtle changes in the non-spatial components of an experience (Colgin et al., 2008; Leutgeb et al., 2005b). Historically the non-spatial information necessary for this rate coding had been through of as arriving from lEC (Deshmukh, 2014; Eichenbaum et al., 2012; Lu et al., 2013; Renno-Costa et al., 2010), completely independent of any spatial input from mEC grid, border, or NGS cells. Yet contrary to this view that there are distinct parallel streams to support spatial

representations and conjunctive rate coding, in chapter 1 we found that conditions that elicit rate remapping in hippocampal place cells also led to changes in the firing patterns of both grid and NGS cells upstream in mEC. In response to subtle manipulations of environmental features, grid cells maintained their spatial firing patterns but adapted their firing rates by redistributing activity across their grid fields. For NGS cells, subtle changes in environment features produced dramatic changes in the spatial firing patterns. Thus, while NGS cells are able to maintain a reliable spatial signal across many repetitions of a singular experience, representation and differentiation of multiple experiences is achieved via the spatial domain, seemingly forgoing any utility of this spatial information in navigational processes.

How then does the hippocampus receive the spatial information used to establish the spatial location of place fields and the non-spatial feature information used to adapt their firing rates? What are the roles of grid and NGS cells in providing the necessary content? Perhaps the most parsimonious explanation would be that the spatial firing of place cells arises through an integration of the grid cell signal, much in the way as has been widely postulated. That the spatial firing of grid and place cells exhibit strong parallels, remaining stable in response to feature manipulations and changing only in response to alterations of an experience's broad spatial components, support this viewpoint. In turn NGS cells, in conjunction with lEC, would contribute the information necessary to determine place field firing rates. The specific characteristics of an experience would be represented in mEC by the spatial firing patterns of NGS cells, which would then be translated to a rate code by hippocampus. In this way mEC would contain two independent processing streams. Grid cells would provide a dedicated spatial signal, with NGS cells acting to supply the information necessary to support episodic memory coding.

However, such a model remains purely correlative and in fact encounters difficulties when considering causal manipulations of the MTL system. Most notably, it fails to account for

disruption of grid cell firing, such as during manipulations of the MSA. Past work has found that by pharmacologically inactivating the MSA, the periodic spatial firing pattern of grid cells can be eliminated (Brandon et al., 2011; Koenig et al., 2011). Yet downstream in the hippocampus, the spatial firing of place cells appears to emerge normally (Brandon et al., 2014; Koenig et al., 2011). Accordingly, it remains difficult to conceptualize how grid cells could act to establish the spatial firing of place cells under normal conditions but be completely uninvolved during inactivations of the MSA. Instead NGS cells, whose spatial firing pattern is largely retained during MSA inactivation (Koenig et al., 2011), may be critical for the generation of hippocampal place fields. Though in this case it becomes necessary to explain how the dramatic changes in spatial firing patterns observed in NGS cells during conditions of rate remapping would not lead to similar changes in the spatial firing patterns of downstream place cells. A third possibility would be that spatial firing of place cells is generated through the combined action of grid and NGS cells. NGS cells could provide the necessary spatial content, with grid cells then acting to refine and anchor it across different environment conditions. In this case one may hypothesize that NGS cells alone could generate place field firing, but that without complementary grid cell input the dramatic changes in the spatial firing of NGS cells observed under conditions of rate remapping would inappropriately be passed downstream to hippocampus. Such a hypothesis could easily be tested by monitoring place cell activity in a rate remapping paradigm during MSA inactivation. If hippocampus were to behave normally, it would indicate that grid cell activity is expendable for both spatial and rate coding by the hippocampus. However, if place fields were formed normally, but were unable to exhibit proper rate coding or could not maintain their spatial locations across feature changes, it would point towards an important role of the grid cell population in either supplying non-spatial content or anchoring the spatial signal.

Our results also provide valuable insight into the behavior of the MTL over time, both in its ability to maintain a long-term representation of spatial content to use for navigation and its coding for the temporal recency of an experience. Considering the hippocampus, chapter 2 described how CA2 network representations changed rapidly over time, presenting a parallel to the highly stable signal previously observed in CA3 (Lu et al., 2015; Mankin et al., 2012). These results provide robust support for theoretical work, presenting a model in which the CA1 region acts to compute the temporal recency (the *when*) of an event through the comparison of a temporally stable CA3 input and a time varying CA2 input. In conjunction with its reliable spatial signal (the *where*) and ability to distinguish between specific experiences (the *what*) through rate remapping, CA1 then contains the necessary *where-what-when* components for encoding all of the facets of episodic memory (Tulving, 1972).

In chapter 3 we followed up on this work to reveal how upstream mEC activity may allow for hippocampus to generate a time varying signal to be used for encoding of elapsed time, while simultaneously maintaining a long-term spatial map. Consistent with the viewpoint that grid cells provide a global metric of space, we found the behavior of grid cells to be highly consistent over periods of minutes and hours, relaying spatial information but no temporal signal. Among the population of non-grid cells, coding was more nuanced. Across non-grid cells, the degree of spatial coding was considerably less precise and less reliable than that of grid cells. Although this baseline degree of similarity was lower, for a large proportion of non-grid cells the degree of similarity of the firing patterns across two sessions was unaffected by the time between them. That is to say, the firing properties of a given cell would be recalled to the same degree 15 minutes later or six hours later, meaning that no information could be extracted about the temporal delay between experiences. Yet for a small subset of non-gird cells, about 10-15% of the population, the representation of a given experience changed considerably over time. Much as

has been observed in CA1 and CA2 (Mankin et al., 2012; Chapter 2), for this subset of non-grid cells representations of a pair of experiences were more dissimilar when separated by six hours than when separated by less than one hour. Thus, this population of time varying non-grid cells may reflect an important source of upstream input for the calculation of temporal recency by the hippocampus. In conjunction, the large portion of temporally stable mEC cells likely serve to anchor downstream hippocampal representations, consistent with findings that elimination of mEC inputs lead to increased instability in the CA1 network (Hales et al., 2014; Schlesiger et al., 2018; Schlesiger et al., 2015).

If indeed the change over time observed in hippocampus arises due to input from the subset of mEC non-grid cells that vary, one would hope to gain a greater understanding of this group of cells, seeking to determine what may set them apart from those that remain stable. In chapter 3 we sought to address this question, asking if cells that change over time perhaps reflect a distinct subset of the mEC population. However, outside of a slight propensity toward anatomical localization to mEC layer III, we were unable to identify any defining characteristics that would allow for *a priori* evaluation of the long-term behavior of individual mEC non-grid cells. While unfortunate, our inability to distinguish between those non-grid cells that change over time and those that do not is perhaps emblematic of a broader limitation in the ability to evaluate the role of mEC. Currently, an understanding of mEC physiology and its relation to downstream hippocampal processing and behavior is limited to correlational comparisons or relatively crude, broad reaching manipulations. Individual cell classes are largely defined according to functional firing properties and their relationship to a set of predefined tuning curves. Yet these functionally defined categories have thus far proven to have no clear correspondence to any underlying anatomical, genetic, morphological, or physiological features of the cells (Boccara et al., 2010; Latuske et al., 2015; Sun et al., 2015; Tang et al., 2014; Zhang

et al., 2013). Furthermore, the conceptualization that mEC cells can be appropriately categorized into discrete classes according to functional firing properties remains questionable. In chapter 1 we identified a critical flaw in past categorization methods that led to a fundamental re-evaluation of the mEC population activity. A recent study by Hardcastle et al. (2017) has also presented a novel approach to the idea of classification. Utilizing unbiased modeling techniques to categorize cells these authors' results had limited correspondence to the standard tuning-curve based methods. And in chapter 3 we described how the degree of spatial tuning observed in mEC cells appeared to be highly influenced by the size of an explored environment rather than necessarily reflecting a fundamental feature of a given cell. Collectively these findings question if mEC is truly composed of discreet classes of functionally distinct cell types, or if instead it is more appropriate to treat cells as representing different points along a continuous spectrum.

Because of these limitations in our understanding of mEC, it has remained virtually impossible to perform targeted manipulations of specific mEC cell types so as to determine their specific roles in MTL processing. While a handful of studies appear to preferentially target grid cell firing properties (Gil et al., 2018; Koenig et al., 2011; Mallory et al., 2018; Miao et al., 2017), our ability to appropriately gauge impacts on non-grid cells remains limited, particularly as we lack a clear understanding of which specific spatio-temporal firing properties of mEC cells are relevant for network processing. While it is assumed that the spatial firing characteristics of grid, border, and NGS cells are relevant for downstream hippocampal firing, such a hypothesis remains untested. In fact, the finding that place fields persist and that distinct spatial maps can be appropriately formed in animals lacking mEC input (Brun et al., 2008a; Hales et al., 2014; Ormond and McNaughton, 2015; Schlesiger et al., 2018) presents an interesting problem for the notion that all spatial content arrives in the hippocampus from mEC. If spatial firing in hippocampus were to arise via integration and refinement of an upstream spatial signal, one

would expect that removal of such input would eliminate downstream place fields. Moving forward, a better ability to selectively target specific subsets of the mEC population will be critical for advancing our understanding. Through the development of new methods or the uncovering of a correspondence between functional firing and underlying cellular properties it will hopefully become possible to perturb specific classes of mEC cells and gain insight into their roles in network processing and behavior. Alternatively, novel behavioral tasks or experimental manipulations may shed light on the properties of mEC cells. Instances in which the responses of cells diverge, such as was seen in chapter 1 in which grid cells maintain their spatial firing following changes to environmental features while NGS cells do not, may prove particularly useful in this endeavor.

Yet it is also important to keep in mind what we have learned from the work presented here and the parallels that are beginning to become clear between hippocampal network coding and upstream mEC activity. Spatial firing patterns, while not always in a periodic grid pattern, are abundant across the mEC population allowing for the establishment of a cognitive map of a space. These spatial firing patterns are largely consistent across repeated exposures to an environment with little systematic alteration over time as would be required for their use in navigational processing. But at the same time a subset of the population exhibits systematic changes over time, perhaps contributing an important temporal signal. Finally, cellular representation in mEC are highly multimodal, representing not only spatial information but also the non-spatial components of an experience. By utilizing this non-spatial coding, mEC cells become able to distinguish between experiences and in turn the network gains the ability to complement its spatial signal with the information necessary to also support episodic memory.

REFERENCES

Aggleton, J.P., Hunt, P.R., and Rawlins, J.N. (1986). The effects of hippocampal lesions upon spatial and non-spatial tests of working memory. Behav Brain Res 19, 133-146.

Aghajan, Z.M., Acharya, L., Moore, J.J., Cushman, J.D., Vuong, C., and Mehta, M.R. (2015). Impaired spatial selectivity and intact phase precession in two-dimensional virtual reality. Nat Neurosci 18, 121-128.

Alexander, G.M., Farris, S., Pirone, J.R., Zheng, C., Colgin, L.L., and Dudek, S.M. (2016). Social and novel contexts modify hippocampal CA2 representations of space. Nat Commun 7, 10300.

Allen, K., Gil, M., Resnik, E., Toader, O., Seeburg, P., and Monyer, H. (2014). Impaired path integration and grid cell spatial periodicity in mice lacking GluA1-containing AMPA receptors. J Neurosci 34, 6245-6259.

Anderson, M.I., and Jeffery, K.J. (2003). Heterogeneous modulation of place cell firing by changes in context. J Neurosci 23, 8827-8835.

Aronov, D., Nevers, R., and Tank, D.W. (2017). Mapping of a non-spatial dimension by the hippocampal-entorhinal circuit. Nature 543, 719-722.

Barry, C., Ginzberg, L.L., O'Keefe, J., and Burgess, N. (2012). Grid cell firing patterns signal environmental novelty by expansion. Proc Natl Acad Sci U S A 109, 17687-17692.

Barry, C., Hayman, R., Burgess, N., and Jeffery, K.J. (2007). Experience-dependent rescaling of entorhinal grids. Nat Neurosci 10, 682-684.

Barry, C., Lever, C., Hayman, R., Hartley, T., Burton, S., O'Keefe, J., Jeffery, K., and Burgess, N. (2006). The boundary vector cell model of place cell firing and spatial memory. Rev Neurosci 17, 71-97.

Bartesaghi, R., and Gessi, T. (2004). Parallel activation of field CA2 and dentate gyrus by synaptically elicited perforant path volleys. Hippocampus 14, 948-963.

Bartesaghi, R., Migliore, M., and Gessi, T. (2006). Input-output relations in the entorhinal cortex-dentate-hippocampal system: evidence for a non-linear transfer of signals. Neuroscience 142, 247-265.

Bellgowan, P.S., Buffalo, E.A., Bodurka, J., and Martin, A. (2009). Lateralized spatial and object memory encoding in entorhinal and perirhinal cortices. Learn Mem 16, 433-438.

Bjerknes, T.L., Langston, R.F., Kruge, I.U., Moser, E.I., and Moser, M.B. (2015). Coherence among head direction cells before eye opening in rat pups. Curr Biol 25, 103-108.

Blair, H.T., Gupta, K., and Zhang, K. (2008). Conversion of a phase- to a rate-coded position signal by a three-stage model of theta cells, grid cells, and place cells. Hippocampus 18, 1239-1255.

Boccara, C.N., Sargolini, F., Thoresen, V.H., Solstad, T., Witter, M.P., Moser, E.I., and Moser, M.B. (2010). Grid cells in pre- and parasubiculum. Nat Neurosci 13, 987-994.

Bonnevie, T., Dunn, B., Fyhn, M., Hafting, T., Derdikman, D., Kubie, J.L., Roudi, Y., Moser, E.I., and Moser, M.B. (2013). Grid cells require excitatory drive from the hippocampus. Nat Neurosci 16, 309-317.

Bostock, E., Muller, R.U., and Kubie, J.L. (1991). Experience-dependent modifications of hippocampal place cell firing. Hippocampus 1, 193-205.

Brandon, M.P., Bogaard, A.R., Libby, C.P., Connerney, M.A., Gupta, K., and Hasselmo, M.E. (2011). Reduction of theta rhythm dissociates grid cell spatial periodicity from directional tuning. Science 332, 595-599.

Brandon, M.P., Koenig, J., Leutgeb, J.K., and Leutgeb, S. (2014). New and distinct hippocampal place codes are generated in a new environment during septal inactivation. Neuron 82, 789-796.

Brun, V.H., Leutgeb, S., Wu, H.Q., Schwarcz, R., Witter, M.P., Moser, E.I., and Moser, M.B. (2008a). Impaired spatial representation in CA1 after lesion of direct input from entorhinal cortex. Neuron 57, 290-302.

Brun, V.H., Solstad, T., Kjelstrup, K.B., Fyhn, M., Witter, M.P., Moser, E.I., and Moser, M.B. (2008b). Progressive increase in grid scale from dorsal to ventral medial entorhinal cortex. Hippocampus 18, 1200-1212.

Bunsey, M., and Eichenbaum, H. (1995). Selective damage to the hippocampal region blocks long-term retention of a natural and nonspatial stimulus-stimulus association. Hippocampus 5, 546-556.

Burak, Y., and Fiete, I.R. (2009). Accurate path integration in continuous attractor network models of grid cells. PLoS Comput Biol 5, e1000291.

Burgess, N., Barry, C., and O'Keefe, J. (2007). An oscillatory interference model of grid cell firing. Hippocampus 17, 801-812.

Burgess, N., Maguire, E.A., and O'Keefe, J. (2002). The human hippocampus and spatial and episodic memory. Neuron 35, 625-641.

Burwell, R.D. (2000). The parahippocampal region: corticocortical connectivity. Ann N Y Acad Sci 911, 25-42.

Bush, D., Barry, C., and Burgess, N. (2014). What do grid cells contribute to place cell firing? Trends Neurosci 37, 136-145.

Buzsaki, G. (2015). Hippocampal sharp wave-ripple: A cognitive biomarker for episodic memory and planning. Hippocampus 25, 1073-1188.

Buzsaki, G., and Moser, E.I. (2013). Memory, navigation and theta rhythm in the hippocampal-entorhinal system. Nat Neurosci 16, 130-138.

Carpenter, F., Manson, D., Jeffery, K., Burgess, N., and Barry, C. (2015). Grid cells form a global representation of connected environments. Curr Biol 25, 1176-1182.

Caruana, D.A., Alexander, G.M., and Dudek, S.M. (2012). New insights into the regulation of synaptic plasticity from an unexpected place: hippocampal area CA2. Learn Mem 19, 391-400.

Cheng, S., and Frank, L.M. (2011). The structure of networks that produce the transformation from grid cells to place cells. Neuroscience 197, 293-306.

Chevaleyre, V., and Siegelbaum, S.A. (2010). Strong CA2 pyramidal neuron synapses define a powerful disynaptic cortico-hippocampal loop. Neuron 66, 560-572.

Clark, R.E., Zola, S.M., and Squire, L.R. (2000). Impaired recognition memory in rats after damage to the hippocampus. J Neurosci 20, 8853-8860.

Colgin, L.L., Moser, E.I., and Moser, M.B. (2008). Understanding memory through hippocampal remapping. Trends Neurosci 31, 469-477.

Cui, Z., Gerfen, C.R., and Young, W.S., 3rd (2013). Hypothalamic and other connections with dorsal CA2 area of the mouse hippocampus. J Comp Neurol 521, 1844-1866.

D'Hooge, R., and De Deyn, P.P. (2001). Applications of the Morris water maze in the study of learning and memory. Brain Res Brain Res Rev 36, 60-90.

de Almeida, L., Idiart, M., and Lisman, J.E. (2009). The input-output transformation of the hippocampal granule cells: from grid cells to place fields. J Neurosci 29, 7504-7512.

Derdikman, D., Whitlock, J.R., Tsao, A., Fyhn, M., Hafting, T., Moser, M.B., and Moser, E.I. (2009). Fragmentation of grid cell maps in a multicompartment environment. Nat Neurosci 12, 1325-1332.

Deshmukh, S.S. (2014). Spatial and Nonspatial Representations in the Lateral Entorhinal Cortex. In Space,Time and Memory in the Hippocampal Formation, D. Derdikman, and J.J. Knierim, eds. (Vienna: Springer Vienna), pp. 127-152.

Deshmukh, S.S., and Knierim, J.J. (2011). Representation of non-spatial and spatial information in the lateral entorhinal cortex. Front Behav Neurosci 5, 69.

Deshmukh, S.S., and Knierim, J.J. (2013). Influence of local objects on hippocampal representations: Landmark vectors and memory. Hippocampus 23, 253-267.

DeVito, L.M., Konigsberg, R., Lykken, C., Sauvage, M., Young, W.S., 3rd, and Eichenbaum, H. (2009). Vasopressin 1b receptor knock-out impairs memory for temporal order. J Neurosci 29, 2676-2683.

Diehl, G.W., Hon, O.J., Leutgeb, S., and Leutgeb, J.K. (2017). Grid and Nongrid Cells in Medial Entorhinal Cortex Represent Spatial Location and Environmental Features with Complementary Coding Schemes. Neuron 94, 83-92 e86.

Dudek, S.M., Alexander, G.M., and Farris, S. (2016). Rediscovering area CA2: unique properties and functions. Nat Rev Neurosci 17, 89-102.

Dusek, J.A., and Eichenbaum, H. (1997). The hippocampus and memory for orderly stimulus relations. Proc Natl Acad Sci U S A 94, 7109-7114.

Ebbinghaus, H. (1913). Memory: A contribution to experimental psychology (New York, NY, US: Teachers College Press).

Eichenbaum, H. (2000). A cortical-hippocampal system for declarative memory. Nat Rev Neurosci 1, 41-50.

Eichenbaum, H. (2014). Time cells in the hippocampus: a new dimension for mapping memories. Nat Rev Neurosci 15, 732-744.

Eichenbaum, H., and Cohen, N.J. (2001). From conditioning to conscious recollection : memory systems of the brain (Upper Saddle River, NJ: Oxford Univ).

Eichenbaum, H., Sauvage, M., Fortin, N., Komorowski, R., and Lipton, P. (2012). Towards a functional organization of episodic memory in the medial temporal lobe. Neurosci Biobehav Rev 36, 1597-1608.

Ennaceur, A., Neave, N., and Aggleton, J.P. (1997). Spontaneous object recognition and object location memory in rats: the effects of lesions in the cingulate cortices, the medial prefrontal cortex, the cingulum bundle and the fornix. Exp Brain Res 113, 509-519.

Estes, W.K. (1955). Statistical theory of spontaneous recovery and regression. Psychol Rev 62, 145-154.

Ezzyat, Y., and Davachi, L. (2014). Similarity breeds proximity: pattern similarity within and across contexts is related to later mnemonic judgments of temporal proximity. Neuron 81, 1179-1189.

Felleman, D.J., and Van Essen, D.C. (1991). Distributed hierarchical processing in the primate cerebral cortex. Cereb Cortex 1, 1-47.

Foster, D.J., and Wilson, M.A. (2006). Reverse replay of behavioural sequences in hippocampal place cells during the awake state. Nature 440, 680-683.

Foster, D.J., and Wilson, M.A. (2007). Hippocampal theta sequences. Hippocampus 17, 1093-1099.

Fuhs, M.C., and Touretzky, D.S. (2006). A spin glass model of path integration in rat medial entorhinal cortex. J Neurosci 26, 4266-4276.

Fyhn, M., Hafting, T., Treves, A., Moser, M.B., and Moser, E.I. (2007). Hippocampal remapping and grid realignment in entorhinal cortex. Nature 446, 190-194.

Fyhn, M., Molden, S., Witter, M.P., Moser, E.I., and Moser, M.B. (2004). Spatial representation in the entorhinal cortex. Science 305, 1258-1264.

Garden, D.L., Dodson, P.D., O'Donnell, C., White, M.D., and Nolan, M.F. (2008). Tuning of synaptic integration in the medial entorhinal cortex to the organization of grid cell firing fields. Neuron 60, 875-889.

Gil, M., Ancau, M., Schlesiger, M.I., Neitz, A., Allen, K., De Marco, R.J., and Monyer, H. (2018). Impaired path integration in mice with disrupted grid cell firing. Nat Neurosci 21, 81-91.

Giocomo, L.M., and Hasselmo, M.E. (2008). Time constants of h current in layer ii stellate cells differ along the dorsal to ventral axis of medial entorhinal cortex. J Neurosci 28, 9414-9425.

Giocomo, L.M., Hussaini, S.A., Zheng, F., Kandel, E.R., Moser, M.B., and Moser, E.I. (2011a). Grid cells use HCN1 channels for spatial scaling. Cell 147, 1159-1170.

Giocomo, L.M., Moser, M.B., and Moser, E.I. (2011b). Computational models of grid cells. Neuron 71, 589-603.

Giocomo, L.M., Zilli, E.A., Fransen, E., and Hasselmo, M.E. (2007). Temporal frequency of subthreshold oscillations scales with entorhinal grid cell field spacing. Science 315, 1719-1722.

Goodridge, J.P., and Taube, J.S. (1997). Interaction between the postsubiculum and anterior thalamus in the generation of head direction cell activity. J Neurosci 17, 9315-9330.

Gothard, K.M., Skaggs, W.E., Moore, K.M., and McNaughton, B.L. (1996). Binding of hippocampal CA1 neural activity to multiple reference frames in a landmark-based navigation task. J Neurosci 16, 823-835.

Gupta, A.S., van der Meer, M.A., Touretzky, D.S., and Redish, A.D. (2012). Segmentation of spatial experience by hippocampal theta sequences. Nat Neurosci 15, 1032-1039.

Hafting, T., Fyhn, M., Bonnevie, T., Moser, M.B., and Moser, E.I. (2008). Hippocampus-independent phase precession in entorhinal grid cells. Nature 453, 1248-1252.

Hafting, T., Fyhn, M., Molden, S., Moser, M.B., and Moser, E.I. (2005). Microstructure of a spatial map in the entorhinal cortex. Nature 436, 801-806.

Hales, J.B., Schlesiger, M.I., Leutgeb, J.K., Squire, L.R., Leutgeb, S., and Clark, R.E. (2014). Medial entorhinal cortex lesions only partially disrupt hippocampal place cells and hippocampus-dependent place memory. Cell Rep 9, 893-901.

Hardcastle, K., Ganguli, S., and Giocomo, L.M. (2015). Environmental boundaries as an error correction mechanism for grid cells. Neuron 86, 827-839.

Hardcastle, K., Maheswaranathan, N., Ganguli, S., and Giocomo, L.M. (2017). A Multiplexed, Heterogeneous, and Adaptive Code for Navigation in Medial Entorhinal Cortex. Neuron 94, 375-387 e377.

Hargreaves, E.L., Rao, G., Lee, I., and Knierim, J.J. (2005). Major dissociation between medial and lateral entorhinal input to dorsal hippocampus. Science 308, 1792-1794.

Hargreaves, E.L., Yoganarasimha, D., and Knierim, J.J. (2007). Cohesiveness of spatial and directional representations recorded from neural ensembles in the anterior thalamus, parasubiculum, medial entorhinal cortex, and hippocampus. Hippocampus 17, 826-841.

Hartley, T., Burgess, N., Lever, C., Cacucci, F., and O'Keefe, J. (2000). Modeling place fields in terms of the cortical inputs to the hippocampus. Hippocampus 10, 369-379.

Hartley, T., Lever, C., Burgess, N., and O'Keefe, J. (2014). Space in the brain: how the hippocampal formation supports spatial cognition. Philos Trans R Soc Lond B Biol Sci 369, 20120510.

Hinman, J.R., Brandon, M.P., Climer, J.R., Chapman, G.W., and Hasselmo, M.E. (2016). Multiple Running Speed Signals in Medial Entorhinal Cortex. Neuron 91, 666-679.

Hitti, F.L., and Siegelbaum, S.A. (2014). The hippocampal CA2 region is essential for social memory. Nature 508, 88-92.

Howard, M.W., and Kahana, M.J. (2002). A Distributed Representation of Temporal Context. Journal of Mathematical Psychology 46, 269-299.

Hsieh, L.T., Gruber, M.J., Jenkins, L.J., and Ranganath, C. (2014). Hippocampal activity patterns carry information about objects in temporal context. Neuron 81, 1165-1178.

James, W. (1890). The principles of psychology (NY, US: Henry Holt and Company).

Jenkins, L.J., and Ranganath, C. (2016). Distinct neural mechanisms for remembering when an event occurred. Hippocampus 26, 554-559.

Johnson, A., and Redish, A.D. (2007). Neural ensembles in CA3 transiently encode paths forward of the animal at a decision point. J Neurosci 27, 12176-12189.

Jones, M.W., and McHugh, T.J. (2011). Updating hippocampal representations: CA2 joins the circuit. Trends Neurosci 34, 526-535.

Kanter, B.R., Lykken, C.M., Avesar, D., Weible, A., Dickinson, J., Dunn, B., Borgesius, N.Z., Roudi, Y., and Kentros, C.G. (2017). A Novel Mechanism for the Grid-to-Place Cell Transformation Revealed by Transgenic Depolarization of Medial Entorhinal Cortex Layer II. Neuron 93, 1480-1492 e1486.

Kay, K., Sosa, M., Chung, J.E., Karlsson, M.P., Larkin, M.C., and Frank, L.M. (2016). A hippocampal network for spatial coding during immobility and sleep. Nature 531, 185-190.

Keene, C.S., Bladon, J., McKenzie, S., Liu, C.D., O'Keefe, J., and Eichenbaum, H. (2016). Complementary Functional Organization of Neuronal Activity Patterns in the Perirhinal, Lateral Entorhinal, and Medial Entorhinal Cortices. J Neurosci 36, 3660-3675.

Kempter, R., Leibold, C., Buzsáki, G., Diba, K., and Schmidt, R. (2012). Quantifying circular–linear associations: Hippocampal phase precession. Journal of Neuroscience Methods 207, 113-124.

Kennedy, P.J., and Shapiro, M.L. (2009). Motivational states activate distinct hippocampal representations to guide goal-directed behaviors. Proc Natl Acad Sci U S A 106, 10805-10810.

Kentros, C., Hargreaves, E., Hawkins, R.D., Kandel, E.R., Shapiro, M., and Muller, R.V. (1998). Abolition of long-term stability of new hippocampal place cell maps by NMDA receptor blockade. Science 280, 2121-2126.

Kentros, C.G., Agnihotri, N.T., Streater, S., Hawkins, R.D., and Kandel, E.R. (2004). Increased attention to spatial context increases both place field stability and spatial memory. Neuron 42, 283-295.

Kesner, R.P., Bolland, B.L., and Dakis, M. (1993). Memory for spatial locations, motor responses, and objects: triple dissociation among the hippocampus, caudate nucleus, and extrastriate visual cortex. Exp Brain Res 93, 462-470.

Killian, N.J., Jutras, M.J., and Buffalo, E.A. (2012). A map of visual space in the primate entorhinal cortex. Nature 491, 761-764.

Kitamura, T., Sun, C., Martin, J., Kitch, L.J., Schnitzer, M.J., and Tonegawa, S. (2015). Entorhinal Cortical Ocean Cells Encode Specific Contexts and Drive Context-Specific Fear Memory. Neuron 87, 1317-1331.

Kjonigsen, L.J., Leergaard, T.B., Witter, M.P., and Bjaalie, J.G. (2011). Digital atlas of anatomical subdivisions and boundaries of the rat hippocampal region. Front Neuroinform 5, 2.

Knierim, J.J. (2002). Dynamic interactions between local surface cues, distal landmarks, and intrinsic circuitry in hippocampal place cells. J Neurosci 22, 6254-6264.

Knierim, J.J., Lee, I., and Hargreaves, E.L. (2006). Hippocampal place cells: parallel input streams, subregional processing, and implications for episodic memory. Hippocampus 16, 755-764.

Knierim, J.J., Neunuebel, J.P., and Deshmukh, S.S. (2014). Functional correlates of the lateral and medial entorhinal cortex: objects, path integration and local-global reference frames. Philos Trans R Soc Lond B Biol Sci 369, 20130369.

Koenig, J., Linder, A.N., Leutgeb, J.K., and Leutgeb, S. (2011). The spatial periodicity of grid cells is not sustained during reduced theta oscillations. Science 332, 592-595.

Kohara, K., Pignatelli, M., Rivest, A.J., Jung, H.Y., Kitamura, T., Suh, J., Frank, D., Kajikawa, K., Mise, N., Obata, Y., *et al.* (2014). Cell type-specific genetic and optogenetic tools reveal hippocampal CA2 circuits. Nat Neurosci 17, 269-279.

Kraus, B.J., Brandon, M.P., Robinson, R.J., 2nd, Connerney, M.A., Hasselmo, M.E., and Eichenbaum, H. (2015). During Running in Place, Grid Cells Integrate Elapsed Time and Distance Run. Neuron 88, 578-589.

Kraus, B.J., Robinson, R.J., 2nd, White, J.A., Eichenbaum, H., and Hasselmo, M.E. (2013). Hippocampal "time cells": time versus path integration. Neuron 78, 1090-1101.

Kropff, E., Carmichael, J.E., Moser, M.B., and Moser, E.I. (2015). Speed cells in the medial entorhinal cortex. Nature 523, 419-424.

Krupic, J., Bauza, M., Burton, S., Barry, C., and O'Keefe, J. (2015). Grid cell symmetry is shaped by environmental geometry. Nature 518, 232-235.

Langston, R.F., Ainge, J.A., Couey, J.J., Canto, C.B., Bjerknes, T.L., Witter, M.P., Moser, E.I., and Moser, M.B. (2010). Development of the spatial representation system in the rat. Science 328, 1576-1580.

Lashley, K.S. (1950). In search of the engram. In Physiological mechanisms in animal behavior (Society's Symposium IV) (Oxford, England: Academic Press), pp. 454-482.

Latuske, P., Toader, O., and Allen, K. (2015). Interspike Intervals Reveal Functionally Distinct Cell Populations in the Medial Entorhinal Cortex. J Neurosci 35, 10963-10976.

Lee, A.K., and Wilson, M.A. (2002). Memory of sequential experience in the hippocampus during slow wave sleep. Neuron 36, 1183-1194.

Lee, H., Wang, C., Deshmukh, S.S., and Knierim, J.J. (2015). Neural Population Evidence of Functional Heterogeneity along the CA3 Transverse Axis: Pattern Completion versus Pattern Separation. Neuron 87, 1093-1105.

Lee, I., Yoganarasimha, D., Rao, G., and Knierim, J.J. (2004). Comparison of population coherence of place cells in hippocampal subfields CA1 and CA3. Nature 430, 456-459.

Lee, S.E., Simons, S.B., Heldt, S.A., Zhao, M., Schroeder, J.P., Vellano, C.P., Cowan, D.P., Ramineni, S., Yates, C.K., Feng, Y., *et al.* (2010). RGS14 is a natural suppressor of both synaptic plasticity in CA2 neurons and hippocampal-based learning and memory. Proc Natl Acad Sci U S A 107, 16994-16998.

Lein, E.S., Callaway, E.M., Albright, T.D., and Gage, F.H. (2005). Redefining the boundaries of the hippocampal CA2 subfield in the mouse using gene expression and 3-dimensional reconstruction. J Comp Neurol 485, 1-10.

Leutgeb, J.K., Leutgeb, S., Moser, M.B., and Moser, E.I. (2007). Pattern separation in the dentate gyrus and CA3 of the hippocampus. Science 315, 961-966.

Leutgeb, J.K., Leutgeb, S., Treves, A., Meyer, R., Barnes, C.A., McNaughton, B.L., Moser, M.B., and Moser, E.I. (2005a). Progressive transformation of hippocampal neuronal representations in "morphed" environments. Neuron 48, 345-358.

Leutgeb, S., Leutgeb, J.K., Barnes, C.A., Moser, E.I., McNaughton, B.L., and Moser, M.B. (2005b). Independent codes for spatial and episodic memory in hippocampal neuronal ensembles. Science 309, 619-623.

Leutgeb, S., Leutgeb, J.K., Moser, M.B., and Moser, E.I. (2005c). Place cells, spatial maps and the population code for memory. Curr Opin Neurobiol 15, 738-746.

Leutgeb, S., Leutgeb, J.K., Treves, A., Moser, M.B., and Moser, E.I. (2004). Distinct ensemble codes in hippocampal areas CA3 and CA1. Science 305, 1295-1298.

Lever, C., Wills, T., Cacucci, F., Burgess, N., and O'Keefe, J. (2002). Long-term plasticity in hippocampal place-cell representation of environmental geometry. Nature 416, 90-94.

Lipton, P.A., White, J.A., and Eichenbaum, H. (2007). Disambiguation of overlapping experiences by neurons in the medial entorhinal cortex. J Neurosci 27, 5787-5795.

Lisman, J., and Redish, A.D. (2009). Prediction, sequences and the hippocampus. Philos Trans R Soc Lond B Biol Sci 364, 1193-1201.

Lorente De Nó, R. (1934). Studies on the structure of the cerebral cortex. II. Continuation of the study of the ammonic system. Journal für Psychologie und Neurologie 46, 113-177.

Lu, L., Igarashi, K.M., Witter, M.P., Moser, E.I., and Moser, M.B. (2015). Topography of Place Maps along the CA3-to-CA2 Axis of the Hippocampus. Neuron 87, 1078-1092.

Lu, L., Leutgeb, J.K., Tsao, A., Henriksen, E.J., Leutgeb, S., Barnes, C.A., Witter, M.P., Moser, M.B., and Moser, E.I. (2013). Impaired hippocampal rate coding after lesions of the lateral entorhinal cortex. Nat Neurosci 16, 1085-1093.

Ludvig, N. (1999). Place cells can flexibly terminate and develop their spatial firing. A new theory for their function. Physiol Behav 67, 57-67.

MacDonald, C.J., Carrow, S., Place, R., and Eichenbaum, H. (2013). Distinct hippocampal time cell sequences represent odor memories in immobilized rats. J Neurosci 33, 14607-14616.

MacDonald, C.J., Lepage, K.Q., Eden, U.T., and Eichenbaum, H. (2011). Hippocampal "time cells" bridge the gap in memory for discontiguous events. Neuron 71, 737-749.

Magloczky, Z., Acsady, L., and Freund, T.F. (1994). Principal cells are the postsynaptic targets of supramammillary afferents in the hippocampus of the rat. Hippocampus 4, 322-334.

Mallory, C.S., Hardcastle, K., Bant, J.S., and Giocomo, L.M. (2018). Grid scale drives the scale and long-term stability of place maps. Nat Neurosci.

Mankin, E.A., Diehl, G.W., Sparks, F.T., Leutgeb, S., and Leutgeb, J.K. (2015). Hippocampal CA2 activity patterns change over time to a larger extent than between spatial contexts. Neuron 85, 190-201.

Mankin, E.A., Sparks, F.T., Slayyeh, B., Sutherland, R.J., Leutgeb, S., and Leutgeb, J.K. (2012). Neuronal code for extended time in the hippocampus. Proc Natl Acad Sci U S A 109, 19462-19467.

Manning, J.R., Polyn, S.M., Baltuch, G.H., Litt, B., and Kahana, M.J. (2011). Oscillatory patterns in temporal lobe reveal context reinstatement during memory search. Proc Natl Acad Sci U S A 108, 12893-12897.

Manns, J.R., Howard, M.W., and Eichenbaum, H. (2007). Gradual changes in hippocampal activity support remembering the order of events. Neuron 56, 530-540.

Marozzi, E., Ginzberg, L.L., Alenda, A., and Jeffery, K.J. (2015). Purely Translational Realignment in Grid Cell Firing Patterns Following Nonmetric Context Change. Cereb Cortex 25, 4619-4627.

Marr, D. (1971). Simple memory: a theory for archicortex. Philos Trans R Soc Lond B Biol Sci 262, 23-81.

Martig, A.K., and Mizumori, S.J. (2011). Ventral tegmental area disruption selectively affects CA1/CA2 but not CA3 place fields during a differential reward working memory task. Hippocampus 21, 172-184.

McDonald, R.J., and White, N.M. (1994). Parallel information processing in the water maze: evidence for independent memory systems involving dorsal striatum and hippocampus. Behav Neural Biol 61, 260-270.

McFarland, W.L., Teitelbaum, H., and Hedges, E.K. (1975). Relationship between hippocampal theta activity and running speed in the rat. J Comp Physiol Psychol 88, 324-328.

McNaughton, B.L., Battaglia, F.P., Jensen, O., Moser, E.I., and Moser, M.B. (2006). Path integration and the neural basis of the 'cognitive map'. Nat Rev Neurosci 7, 663-678.

McNaughton, B.L., and Morris, R.G.M. (1987). Hippocampal synaptic enhancement and information storage within a distributed memory system. Trends in Neurosciences 10, 408-415.

Miao, C., Cao, Q., Ito, H.T., Yamahachi, H., Witter, M.P., Moser, M.B., and Moser, E.I. (2015). Hippocampal Remapping after Partial Inactivation of the Medial Entorhinal Cortex. Neuron 88, 590-603.

Miao, C., Cao, Q., Moser, M.B., and Moser, E.I. (2017). Parvalbumin and Somatostatin Interneurons Control Different Space-Coding Networks in the Medial Entorhinal Cortex. Cell 171, 507-521 e517.

Mishkin, M. (1978). Memory in monkeys severely impaired by combined but not by separate removal of amygdala and hippocampus. Nature 273, 297-298.

Mitra, P., and Bokil, H. (2008). Observed brain dynamics (Oxford ; New York: Oxford University Press).

Moita, M.A., Rosis, S., Zhou, Y., LeDoux, J.E., and Blair, H.T. (2004). Putting fear in its place: remapping of hippocampal place cells during fear conditioning. J Neurosci 24, 7015-7023.

Morris, R. (1984). Developments of a water-maze procedure for studying spatial learning in the rat. J Neurosci Methods 11, 47-60.

Morris, R.G., Garrud, P., Rawlins, J.N., and O'Keefe, J. (1982). Place navigation impaired in rats with hippocampal lesions. Nature 297, 681-683.

Morris, R.G.M. (1981). Spatial localization does not require the presence of local cues. Learning and Motivation 12, 239-260.

Moser, E.I., Kropff, E., and Moser, M.B. (2008). Place cells, grid cells, and the brain's spatial representation system. Annu Rev Neurosci 31, 69-89.

Moser, E.I., Moser, M.B., and McNaughton, B.L. (2017). Spatial representation in the hippocampal formation: a history. Nat Neurosci 20, 1448-1464.

Moser, E.I., Roudi, Y., Witter, M.P., Kentros, C., Bonhoeffer, T., and Moser, M.B. (2014). Grid cells and cortical representation. Nat Rev Neurosci 15, 466-481.

Muller, R.U., and Kubie, J.L. (1987). The effects of changes in the environment on the spatial firing of hippocampal complex-spike cells. J Neurosci 7, 1951-1968.

Muller, R.U., Kubie, J.L., and Ranck, J.B., Jr. (1987). Spatial firing patterns of hippocampal complex-spike cells in a fixed environment. J Neurosci 7, 1935-1950.

Neunuebel, J.P., Yoganarasimha, D., Rao, G., and Knierim, J.J. (2013). Conflicts between local and global spatial frameworks dissociate neural representations of the lateral and medial entorhinal cortex. J Neurosci 33, 9246-9258.

Newman, E.L., Climer, J.R., and Hasselmo, M.E. (2014). Grid cell spatial tuning reduced following systemic muscarinic receptor blockade. Hippocampus 24, 643-655.

Newman, E.L., Gillet, S.N., Climer, J.R., and Hasselmo, M.E. (2013). Cholinergic blockade reduces theta-gamma phase amplitude coupling and speed modulation of theta frequency consistent with behavioral effects on encoding. J Neurosci 33, 19635-19646.

Newman, E.L., and Hasselmo, M.E. (2014). Grid cell firing properties vary as a function of theta phase locking preferences in the rat medial entorhinal cortex. Front Syst Neurosci 8, 193.

Nielson, D.M., Smith, T.A., Sreekumar, V., Dennis, S., and Sederberg, P.B. (2015). Human hippocampus represents space and time during retrieval of real-world memories. Proc Natl Acad Sci U S A 112, 11078-11083.

O'Keefe, J. (1976). Place units in the hippocampus of the freely moving rat. Exp Neurol 51, 78-109.

O'Keefe, J., and Burgess, N. (1996). Geometric determinants of the place fields of hippocampal neurons. Nature 381, 425-428.

O'Keefe, J., and Dostrovsky, J. (1971). The hippocampus as a spatial map. Preliminary evidence from unit activity in the freely-moving rat. Brain Res 34, 171-175.

O'Keefe, J., and Nadel, L. (1978). The hippocampus as a cognitive map (Oxford: Clarendon Press).

O'Keefe, J., Nadel, L., Keightley, S., and Kill, D. (1975). Fornix lesions selectively abolish place learning in the rat. Exp Neurol 48, 152-166.

O'Keefe, J., and Recce, M.L. (1993). Phase relationship between hippocampal place units and the EEG theta rhythm. Hippocampus 3, 317-330.

Oliva, A., Fernandez-Ruiz, A., Buzsaki, G., and Berenyi, A. (2016). Role of Hippocampal CA2 Region in Triggering Sharp-Wave Ripples. Neuron 91, 1342-1355.

Ormond, J., and McNaughton, B.L. (2015). Place field expansion after focal MEC inactivations is consistent with loss of Fourier components and path integrator gain reduction. Proc Natl Acad Sci U S A 112, 4116-4121.

Pagani, J.H., Zhao, M., Cui, Z., Avram, S.K., Caruana, D.A., Dudek, S.M., and Young, W.S. (2015). Role of the vasopressin 1b receptor in rodent aggressive behavior and synaptic plasticity in hippocampal area CA2. Mol Psychiatry 20, 490-499.

Pan, W.X., and McNaughton, N. (2004). The supramammillary area: its organization, functions and relationship to the hippocampus. Prog Neurobiol 74, 127-166.

Parkinson, J.K., Murray, E.A., and Mishkin, M. (1988). A selective mnemonic role for the hippocampus in monkeys: memory for the location of objects. J Neurosci 8, 4159-4167.

Pastalkova, E., Itskov, V., Amarasingham, A., and Buzsaki, G. (2008). Internally generated cell assembly sequences in the rat hippocampus. Science 321, 1322-1327.

Pavlov, I.P. (1927). Conditioned reflexes: an investigation of the physiological activity of the cerebral cortex (Oxford, England: Oxford Univ. Press).

Perez-Escobar, J.A., Kornienko, O., Latuske, P., Kohler, L., and Allen, K. (2016). Visual landmarks sharpen grid cell metric and confer context specificity to neurons of the medial entorhinal cortex. Elife 5.

Pfeiffer, B.E., and Foster, D.J. (2013). Hippocampal place-cell sequences depict future paths to remembered goals. Nature 497, 74-79.

Polyn, S.M., Norman, K.A., and Kahana, M.J. (2009). A context maintenance and retrieval model of organizational processes in free recall. Psychol Rev 116, 129-156.

Quian Quiroga, R., Kraskov, A., Koch, C., and Fried, I. (2009). Explicit encoding of multimodal percepts by single neurons in the human brain. Curr Biol 19, 1308-1313.

Quirk, G.J., Muller, R.U., and Kubie, J.L. (1990). The firing of hippocampal place cells in the dark depends on the rat's recent experience. J Neurosci 10, 2008-2017.

Quirk, G.J., Muller, R.U., Kubie, J.L., and Ranck, J.B., Jr. (1992). The positional firing properties of medial entorhinal neurons: description and comparison with hippocampal place cells. J Neurosci 12, 1945-1963.

Raaijmakers, J.G.W., and Mensink, G.J.M.A. (1988). A model for interference and forgetting. Psychological Review 95, 434 - 455.

Racine, R.J., and Kimble, D.P. (1965). Hippocampal lesions and delayed alternation in the rat. Psychon Sci 3, 285-286.

Ratzliff, A.D., and Soltesz, I. (2001). Differential immunoreactivity for alpha-actinin-2, an N-methyl-D-aspartate-receptor/actin binding protein, in hippocampal interneurons. Neuroscience 103, 337-349.

Redish, A.D., Battaglia, F.P., Chawla, M.K., Ekstrom, A.D., Gerrard, J.L., Lipa, P., Rosenzweig, E.S., Worley, P.F., Guzowski, J.F., McNaughton, B.L., and Barnes, C.A. (2001). Independence of firing correlates of anatomically proximate hippocampal pyramidal cells. J Neurosci 21, RC134.

Renno-Costa, C., Lisman, J.E., and Verschure, P.F. (2010). The mechanism of rate remapping in the dentate gyrus. Neuron 68, 1051-1058.

Robinson, N.T.M., Priestley, J.B., Rueckemann, J.W., Garcia, A.D., Smeglin, V.A., Marino, F.A., and Eichenbaum, H. (2017). Medial Entorhinal Cortex Selectively Supports Temporal Coding by Hippocampal Neurons. Neuron 94, 677-688 e676.

Rolls, E.T. (1989). Functions of neuronal networks in the hippocampus and neocortex in memory. In Neural models of plasticity: Experimental and theoretical approaches (San Diego, CA, US: Academic Press), pp. 240-265.

Rolls, E.T., Stringer, S.M., and Elliot, T. (2006). Entorhinal cortex grid cells can map to hippocampal place cells by competitive learning. Network 17, 447-465.

Rolls, E.T., Treves, A., Tovee, M.J., and Panzeri, S. (1997). Information in the neuronal representation of individual stimuli in the primate temporal visual cortex. J Comput Neurosci 4, 309-333.

Rowland, D.C., Weible, A.P., Wickersham, I.R., Wu, H., Mayford, M., Witter, M.P., and Kentros, C.G. (2013). Transgenically targeted rabies virus demonstrates a major monosynaptic projection from hippocampal area CA2 to medial entorhinal layer II neurons. J Neurosci 33, 14889-14898.

Royer, S., Sirota, A., Patel, J., and Buzsaki, G. (2010). Distinct representations and theta dynamics in dorsal and ventral hippocampus. J Neurosci 30, 1777-1787.

Rubin, A., Geva, N., Sheintuch, L., and Ziv, Y. (2015). Hippocampal ensemble dynamics timestamp events in long-term memory. Elife 4.

Rueckemann, J.W., DiMauro, A.J., Rangel, L.M., Han, X., Boyden, E.S., and Eichenbaum, H. (2016). Transient optogenetic inactivation of the medial entorhinal cortex biases the active population of hippocampal neurons. Hippocampus 26, 246-260.

Sargolini, F., Fyhn, M., Hafting, T., McNaughton, B.L., Witter, M.P., Moser, M.B., and Moser, E.I. (2006). Conjunctive representation of position, direction, and velocity in entorhinal cortex. Science 312, 758-762.

Save, E., Poucet, B., Foreman, N., and Buhot, M.C. (1992). Object exploration and reactions to spatial and nonspatial changes in hooded rats following damage to parietal cortex or hippocampal formation. Behav Neurosci 106, 447-456.

Savelli, F., Luck, J.D., and Knierim, J.J. (2017). Framing of grid cells within and beyond navigation boundaries. Elife 6.

Savelli, F., Yoganarasimha, D., and Knierim, J.J. (2008). Influence of boundary removal on the spatial representations of the medial entorhinal cortex. Hippocampus 18, 1270-1282.

Schlesiger, M.I., Boublil, B.L., Hales, J.B., Leutgeb, J.K., and Leutgeb, S. (2018). Hippocampal Global Remapping Can Occur without Input from the Medial Entorhinal Cortex. Cell Rep 22, 3152-3159.

Schlesiger, M.I., Cannova, C.C., Boublil, B.L., Hales, J.B., Mankin, E.A., Brandon, M.P., Leutgeb, J.K., Leibold, C., and Leutgeb, S. (2015). The medial entorhinal cortex is necessary for temporal organization of hippocampal neuronal activity. Nat Neurosci 18, 1123-1132.

Schmitzer-Torbert, N., Jackson, J., Henze, D., Harris, K., and Redish, A.D. (2005). Quantitative measures of cluster quality for use in extracellular recordings. Neuroscience 131, 1-11.

Scoville, W.B., and Milner, B. (1957). Loss of recent memory after bilateral hippocampal lesions. J Neurol Neurosurg Psychiatry 20, 11-21.

Shapiro, M.L., Tanila, H., and Eichenbaum, H. (1997). Cues that hippocampal place cells encode: dynamic and hierarchical representation of local and distal stimuli. Hippocampus 7, 624-642.

Shen, J., Barnes, C.A., McNaughton, B.L., Skaggs, W.E., and Weaver, K.L. (1997). The effect of aging on experience-dependent plasticity of hippocampal place cells. J Neurosci 17, 6769-6782.

Simons, S.B., Caruana, D.A., Zhao, M., and Dudek, S.M. (2011). Caffeine-induced synaptic potentiation in hippocampal CA2 neurons. Nat Neurosci 15, 23-25.

Simons, S.B., Escobedo, Y., Yasuda, R., and Dudek, S.M. (2009). Regional differences in hippocampal calcium handling provide a cellular mechanism for limiting plasticity. Proceedings of the National Academy of Sciences 106, 14080-14084.

Skaggs, W.E., McNaughton, B.L., Gothard, K.M., and Markus, E.J. (1993). An information-theoretic approach to deciphering the hippocampal code. Advances in Neural Information Processing Systems 5, 1030-1037.

Skillings, J.H., and Mack, G.A. (1981). On the Use of a Friedman-Type Statistic in Balanced and Un-Balanced Block-Designs. Technometrics 23, 171-177.

Skinner, B.F. (1938). The behavior of organisms: an experimental analysis (Oxford, England: Appleton-Century).

Slawinska, U., and Kasicki, S. (1998). The frequency of rat's hippocampal theta rhythm is related to the speed of locomotion. Brain Res 796, 327-331.

Solstad, T., Boccara, C.N., Kropff, E., Moser, M.B., and Moser, E.I. (2008). Representation of geometric borders in the entorhinal cortex. Science 322, 1865-1868.

Solstad, T., Moser, E.I., and Einevoll, G.T. (2006). From grid cells to place cells: a mathematical model. Hippocampus 16, 1026-1031.

Squire, L.R. (1982). The neuropsychology of human memory. Annu Rev Neurosci 5, 241-273.

Squire, L.R., and Zola-Morgan, S. (1983). The neurology of memory: the case for correspondence between the findings for human and nonhuman primate. In The Physiological Basis of Memory (Second Edition), J.A. Deutsch, ed. (Academic Press), pp. 199-268.

Squire, L.R., and Zola-Morgan, S. (1991). The medial temporal lobe memory system. Science 253, 1380-1386.

Stensola, H., Stensola, T., Solstad, T., Froland, K., Moser, M.B., and Moser, E.I. (2012). The entorhinal grid map is discretized. Nature 492, 72-78.

Stensola, T., Stensola, H., Moser, M.B., and Moser, E.I. (2015). Shearing-induced asymmetry in entorhinal grid cells. Nature 518, 207-212.

Stepanek, L., and Doupe, A.J. (2010). Activity in a cortical-basal ganglia circuit for song is required for social context-dependent vocal variability. J Neurophysiol 104, 2474-2486.

Stevenson, E.L., and Caldwell, H.K. (2014). Lesions to the CA2 region of the hippocampus impair social memory in mice. Eur J Neurosci 40, 3294-3301.

Stewart, M., and Fox, S.E. (1990). Do septal neurons pace the hippocampal theta rhythm? Trends Neurosci 13, 163-168.

Sun, C., Kitamura, T., Yamamoto, J., Martin, J., Pignatelli, M., Kitch, L.J., Schnitzer, M.J., and Tonegawa, S. (2015). Distinct speed dependence of entorhinal island and ocean cells, including respective grid cells. Proc Natl Acad Sci U S A 112, 9466-9471.

Sutherland, R.J., Kolb, B., and Whishaw, I.Q. (1982). Spatial mapping: definitive disruption by hippocampal or medial frontal cortical damage in the rat. Neurosci Lett 31, 271-276.

Tang, Q., Burgalossi, A., Ebbesen, C.L., Ray, S., Naumann, R., Schmidt, H., Spicher, D., and Brecht, M. (2014). Pyramidal and stellate cell specificity of grid and border representations in layer 2 of medial entorhinal cortex. Neuron 84, 1191-1197.

Tang, Q., Ebbesen, C.L., Sanguinetti-Scheck, J.I., Preston-Ferrer, P., Gundlfinger, A., Winterer, J., Beed, P., Ray, S., Naumann, R., Schmitz, D., *et al.* (2015). Anatomical Organization and Spatiotemporal Firing Patterns of Layer 3 Neurons in the Rat Medial Entorhinal Cortex. J Neurosci 35, 12346-12354.

Taube, J.S. (2007). The head direction signal: origins and sensory-motor integration. Annu Rev Neurosci 30, 181-207.

Taube, J.S., Muller, R.U., and Ranck, J.B., Jr. (1990). Head-direction cells recorded from the postsubiculum in freely moving rats. I. Description and quantitative analysis. J Neurosci 10, 420-435.

Thompson, L.T., and Best, P.J. (1989). Place cells and silent cells in the hippocampus of freely-behaving rats. J Neurosci 9, 2382-2390.

Thorndike, E.L. (1898). Animal intelligence: An experimental study of the associative processes in animals. The Psychological Review: Monograph Supplements 2, i-109.

Tolman, E.C. (1948). Cognitive maps in rats and men. Psychological Review 55, 189-208.

Treves, A., and Rolls, E.T. (1994). Computational analysis of the role of the hippocampus in memory. Hippocampus 4, 374-391.

Tsao, A., Moser, M.B., and Moser, E.I. (2013). Traces of experience in the lateral entorhinal cortex. Curr Biol 23, 399-405.

Tulving, E. (1972). Episodic and semantic memory. In Organization of memory (Oxford, England: Academic Press), pp. xiii, 423-xiii, 423.

van Strien, N.M., Cappaert, N.L., and Witter, M.P. (2009). The anatomy of memory: an interactive overview of the parahippocampal-hippocampal network. Nat Rev Neurosci 10, 272-282.

Varga, C., Lee, S.Y., and Soltesz, I. (2010). Target-selective GABAergic control of entorhinal cortex output. Nat Neurosci 13, 822-824.

Vazdarjanova, A., and Guzowski, J.F. (2004). Differences in hippocampal neuronal population responses to modifications of an environmental context: evidence for distinct, yet complementary, functions of CA3 and CA1 ensembles. J Neurosci 24, 6489-6496.

Victor, M., and Agamanolis, D. (1990). Amnesia due to Lesions Confined to the Hippocampus: A Clinical-Pathologic Study. J Cogn Neurosci 2, 246-257.

Wang, M.E., Wann, E.G., Yuan, R.K., Ramos Alvarez, M.M., Stead, S.M., and Muzzio, I.A. (2012). Long-term stabilization of place cell remapping produced by a fearful experience. J Neurosci 32, 15802-15814.

Wang, Y., Romani, S., Lustig, B., Leonardo, A., and Pastalkova, E. (2015). Theta sequences are essential for internally generated hippocampal firing fields. Nat Neurosci 18, 282-288.

Wernle, T., Waaga, T., Morreaunet, M., Treves, A., Moser, M.B., and Moser, E.I. (2018). Integration of grid maps in merged environments. Nat Neurosci 21, 92-101.

Wersinger, S.R., Ginns, E.I., O'Carroll, A.M., Lolait, S.J., and Young, W.S., 3rd (2002). Vasopressin V1b receptor knockout reduces aggressive behavior in male mice. Mol Psychiatry 7, 975-984.

Wikenheiser, A.M., and Redish, A.D. (2015). Hippocampal theta sequences reflect current goals. Nat Neurosci 18, 289-294.

Wills, T.J., Cacucci, F., Burgess, N., and O'Keefe, J. (2010). Development of the hippocampal cognitive map in preweanling rats. Science 328, 1573-1576.

Wilson, M.A., and McNaughton, B.L. (1993). Dynamics of the hippocampal ensemble code for space. Science 261, 1055-1058.

Winter, S.S., Clark, B.J., and Taube, J.S. (2015a). Disruption of the head direction cell network impairs the parahippocampal grid cell signal. Science 347, 870-874.

Winter, S.S., Mehlman, M.L., Clark, B.J., and Taube, J.S. (2015b). Passive Transport Disrupts Grid Signals in the Parahippocampal Cortex. Curr Biol 25, 2493-2502.

Wintzer, M.E., Boehringer, R., Polygalov, D., and McHugh, T.J. (2014). The hippocampal CA2 ensemble is sensitive to contextual change. J Neurosci 34, 3056-3066.

Wirth, S., Yanike, M., Frank, L.M., Smith, A.C., Brown, E.N., and Suzuki, W.A. (2003). Single neurons in the monkey hippocampus and learning of new associations. Science 300, 1578-1581.

Witter, M.P. (2007). Intrinsic and extrinsic wiring of CA3: indications for connectional heterogeneity. Learn Mem 14, 705-713.

Witter, M.P., and Amaral, D.G. (2004). Hippocampal Formation. In The Rat Nervous System, G. Paxinos, ed. (Burlington: Academic Press), pp. 635-704.

Witter, M.P., Groenewegen, H.J., Lopes da Silva, F.H., and Lohman, A.H. (1989). Functional organization of the extrinsic and intrinsic circuitry of the parahippocampal region. Prog Neurobiol 33, 161-253.

Wolpert, D.M., and Flanagan, J.R. (2001). Motor prediction. Curr Biol 11, R729-732.

Wood, E.R., Dudchenko, P.A., and Eichenbaum, H. (1999). The global record of memory in hippocampal neuronal activity. Nature 397, 613-616.

Wood, E.R., Dudchenko, P.A., Robitsek, R.J., and Eichenbaum, H. (2000). Hippocampal neurons encode information about different types of memory episodes occurring in the same location. Neuron 27, 623-633.

Woodhams, P.L., Celio, M.R., Ulfig, N., and Witter, M.P. (1993). Morphological and functional correlates of borders in the entorhinal cortex and hippocampus. Hippocampus 3 Spec No, 303-311.

Wu, H.G., Miyamoto, Y.R., Gonzalez Castro, L.N., Olveczky, B.P., and Smith, M.A. (2014). Temporal structure of motor variability is dynamically regulated and predicts motor learning ability. Nat Neurosci 17, 312-321.

Wyszynski, M., Kharazia, V., Shanghvi, R., Rao, A., Beggs, A.H., Craig, A.M., Weinberg, R., and Sheng, M. (1998). Differential regional expression and ultrastructural localization of alpha-actinin-2, a putative NMDA receptor-anchoring protein, in rat brain. J Neurosci 18, 1383-1392.

Yoganarasimha, D., and Knierim, J.J. (2005). Coupling between place cells and head direction cells during relative translations and rotations of distal landmarks. Exp Brain Res 160, 344-359.

Yoganarasimha, D., Rao, G., and Knierim, J.J. (2011). Lateral entorhinal neurons are not spatially selective in cue-rich environments. Hippocampus 21, 1363-1374.

Yoon, K., Lewallen, S., Kinkhabwala, A.A., Tank, D.W., and Fiete, I.R. (2016). Grid Cell Responses in 1D Environments Assessed as Slices through a 2D Lattice. Neuron 89, 1086-1099.

Young, W.S., Li, J., Wersinger, S.R., and Palkovits, M. (2006). The vasopressin 1b receptor is prominent in the hippocampal area CA2 where it is unaffected by restraint stress or adrenalectomy. Neuroscience 143, 1031-1039.

Zhang, S.J., Ye, J., Miao, C., Tsao, A., Cerniauskas, I., Ledergerber, D., Moser, M.B., and Moser, E.I. (2013). Optogenetic dissection of entorhinal-hippocampal functional connectivity. Science 340, 1232627.

Zhao, M., Choi, Y.S., Obrietan, K., and Dudek, S.M. (2007). Synaptic plasticity (and the lack thereof) in hippocampal CA2 neurons. J Neurosci 27, 12025-12032.

Zhao, X., Lein, E.S., He, A., Smith, S.C., Aston, C., and Gage, F.H. (2001). Transcriptional profiling reveals strict boundaries between hippocampal subregions. J Comp Neurol 441, 187-196.

Ziv, Y., Burns, L.D., Cocker, E.D., Hamel, E.O., Ghosh, K.K., Kitch, L.J., El Gamal, A., and Schnitzer, M.J. (2013). Long-term dynamics of CA1 hippocampal place codes. Nat Neurosci 16, 264-266.

Zola-Morgan, S., and Squire, L.R. (1986). Memory impairment in monkeys following lesions limited to the hippocampus. Behav Neurosci 100, 155-160.

Zola-Morgan, S., Squire, L.R., and Amaral, D.G. (1986). Human amnesia and the medial temporal region: enduring memory impairment following a bilateral lesion limited to field CA1 of the hippocampus. J Neurosci 6, 2950-2967.